UNIVERSITÉ DE SHERBROOKE
Faculté de génie
Département de génie civil et de génie du bâtiment

Étude de la réhabilitation sismique d'un pont avec des isolateurs en caoutchouc à basse température par le biais de surfaces de fragilité

Study of the seismic retrofitting of a bridge with rubber isolators in cold environment through fragility surfaces

Thèse de doctorat
Specialité: génie civil

Pedro Alexandre CONDE BANDINI

Sherbrooke (Québec) Canada

Avril 2021

JURY MEMBERS

Patrick PAULTRE

Supervisor

Jamie Ellen PADGETT

Co-supervisor

Charles-Philippe LAMARCHE

Examiner

Georgios BALOMENOS

Examiner

Yazhou (Tim) XIE

Examiner

RÉSUMÉ

Au Québec, Canada, en raison du vieillissement et de détails insuffisants de dimensionnement sismique, les ponts sont susceptibles de subir des dommages importants en cas de fort séisme. Pour améliorer la performance sismique de l'inventaire des ponts de la province, le remplacement des appareils d'appui classiques par des isolateurs en caoutchouc naturel s'est avéré une mesure de réhabilitation potentiellement efficace. Cependant, les variations des propriétés mécaniques des isolateurs dues aux conditions environnementales peuvent affecter la performance sismique. Par exemple, le caoutchouc subit un raidissement important lorsqu'il est exposé aux basses températures, comme celles typiquement observées pendant les hivers dans l'est du Canada. Dans les ponts, le raidissement thermique des isolateurs augmente les forces transmises à la sous-structure, qui devient alors plus susceptible d'être endommagée. Une étude plus détaillée des effets thermiques sur la performance sismique des ponts provinciaux typiques est donc nécessaire. Des surfaces de fragilité sont donc utilisées pour évaluer la vulnérabilité d'un pont typique au Québec réhabilité avec des isolateurs en caoutchouc naturel sous les actions concomitantes des séismes et des basses températures. Les ponts sont composés de plusieurs éléments différents ayant des comportements distincts et des interactions complexes sous une excitation sismique. En raison de l'importance de la contribution de plusieurs composants à la fragilité du pont, la première partie de cette étude se concentre sur la construction de modèles probabilistes multivariés de demande sismique (PSDM). On a critiqué la validité des hypothèses couramment adoptées et leur impact sur les estimations de fragilité n'est pas entièrement compris. Une approche PSDM multivariée est donc développée en couplant l'analyse de bandes multiples et les modèles de mélange gaussien. La nouvelle approche capture de manière concomitante la complexité de la réponse dynamique et modélise les incertitudes et la corrélation. On évalue ensuite le biais potentiel introduit par une mauvaise modélisation sur les estimations de fragilité et de risque d'un pont réel tel que construit. Cette stratégie PSDM est ensuite adoptée pour traduire la réponse des composants du pont de l'étude de cas lorsqu'il est réhabilité. Les surfaces de fragilité basées sur la régression logistique décrivent les effets du raidissement thermique des isolateurs sur les performances du pont, tant au niveau des composants que du système. Une combinaison bénéfique est révélée entre l'effet de découplage des isolateurs et l'action de retenue latérale des murs en fonction des écarts fournis. La dérivation des surfaces de fragilité pour les ponts isolés dans les régions froides jette un nouvel éclairage sur les défis de la réhabilitation des structures exposées à de multiples environnements extrêmes (sismiques et thermiques). Dans l'ensemble, les résultats présentés peuvent faciliter la modélisation de la vulnérabilité sismique et l'évaluation de la réhabilitation de ces systèmes complexes et avoir des répercussions pratiques importantes. Les idées et les avancées méthodologiques peuvent susciter des recherches et des applications bien au-delà des structures étudiées dans la thèse, et en avoir un large impact.

Mots-clés : Ponts, Fragilité, Réhabiliation, Isolation sismique, Basses températures

ABSTRACT

In Quebec, Canada, due to aging and deficient seismic detailing, bridges are susceptible to important damage in the occurrence of a strong earthquake. To enhance the seismic performance of the provincial bridge inventory, the replacement of typical bearings with natural rubber isolators has shown to be a potentially efficient retrofitting measure. However, variations in the mechanical properties of the isolators due to environmental conditions can affect the seismic performance. For instance, rubber undergoes substantial stiffening when exposed to low temperatures, as those typically observed during winter in eastern Canada. In bridge-type structures, the thermal stiffening of isolators increases the forces transmitted to the substructure, which in turn becomes more prone to damage. A more detailed consideration of the thermal effects on the seismic performance of typical provincial bridges is thus necessary. In this study, fragility surfaces are used to assess the vulnerability of a typical bridge in Quebec when retrofitted with natural rubber isolators under the concomitant actions of earthquakes and low temperatures. Bridges are composed of several different components with distinguished behaviors and complex interactions under seismic excitation. Owing to the importance of the contribution of different components to the bridge fragility, the first part of this study focuses on the construction of multivariate probabilistic seismic demand models (PSDM). The validity of the commonly adopted assumptions has been criticized and their impact on fragility estimates is not fully understood. A multivariate PSDM approach is thus developed coupling the multiple-stripe analysis and Gaussian mixture models. The novel approach concomitantly captures the complexity of the dynamic response of multicomponent structures and models their uncertainties and correlation. The proposed approach is then used to assess the potential bias introduced by poor modeling on fragility and risk estimates of a real as-built case-study bridge. This PSDM strategy then is adopted to translate the uncertainty and the correlation of the response of the case-study bridge components when retrofitted. Fragility surfaces based on logistic regression depict the effects of thermal stiffening of isolators on the performance of the bridge in both component- and system-level. A beneficial combination is revealed between the decoupling effect provided by isolators and the lateral restraining action of the abutment wing walls depending on the provide clearances. The derivation of fragility surfaces for isolated bridges in cold regions sheds new light on the challenges of retrofitting structures exposed to multiple extreme environments (e.g., seismic and thermal). Overall the presented results can facilitate seismic vulnerability modeling and retrofit assessment of these complex systems and afford valuable practical impacts. The insights and methodological advances can prompt research and applications well beyond the case study structures considered in the thesis, and have broad impacts.

Keywords: Bridges, Fragility, Retrofitting, Seismic isolation, Low temperatures

"(...) all calculations, no matter how sophisticated and complex, cannot be more than rough approximations of the natural phenomenon they try to represent by means of a mathematical model".
- Félix Candela

To Silvia, Luiz A., Luiz F., Geneviève, and Flora

ACKNOWLEDGEMENTS

I start by thanking Prof. Paultre for the opportunity, trust, and support that allowed me to conduct a research on this rather challenging, but encouraging subject. I am truly grateful for being part of the CRGP research group directed by Prof. Paultre. I gratefully acknowledge Prof. Padgett at Rice University for her substantial contribution to this work, first by welcoming me in her research group as a visitor, and for her guidance as co-advisor. I am also greatly thankful to Prof. Siqueira at *Universidade Estadual de Campinas*, where I spent crucial years on my formation as civil engineer. Prof. Siqueira has contributed immensely to this research with long and meaningful discussions, and valuable advices. I would like to acknowledge the support from the current and past members of the CRGP and the department of civil engineering and building engineering at the *Université de Sherbrooke*, particularly to Anderssen Barbosa, Rodrigo Torres, Steeve Ambroise, Olivier Gauron, and Luis Zuluaga. I specially thank my South-American teammate and friend Rocio Segura for the countless times we discussed our research projects and life in general.

I am greatly thankful for the financial support of the *Conselho Nacional de Pesquisa e Desenvolvimento Científico* (CNPq), the Natural Sciences and Engineering Research Council of Canada (NSERC), and the *Fonds de Recherche du Québec – Nature et Technologies* (FRQNT), and the *Centre d'Études Interuniversitaires des Structures sous Charges Extrêmes* (CEISCE). Computational resources for this work were provided by Compute Canada and *Calcul Québec*. I would also like to acknowledge the support provided by the *Ministère des Transports du Québec* with the required data on the case-study structure.

Finally, I would like to express my gratefulness to all my family and friends. My experience in Sherbrooke would not be as pleasant and colorful without Guilherme, Livia, Franciele, Ayo, Romain, Teura, Matthieu, Luca, François, Claire, Azenor, Renaud, Marc-Antoine, and Élyse. I have also been inspired by friends who are far: Pedro, Raquel, Gabriel, Rabelo, Augusto, Giul, Xuxo, Elisa, Pedrinho, Michel, Damaris, Fernando, and Marcelo. I want to express all my gratitude to my wife and friend Geneviève for her love and unconditional support since we first met. She has been a great source of motivation, particularly during the past year. At last, but most importantly, I thank my parents Silvia and Luiz Antonio, and my brother Luiz Fernando, for all the encouragement during my whole life, and for being there whenever I needed despite the distance.

TABLE OF CONTENTS

LIST OF FIGURES

LIST OF TABLES

LIST OF SYMBOLS

a	Intercept of linear regression
b	Slope of linear regression
$f(\cdot)$	Probability density function
$f(\cdot\|\cdot)$	Posterior probability density function
f'_c	Concrete compressive strength
f_y	Steel yielding stress
$\hat{f}(\mathbf{x})$	Surrogate model with predictors $\mathbf{x}$
$F(\cdot)$	Cumulative distribution function
$\hat{F}(\cdot)$	Empirical cumulative distribution function
g	Gravity acceleration
G	Shear modulus
$G(\cdot\|\cdot)$	Conditional complementary cumulative distribution function
IM_i	Conditioned intensity measure
IM_j	Conditioning intensity measure
K_{eff}	Effective lateral stiffness
K_1	Initial lateral stiffness
K_2	Post-activation lateral stiffness
$L_{n,\alpha}$	Lilliefors critical statistics for n samples in the significance level α
m_X	Median of random variable X
n	Number of observed data points
N	Total number of samples
p	Number of parameters
$\mathbf{P}$	Vector of predictors
p_i	i^{th} predictor
p_f	Probability of collapse or damage state exceedance
$s(x)$	Sample standard deviation of random variable X
$S_a(T)$	(Pseudo) Spectral acceleration at natural period T
$S_a(T_1)$	(Pseudo) Spectral acceleration at the fundamental period T_1
$S_{a,Avg}$	Average spectral acceleration over a range of periods
T	Natural vibration period
T_1	Fundamental vibration period
W	Seismic weight
$\bar{x}$	Sample mean of random variable X
$\mathbf{X}$	Multivariate random variable
z	Number of collapse or damage state exceedance cases
z_X	Standard score of random variable X
β	Regression coefficient
δ	Drift ratio
Δ	Displacement or deformation
ε	Normally distributed error
ε_j	Residual of intensity measure in terms of standard deviation

ε_c	Concrete compressive strain
ε_{cu}	Concrete crushing compressive strain
ε_{st}	Steel strain
ε_y	Steel yielding strain
γ	Shear strain
λ_X	Logarithmic of median or random variable X
$\lambda(\cdot)$	Mean annual frequency of exceedance
μ_X	Mean of random variable X
μ_Δ	Displacement ductility
$\boldsymbol{\mu}_k$	Mean vector of cluster k
$\Phi(\cdot)$	Standard normal cumulative distribution function
π_k	Mixture proportion of cluster k
$\boldsymbol{\Psi}$	Vector of hyperparameters of Gaussian mixture model
ρ_t	Transverse reinforcement ratio
ρ_{XY}	Pearson correlation coefficient between X and Y
σ	Standard deviation
$\boldsymbol{\Sigma}_k$	Covariance matrix of cluster k
θ	Temperature
$\bar{\theta}_{daily}$	Mean daily temperature
$\boldsymbol{\Theta}$	Set of fragility function parameters
ξ_{eff}	Effective damping ratio
ζ_X	Dispersion of random variable X
$\mathcal{F}$	Collapse or damage state exceedance event
$\mathcal{L}(\cdot)$	Likelihood

LIST OF ACRONYMS

3D	Three-dimensional
AASHTO	American association of state highway and transportation officials
BIC	Bayesian information criterion
CCDF	Complementary cumulative distribution function
CDF	Cumulative distribution function
CHBDC	Canadian highway bridge design code
CID	Climate identifier
CGC	*Commission géologique du Canada*
CRGP	*Centre de recherche en génie parasismique et en dynamique des structures*
CS	Conditional spectrum
CSA	Canadian standards association
CSUS	Central and southeastern United States
DS	Damage state
DV	Decision variable
ECDF	Empirical cumulative distribution function
EDC	Energy dissipated per cycle
EDP	Engineering demand parameter
EM	Expectation-maximization
GCIM	generalized conditional intensity measure
GM	Gaussian mixture
GMM	Ground motion model
GMSDM	Gaussian mixture seismic demand model
GSC	Geological survey of Canada
HAZUS	Hazard U.S.
HDRB	High-damping rubber bearing
IDA	Incremental dynamic analysis
IM	Intensity measure
K-S	Kolmogorov-Smirnov
LR	Logistic regression
MAF	Mean annual frequency
MSA	Multiple-stripe analysis
MSC	Multi-span continuous
ML	Machine learning
NBCC	National building code of Canada
NGA-E	Next generation attenuation model – East
NGA-W2	Next generation attenuation model – West-2
NRB	Natural rubber bearing
NRC	Natural resources Canada
OpenSees	Open system for earthquake engineering simulation
OQ	OpenQuake
PBEE	Performance-based earthquake engineering

PBSD	Performance-based seismic design
PDF	Probability density function
PEER	Pacific earthquake engineering research center
PGA	Peak ground acceleration
PGV	Peak ground velocity
PSD	Probabilistic seismic demand
PSDM	Probabilistic seismic demand model
PSHA	Probabilistic seismic hazard analysis
RC	Reinforced concrete
RF	Random forest
RHA	Response history analysis
SVM	Support vector machines
UdeS	Université de Sherbrooke
UHS	Uniform hazard spectrum

CHAPTER 1

INTRODUCTION

1.1 Problem description and background

Beyond life and economic losses caused by strong earthquakes, the traffic interruption due to the lower serviceability of a damaged bridge may have substantial social and financial consequences to a country or a region on the aftermath of a seismic event. Past earthquakes caused the collapse of, or severe damage to, numerous major bridges, even to those that were at least nominally engineered to resist earthquakes, corresponding to life losses, service disruption, and major repairing cost [214, 181]. As a result of the post-event experiences allied to theoretical and experimental studies, the knowledge on the seismic behavior of structures and their design has evolved significantly in the last decades. One outcome of this evolution is performance-based earthquake engineering (PBEE), a design process that attempts to rationally and scientifically link decision-making for asset design with seismic input, facility response, and potential facility damage, based on proper consideration of uncertainties. The main purpose of PBEE is to build structures with predictable seismic performance, promoting optimized designs to fulfill the performance criteria resulting in efficiency of time and cost [73, 182]. And seismic fragility analysis has proven to be a valuable tool for performance assessment of structures, playing a central role in PBEE [185, 20].

Seismic fragility is a term employed by the earthquake engineering community to express a structure's susceptibility to damage caused by earthquakes. Typically depicted as fragility curves, this analysis has evolved from empirical approaches (subject to expert judgment) to current analytical formulations conditioned on multiple system parameters [110]. Numerous examples of application are found in the literature, from structure-specific [86, 251] to portfolios cases [198, 207, 250, 243]; with simple formulations using linear regression [199] to more complex ones employing statistical learning techniques to establish probabilistic relationships between system parameters and responses and to assess the importance of each parameter [85, 168]. Furthermore, as performance criteria relate damage limit states with sought structural functionality; for multi-component structures, such as highway bridges, damage limit states are formulated at two levels: component and system. More specifically, components are assessed for damage and corresponding repair costs or repair times are estimated; whereas the system level addresses the overall performance of

the bridge as a whole—in terms of lane closures, allowed axle loads, and speed limits—in a post-earthquake scenario. Therefore, methodologies that rationally account for the uncertainty on the seismic demand and on the interaction between bridge components are crucial in the assessment of the system seismic fragility. Traditional methodologies rely on simplifying assumptions, which have been verified mainly for multistory buildings, while their validity for bridge-type structures should still be explored.

Fragility analysis has been broadly used in the assessment of the vulnerability of regional structure portfolios (e.g., bridges [198, 30] and ports [171]), rehabilitation prioritization [205], and restoration plans [42, 131, 132]. In effect, due to the particularities of the construction systems used and the characteristics of the seismicity of the different regions, it is essential to perform a seismic risk analysis for the structures belonging to a specific region. The province of Quebec, Canada, counts with more than 2 600 multi-span bridges in its road network, of which 75% are more than 35 years old [248]. Given their advanced age and the lack of seismic detailing, these bridges may be vulnerable to future earthquake events. Aiming to prevent a disruption of the transportation network in Quebec and to contribute on a retrofitting prioritization plan, these provincial bridges had their seismic fragility assessed. Accordingly, high susceptibility to extensive damage and consequential service disruption were identified for most bridge classes in as-built configuration for a likely future earthquake [248, 251]. While using natural rubber bearing (NRB) seismic isolators to retrofit the bridge inventory in the province has shown to be potentially effective in reducing the seismic fragility in nominal conditions [245, 243], in regions with severely cold winters, this rehabilitation measure requires the consideration of concomitant events of earthquake loading and thermal stiffening due to subfreezing temperatures [57].

Ideally, the problem of quantifying the impact of low temperatures on the seismic performance of isolated bridges should be probabilistic [118]. Accordingly, a few recent studies used probability-based frameworks to investigate this phenomenon [190, 40, 98]. Limitations of these studies rely on the adoption of either oversimplified numerical models, neglecting the interaction between the multiple bridge component, or limited assumptions on the damage states of isolators. With contemporary computational resources and data availability, machine-learning (ML) techniques have become popular in the earthquake engineering community, providing powerful statistical tools to better handle uncertainty [224, 265]. Consequently, refined density modeling techniques for probabilistic seismic demand modeling can be developed. In addition, classification-based parameterized fragility functions can readily estimate the performance of structures conditional on the occurrence of concurrent events. Therefore, an efficient framework is envisioned to assess the

impact of severe winter conditions on the seismic response of retrofitted bridges with NRB isolators.

1.2 Objectives

This study is part of one of the research axes of the *Centre de recherche en génie parasismique et en dynamique des structures* (CRGP – Earthquake engineering and structural dynamics research center) at the Université de Sherbrooke (UdeS) on the evaluation of the seismic vulnerability of infrastructures in Canada. Several previous projects performed by the CRGP employed methodologies for using fragility curves for structural performance assessment mainly in the area of bridges [248, 251, 245, 243, 103, 280], concrete gravity dams [39, 38, 230, 231], and masonry walls [147]. In a continuous effort to contribute to the science and practice of earthquake hazard mitigation, the general objective of this research is to use a probabilistic framework to further improve the understanding of the performance assessment of typical highway bridges retrofitted with natural rubber isolators when subjected combined hazards of seismic and cold weather environment.

To achieve the overarching research objective, the following specific objectives are further detailed:

1. to update and parameterize the finite element model of the case-study bridge to consider variations in mechanical properties and geometry;
2. to characterize the seismic hazard at the bridge by performing a probabilistic seismic hazard analysis based on the most recent ground motion models and seismic hazard developments in Canada;
3. to select ground motion records that are consistent with the characterized seismic hazard using the generalized conditional intensity measure approach;
4. to incorporate the recent findings in capacity modeling of bridge columns and seismic isolators in accordance to the performance criteria defined in the 2014 edition of the Canadian highway bridge design code CSA S6-14 [57];
5. to explore the validity of traditional hypotheses used by probabilistic seismic demand modeling approaches for multicomponent structures and their potential bias propagated into the system fragility;
6. to conceive the isolation system based on natural rubber seismic isolators for the case-study bridge in accordance to the CSA S6-14 performance criteria;
7. to collect climate data at the bridge site to represent the expected thermal stiffening effects on natural rubber isolators; and

8. to leverage the features of parameterized seismic fragility functions to assess the performance of the case-study bridge in its retrofitted configuration with natural rubber bearings under concomitant earthquake loadings and thermal effects, considering both component- and system-level fragilities.

This study focuses on a specific case-study structure. The Chemin des Dalles overpass is a three-span continuous concrete girder bridge located over highway 55 near Trois-Rivières in Quebec, Eastern Canada (Figure 1.1). This bridge was designed in 1975 and built in 1979. The seismic detailing of the bent columns might be classified as deficient when compared to current criteria found in the CSA S6-14. Further details on the case-study bridge geometry and numerical model are found in Chapters 3 and 4 for its as-built and isolated configurations, respectively. This structure has been extensively studied by the CRGP, and information has been gathered on ambient vibration data, soil condition, component capacity, and finite element modeling [221, 251, 244, 280]. Furthermore, this bridge presents numerous similarities to the average bridge in Quebec defined by Tavares [250], as further detailed in Appendix A.

1.3 Research contribution

As advancements in other fields of seismic hazard mitigation are made, their integration into the science of earthquake engineering becomes mandatory. In 2015, the Geological Survey of Canada (GSC) published the fifth generation of seismic hazard models of Canada, the first fully probabilistic generation in the country [1]. This means that these seismic hazard models are completely based on probabilistic seismic hazard analysis (PSHA). Allied to the refined outcomes of PSHA, hazard consistent ground record selection methods—e.g., the conditional spectrum (CS) approach [25, 21, 125, 27] and its generalization, the generalized conditional intensity measure (GCIM) approach [43, 45]—have become more accessible. A methodology coupling the results from PSHA and record selection based on GCIM has already lead to less conservative fragility functions for a concrete gravity dam in eastern Canada [230], whilst the outcomes of its application to highway bridges are explored in the present work. This rigorous ground motion record selection enables an optimal and consistent propagation of record-to-record variability, which in turn facilitates a refined assessment of the uncertainty on the seismic demand of multicomponent structures.

At the time that risk-based methods become more mainstream yet critics remain regarding the uncertainties present in risk estimates. And as both fundamental knowledge and computing power increase, opportunities to improve uncertainty estimation are identified. A novel approach is proposed to model the joint density of the seismic demand for multicom-

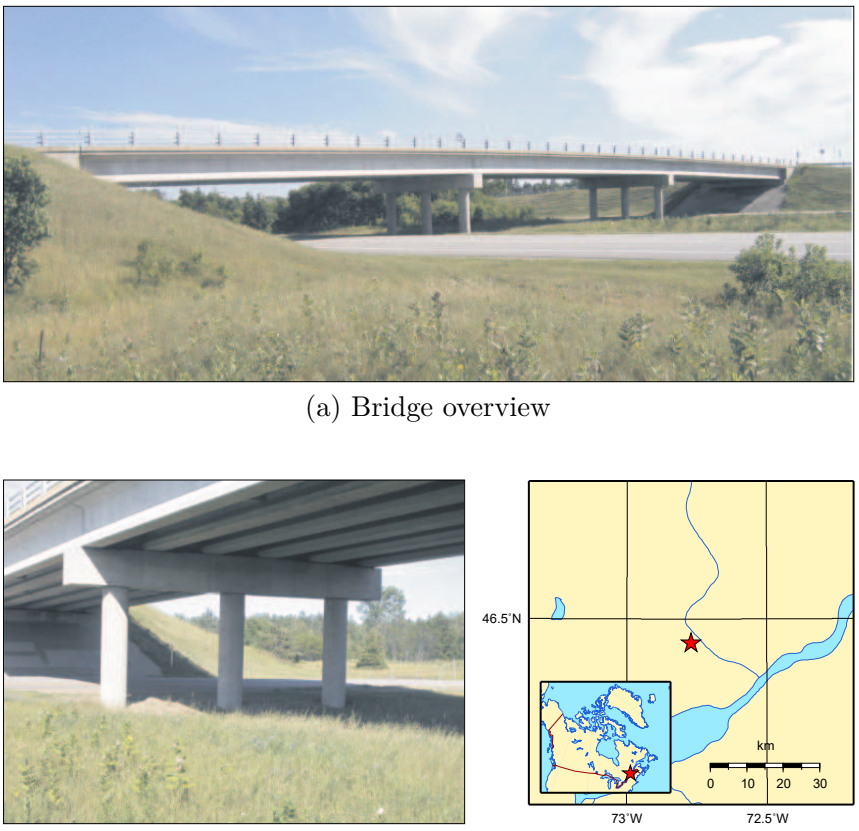

(a) Bridge overview

(b) Bent detail

(c) Bridge location

Figure 1.1 Chemin des Dalles overpass over highway 55 in Quebec, Eastern Canada (photography credits to Roy [220]; map generated by the GSC Hazard Calculator [193])

ponent structures, which profits from the stratified structure of demand data generated according to multiple-stripe analysis (MSA) [124], and the refined density modeling of Gaussian mixtures. The proposed methodology is thus eminently flexible in terms of adopted assumptions and it is leveraged to assess the potential bias introduced in fragility analysis caused by restrictive assumptions found in traditional probabilistic seismic demand modeling.

The proposed approach is then used within a probabilistic framework to assess the impact of thermal stiffening of natural rubber isolators on the performance of a retrofitted bridge in severe winter conditions. A holistic understanding of the bridge seismic performance under the effects of cold weather temperatures is provided considering the correlation of the seismic demand of the case-study bridge critical components, and the individual contribution of these components to the fragility of the whole system. To this end, parameterized fragility functions conditioned on seismic intensity and air temperature are developed for the first time in the performance assessment of an isolated bridge in cold regions. The

global aspect of this study provides an insightful example on how combining isolators and lateral restraining structures may be beneficial for the bridge performance at subfreezing temperatures.

Finally, this study is focused on a single case-study bridge that has been extensively studied (e.g., previous studies gathered relevant information on this structure and comprehensive data is available on its structural and dynamic properties, capacity, site conditions, and numerical model). Besides the relevant information acquired by the past studies, its significance with respect to the regional bridge inventory should be understood. Indeed, multi-span continuous (MSC) concrete bridges, such as the Chemin des Dalles bridge, are the second most important class in Quebec, representing 21% of the multi-span bridge inventory, behind simply supported concrete bridges (25%) and followed by continuous thick slab bridges (11%) [250]. The case-study bridge is also similar to the average bridge in Quebec [248] (see details in the Appendix A), defined to represent a typical bridge in the region. Therefore, the case-study bridge is a real structure that is chosen to demonstrate an application of the adopted framework rather than using a hypothetical case study. The conclusions from this study can, thus, provide meaningful insights on the seismic performance of other typical bridges in the province.

1.4 Document outline

This thesis has a combined format and is composed of traditional chapters and two articles. Chapter 2 provides a state-of-the-art review on the seismic performance assessment of highway bridges. Chapter 3 (Article No. 1), the limitations of statistical tools commonly used in seismic fragility of bridges led to the development of a new probabilistic seismic demand model, which is described and applied to the case-study bridge. In Chapter 4 (Article No. 2), the performance of the retrofitted version of case-study bridge under concomitant events of earthquakes and low temperatures is assessed using fragility surfaces. Chapter 5 presents the main conclusions and recommendations for future work. As supplementary material, Appendix A details the average bridge in Quebec and its resemblance to the case-study bridge. The hazard characterization at the bridge site comprising seismic hazard and climate data is described in Appendix B. Appendix C presents the aspects of the seismic ground motion record selection algorithm, while the selected suites are further detailed in Appendix D. Finally, in Appendix E, a validation of the proposed probabilistic seismic modeling strategy is performed by comparing the resulting fragility estimates to bootstrap-based fragility curves. Numbered citations and alphabetical list of references are adopted.

1.5 Contexte de l'étude et problématique

Au-delà des pertes humaines et économiques causées par de forts tremblements de terre, l'interruption du trafic due à la moindre capacité de fonctionnement d'un pont endommagé peut avoir des conséquences sociales et financières importantes pour un pays ou une région à la suite d'un événement sismique. En effet, certains événements sismiques ont provoqué l'effondrement ou de graves dommages à de nombreux ponts importants (même à ceux qui étaient au moins nominalement conçus pour résister aux tremblements de terre), ce qui a entraîné des pertes de vies humaines, des interruptions de service et des coûts de réparation importants [214, 181]. Dues à l'expertise acquise à la suite de ces événements alliée aux études théoriques et expérimentales, les connaissances sur le comportement sismique des structures et leur conception ont considérablement évolué au cours des dernières décennies. L'un des résultats de cette évolution est le génie parasismique basé sur la performance (PBEE), un processus de conception qui tente de relier rationnellement et scientifiquement la prise de décision pour la conception des infrastructures avec les données sismiques, la réponse des installations et les dommages potentiels. L'objectif principal de la PBEE est de construire des structures dont la performance sismique est prévisible, en encourageant l'optimisation des conceptions pour répondre aux critères de performance, ce qui permet de gagner du temps et de réduire les coûts [73, 182]. L'analyse de fragilité sismique s'est avérée être un outil précieux pour l'évaluation de la performance des structures, jouant un rôle central dans l'évaluation des risques [185, 20].

La fragilité sismique est un terme employé par la communauté du génie parasismique pour exprimer la susceptibilité d'une structure aux dommages causés par les séismes. Généralement représentée sous forme de courbes de fragilité, cette analyse a évolué depuis des approches empiriques (soumises au jugement d'experts) jusqu'aux formulations analytiques actuelles conditionnées par de multiples paramètres du système [110]. On trouve de nombreux exemples d'application dans la littérature, depuis les cas de structures spécifiques [86, 251] jusqu'aux cas d'inventaires [198, 207, 250, 243] ; de formulations simples utilisant la régression linéaire [199] à des formulations plus complexes employant des techniques d'apprentissage statistique pour établir des relations probabilistes entre les paramètres du système et les réponses et pour évaluer l'importance de chaque paramètre [85, 168]. En outre, comme les critères de performance relient les états limites d'endommagement à la fonctionnalité structurelle requise, pour les structures à composants multiples, comme les ponts routiers, les états limites d'endommagement sont formulés à deux niveaux : composant (local) et système (global). Plus précisément, les composants sont évalués pour les dommages et les coûts de réparation correspondants ou les temps de réparation sont

estimés, tandis que le niveau système concerne la performance globale du pont dans son ensemble—en matière de fermetures de voies, de charges par essieu autorisées et de limites de vitesse—dans un scénario post-séisme. Par conséquent, les méthodologies qui tiennent compte de manière rationnelle de l'incertitude sur la demande sismique et sur l'interaction entre les composants du pont sont les plus critiques sont cruciales pour l'évaluation de la fragilité sismique du système. Les méthodologies traditionnelles s'appuient sur des hypothèses simplificatrices qui ont été vérifiées principalement pour des bâtiments multi-étagés, alors que leur validité pour les structures du type pont doit encore être explorée.

L'analyse de fragilité a été largement utilisée pour l'évaluation de la vulnérabilité des portfolios de structures régionales (e.g., pour les ponts [198, 30] et pour les ports [171]), de la priorisation de la réhabilitation [205] et des plans de restoration [42, 131, 132]. En effet, en raison des particularités des systèmes de construction utilisés et des caractéristiques de la sismicité des différentes régions, il est essentiel de réaliser une analyse du risque sismique pour les structures appartenant à une région spécifique. La province de Québec, au Canada, compte plus de 2 600 ponts à travées multiples dans son réseau routier, dont 75% ont plus de 35 ans [248]. Compte tenu de leur âge avancé et de l'absence de détails sismiques, ces ponts peuvent être vulnérables aux futurs séismes. Afin d'éviter une perturbation du réseau de transport au Québec et de contribuer à l'élaboration d'un plan de réhabilitation prioritaire, la fragilité sismique de ces ponts provinciaux a été évaluée [251]. En conséquence, une forte susceptibilité à des dommages importants et à une interruption de service conséquente a été identifiée pour la plupart des classes de ponts tels que construits pour un probable tremblement de terre futur. Bien que l'utilisation d'isolateurs sismiques en caoutchouc naturel (NRB) pour réhabiliter les ponts de la province se soit avérée potentiellement efficace pour réduire la fragilité sismique dans des conditions nominales [245, 243], dans les régions où les hivers sont très froids, cette mesure de réhabilitation nécessite la prise en compte des événements concomitants de la charge sismique et du raidissement thermique des isolateurs dû aux températures inférieures au point de congélation [57].

Idéalement, l'étude de la quantification de l'impact des basses températures sur la performance sismique des ponts isolés devrait être probabiliste [118]. En conséquence, quelques études récentes ont utilisé des cadres basés sur les probabilités pour étudier ce phénomène [190, 40, 98]. Les limites de ces études reposent sur l'adoption de l'adoption de modèles numériques trop simplifiés, négligeant l'interaction entre les multiples composants du pont, ou d'hypothèses limitées sur l'endommagement des ponts. ou d'hypothèses limitées sur les états d'endommagement des isolateurs. Avec les ressources de calcul ressources

informatiques et la disponibilité des données, les techniques d'apprentissage automatique (ML) sont devenues populaires dans la communauté du génie parasismique, fournissant des outils statistiques puissants pour mieux gérer l'incertitude [224, 265]. Par conséquent, des techniques raffinées de modélisation probabiliste de la demande sismique peuvent être développées. De plus, les fonctions de fragilité paramétrées basées sur la classification peuvent facilement estimer la performance des structures en fonction de l'occurrence d'événements simultanés. Par conséquent, une méthodologie efficace est envisagée pour évaluer l'impact des conditions hivernales sévères sur la réponse sismique des ponts modernisés avec des isolateurs NRB.

1.6 Objectifs

Cette étude s'inscrit dans l'un des axes de recherche du Centre de recherche en génie parasismique et en dynamique des structures (CRGP) sur l'évaluation de la vulnérabilité sismique des infrastructures au Canada. Plusieurs projets antérieurs réalisés par le CRGP ont employé des courbes de fragilité pour l'évaluation de la performance des structures, surtout dans le domaine des ponts [248, 251, 245, 243, 103, 280], des barrages-poids en béton [39, 38, 230, 231], et des murs en maçonnerie [147]. Dans un effort continu pour contribuer à la science et à la pratique de l'atténuation des risques sismiques, l'objectif général de cette recherche est d'utiliser une méthodologie probabiliste pour améliorer davantage l'évaluation de la performance sismique des ponts routiers typiques réhabilités avec des isolateurs en caoutchouc naturel dans un environnement à basse température.

Pour atteindre l'objectif principal de la recherche, les objectifs spécifiques suivants sont détaillés :

1. mettre à jour et paramétrer le modèle par éléments finis du pont de l'étude de cas afin de prendre en compte les variations des propriétés mécaniques et de la géométrie;

2. caractériser l'aléa sismique au niveau du pont en effectuant une analyse probabiliste de l'aléa sismique basée sur les modèles de mouvement du sol les plus récents et les développements de l'aléa sismique au Canada ;

3. sélectionner les accélérogrammes cohérents avec l'aléa sismique caractérisé en utilisant l'approche de la mesure d'intensité conditionnelle généralisée (GCIM) ;

4. intégrer les résultats récents de la modélisation de la capacité des colonnes de pont et des isolateurs sismiques conformément aux critères de performance définis par l'édition 2014 du code canadien sur le calcul des ponts routiers CSA S6-14 [57] ;

5. d'explorer la validité des hypothèses traditionnelles utilisées par les approches de modélisation probabiliste de la demande sismique pour les composants multiples et leur biais potentiel propagé dans la fragilité du système ;
6. concevoir un système d'isolation basé sur des isolateurs sismiques en caoutchouc naturel pour le pont de l'étude de cas, conformément aux critères de performance du code CSA S6-14;
7. recueillir des données climatiques sur le site du pont afin de représenter les effets attendus du raidissement thermique sur les isolateurs en caoutchouc naturel; et
8. exploiter les caractéristiques des fonctions de fragilité sismique paramétrées pour évaluer la performance du pont de l'étude de cas dans sa configuration réhabilitée avec des appuis en caoutchouc naturel sous des charges sismiques et des effets thermiques concomitants, en tenant compte à la fois de la les fragilités au niveau des composants et du système.

Cette étude se concentre sur l'étude de cas d'une structure spécifique. Le pont du Chemin des Dalles est un pont à poutres continues en béton à trois travées situé au-dessus de l'autoroute 55 près de Trois-Rivières, au Québec, dans l'est du Canada (Figure 1.2). Ce pont a été conçu en 1975 et construit en 1979. Les détails sismiques des colonnes courbées pourraient être classés comme déficients par rapport aux critères actuels du code CSA S6-14. Plus d'amples détails sur la géométrie et le modèle numérique du pont de l'étude de cas se trouvent dans les chapitres 3 et 4 pour les configurations telle que construite et isolée, respectivement. Cette structure a été étudiée en profondeur par le CRGP, et des informations ont été recueillies sur les données de vibrations ambiantes, l'état du sol, la capacité des composants et la modélisation par éléments finis [221, 251, 244, 280]. En outre, ce pont présente plusieurs ressemblances avec le pont moyen du Québec défini par Tavares [250], tel que détaillé dans l'annexe A.

1.7 Contribution de la recherche

À mesure que des progrès sont réalisés dans d'autres domaines de l'atténuation des risques sismiques, leur intégration dans la science du génie parasismique devient obligatoire. En 2015, la Commission géologique du Canada (CGC) a publié la cinquième génération de modèles d'aléas sismiques du Canada, la première génération entièrement probabiliste du pays [1]. Cela signifie que ces modèles sont entièrement basés sur l'analyse probabiliste d'aléa sismique (PSHA). Parallèlement aux résultats raffinés de la PSHA, des méthodes de sélection d'accélérogrammes cohérents avec l'aléa—par exemple, l'approche du spectre conditionnel (CS) [25, 21, 125, 27] et sa généralisation, l'approche de la mesure de l'intensité conditionnelle généralisée (GCIM) [43, 45]—sont devenues plus accessibles.

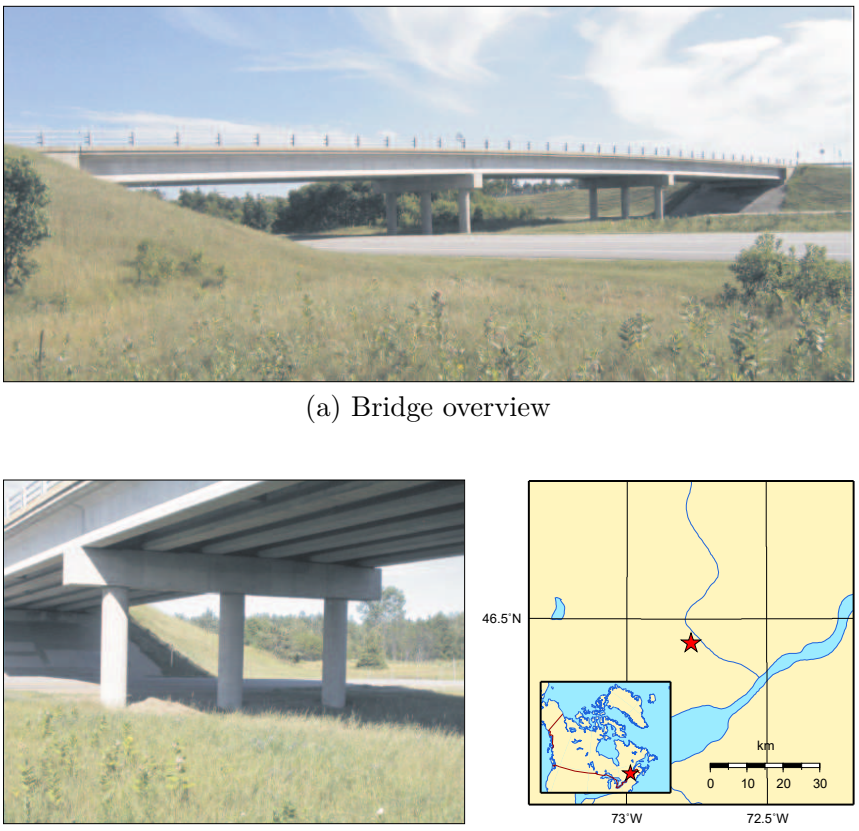

(a) Bridge overview

(b) Bent detail

(c) Bridge location

Figure 1.2 Pont du Chemin des Dalles au-dessus de l'autoroute 55 au Québec, dans l'est du Canada (crédits photographiques à Roy [220] ; carte générée par le calculatrice d'aléa sismique de la CGC [193])

Une méthodologie couplant les résultats de PSHA et la sélection d'enregistrements de mouvement du sol basée sur la méthode GCIM a déjà conduit à des fonctions de fragilité moins conservatrices pour un barrage-poids en béton dans l'est du Canada [230], tandis que les résultats de son application aux ponts routiers sont explorés dans le présent travail. Cette sélection rigoureuse d'accélérogrammes permet une propagation optimale et cohérente de la variabilité d'un enregistrement à l'autre. Cela facilite une évaluation raffinée de l'incertitude sur la demande sismique dans les structures multicomposantes.

Alors que les méthodes basées sur le risque deviennent plus courantes, des critiques subsistent quant aux incertitudes présentes dans les estimations du risque sismique. Alors que les connaissances fondamentales et la puissance de calcul, des circonstances opportunes sont identifiées à améliorer l'estimation d'incertitudes. Une nouvelle approche est proposée pour modéliser la densité conjointe de la demande sismique des structures multicomposantes, qui bénéficie de la structure en bandes des données de demande générées selon l'analyse à bandes multiples (MSA) [124], et de la modélisation raffinée de la densité

des mélanges gaussiens. La méthodologie proposée est donc éminemment flexible en termes d'hypothèses adoptées et elle est utilisée pour évaluer le biais potentiel introduit dans les calculs de fragilité causé par les hypothèses restrictives trouvées dans les méthodologies plus traditionnelles.

L'approche proposée est ensuite utilisée dans un cadre probabiliste pour évaluer l'impact du raidissement thermique des isolateurs en caoutchouc naturel sur la performance d'un pont réhabilité dans des conditions hivernales sévères. Une compréhension holistique de la performance sismique du pont sous les effets des températures froides est fournie en tenant compte de la corrélation de la demande sismique des composants critiques du pont étudiés, et la contribution individuelle de ces composants à la fragilité de l'ensemble du système. À cette fin, des fonctions de fragilité paramétrées conditionnées par l'intensité sismique et la température développées pour la première fois dans l'évaluation de la performance d'un pont isolé en région froide. L'aspect global de cette étude fournit un exemple perspicace sur la façon dont la combinaison d'isolateurs et de structures de retenue latérale peut être bénéfique pour la performance d'un pont réhabilité à des températures inférieures au point de congélation.

Enfin, cette étude se concentre sur un seul cas de pont ayant fait l'objet d'études approfondies. Par exemple, des études antérieures ont rassemblé des informations pertinentes sur cette structure et des données complètes sont disponibles sur les propriétés structurelles et dynamiques, la capacité des composants, les conditions du site et le modèle numérique. Outre les informations pertinentes acquises par les études antérieures, son importance par rapport à l'inventaire régional des ponts doit être comprise. En effet, des ponts continus en béton à travées multiples (MSC), tel que le pont du Chemin des Dalles, constituent la deuxième catégorie la plus importante au Québec. Ils représentent 21% de l'inventaire provincial des ponts à travées multiples, après les ponts en béton simplement appuyés (25%) et les ponts à dalles épaisses continues (11%) [250]. En plus, le pont de l'étude de cas est semblable au pont moyen du Québec [248] (voir les détails dans l'annexe A) défini pour représenter un pont typique de la région. Par conséquent, le pont du Chemin des Dalles est une structure réelle qui est choisie pour présenter une application du cadre adopté plutôt que d'utiliser une structure hypothétique. Les conclusions de cette étude peuvent donc fournir des indications significatives sur la performance sismique d'autres ponts typiques de la province.

1.8 Structure du document

Cette thèse a un format combiné et est composée de chapitres traditionnels et de deux articles. Le chapitre 2 présente l'état-de-l'art de évaluation de la performance sismique des ponts routiers. Dans le chapitre 3 (Article No. 1), les limitations des outils statistiques trouvées dans les méthodes traditionnelles utilisées dans l'évaluation de la performance sismique conduisent à l'élaboration d'un nouveau modèle probabiliste de la demande sismique. Cette nouvelle approche est décrite et appliquée au pont de l'étude de cas dans sa configuration telle que construite. Dans le chapitre 4 (Article No. 2), une application de l'approche PSDM proposée, combinée aux données climatiques et à la modélisation de la rigidité thermique du caoutchouc, est utilisée pour évaluer la performance du pont isolé sous les événements concomitants d'un tremblement de terre et de températures extrêmement basses en utilisant des fonctions de fragilité paramétrées. Le chapitre 5 présente les principales conclusions et recommandations pour les travaux futurs. En tant que matériel supplémentaire, l'annexe A détaille le pont moyen au Québec et sa ressemblance avec le pont de l'étude de cas. La caractérisation de l'aléa sur l'endroit du pont, comprenant des données sur l'aléa sismique et le climat, est décrite en annexe B. L'annexe C présente les aspects de l'algorithme de sélection de sismique, tandis que les suites sélectionnées sont détaillées dans l'annexe D. Enfin, dans l'annexe E, on conduit la validation de la stratégie proposée pour la modélisation sismique probabiliste en comparant les courbes de fragilité résultantes aux courbes de fragilité basées sur l'approche *bootstrap*. On adopte les citations numérotées et la liste alphabétique des références.

CHAPTER 2

PROBABILISTIC SEISMIC PERFORMANCE ASSESSMENT OF HIGHWAY BRIDGES

The state-of-the-art presented here is based on a comprehensive literature review focused on the loads and expected damage to bridge components during an earthquake, the seismic performance criteria for bridges, the probabilistic seismic risk assessment involving fragility analysis, the development of analytical fragility functions, and the performance enhancement through retrofitting with laminated-rubber isolators. The analytical framework for fragility analysis is further detailed with respect to the construction of the probabilistic relationship between structural response and seismic excitation, the definition of fragility according to structural reliability theory, and the construction of fragility functions. Although this literature review is focused on the seismic performance assessment of highway bridges, the exposed concepts and tools for seismic risk analysis are not limited to bridges, and other types of structures are discussed when convenient.

2.1 Expected loads, damage, and failure modes

Bridges are structures that provide a roadway or walkway to overcome an obstacle. Such structures are expected to withstand construction, permanent, transitory, and exceptional loads during their design life, and are essential for the transportation of people and goods through a country's road network. Some seismic events, such as the 1989 Loma Pietra (U.S.), the 1994 Northridge (U.S.), the 1995 Kobe (Japan), and the 2010 Maule (Chile) have caused the collapse of, or severe damage to, numerous major bridges, even to those that were at least nominally engineered to resist earthquakes [214, 181]. To be able to effectively design either new bridges or retrofit measures for existing bridges, a clear understanding of potential problem areas is essential. There is no better way of developing this understanding than by a systematic examination and categorization of failures and damage that have occurred to bridges in earlier earthquakes [214].

During seismic events, bridges are subjected to gravity and earthquake loads. Earthquakes lead to vertical and horizontal ground motions that can result in the failure of bridge components. The horizontal components of the ground motion contribute mainly to the flexural damage to columns or piers, and to the deck misalignment and falling off the supports. The vertical ground motion causes significant fluctuating axial forces in columns

or piers, which may induce outward buckling or crushing [209]. It can also result in significant amplification of the bending moment in the mid-span, which may lead to the bending failure of the deck. Moreover, both vertical and horizontal ground motions may cause the liquefaction of the soil at the bridge foundations, resulting in structural collapse due to the loss of load-carrying capacity of the foundation [79].

Seismic-induced failures of bridges are mostly related to supports (abutments, piles, and columns), decks, and bearings. Even though the deck is expected to remain elastic, in simply supported bridges, either single-span or multi-span, it can fall off or slide away from the supports (unseating) due to large horizontal ground motions. The oblique impact of skewed bridges tends to make the deck rotate in the horizontal plane, resulting in unseating at the acute corners [214, 79]. The deck can also experience impact between adjacent spans and between the end span and the abutment (pounding), as a result of large horizontal movements. Such impact can lead to failure of rocker bearings in the form of toppling, shear failure of the steel bearings, and the failure of the abutment back-walls. The presence of soft soil and incompletely consolidated abutment fill has led to slumping of the fill and abutment rotation, consequently causing the failure of back wall and pile support. Finally, bridge columns tend to fail in three modes, i.e., flexural failure, shear failure, and crushing failure [214, 79]. Modern design codes, however, prevent shear failure to happen in columns, allowing only the flexural type [216]. For reinforced concrete bridges, observed weaknesses are summarized in Table 2.1.

2.2 Seismic performance of bridges

As described earlier, important seismic events occurred in the 1990 decade and later caused an amount of damage, economic loss due to downtime and repair cost that were perceived as unacceptably high by the structural engineering community. Motivated by this perception, the first generation of performance-based earthquake engineering (PBEE) was established by the beginning of the current century [114]. The main objective of PBEE is to introduce a design framework which results in the sought system performances at various intensity levels of seismic hazard, giving more control over the loss in the case of an extreme event and removing unnecessary conservatism. A comprehensive literature review on the worldwide application of performance-based seismic design (PBSD) is given by Tavares [250], whilst a survey on state departments of transportation in the U.S. was conducted by the Transportation Research Board resulted in the summary of the current state of knowledge and practice for PBSD [253]. The main advantages of PBSD are [188]:

– more control over the loss in case of an extreme event, since the choice of the performance lies with the asset manager;

Table 2.1 Failure modes for bridge components [214, 92].

Structural component	Failure mode
Piers/Columns	– Flexural failures in plastic hinges with inadequate confinement – Shear failure in short single columns, piers, multi-columns bents, columns with flares, and other accidental restraints and columns in skewed bridges – Inappropriate location of lap splices in pier members, causing shear failures – Compressive failures of columns and piers with corresponding rebar buckling and stirrup openings and ruptures
Abutments	– Backfill settlement and erosion resulting in rotation of the abutment with damage to back wall and pile support.
Deck	– Pounding and unseating at hinge seats and girder supports
Foundation	– Uplifting and overturning of bridge foundations and piers with inadequate anchorage at the base – Footing failures caused by soil liquefaction and differential settlements – Pullout failure caused by inadequate development of column longitudinal reinforcement
Restrainers	– Overstressing of seismic restrainers leading to local failure
Bearings	– Slippage – Shear failure

– unnecessary conservatism is removed or reduced for some parameters and unidentified deficiencies are discovered for others;
– a more reliable structural design can be produced when compared to traditional prescriptive procedures.

2.2.1 First and second generation PBEE

Many codes and standards are globally moving towards a conception based on functional objectives of service and damage limits subject to explicit demonstration of the design meeting the performance criteria [253]. Even though the specified demand levels are different for each regulatory agency, the design levels are essentially the same (i.e., at the lower design level the structure should remain functional and at the higher design level the structure should avoid collapse) [276]. For instance, the 2014 edition of the Canadian highway bridge design code (CHBDC) CSA S6-14 [57] adopted the performance-based seismic design as the mandatory approach for the design of new bridges and for

the rehabilitation of existing bridges. The CHBDC's performance criteria establish the correlation amongst damage stage, service level, and prescribed probability demand levels (Figure 2.1). The intent of the importance categories is to provide owners and regulatory agencies with the necessary information to manage risk and prioritize their inventory to facilitate emergency response, economic recovery, and impact on available resources [56]. The performance criteria describe the service levels to be met according to the damage stage. The latter is translated by the following response parameters: bridge general behavior, concrete spalling, steel yielding, condition of connections, displacements, bearings and joints, restrainers, foundations, and seismic capacity for aftershocks, to name a few.

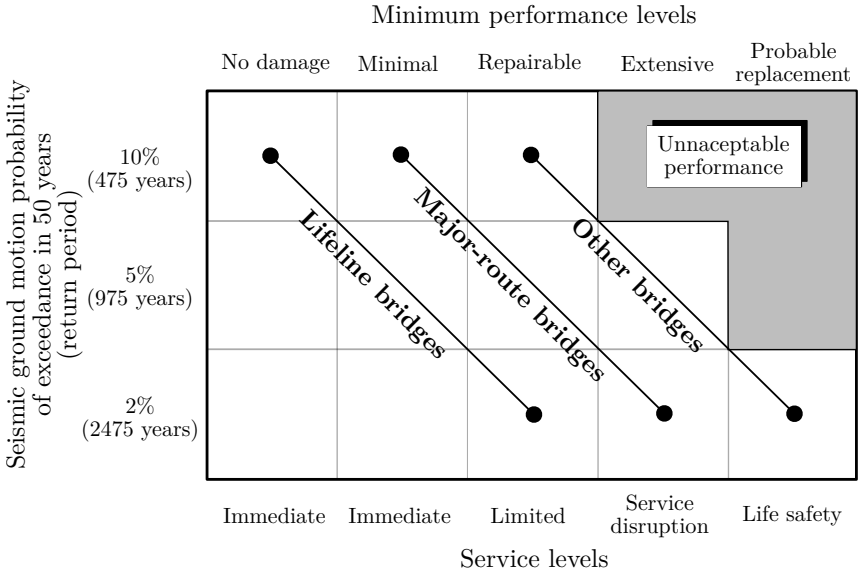

Figure 2.1 Performance-based seismic design in the CHBDC CSA S6-14 [57]

The performance criteria describe the service levels to be met according to the damage stage. The latter is translated by the following response parameters: bridge general behavior, concrete spalling, steel yielding, condition of connections, displacements, bearings and joints, restrainers, foundations, and seismic capacity for aftershocks, to name a few. Four service levels are presented in the CHBDC, namely immediate, limited, service disruption, and life safety; which are paired to respective damage states: minimal, repairable, extensive, and probable replacement. The damage states are qualitatively described in Table 2.2. It is important to notice that these definitions are similar to those classified as slight, moderate, extensive, and complete damage states by the Federal Emergency Management Agency's (FEMA) software Hazard U.S. – Multi-Hazard (HAZUS-MH) for bridges [93] (which have been extensively used in fragility analyses, as discussed in Section 2.2.3).

Table 2.2 General bridge damage states adapted from the CSA S6-14 [57]

Damage state	General damage description
Minimal	Bridge shall remain essentially elastic with minor damage that does not affect the performance level of the structure.
Repairable	There may be some inelastic behavior and moderate damage may occur; however, primary members shall not need to be replaced, shall be repairable in place, and shall be capable of supporting the dead plus full live load.
Extensive	Inelastic behavior is expected. Members might have extensive visible damage, such as spalling of concrete and buckling of braces but strength degradation shall not occur. Members shall be capable of supporting the dead plus 50% live loads, excluding impacts, including P-delta effects, without collapse.
Probable replacement	Bridge spans shall remain in place but the bridge might be unusable and might have to be extensively repaired or replaced. Extensive distortion of beams and column panels might occur. Fractures at moment connections might occur but shear connections shall remain intact. Members shall be capable of supporting the dead plus 30% live loads, excluding impacts, but including P-delta effects, without collapse.

These damage stage are related to such qualitative as quantitative response parameters, e.g., strains, drifts, cracks, yielding, from minimum damage to probable replacement. The service level is referred to the bridge post-earthquake degree of functionality, from immediate use to life safety. Table 2.3 summarizes the minimum performance requirements for each bridge importance category demanded by the CHBDC in terms of engineering quantities.

Table 2.3 Performance criteria adapted from the CSA S6-14 [57].

Damage state	Criteria
Minimum	Concrete compressive strains (ε_c) $\leq$ 0.004 and steel strains (ε_{st}) $\leq$ yield strain (ε_y)
Repairable	Steel strains (ε_{st}) $\leq$ 0.015
Extensive	Confined core concrete strain (ε_{cc}) $\leq$ concrete crushing strain (ε_{cu}). Steel strains $\leq$ 0.05
Probable replacement	Bridge spans shall remain in place but the bridge may be unusable and may have to be extensively repaired or replaced

Performance-based earthquake engineering, when implement at the highest level, should be comprehensive in consideration of the uncertainties related to the seismic hazard and its outcomes on facilities. The PBSD framework of the CSA S6-14 is, therefore, deterministic, in accordance to the first generation PBEE, in which design objectives relate

intensity levels of seismic hazard to target performance criteria and do not possess probability distributions [114]. This approach incorporates no uncertainty propagation, instead introducing any probability or safety at the input intensity and expecting it to be naturally propagated to the output response. Therefore, they are not risk consistent and, although, they may have appeared in the literature as performance-based, by the current understanding of PBEE, they are not: there is no hazard curve and no uncertainty propagation, thus no proper probabilistic implementation [255].

Considering the shortcomings of the first-generation procedures, a more robust PBEE methodology was proposed in the Pacific Earthquake Engineering Research (PEER) Center by Cornell and Krawinkler [73]. A key feature of the PEER PBEE methodology is the calculation of performance in a rigorous probabilistic manner without relying on expert opinion. Accordingly, uncertainties in earthquake intensity, ground motion characteristics, structural response, physical damage, and economic and human losses are explicitly considered in the method. The entire PEER PBEE methodology is summarized by applying the total probability theorem, as it assesses the structural performance in terms of the mean annual frequency of decision variables (DV), such as casualties, monetary loss, and down time. This estimation is computed using, continuous damage measures (DM) or discrete damage states (DS), which are defined based on appropriate engineering demand parameters (EDP), associated with seismic ground motions at a range of intensity measure (IM) levels:

$$\lambda(\mathrm{DV}) = \int_{\mathrm{DS}} \int_{\mathrm{EDP}} \int_{\mathrm{IM}} G(\mathrm{DV}|\mathrm{DS}) \,|\, \mathrm{d}G(\mathrm{DS}|\mathrm{EDP})| \,|\, \mathrm{d}G(\mathrm{EDP}|\mathrm{IM})| \,|\, \mathrm{d}\lambda(\mathrm{IM})| \tag{2.1}$$

where $G(X|Y) = \Pr(X > x|Y = y)$ is the conditional complementary cumulative distribution function (CCDF) of a random variable X exceeding a certain value x given the occurrence of another random variable $Y = y$ [78]. This formulation is intrinsically related to probabilistic risk assessment, supplying a rational safety assessment tool by dealing with the numerous sources of uncertainties that may impact on the bridge performance. It can be used to provide a quantitative basis for decision-making in the face of uncertainty and insights not otherwise obtainable from deterministic analyses of extreme events [89, 91, 90]. It provides, thus, a conceptual method for estimating the mean annual frequency (MAF) of exceeding a target parameter and verifying whether a design complies with a stated objective. Therefore, a performance objective can be defined by calculating the probability of exceeding a target value of DV, DS or EDP, within a time span, depending on how ambitious or demanding an owner or regulatory agency may be. Depending on the order

of integration of Equation 2.1, fragility analysis may have a central role in the assessment of a structure's seismic performance [20].

2.2.2 Seismic fragility analysis

A seismic fragility model of a structure provides a tool for rational safety assessment and decision-making using a probabilistic framework to manage the various sources of uncertainty that affect the structure's performance during an earthquake. The seismic fragility of an engineered system depicts the conditional probability of violating a damage state DS under a specific hazard with intensity IM = im, i.e.:

$$\text{Fragility} = \Pr(\text{DS}|\text{IM} = im) \tag{2.2}$$

where $\Pr(\cdot|\cdot)$ represents the conditional probability function [91]. The depiction of fragility functions for a given damage state is a fragility curve when it is conditioned on a single intensity measure, whereas conditioning the fragility on two parameters (e.g., an IM and another system parameter) determines a fragility surface. For example, based on the fragility data of a bridge in Eastern Canada [33], the enhancement of the bridge fragility due to increased concrete confinement in bridge columns is illustrated in Figure 2.2. While the fragility curves indicate the bridge performance for discrete values of transverse reinforcement ratio (ρ_t), a continuous appreciation is provided by fragility surfaces. More details on fragility curves and surfaces are discussed in Section 2.5

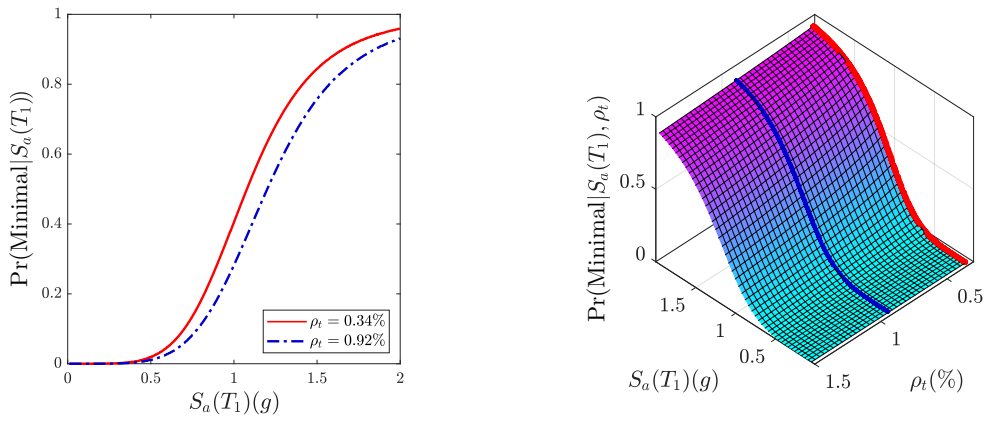

(a) (b)

Figure 2.2 Depiction of fragility functions as (a) curves and (b) surface for minimal damage with respect to transverse reinforcement ratio of bridge columns (based on the data from Bandini et al. [33])

Three main approaches for the development of fragility functions for a structure are found in the literature, namely judgmental, empirical, and analytical [185]. These approaches

differ in the accuracy of the results of the vulnerability assessment, and in the resources demanded to perform the analysis. These three types are briefly discussed hereafter regarding their advantages and disadvantages.

The judgmental (or expert-based) fragility analysis is one of the oldest and simplest methods for deriving fragility functions. In such method, an expert panel is submitted to a survey for the estimative of probable damage distribution on several components of a typical highway bridge under different earthquake intensities. The method is strongly dependent on the questionnaire used, experience of the panel and the number of experts consulted (e.g., [197, 203]). The reliability of expert-based fragility curves is questionable because they generally rely on non-quantified uncertainties, often biased judgments, development upon specific structural types, typical configurations, detailing, and materials [185].

Empirical fragility analysis is based on damage distributions from post-earthquake field observations or reconnaissance reports. This method provides a more realistic picture when compared to expert-based, but it still lacks generality and is usually associated with a large degree of uncertainty. For instance, empirical fragility curves were built based on damage data from the Kobe earthquake (Japan, 1995) considering three damage states (i.e., minor, moderate, and major damage). The fragility curves of expressway bridge structures in Japan are illustrated in Figure 2.3 based on two studies (S – Shinozuka et al. [235], Y – Yamazaki et al. [269]) and present significant differences particularly for minor and moderate damage.

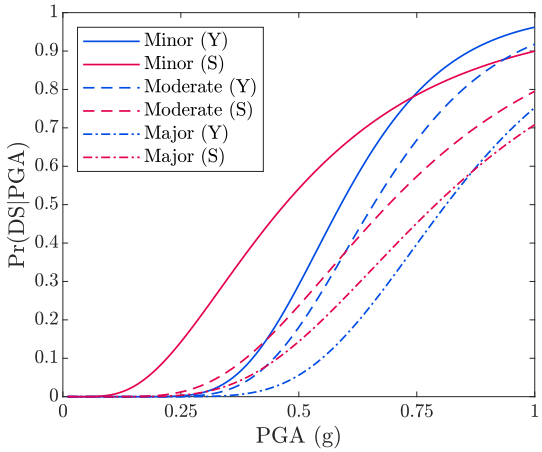

Figure 2.3 Comparison of empirical fragility curves based on damage data from the 1995 Kobe earthquake for the same bridge (S – Shinozuka et al. [235], Y – Yamazaki et al. [269])

The analytical fragility analysis is the most used method for the development of bridge fragility curves. Its popularity is related to its increased degree of reliability and for being a less biased method. Moreover, it is the appropriate method for the fragility analysis when one lacks adequate damage data. A variety of analytical methods has been used on the development of seismic fragility curves for bridges, such as capacity spectrum-based analysis [164], probabilistic seismic demand model [64, 199], multiple-stripe analysis [22], and incremental dynamic analysis [20]. The main inconvenience of this approach lies on the amount of computational time required for the analysis. Although it has not yet been incorporated into design guidelines, analytical seismic fragility analysis has become widely popular, providing a more reliable and objective framework to calculate the probability of observing structural damage than its empirical and judgmental counterparts. Fragility analysis can support insights into the relative seismic performance of highway bridges as well as the effectiveness of prospective retrofit options, that aim to reduce the seismic risk to bridges, given potential uncertainties in structural performance, retrofit impact, and seismic hazard [243]. It has already been used in design optimization of isolation and damping devices for bridges [266], and its application has been expanded beyond earthquake engineering, gaining acceptance in the risk assessment of structures subject to other hazards, such as hurricanes [11, 12, 37, 29, 30]. Moreover, fragility functions are extremely valuable in regions of moderate seismicity (e.g., eastern Canada and central and southeastern U.S.), where scarcity of empirical data of earthquake damage requires risk evaluation to be based on analytical methods with explicit account for the uncertainty inherent in the performance assessment [215].

Additionally, considering that large-scale experiments involving entire bridge models or full-scale components are expensive, bridge fragility curves obtained from experimental data of shaking-table tests have been very limited, and are a less expressive approach in fragility analysis. Such type of analysis has already been conducted providing actual damage condition, yet showing limitations due to a lack of adequate data points at all damage stages and weak correlation between geometry and structural properties [185]. As an alternative, a hybrid approach may be adopted to construct fragility curves using a combination of two or more of the previously discussed techniques in an attempt to overcome their various limitations. For instance, it may aim in reducing the computational effort of analytical modeling, while compensating for subjective biases that are present on the judgmental approach [227, 92, 185].

2.2.3 Damage state capacity models

A probabilistic seismic capacity model of a bridge component describes the component's ability to sustain seismic demands before suffering damage considering uncertainties. The definition and selection of realistic damage states are a paramount step in fragility analysis, since the quantification of damage stages has a direct effect on the determination of the parameters that influence the shape of the fragility function [92]. Given the dynamic nature of earthquake loadings and most of the mass being concentrated on the superstructure, substructure components are prone to undergo severe damage during seismic events, and understanding their capacity is essential in the establishment of performance criteria for bridges [234]. Several seismic fragility analyses of bridges (e.g., [243, 250, 247, 198, 207, 273]) were based on the definition of limit states provided by the Federal Emergency Management Agency (FEMA) in the software manual for HAZUS-MH (Hazards U.S. – Multi-hazard) [95, 93] (Table 2.4).

Table 2.4 Bridge damage states according to FEMA HAZUS-MH [93]

Damage state	General damage description
Slight	Minor cracking and spalling to the abutment, cracks in shear keys at abutments, minor spalling and cracks at hinges, minor spalling at the column (damage requires no more than cosmetic repair) or minor cracking to the deck.
Moderate	Any column experiencing moderate (shear cracks) cracking and spalling (column structurally still sound), moderate movement of the abutment (<5 cm), extensive cracking and spalling of shear keys, any connection having cracked shear keys or bent bolts, keeper bar failure without unseating, rocker bearing failure or moderate settlement of the approach.
Extensive	Any column degrading without collapse - shear failure - (column structurally unsafe), significant residual movement at connections, or major settlement approach, vertical offset of the abutment, differential settlement at connections, shear key failure at abutments.
Complete	Any column collapsing and connection losing all bearing support, which may lead to imminent deck collapse, tilting of the substructure due to foundation failure.

The damage states described in Table 2.4 are qualitative, and, in order to develop fragility functions, these must be translated into structural demand quantities, known as engineering demand parameters (EDP) (e.g., displacement or curvature ductility, drift ratio, and deformation). The strength of non-seismically design columns has been established via analytical [64], numerical [249], and experimental [222] models. Well confined concrete bridge columns combining analytical and experimental approaches [149]. A comprehensive work was performed by Nielson [197] to analytically determine the damage state quantities of

several bridge components, namely curvature ductility for columns, longitudinal and transverse deformations for four sorts of bearings (steel rocker, steel-fixed, elastomer-fixed, and elastomeric expansion), and active, passive and transverse deformation for non-integral abutments. A Bayesian approach was then used to update the physics-based values with the results of a survey based on the judgment of experimented engineers. These damage states have been extensively adopted in the seismic fragility assessment of bridges (e.g., [207, 109, 85]) and were later adapted to the representative bridges in eastern Canada [248]. Damage states of natural rubber seismic isolators were defined through the combination of numerical and experimental analyses [245, 103].

Finally, an accurate estimation of the seismic fragility can only be achieved when capacity is also treated as a random variable. An elegant estimation of the component fragility would only be possible with a series of large-scale experiments, and thus the uncertain capacity approach should not be adopted if such information is missing. Obviously, despite the number of laboratory tests performed to estimate various capacities of different structural systems, there will always be a lack of information as specific setups only have or can be tested [20]. Recent efforts in integrating machine-learning techniques to propagate uncertainty into capacity models may address this issue (e.g., [167, 155, 156]). Nonetheless, in the absence of test data, it is suggested to assume that component strength follows normal or lognormal distributions [168]. Recommendations on dispersion values are found in the work of Nielson [197] and in FEMA P-58 [94].

2.3 Characterization of seismic hazard and record selection

A consistent seismic fragility analysis requires the use of ground motion accelerograms that describes the specificities of the seismic hazard at the investigated site. This can be achieved by the characterization of the seismic hazard at the site (i.e., establishing the recurrence rate of an earthquake scenario), followed by a representative selection of ground motion records (i.e., choosing earthquake signals that are coherent to the seismic hazard from a database). Estimating the recurrence rate of observing an earthquake scenario can be accomplished either by a deterministic or a probabilistic approach, using geology and historical seismicity data. The deterministic seismic hazard analysis method identifies earthquake sources and interpret the strongest earthquake that each source is capable of producing regardless of time. The main objective is to identify the largest earthquake that appears possible along a recognized fault as a result of known or presumed tectonic activity. The main advantages of the deterministic seismic hazard analysis procedure are

its simplicity to apply and conservative results for well-defined tectonic features, such as the Cascadia subduction zone in the Pacific northwest and the San Andreas fault in California. The disadvantages of this type of analysis include the difficulty of applying it to distributed sources close to the site where the source-to-site distance is complex. Also, uncertainty is not handled well by the deterministic seismic hazard analysis procedure as it provides no information on the likelihood of the controlling earthquake occurring at the site of interest. Finally, it supplies no information on the level of shaking a structure may endure over its lifespan form earthquakes occurring along faults other than the one controlling the definition of the seismic hazard at the site [96]. The limitations of the deterministic approach can be surpassed by a probabilistic framework, which is further detailed next.

2.3.1 Probabilistic seismic hazard analysis

The probabilistic seismic hazard analysis (PSHA), originally proposed by [71], attempts to provide annual rates of exceedance of a given ground motion intensity at a specific site. The application of PSHA usually requires four steps [96]:

Step 1. Definition of seismic sources : for a given site, geographic zones representing seismotectonic sources are defined and, for each zone, it is presumed that the probability of earthquake occurrence is the same for the entire surface area.

Step 2. Definition of seismicity model : historical seismicity is used to establish the parameters of a magnitude-recurrence relation of the type $\log N = A - bM$ for each source. A maximum magnitude $M_{\max}$ is also defined for each source.

Step 3. Definition of a ground motion model : a ground motion model (GMM) (also known as an attenuation relationship or ground motion prediction equation) is determined between each source and a given site. This model establishes the relationship between the expected value of a given intensity measure and the rupture characteristics, such as magnitude and source-to-site distance.

Step 4. Calculation of the hazard curve for the site : the GMMs are combined with the magnitude-recurrence relationships to calculate the annual recurrence rate of exceedance for a chosen ground motion level at any given site. The total recurrence rate at the site is obtained by adding up the recurrence rates from each source and a theoretical probability distribution is used (usually Poisson's). Finally, the hazard curve is generated, which represents the relationship between the annual recurrence rate and the seismic parameter of interest.

A seismic hazard map for a region is created by repeating these four steps on a grid for each given site in the region, for a chosen seismic parameter, and using contour lines based on

the same annual probability of exceedance. An example of seismic hazard map of Canada is presented in Figure 2.4. The PSHA procedure can be used with any seismic parameter IM of interest if a GMM for this parameter is known. Generally, a site is influenced by many seismic sources of different geometries and surface areas. A numerical integration is carried out to evaluate the recurrence rate N for a given site. For a value of the seismic parameter of interest IM $= im$ at a given site, all contributions to the total recurrence rate N are considered by dividing each seismic source in sectors of smaller surface areas. The contributions of all sectors from all sources ΔN are then added to obtain the final recurrence rate.

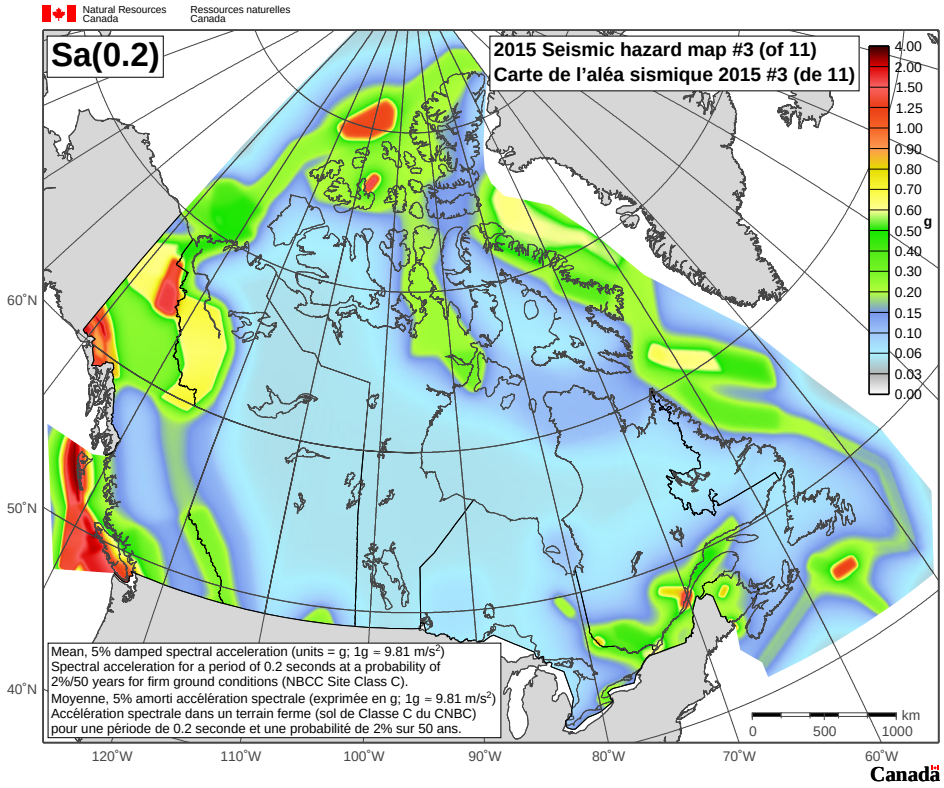

Figure 2.4 Seismic hazard map of Canada for spectral acceleration at 0.2 s period and 5% damping [194].

Regarding uncertainties, the PSHA procedure provides a systematic framework for their treatment, considering both epistemic and aleatory uncertainties about the seismic model. Aleatory uncertainties are treated by modeling the GMM with a lognormal distribution that is characterized by a mean value and by the standard deviation of the logarithmic of the ground motion parameter of interest at a given magnitude and distance. Historically, the standard deviation has been assumed constant for all magnitudes and distances.

Epistemic uncertainty arises from the modeling assumptions, unknown properties and parameters, and extrapolation of data beyond their observed range. The use of logic trees provides a convenient framework for the explicit treatment of epistemic uncertainty in seismic hazard analysis. A logic tree consists of a series of nodes at which models are specified, and a number of branches that represent the different models under consideration. Each alternative model is assigned a weighting factor representing the likelihood of that model being correct and the sum of the weights from each branch connected to a node must equate 1.0. A seismic hazard analysis is carried out for each combination of models associated with a terminal branch and the result of each analysis is weighted by relative likelihood of its particular combination of branches. The final result is the sum of the weighted individual results. For instance, the PSHA in the open source software OpenQuake (OQ) engine is based on logic trees [239, 238].

Finally, the estimation of the contribution of an expected earthquake scenario at the site according to a specific exceedance recurrence rate given that a ground motion intensity measure of recurrence rate $\lambda(\text{IM})$ is observed can be accomplished by seismic deaggregation (or disaggregation). Traditional seismic deaggregation [174, 34] provides $\Pr(\theta_{rup}|\text{IM} > im)$ which is the conditional probability of observing an earthquake of certain rupture properties θ_{rup} given that a ground motion exceedance has occurred (i.e., $IM > im$). Alternatively, seismic deaggregation can express the conditional probability of (at least one) ground motion exceedance in a time span (or return period T_{ret}), given the occurrence of earthquakes of certain rupture properties (i.e., $\Pr(\text{IM} > im|\theta_{rup}, T_{ret})$), as in the OQ engine. A simple conversion from the alternative deaggregation to the traditional formulation involves the use of the Poisson distribution. Seismic deaggregation is an essential step to determine the parameters of ground motion models used to construct conditional target distributions for record selection, as detailed next.

2.3.2 Ground motion record selection

The selection of a suite of ground motions that are representative of the seismic scenario at a site of interest is crucial to consistently propagate the record-to-record variability and the uncertainty about the seismic hazard into the seismic fragility analysis [152]. Traditionally, ground motion records are selected to match the uniform hazard spectrum (UHS) at the site. Several seismic fragility analyses were conducted using UHS as the target spectrum for bridges [64, 197, 243, 248, 207] and other structures [39, 90, 146]. The UHS is, however, a design spectrum built upon different earthquake events with different magnitudes and distances, with the same probability of exceedance for all periods. Thus, the UHS does not represent the response spectrum of any individual seismic excitation

and has been recently considered unsuitable to be a target spectrum for record selection due to its inherent conservatism [21, 252, 75].

The conditional spectrum approach [21, 125] came up as a refined approach for record selection by representing a more rational target spectrum than the UHS. The target spectrum in the CS approach is built upon a multivariate lognormal distribution of spectral accelerations at multiple vibration periods conditioned on the occurrence of a specific spectral acceleration level $S_a(T^*)$, where T^* is the conditioning period (usually chosen as the structure's fundamental period T_1). Starting from the well-accepted assumption that seismic spectral quantities are lognormally distributed, for a single seismic rupture rup_k, the conditional distribution of spectral accelerations given the occurrence of a particular spectral acceleration value at the conditioning period $S_a(T_j = T^*) = s_{a,j}$ has a lognormal distribution defined by the following mean:

$$\mu_{\ln S_{a,i}|Rup,S_{a,j}}(rup_k, s_{a,j}) = \mu_{\ln S_{a,i}|Rup}(rup_k) + \sigma_{\ln S_{a,i}|Rup}(rup_k)\rho_{j,i}\varepsilon_j \tag{2.3}$$

and standard deviation:

$$\sigma_{\ln S_{a,i}|Rup,S_{a,j}}(rup_k, s_{a,j}) = \sigma_{\ln S_{a,i}|Rup}(rup_k)\sqrt{1-\rho_{j,i}^2} \tag{2.4}$$

where $\mu_{\ln S_{a,i}|Rup,S_{a,j}}(rup_k, s_{a,j})$ and $\sigma_{\ln S_{a,i}|Rup,S_{a,j}}(rup_k, s_{a,j})$ are the mean and standard deviation of $\ln S_{a,i}$ given the occurrence of $S_{a,j} = s_{a,j}$ and the specific earthquake rupture scenario $Rup = rup_k$; $\mu_{\ln S_{a,i}|Rup}(rup_k)$ and $\sigma_{\ln S_{a,i}|Rup}(rup_k)$ are the mean and standard deviation of $\ln S_{a,i}$ given the rupture scenario (provided by a ground motion model); and $\rho_{j,i} = \rho(T_j, T_i)$ is the Pearson correlation coefficient between $\varepsilon_j = \varepsilon(T_j)$ and $\varepsilon_i = \varepsilon(T_i)$ (assumed independent of Rup) [26, 76], being $\varepsilon_j = \varepsilon(T_j)$ the difference between $\ln S_{a,j}$ and the mean value $\mu_{\ln S_{a,j}|Rup}(rup_k)$ in terms of standard deviation, hence:

$$\varepsilon_j = \varepsilon(T_j) = \frac{\ln S_{a,j} - \mu_{\ln S_{a,j}|Rup}(rup_k)}{\sigma_{\ln S_{a,j}|Rup}(rup_k)} \tag{2.5}$$

A ground motion record selection algorithm with greedy optimization was proposed by Jayaram and Baker [125] and further improved by Baker and Lee [27]. Basically, the target conditional spectrum distribution (built upon Equations 2.3 and 2.4 for a range of vibration periods) is used to draw N_{gm} acceleration spectrum samples, where N_{gm} is the number of records to be selected. Real ground motion record spectra from a database are first scaled to match the conditional $S_a(T^*)$ and the N_{gm} spectra that best fit the spectrum samples are then selected. In this way, the selected spectra automatically respect the mean

and standard deviation of the target CS. Besides being consistent to hazard, the scaling factor of the chosen records may also be limited, avoiding thus the introduction of bias due to excessively high scale factor [154]. The adoption of the CS in some studies resulted in lower structural response when compared to the application of more conventional spectra, say the UHS (e.g., [21, 252, 76, 38]). For the reasons listed above, the use of the CS has been recommended over the UHS as target spectrum in the last decade [28].

The formulation presented in Equations 2.3 and 2.4 were proposed by Lin et al. [151] who evaluated the impact of incorporating multiple earthquake rupture scenarios and ground motion models using approximated and an 'exact' formulation to build the conditional spectrum distribution. For cases with significant hazard contributions from multiple earthquake sources, the 'exact' calculation methods are recommended, in which deaggregation results are used as weights for rupture scenarios and GMMs to build the conditional spectrum. Conversely, for simpler cases, the approximations are rather satisfactory. In this sense, the simplest approximated calculation is based on an expected seismic rupture scenario $Rup = \overline{rup}$ defined, for example, by expected earthquake magnitude $\bar{M}$, source-to-site distance $\bar{R}$, and epsilon $\bar{\varepsilon}$ provided by seismic deaggregation.

Although indicated as a more rational approach for record selection, a couple of limitations on the adoption of the conditional spectrum as the target distribution have been raised [43]. The first drawback is related to representing ground motions only in terms of spectral accelerations, whereas it is well acknowledged that the severity of ground motions depends, in general, on its intensity, frequency content, and duration (e.g., [60, 61]). A second critical remark regards the type of structural system considered in past studies. While disregarding other characteristics of ground motions than spectral response was justified in assessing single-degree-of-freedom or multi-degree-of-freedom representations of multi-story structures with peak inter-story drift ratio as a response parameter of interest, spectral acceleration may not cover for an arbitrary response measure for any arbitrary system.

To overcome these limitations, Bradley [43, 45] proposed the generalized conditional intensity measure approach. The GCIM approach is an extension of the CS approach to seismic intensity quantities other than spectral accelerations. The hypothesis of lognormality of S_a is extended to any intensity measure. Therefore, the target conditional-IM distribution is a multivariate lognormal distribution of a vector of intensity measures **IM** conditioned on the occurrence of the conditioning intensity quantity IM_j. The GCIM formulation is analogous to that of the CS approach and is presented in the Appendix C for brevity. In this approach, any intensity measure may be used, for instance peak ground acceleration

(PGA), peak ground velocity (PGV), peak ground displacement (PGD), Arias intensity (I_A), spectrum intensity (SI), and significant duration (Ds_{575} or Ds_{595}), to name a few. The choice of IMs to build the target GCIM distribution relies, however, on the availability of ground motion models on these intensity measures at the site of interest. Moreover, correlation between the epsilon values of these intensity quantities must be known (e.g., [26, 44, 46, 51, 24]).

Besides the selection method, two important questions have been raised regarding ground motion record selection in the context of fragility analysis. First, which conditioning intensity measure should be chosen? And what is the minimum required number of ground motions to be used? In general, it is recommended that the conditioning intensity measure is selected such that it captures the amplitude of ground motion in the region of vibration frequencies that govern the predominant physical mechanism controlling the seismic response of the problem considered [47]. Regarding the number of required accelerograms, it might seem straightforward that using a large number of ground motions for RHA can reduce the standard error in the predicted structural seismic demand based on classical statistical theory [35]. It is, however, impractical to implement a large number of records, given that the main reason for using a limited set is the computational burden associated with performing numerous RHAs [135]. Additionally, due to the limited size of databases of recorded ground motion time histories, selecting a large number of records that are hazard consistent (i.e., that show a satisfactory fit with a target distribution of IMs like the GCIM) might be rather challenging [49].

Although the conditioning IM of the fragility functions is not necessarily the same of the record selection step (using CS or GCIM), there are some advantages in considering the same intensity measure in these two steps. For instance, when a conditional-IM-based approach for ground motion selection is coupled with multiple-stripe analysis [124], the record-to-record variability is more efficiently propagated into the fragility analysis [22, 38]. As verified by Bradley [47], the seismic demand hazard (i.e., the convolution of the conditional probability of exceeding a level of demand given the occurrence of seismic intensity level with the rate of exceedance of the same IM) is independent of the choice of conditioning intensity measure. Nevertheless, the distribution of seismic demand given ground motions with an intensity measure of a specified rate of exceedance is not unique and depends on the conditioning IM chosen used.

The criteria that guide the selection of an optimal conditioning IM for fragility analysis may involve the IM's efficiency (a measure of variation), practicality (a measure of correlation), sufficiency (a measure of statistical independence of causal ground motion parameters),

and hazard computability (a measure of the effort to probabilistically estimate the seismic hazard). Alternatively, proficiency (a composite measure of variation and correlation) can be used as a more efficient parameter [208]. For bridge-specific fragility analysis, the spectral acceleration at the fundamental period ($S_a(T_1)$) has been deemed appropriated, whereas the adoption of PGA and PGV have been suggested in the case of bridge portfolios or isolated bridges [208, 19, 275]. Moreover, because the response of bridges to ground shaking is not necessarily governed by its fundamental vibration mode, it has been argued that a intensity measure that covers a range of periods (and consequently, the respective mode shapes) may be better suited. An example is the average spectral acceleration, defined as [140]:

$$S_{a,Avg} = \left[\prod_{i=1}^{n} S_a(T_i)\right]^{1/n} \tag{2.6}$$

which is the geometric mean of spectral accelerations over a range of periods. An adaptation of the CS approach to build a multivariate lognormal distribution conditioned on $S_{a,Avg}$ was also developed and can be built upon an indirect method that defines ground motion models for the average spectral acceleration [138, 139].

With respect to the number of accelerograms, in general, there is not a unique guidance regarding how many ground motion records are necessary to perform seismic demand analysis, as a wide range of required number of accelerograms is pointed by several studies and standards (e.g., [201, 57, 104, 22, 6]). Accordingly, the number of required ground motion time histories may depend on: (i) the type of analysis (e.g., design, fragility, or risk); (ii) the chosen strategy to generate the demand dataset (as seen later in Section 2.4.1); (iii) the efficiency of the conditioning IM; (iv) and the damage state level [135]. More recently, design codes (e.g., [57, 6]) have recommended the use of 11 ground motion sets (considering two horizontal and one vertical directions). In the case of seismic fragility or risk analysis, more records may be necessary to better capture the record-to-record variability and depend on the type of structure in study [135].

2.4 Probabilistic seismic demand modeling

Intermediate steps of a PBEE probabilistic framework may include the definition of a model that correlates the seismic demand and the earthquake intensity, known as a probabilistic seismic demand model (PSDM) [158]. This approach aims to treat the uncertainties (both structural and seismic) by replacing the limited numerical simulations with a probabilistic model relating the input and the output of the dynamic analyses. The definition of a PSDM is commonly coupled with cloud analysis (as described in the following

section) (e.g., [72, 158, 199, 206, 237]. In a broader interpretation, PSDM is considered here as a surrogate to translate uncertainty of the limited observed demand dataset with respect to the seismic intensity and other parameters of interest. The construction of a PSDM starts by choosing the rules to generate the seismic demand dataset, which is then used to fit a statistical model. Once the model is built, it can be applied to calculate the seismic fragility using either an analytical or numerical approach. Different strategies are found in the literature to collect the demand data and to adjust a probabilistic model. These strategies are discussed next.

2.4.1 Seismic demand data collection strategies

Typical seismic demand data collection strategies are: (i) cloud analysis, (ii) incremental dynamic analysis (IDA), and (iii) multiple-stripe analysis (MSA) (Figure 2.5). Each collection strategy presents its advantages in terms of choice of record selection and scaling, practicality, and adopted hypotheses [161, 87, 104, 22]. Once demand data are gathered, a PSDM is traditionally built using simple techniques such as linear regression (when cloud analysis is used) or fitting parametric distributions—usually lognormal—if IDA or MSA is employed. A broad discussion on seismic demand data collection strategies and their applications to fragility analysis is provided by Bakalis and Vamvatsikos [20].

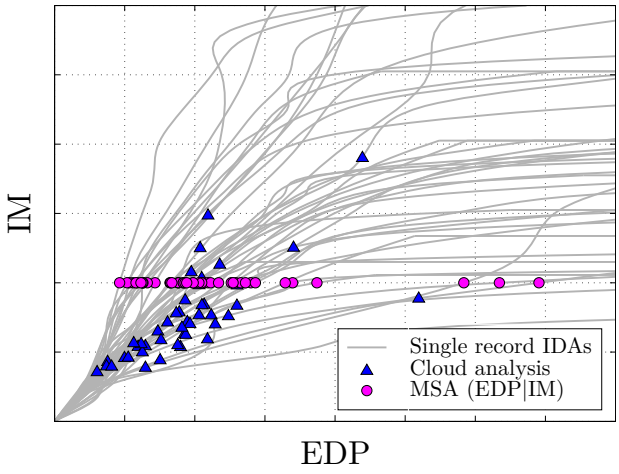

Figure 2.5 Example of different seismic demand data collection strategies (adapted from Bakalis and Vamvatsikos [20])

Cloud analysis is the most straightforward strategy, consisting on gathering peak demand data generated from response history analyses performed with (typically unscaled) ground motions over a range of intensity measure levels. A scatter plot of the seismic demand data with respect to an intensity measure shows a cloud of points, which gives the name of this strategy. Linear regression is then employed in the logarithmic transformed space to define a continuous function of the median and dispersion of the EDP with respect to the chosen

IM. This strategy has been widely employed on the seismic performance assessment of bridges for its simplicity and tractability in fragility analysis (e.g., [158, 199, 206, 248, 243]). When linear regression is adopted, the relationship between EDP and IM is linear in the log-transformed space, assuming that the demand follows a lognormal distribution. The dispersion is commonly assumed independent of the IM level (homoscedasticity).

Incremental dynamic analysis may be seen as the dynamic equivalent to the static pushover analysis. It is a parametric analysis method that has emerged in several different forms to estimate more thoroughly the structural performance under seismic loads. In brief, IDA involves subjecting a structural model to (typically) a set of ground motion record, each scaled to multiple levels of the same intensity measure, thus producing continuous curves of seismic demand as a function of the chosen IM [257]. Although IDA may require a smaller ground motion suite than cloud analysis, the continuous structure of the IDA results allows to better capture a potential nonlinear relationship between demand and seismic intensity and heteroscedasticity (i.e., the dispersion of the demand is conditional on the IM level) in a non-parametric form. Careful must be taken, however, on using unrealistic scaling factors on ground motion records to avoid the introduction of bias [154].

Multiple-stripe analysis [124] organizes demand data at a set of discrete IM levels, which are called stripes. Although it can be interpreted as a discrete version of incremental dynamic analysis, MSA is preferred over IDA due to: the possibility to use different record sets for each seismic intensity level of interest, limited scale factor, and higher efficiency to account for seismic variability (i.e., fewer RHAs are required) [154, 87, 22]. If a deterministic capacity model is adopted (i.e., no uncertainty is considered on capacity), fragility estimates can be readily calculated using MSA. For a given intensity measure level $\mathrm{IM} = im_j$, the corresponding fragility estimate $p_{f,j}$ is approximated as the ratio between the number of cases where the demand is greater than the capacity and the number of RHAs in the stripe. Then, a fragility function can be fitted on the fragility estimates across multiple IM levels. When uncertainty on the capacity is considered using a probabilistic model, however, this estimation is facilitated by fitting a probabilistic model to the demand (as discussed in the Section 2.4.2).

Moreover, MSA is suitable to be paired with conditional IM-based record selection approaches (e.g., the CS or the GCIM), assuring the consistency of the ground motions to the site seismic hazard, better capturing locally the record-to-record variability, and avoiding unnecessary conservatism. This feature may, however, be seen as a potential drawback of the multiple-stripe analysis, because several ground motion sets must be selected to cover a significative range of seismic IM levels used in fragility analysis. Important IM levels to

generate a fragility curve should cover mainly the lower tail of the CDF curve and slightly above its median (i.e., a probability of exceeding a damage state of 50%) [22].

2.4.2 Relationship between seismic demand and intensity

Once the seismic demand data is obtained following one of the collection schemes, the probabilistic conditional relationship EDP|IM is constructed. Classical PSDMs assume that this relationship is nonlinear, assigning a parametric surrogate model to correlate the median of the EDP and the intensity measure. The adoption of IDA or MSA allows the estimation of the demands statistics that are conditioned on the IM levels. The inclusion of other system variables (e.g., material and geometrical uncertainties) may be treated using more advanced surrogate models.

The power-law model

Cornell et al. [72] proposed a power-law model between the median structural demand $m_{\mathrm{EDP|IM}}$ and the intensity measure as follows [20]:

$$m_{\mathrm{EDP|IM}} = a\mathrm{IM}^{b}\varepsilon \tag{2.7}$$

where a and b are the model parameters, and ε is the error resulting from lack-of-fit, which is assumed to follow a lognormal distribution with median equal to unity and dispersion $\zeta_{\mathrm{D|IM}}$.

Linear regression can be performed on the logarithms of the intensity measure levels and peak responses from RHAs to define the demand model once Equation 2.7 is rearranged in the following form:

$$\ln(m_{\mathrm{EDP|IM}}) = \ln(a) + b\ln(\mathrm{IM}) + \ln(\varepsilon) \tag{2.8}$$

where a and b are the regression coefficients (intercept and slope, respectively).

Typically, homoscedasticity is assumed, approximating the dispersion a constant value:

$$\zeta_{\mathrm{D|IM}} \equiv \zeta_D \approx \sqrt{\frac{\sum_{i=1}^{N}\left(\ln(d_i) - \ln(a\mathrm{IM}^{b})\right)}{N-2}} \tag{2.9}$$

where N is the number of RHAs and d_i are the peak demands from the RHAs.

Therefore, the power-law approach models the seismic demand as a conditional lognormal distribution of the form $\mathrm{EDP|IM} \sim \mathrm{LN}(a\mathrm{IM}^{b}, \zeta_D)$. This formulation was first proposed to represent the maximum inter-story drift of steel moment-resisting frame buildings as a

function of the spectral acceleration at the fundamental period [237, 72]. The hypothesis that this quantity of seismic demand follows a lognormal distribution was then tested and validated. This model was later extensively used to represent the behavior of other types of structures, including highway bridges (e.g., [64, 199, 162, 207]).

Up to this point, the power-law model is a component-level PSDM. In the case of multi-component structures, the consideration of multiple structural elements that can undergo damage (either simultaneously or not) requires the inclusion of the dependence between pairs of these various component EDPs. Nielson and DesRoches [199] proposed the joint probabilistic seismic demand model (JPSDM) based on this principle to account for the contribution of multiple critical bridge components on the system (whole bridge) fragility. The JPSDM is thus a multivariate lognormal distribution constructed upon the component marginal distributions defined by Equation 2.7 and a linear correlation structure defined by the Pearson correlation coefficient (Equation 2.10). The correlation coefficient ρ_{XY} is a measurement of the linear dependence between two random variables X and Y and always falls within the closed interval $[-1, 1]$ [35]. Considering a pair of components EDPs, the correlation coefficient is estimated from the peak demand samples d_i as:

$$\rho_{12} = \frac{1}{N} \sum_{i=1}^{N} \left(\frac{\ln(d_{1,i}) - \hat{d_1}}{s_1} \right) \left(\frac{\ln(d_{2,i}) - \hat{d_2}}{s_1} \right) \tag{2.10}$$

where $\hat{d}$ and s are, respectively, the sample mean and standard deviation in the log-transformed space. The JPSDM methodology has been broadly employed for the assessment of bridge seismic performance since then (e.g., [207, 248, 243, 273, 110, 216]). An important remark about this formulation is the fact that the correlation structure neglects any local effect of the seismic intensity levels as it uses the entire dataset to estimate the pairwise correlation coefficients. Nielson [197] suggested that the variation on the correlation coefficients for increasing IM levels could be neglected based on the results of RHAs using a set of 30 synthetic ground motions all scaled to several levels of spectral acceleration. Contrarily, the results of Lupoi et al. [157] suggested the significant dependence of the correlation coefficients of peak responses of piers in long bridges on the IM level.

Besides the observations on the influence of the seismic intensity on the correlation, the hypothesis of linear dependence, although widely employed, is not always valid. For instance, Brandenberg et al. [53] reported nonlinear correlation between bridge component responses when studying typical bridge classes in California. An option to model the nonlinear dependence is to adopt a copula technique (e.g., [115, 116, 279, 278]), which offers a flexible way of describing nonlinear dependence amongst multivariate data separately

from their marginal distributions. It also serves as a powerful tool for modeling nonlinearly-interrelated multivariate data, as well as simulating. Thus, as a trade-off to the simplicity of the power-law model and the JPSDM, restrictive hypotheses make Equation 2.7 hardly capable of globally representing the richness of dynamic response of all kinds of structural systems [20]. An enhanced model can be obtained by considering bilinear or piecewise regression on the observed demand data [158, 99]. Otherwise, MSA- or IDA-based demand models or more advanced surrogate models may be better options to be explored.

MSA- or IDA-based demand models

When demand data is generated following either IDA or MSA rules, modeling the EDP|IM is quite straightforward, suffice an adequate number of ground motion records per IM level of interest is used [20]. In this case, probabilistic distributions can be fitted to the observed dynamic responses at each level of intensity measure, and the lognormal distribution is often chosen (e.g., [49, 50, 48, 241]). Lognormality of seismic demand was introduced by Shome and Cornell [237] as an extrapolation of the classical assumption on the lognormal distribution of seismic intensity measures. It has been validated in some studies since then using either single-degree-of-freedom or two-dimensional frame models [77, 10, 123]. If few stripes are used within the MSA framework, piecewise regression can be employed on the fitted parameters of the lognormal distributions (median and dispersion) to obtain a continuous model. Recommendations in this case are given by Bradley [50]

Nevertheless, in the case of bridges, the lognormal assumption might not be valid for all its critical components, and more refined density estimations may be used instead. Examples are the nonparametric Kernel density distribution [130] and random forest [168]; or a parametric approach based on mixture of Gaussians (as proposed in Chapter 3). In the case of multiple component structures, marginal fitted distributions can be coupled with a correlation structure obtained at each IM level of interest. For instance, Equation 2.10 can be adapted by replacing N with the number of ground motion records at the investigated IM level to estimate a linear correlation coefficient conditional on the seismic intensity $\rho_{XY|\mathrm{IM}}$. Therefore, this approach also addresses the dependence of the correlation coefficient to the level of seismic intensity. Additionally, as proposed in Chapter 3, coupling MSA with Gaussian mixture models can be a powerful tool to account for nonlinear dependence and discontinuities in the seismic response.

Therefore, the power of a MSA- or IDA-based demand model comes from being conditioned on the chosen IM without presuming a parametric formulation to model the variation of a EDP over a range of ground shaking intensities. This aspect can be paramount to avoid propagating significant bias into the risk assessment. An inconvenience of this approach,

however, is that it cannot treat explicitly the uncertainty related to other system parameters (for instance, those related to material or geometry). Multi-parameters surrogate models may address these issues and are discussed next.

Multi-parameter surrogate models

A surrogate model (or metamodel) is an analytical model that substitutes the real experiments or simulations [97]. If the predicted output variable is $y = f(\mathbf{x})$, the objective is to develop a surrogate model to approximate the relationship between the output y and the input vector $\mathbf{x}$. Then, the surrogate demand model $\hat{y} = \hat{f}(\mathbf{x})$ statistically predicts this complex and implicit relationship as

$$y = \hat{f}(\mathbf{x}) + \varepsilon \tag{2.11}$$

where ε is the total error resulting from lack-of-fit and is typically assumed as $\varepsilon \sim \mathrm{N}(0, \sigma^2)$ (i.e., the error follows a normal distribution with zero mean and variance σ^2) [242, 134]. In probabilistic seismic demand modeling, y is the structural dynamic response, while $\mathbf{x} = [\mathrm{IM}, \mathbf{p}]$ is the predictor (or covariate) vector, which gathers the seismic intensity measure IM and the m other relevant structural and environmental parameters $\mathbf{p} = [p_1, \ldots, p_m]$. Similarities between Equations 2.11 and 2.8 are quite evident. In fact, the power law is a surrogate model that only considers explicitly the influence of the seismic input.

With the increasing availability of data and popularity of machine-learning applications, the problem of surrogate modeling has been handled with supervised learning methods for regression, given that seismic demands are real-valued continuous quantities [265]. The scientific challenge of supervised learning resides in the training a model that is as accurate as possible, using as few simulation evaluations as possible. Generally, the process of generating a surrogate model can be described in three steps which may be interleaved iteratively [97]: (1) preparing the training data and selecting the modeling approach; (2) parameters estimating and training the surrogate model; and (3) validation and testing. There is no universally best surrogate model [186] and, as verified in some applications of surrogate models for bridge demand modeling, a given method may be better fitted to certain bridge class (e.g., [109, 128]).

Polynomial response surface (PRS) models is a multi-dimensional surface that predicts desired responses using a computationally efficient closed-form polynomial function developed from a set number of input variables [186]. The general form a PRS model is:

$$\hat{y} = \mathbf{bX} \tag{2.12}$$

where $\hat{y}$ is the predicted value of the component responses, $\mathbf{X}$ is the matrix of basis functions, and $\mathbf{b} = [b_0, b_1, b_2, \ldots, b_B]^\intercal$ are the regression coefficients obtained by minimizing a loss function [117], with B being the number of terms in the basis functions.

Although not a state-of-the-art algorithm, advantages of a PRS model include its ease and speed of computation, and the intuitive nature of interpreting its coefficients [117], affirming its popularity in past studies involving bridge fragilities (e.g., [232, 233, 110, 218, 210, 128, 180, 33, 258]). Second degree response surface polynomials can be adopted because of enhanced goodness-of-fit measures in comparison to first degree polynomial models [109]. Higher order polynomials are quite rare, but are also found for other structures. For instance, a fourth order PRS was the most suitable metamodel for a concrete gravity dam in eastern Canada [231]. A stepwise regression technique might be integrated to obtain the most optimal form of Equation 2.12 by systematically adding and removing terms from the model according to their statistical significance. Additionally, regularization techniques may enhance a metamodel's prediction capability on unseen test data, especially when pairwise correlation between individual predictors is observed [169, 180].

Other algorithms have shown a good performance in modeling the seismic response of highway bridges. The nonparametric multivariate adaptive regression splines (MARS) [100] showed better prediction capabilities than PRS, radial basis function networks, and support vector machines for regression when modeling the response of non-seismically designed multi-span simply supported concrete bridges in Central and South Eastern US [109]. The enhanced performance of MARS was attributed to its adaptive nature, which partitions the input domain, fits a series of models with lower error, and then combines them into an ensemble. Kriging-based metamodels—interpolation algorithms based on the spatial correlation between observed data points—showed improved performance when coupled with a uniform design approach for a three-span simply support concrete bridge [277].

The regression algorithms presented until this point were employed to model the response of bridge components separately (i.e., they were single output methods) and did not account for the interaction between the diverse components. Ghosh et al. [110] combined the JPSDM [199] with multiple PRS component surrogate models, in which the pairwise component correlations were based on the observed data and were simply calculated according to Equation 2.10. The PRS component surrogate models were, however, all trained separately. Mangalathu et al. [165] used multi-output artificial neural networks (ANN) to build a surrogate model that implicitly accounts for the dependent bridge component responses. Attempting to simulate the networked structure of biological brain neurons,

ANN comprehends a suite of interconnected processing nodes (or neurons) associated to three types of layers, namely input, hidden, and output. In summary, model variables in the input layer are weighted and fed into the hidden layer that consists of a series of nonlinear relationships (such as sigmoidal functions). The latter are then further weighted and fed into the output layer. Connection weights are learned in the forward propagation and updated through a training process that minimizes the prediction error, which is typically propagated in the backward direction [41, 265].

Although the multi-output ANN used by Mangalathu et al. [165] considers the dependence of the component responses in the output layer, the correlations of the model residuals were neglected. The latter are crucial for uncertainty propagation and should be included in probabilistic seismic response analysis. To address this issue, multivariate surrogate demand models (MvSDM) for bridges were investigated by Du and Padgett [85]. Generally, MvSDMs establish the mapping between p predictors and m dependent demand quantities, as expressed by:

$$\hat{\mathbf{y}} = \tilde{\mathbf{y}}(\mathbf{x}) + \boldsymbol{\varepsilon}(\mathbf{x}) \tag{2.13}$$

where the model prediction $\hat{\mathbf{y}}$ is comprised of the point estimates from a multivariate systematic trend model $\tilde{\mathbf{y}}(\mathbf{x})$ and the correlated model errors $\boldsymbol{\varepsilon}(\mathbf{x})$. Therefore, a two-step procedure is necessary in this case, to first train the multivariate systematic trend model, and then to fit an error covariance model on the residuals. For a typical three-span concrete girder case-study bridge in the Central and Southeastern U.S. (CSUS), kernel partial least squares regression (PLSR) and ANN outperformed multivariate linear regression and linear PLSR in modeling the multivariate systematic trend. Regarding the error covariance model, sample regression residual covariance was deemed a reasonable option for its mathematical consistency, ease of implementation and computational efficiency, and good agreement with the benchmark fragilities, when compared to the JPSDM approach and multi-output Gaussian process. It was argued that the JPSDM method tends to overestimate the error correlations and underestimate the system fragility, besides the fact that its formulation presents one potential mathematical inconsistency. The error term correlations are assumed to be equal to the sample demand correlations irrespective of the regression model in the JPSDM method, whereas the regression standard deviation depends on the adopted regression model [85].

2.5 Analytical fragility functions of bridges

Analytical fragility curves are based on structural models that characterize the performance limit state of the structure. The performance of the structure is a function of some

vector of basic variables $\mathbf{X}$. These variables determine both the capacity of a structure to withstand a load and the demand placed on the structure, including material properties and geometry. They could also include environmental variables that might in some way affect the capacity. Basic variables can be either deterministic or random variables. The limit state equation, also known as the performance function, can then be expressed in terms of safety margin as the difference between capacity $R(\mathbf{X})$ and demand $S(\mathbf{X})$:

$$Z = g(R, S) = R(\mathbf{X}) - S(\mathbf{X}) \tag{2.14}$$

However, this formulation is still not the most general, since it assumes that there are distinct capacity and demand values. This distinction is not possible in many structural reliability problems. The general structural reliability problem is thus established in terms of a limit state function $g = g(\mathbf{X})$ (Figure 2.6). The solution space consists of three regions: $g(\mathbf{X}) < 0$ is the failure domain (failure state); $g(\mathbf{X}) = 0$ is the limit state surface (limiting state); and $g(\mathbf{X}) > 0$ is the safe domain (survival state). The probability of failure p_f is given by integration of a multivariate density function for the n-dimensional vector of basic random variables over the failure domain $\Omega \equiv \{\mathbf{X} : g(\mathbf{X}) \leq 0\}$ [81]

$$\text{Fragility} = p_f = \Pr(g(\mathbf{X}) \leq 0) = \int_{\Omega} f_{\mathbf{X}}(\mathbf{x}) \mathrm{d}\mathbf{x} \tag{2.15}$$

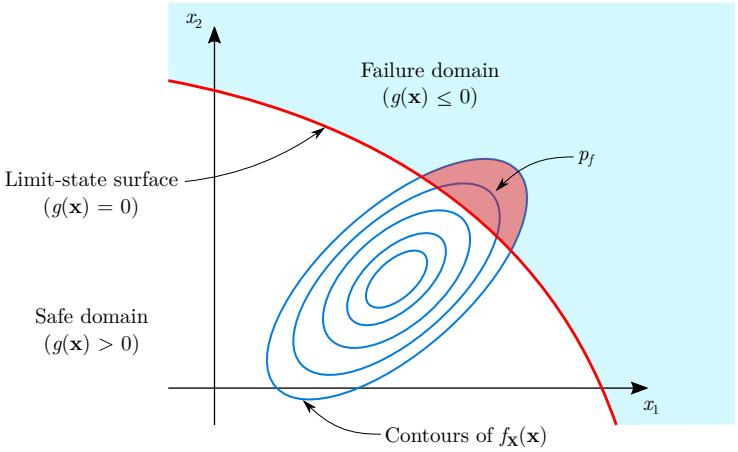

Figure 2.6 Graphical description of structural reliability problems (adapted from Der Kiureghian [81])

This integral may be solved analytically by methods such as the First-Order Second-Moment (FOSM) analysis, the First-Order Reliability Method (FORM), and the Second-Order Reliability Method (SORM). It can also be solved numerically by sampling methods

such as Monte Carlo simulations (MCS) or Latin hypercube simulations (LHS), or by a surrogate modeling technique, such as the Response Surface Method (SRM) [227].

For complex systems characterized by many basic variables and several failure modes, for which the definition of limit state functions is difficult, it is necessary to employ a sampling method in order to generate fragility functions. The main method is the Monte Carlo simulation, which is the most general approach since it does not assume any probability distribution to the fragility. Its employment requires the generation of numerous samples of the system, using the probability density functions of the basic random variables and the assessing the exceedance of a limit state for a given load. Once the procedure is applied for N samples, the probability of failure or the fragility p_f is expressed by:

$$p_f = \frac{z}{N} \tag{2.16}$$

where z is the number of simulations violating a limit state.

The MCS is a robust and straightforward method. However, its convergence rate is low, since it might demand many thousands of simulations to converge and, if the number of random variables is elevated, the MCS can be computationally very expensive, especially when the finite element method is used [31]. Other than that, the MCS is always subject to sampling error because the number of simulations cannot be infinite. Other efficient sampling methods, e.g., Latin Hypercube simulations, might be instead of Monte Carlo sampling to reduce computational effort. The basic approach to estimating fragility is the same [227, 145].

2.5.1 Component- and system-level fragility

In PBEE, performance criteria relate damage limit states to the sought structural functionality, and for multicomponent structures, such as highway bridges, damage limit states are formulated at two levels: component and system. Often, component level damages are used to estimate repair actions and costs, while system-level performance from this combination of component damages often relates to outcomes such as lane closures, load or speed restrictions [160, 199, 206, 243, 127]. The evolution of component-level and system-level bridge fragility assessment is briefly presented here.

Initially, some studies developed fragility curves for bridges on the assumption that the fragility of one critical component (usually piers or columns) was representative of the fragility of the bridges system as a whole [235, 133, 159]. Even though this simplifying approach may be appropriate for bridges whose seismic response is predominantly governed by their columns, other components may be vulnerable and contribute significantly to the

system vulnerability. Hence, all critical components should be considered in order to avoid significant errors in the estimation of bridge fragilities. This lead Choi et al. [64] to use the first-order reliability theory to establish upper and lower bounds on the system fragility $p_{f,sys}$ assuming a series configuration of the bridge components. The lower bound is taken as the maximum component fragility $p_{f,comp,i}$ and the upper bound is a combination of the component fragilities. Thus, the system fragility is bounded as:

$$\max_{i=1}^{m}(p_{f,comp,i}) \leq p_{f,sys} \leq 1 - \prod_{i=1}^{m}(1 - p_{f,comp,i}) \tag{2.17}$$

where m is the total number of components.

With the introduction of the JPSDM approach by Nielson and DesRoches [199], the contribution of multiple critical components to the system fragility was facilitated. By assuming the bridge as a series system, the probability of exceeding the system damage state is:

$$p_{f,sys} = \Pr\left(\bigcup_{i=1}^{m} \mathcal{F}_{comp,i}\right) \tag{2.18}$$

where $\mathcal{F}_{comp,i}$ represents the damage state violation event of the i^{th} component. According to Equation 2.18, when Monte Carlo sampling is used, the numerical approximation of the system fragility is simply taken as the ratio between the number of samples in which at least one of the components has its capacity exceeded by the demand, and the total number of samples [110]. This methodology was extensively employed on the fragility analysis of bridges (e.g., [206, 207, 250, 251, 243, 247]). With this methodology it was possible to identify that the ultimate impact of a retrofit measure on the system fragility is a function of the relative vulnerability of the various components in the system and the influence of the retrofit on shifting those vulnerabilities [207]. For instance, Siqueira et al. [243] verified that, although the introduction of seismic isolators reduced significantly the fragility of columns in MSC concrete bridges (which controlled the system fragility in their as-built configuration), the abutment wing walls became more susceptible to be damaged and controlled the system fragility of the retrofitted bridge for moderate and extensive damage states.

Later, by recognizing that the damage to different critical components have different consequences to the bridge serviceability (in terms of closure and repair implications), Zakeri et al. [273] added the importance of the component into Equation 2.18. The components were classified as primary or secondary in accordance to their importance for the bridge stability under traffic or a subsequent seismic event. Columns that reach instability or

a deck that reach unseating limit state were classified as primary components (the only components to contribute to complete damage state of the bridge). Secondary components (e.g., shear keys, abutments, and bearings) are assumed to contribute to earlier damage states of the whole system (slight, moderate, and extensive) since their complete failure would not have a similar consequence as that of primary components. By numbering the limit states progressively from 1 to 4, the system fragility is calculated by

$$p_{f,sys} = \begin{cases} \Pr\left(\bigcup_{i=1}^{m_p+m_s} \mathcal{F}_{comp,i,j}\right) & \text{for } j \leq 3 \\ \Pr\left(\bigcup_{i=1}^{m_p} \mathcal{F}_{comp,i,j}\right) & \text{for } j = 4 \end{cases} \tag{2.19}$$

where m_p and m_s are the total numbers of primary and secondary components, respectively, and j is the damage state index. This approach was also adopted in the assessment of the evolution of seismic bridge design through time [216].

2.5.2 Single-parameter seismic fragility functions

Several studies demonstrated that seismic fragility can be appropriately represented by a lognormal distribution [89, 90, 39]. Hence, the seismic fragility of a damage state DS is often modeled as following a lognormal law expressed by

$$\Pr(\text{DS}|\text{IM} = im) = p_f(im) = \Phi\left(\frac{\ln(im/m_R)}{\zeta_R}\right) \tag{2.20}$$

where $\Phi(\cdot)$ is the cumulative distribution function (CDF) of the standard normal distribution, im is the demand variable or the control variable defined by the intensity measure, m_R is the median of the capacity (expressed in units that are dimensionally consistent with the demand variable IM), and ζ_R is the logarithmic standard deviation of the capacity, which involves the epistemic and aleatory uncertainties, ζ_{RU} and ζ_{RR}, respectively, in the following form

$$\zeta_R = \sqrt{\zeta_{RU}^2 + \zeta_{RR}^2} \tag{2.21}$$

The epistemic uncertainty is often obtained by values found in the literature, however, due to the lack of data, this source of uncertainty is often neglected or combined with the aleatory uncertainty without further details. Other distributions such as the Weibull, normal, and logistic might as well be used for the definition of fragility [89, 36].

The fragility functions are generated by computing the probability of failure (Equation 2.16) for numerous levels of seismic intensity:

$$p_f(im_j) = \frac{z_j}{N} \tag{2.22}$$

where z_j is the number of observed samples with damage state exceedance at the seismic quantity im_j. Different probabilities of failure might be obtained by scaling a restricted set of ground motions within a range of intensity measure (as by incremental dynamic analysis) or by selecting different ground motions for each IM level of interest (as by multiple-stripe analysis). The latter is preferred since the frequency content and the properties of a seismic record are strongly dependent on its intensity, although such approach requires a larger number of compatible accelerograms [22]. The system fragility can be estimated using Equation 2.20 once the number of points of probabilities of failure is sufficient.

Fitting the parameters of Equation 2.20 is usually performed via maximum likelihood estimation (MLE) or least squares method. The MLE method was adopted by Shinozuka et al. [236] for the development of empirical fragility curves for bridges after the 1995 Kobe earthquake and for the development of analytical fragility curves for the region of Memphis. Given the response to each model sample, the parameters of the lognormal distribution expressed in Equation 2.20 (median and dispersion) can be estimated by maximizing the likelihood function, which is established by

$$\text{Likelihood} = \prod_{j=1}^{N} [p_f(im_j)]^{x_j} [1 - p_f(im_j)]^{1-x_j} \tag{2.23}$$

where $p_f(im_j)$ is expressed by Equation 2.20, im_j is the intensity measure in the sample of interest j, N is the total number of samples, and $x_j = 1$ or 0 if the limit state was whether reached or not.

The MLE was later deemed by Baker [22] as an efficient method for the fitting of analytical fragility functions once coupled with multiple-stripe analysis. By taking the binomial distribution for the probability of observing z_j collapses out of n_j ground motions for a given intensity measure IM $= im_j$, the likelihood for the entire set of intensity measures $j = 1, \ldots, m$ is defined as

$$\text{Likelihood} = \prod_{j=1}^{m} \binom{z_j}{n_j} [p_f(im_j)]^{z_j} [1 - p_f(im_j)]^{n_j - z_j} \tag{2.24}$$

where $p_f(im_j)$ is the probability that structure will reach a given limit state when subject to a ground motion with intensity measure im_j (Equation 2.20).

The parameters m_R and ζ_R of the fragility function are estimated by maximizing likelihood, that can be performed more easily by taking the logarithm of the likelihood function.

Hence the estimated parameters are obtained by the solution of

$$\left\{\widehat{m_R}, \widehat{\zeta_R}\right\} = \underset{m_R,\beta_R}{\arg\max} \sum_{j=1}^{m} \left\{ \ln \binom{z_j}{n_j} + z_j \ln\left[p_f(im_j)\right] + (n_j - z_j) \ln\left[1 - p_f(im_j)\right] \right\} \quad (2.25)$$

where the pair $(\widehat{m_R}, \widehat{\zeta_R})$ is the estimate of the fragility function parameters.

Using the least-squares method, the distribution parameters are estimated by solving the following optimization problem

$$\left\{\widehat{m_R}, \widehat{\zeta_R}\right\} = \underset{m_R,\beta_R}{\arg\min} \sum_{j=1}^{m} \left[\frac{z_i}{n_j} - p_f(im_j) \right]^2 \quad (2.26)$$

where the variables are the same as previously stated. If the method is employed in the log-transformed space, the optimization is performed with the following quantities $im_j^* = \ln(im_j)$ and $p_f^* = \Phi^{-1}\left(z_j/n_j\right)$.

From a statistical point of view, the maximum likelihood method is preferred, because the least-squares method ignores the fundamental property of the data that states the variance of the observed fractions of collapse is nonconstant. This property violates the requirements of least squares fitting [22]. Nevertheless, the least-squares regression method requires far fewer time history analyses to obtain an accurate fragility curve than the maximum likelihood approach [104].

The seismic fragility analysis of bridges is acknowledged as an efficient approach for asset management and retrofitting planning. Accordingly, this method has been extensively employed to assess the vulnerability of bridge portfolios [200, 248, 170] and to show the performance enhancement caused by retrofit measures, such as shear keys, expansion joints, restrainer cables, columns steel jacketing, seat extenders, steel plates, and seismic isolators [206, 207, 243, 259]. The impact of a vast diversity of parameters on the seismic vulnerability of bridges have been investigated with the use of fragility analysis, for instance seismic motion directionality [247], skew angle [270, 273, 274], and temporal evolution of seismic design principles [215, 216]. In all these cases, the fragility functions were built separately for each parameter of interest. Recent methods have combined these analyses into a single one, introducing the concept of parameterized fragility functions.

2.5.3 Parameterized fragility functions

The development of single-parameter seismic fragility curves evolved to the generation of parameterized fragility functions, which concomitantly depict the fragility with respect to a

seismic intensity measure and a set of system parameters (e.g., column reinforcement ratio, skew angle, span length, or time) [112]. It avoids the costly reanalysis for each new set of parameter combination that would be required using single-parameter fragility curves [109]. Moreover, it is sustained that a single intensity measure cannot fully represent the effect of an earthquake on the seismic response of the structure. Hence, it is expected that the use of more than one uncorrelated ground motion parameters would lead to a significant reduction in the scatter in the fragility function [105]. Therefore, a parameterized seismic fragility function is a multivariate conditional probability of reaching or exceeding a given damage state DS upon the observation of (at least) one seismic intensity measure IM $= im$ and a vector of parameters $\mathbf{P} = \mathbf{p}$, as expressed by:

$$p_f(im, \mathbf{p}) = \Pr(\text{DS}|\text{IM} = im, \mathbf{P} = \mathbf{p}) \tag{2.27}$$

For fragility surfaces involving two ground motion parameters, care must be taken in the selection of the IMs. Both parameters should be well correlated with the response of the structure in order to provide an efficient representation of the damage probability. Nevertheless, the two IM parameters should not be well correlated with each other in order to avoid such a surface to show nothing more than a single-parameter curve. A procedure for IM pair selection was proposed by [106] which is based on the ranking of ground motion parameters into clusters and a final judgment with respect to correlation coefficients.

Different methods to fit the analytical damage data to a fragility model have been proposed and depend on the dimensionality of the problem. Solutions to fitting fragility surfaces (bivariate fragility functions) may employ the maximum likelihood method to estimate the joint distribution parameters of a bivariate lognormal distribution in a similar way to fragility curves (e.g., [271]). Alternatively, regression can be employed upon the parameters of multiple fragility curves to build fragility surfaces, whereas multivariate parameterized fragility functions may be established using supervised learning techniques for classification.

Regression on the parameters of multiple fragility curves

Brandenberg et al. [53] proposed a methodology to developed demand fragility surfaces in which one conditional parameter was a seismic IM and the second variable was an engineering demand parameter. The methodology is based on the linear regression of the fragility parameters of multiple fragility curves. The fragility functions at every EDP level are assumed to follow a lognormal distribution with the following parameters: logarithmic

mean $\lambda_R = \ln(m_R)$, logarithmic standard deviation ζ_R, and peak probability $p_{f,\max}$. Linear regression is then performed in the logarithm of EDP to fit an intercept β_0 and a slope β_1 value for each fragility parameter, as follows:

$$\lambda_R = \beta_{0,\lambda} + \beta_{1,\lambda} \ln(edp) \tag{2.28}$$

$$\zeta_R = \beta_{0,\zeta} + \beta_{1,\zeta} \ln(edp) \tag{2.29}$$

$$p_{f,\max} = \beta_{0,p} + \beta_{1,p} \ln(edp) \leq 1 \tag{2.30}$$

Therefore, the demand fragility surface is fully defined by six regression coefficients as in:

$$\Pr(\text{EDP} < edp|\text{IM} = im) = \Phi\left(\frac{\ln(im) - [\beta_{0,\lambda} + \beta_{1,\lambda}\ln(edp)]}{\beta_{0,\zeta} + \beta_{1,\zeta}\ln(edp)}\right)[\beta_{0,p} + \beta_{1,p}\ln(edp)] \tag{2.31}$$

This method was used to assess the impact of the design era, structure type, and pile type on the fragility of bridge classes in California [53]. A similar formulation was adopted by Ghosh and Padgett [108] in the study of the time-dependent vulnerability of MSC steel girder bridges in the central and southeastern US due to corrosion in the reinforced concrete columns and steel bearings. In this case, however, the temporal increase of the bridge fragility along its service life was modeled by a quadratic law only on the median and dispersion of the fragility curves. The continuous time-dependent seismic fragility was thus formulated as:

$$\Pr(\text{DS}|\text{IM} = im, t) = \Phi\left(\frac{\ln(im) - \ln[\beta_{0,m} + \beta_{1,m}t + \beta_{2,m}t^2]}{\beta_{0,\zeta} + \beta_{1,\zeta}t + \beta_{2,\zeta}t^2}\right) \tag{2.32}$$

where $\beta_{i,m}$ and $\beta_{i,\zeta}$ $(i = 0, 1, 2)$ are the regression parameters of the quadratic model for the median and dispersion, respectively. This same model was also adopted in the generation of time-dependent seismic fragility curves of bridges subject to variation of scour depth [119].

More recently, Segura et al. [231] coupled the Brandenberg's method with the use of multiple-stripe analysis [124] to fit fragility surfaces. Moreover, the formulation was generalized to any type of probabilistic distribution CDF to fit the multiple fragility curves (e.g., lognormal, normal, or Weibull), and arbitrary basis function for the regression on the fragility parameters (e.g., polynomial, exponential, or Gaussian). Hence, the fragility surface is defined as:

$$\Pr(\text{DS}|\text{IM} = im, p) = F\left(im; \boldsymbol{\Theta}(p)\right) \tag{2.33}$$

where $F(\cdot)$ is the CDF of a given distribution on IM with parameters $\boldsymbol{\Theta}$, which in turn are functions of the predictor p. The choice of the best combination of distribution type and basis function for the CDF parameters can be based, for instance, on cross-validation. This formulation was used to investigate the impact of several structural variables on the seismic performance of a concrete gravity dam in eastern Canada, and it was facilitated through the use of a surrogate demand model [231].

Classification techniques

Building a parameterized fragility function can be seen as a problem of distinguishing between two regions of either damage state exceedance or non-exceedance. And supervised learning techniques for discrete data (i.e., classification) are well suited for this task [186, 136]. Several classification techniques are available in the literature, and the most adopted in fragility assessment are notably logistic regression (LR), support vector machines (SVM), and random forest (RF). These classification methods are briefly discussed next. Other data-driven algorithms, such as naïve Bayes, linear discriminant analysis, quadratic discriminant analysis, or Gaussian process classification have not popularized as much in fragility or risk assessment [265], and are not discussed here.

Logistic regression, as a regression-based classifier, is the extension of linear regression (e.g., Equation 2.12) for classification problems and, consequently, LR is commonly outperformed by other classification algorithms. Nonetheless, its prevalence, historical importance, and simple formulation make it a popular choice in fragility analysis (e.g., [25, 141, 109, 110, 218, 128, 33]). Logistic regression is commonly used for data classification as a multivariate technique to estimate the probability that an event occurs when discrete outcomes are present (e.g., the damage state exceedance DS = 1 or non-exceedance DS = 0). The general form of the logistic regression model applied to estimate the probability of DS exceedance conditioned on the seismic intensity measure and a vector of structural predictors is:

$$\Pr(\text{DS}|\text{IM} = im, \mathbf{P} = \mathbf{p}) = \frac{\mathrm{e}^{g(im,\mathbf{p})}}{1 + \mathrm{e}^{g(im,\mathbf{p})}} \tag{2.34}$$

where $g(\mathbf{x})$ is the logit function, which usually consists of a linear combination of basis functions on the predictors $\mathbf{x} = [im, \mathbf{p}]$, whose coefficients are estimated by the maximum likelihood method [2]. Conversely to linear regression, it is not possible to find a closed-form solution for the coefficients using maximum likelihood estimation and therefore an iterative method is used to solve for them [117]. Regularization techniques (e.g., Lasso, ridge, or elastic net) can be integrated to LR to allow for identification of relevant predictors and to remove less significant variables of the fragility function [169]. The ease on

interpreting the coefficients of a LR model is one of the main attractive features of this algorithm for fragility analysis [141]. A standardization of the predictors before training the model facilitates the interpretability and the comparison of the importance between predictors.

Support vector machines are based on the structural risk minimization principle and aim at minimizing an upper bound of the generalization error. A binary SVM uses a number of support vectors which are a subset of the training data to construct a hyperplane to define the boundary between the two classes. In SVMs, some nonlinear kernel functions are used to map the training data into a higher dimensional feature where the data are linearly separable. There can be more than one possible hyperplane to separate the data so the one with the maximum margin on separation will be selected. The use of nonlinear kernel function enables the SVMs to define complex decision functions, optimally separating two classes of data samples [41, 186, 163].

A random forest is a large set of uncorrelated decision trees (DT) to classify the categorical data based on the model parameters. Decision trees are a machine-learning algorithm that recursively partitions the input space and defines a local model in each resulting region of the input space. A cost function is applied together with a greedy construction procedure to find the optimal partitioning of the data. To overcome the potential overfitting and instability issues associated with a single tree, RF constructs a multitude of DTs at training and outputs the mean predictions of individual trees. The training algorithm generates RFs by bootstrap aggregating or bagging. In order to keep uncorrelated predictors in the final model, RF uses a randomly selected subset of the problem variables in the DTs [186]. Random forests are easy to train and implement and, in contrast to other methods, random forests are not sensitive to outliers. Each decision tree tests the input model parameters, and predicts the structure failure. Therefore, unlike SVMs, each decision tree is easy to interpret. The trained random forest model decides the structure failure class for the given model parameters based on the majority vote:

$$P_f = \text{majority vote}\left\{P_n(\mathbf{x})\right\}_1^N \tag{2.35}$$

where P_n is the vote cast by the nth tree and N is the total number of trees [12].

In general, the evaluation of the prediction capabilities of a classification model comprises quantifying the number of successful classification against misclassifications, and several methods are found in the literature for this task. One of the simplest methods is the confusion matrix. For a binary dependent variable, a confusion matrix depicts the percentages

of true positive, true negative, false positive, and false negative. These four values can also be combined into the misclassification error (ME), which is one the most common goodness-of-fit measures for classifier models. Although this is not the definition of the mean square error MSE, for binary data, the ME provides the same numeric value as MSE. Hence, it can be used to compare classifier models even with those based on regression, for instance, the logistic regression model. Another metric that is widely used as a measure of goodness-of-fit in statistical learning is the accuracy, which by definition is $1 - ME$. Furthermore, the confusion matrix also offers valuable insight into the performance of surrogate models as classifiers by comparing the actual versus the predicted class of data [12].

2.6 Performance enhancement using laminated-rubber isolators

Enhancing the seismic performance of an existing bridge can be achieved by means of retrofitting, which consists on the practice of modifying structures and structural components or adding supplementary elements to reduce their overall seismic vulnerability [263]. Structural damages observed during seismic events are due to the dissipation of the energy input on the structure by the earthquake. To avoid or mitigate these damages, the main tools in seismic engineering of bridges consist on reducing the amount of induced energy, strengthening key components, providing the bridge with means of dissipating energy other than deteriorating its components, or any combination of the three. Examples of retrofitting measures for highway bridges involve column jacketing, isolation with elastomeric bearings, stability enhancement of footings, and installation of restrainer cables, seat extenders, or shear keys, to name a few [204, 214]. The effectiveness of the retrofit measure in improving system fragility is conditional to which bridge type and damage state are being investigated [207]. For instance, replacing steel bearings with elastomeric isolators could reduce significantly the vulnerability to slight damage of MSC concrete girder bridges in the CSUS (Figure 2.7a), while bent columns could be efficiently protected by the installation of natural rubber isolators in Quebec, reducing the system fragility against slight damage for the same type of bridge (Figure 2.7).

Seismic isolation with elastomeric bearings also showed to effectively reduce the fragility for more severe damage states, although to a lesser extent than for slight damage [207, 243]. The main advantage of seismic design with isolation is the immediate post-event serviceability of the bridge, given that the substructure is expected to remain elastic with minor or no damage. Moreover, as seismic forces are significantly reduced, the demand on

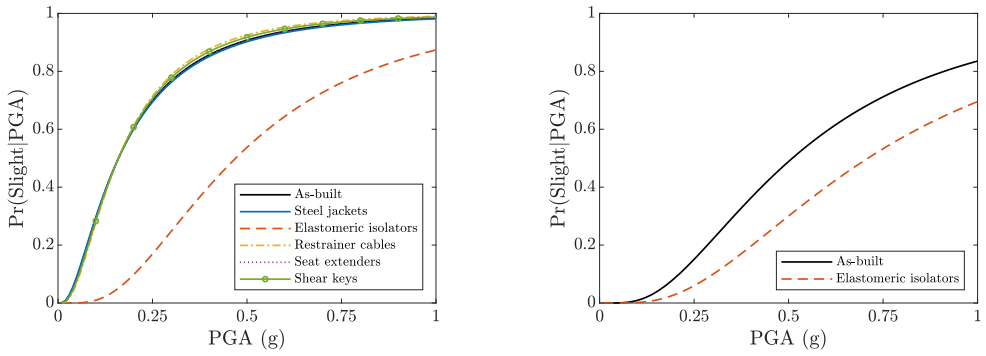

(a) **(b)**

Figure 2.7 Fragility curves MSC concrete girder bridge class in (a) CSUS and (b) Quebec considering retrofitting options (respectively based on data by Padgett and DesRoches [207] and Siqueira et al. [243])

the conventional construction materials is also less important. The construction costs of an isolated structure are comparable or in some cases even lower than traditional seismically designed counterparts with the major advantage that no reparation is required after a strong earthquake [226, 266]. This retrofitting technique is further detailed with respect to its principles, common types of isolation units, and potential issues that should be addressed in the study of the seismic response of bridges isolated with natural rubber bearings.

2.6.1 The principle of seismic isolation

Two main classes of seismic control methods are distinguished with respect to the adopted damage mitigation approach: (i) frequency-dependent methods, which shifts the structural natural frequencies out of the earthquake's dominant frequencies; or (ii) the frequency-independent methods, which focus only on energy dissipation. From these classes, seismic control methods are further categorized as active, passive, semi-active, or hybrid. Amongst them, seismic isolation is thus classified as a passive, non-resonant, frequency-dependent method [144]. Based on the vibration isolation theory, the principle of seismic base isolation is characterized by the modification of a structure's global stiffness with the goal of decoupling the structure movement from the excitation source (i.e., from the soil in the seismic case). This decoupling is achieved by the introduction of flexible elements into the lateral stiffening system of the structure. Consequently, the structure's fundamental frequencies are lowered and shifted from the range of seismic dominant frequencies. Because the vibration modes are orthogonal with respect to mass and stiffness, a significant part of the seismic energy is reflected or transmitted to vibration modes that have a weak influence on the structural response. Additionally, the presence of a damping device per-

forms the dissipation of the part of the seismic energy that is transmitted to the structure. The greater flexibility may also cause large displacements of the superstructure (the isolated part of the structure) and the damping devices are responsible for keeping the those displacements in an acceptable range.

In a conventional structure, all the seismic energy is transferred to the elements in the form of strain energy. For low damping materials (e.g., concrete), energy dissipation takes place by causing the deterioration of structural elements. For instance, in the case of highway bridges, plastic hinges are formed at the ends of pier columns during a severe ground shake (Figure 2.8a). This phenomenon is explained by the large inertial forces that come from the superstructure (where the largest portion of the mass is concentrated) into the pier columns. By decoupling the bridge's superstructure (i.e., deck and girders) from its substructure (i.e., piers, abutments, and foundation) by means of seismic isolation, weaker inertial forces are transmitted to the pier columns, thus avoiding extensive damage to these elements (Figure 2.8b).

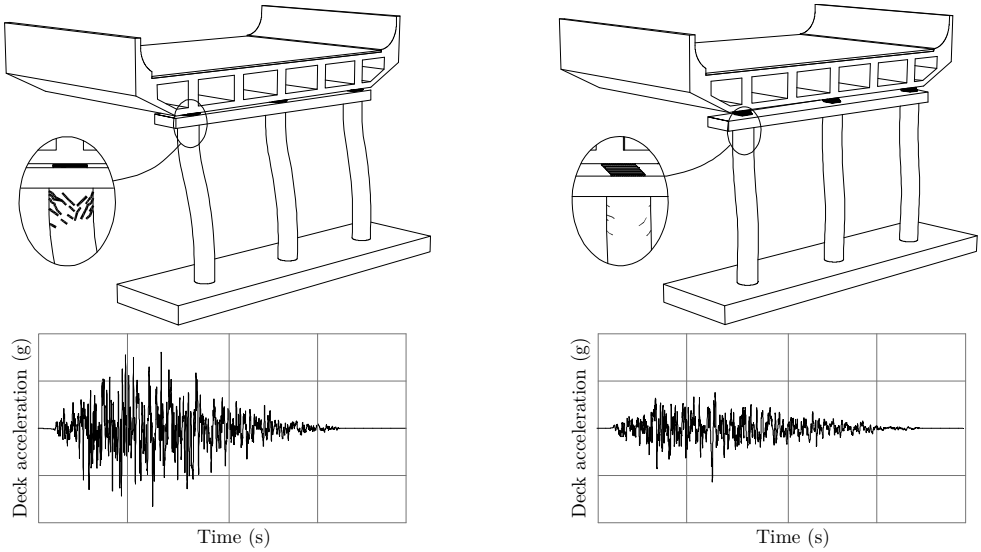

(a) Conventional seismic design (b) Seismic design with isolation

Figure 2.8 Principle of bridge seismic isolation (adapted from Sanda [226])

Isolation units composed by flexible devices are the most commonly used, and the majority of them employ elastomeric isolators due to their low costs for production, installation, and maintenance. Several types of seismic isolation devices are found in the market, for instance elastomeric bearings, friction pendulum system, Eradiquake system, shape memory alloys, resilient friction-based isolator, and rocking system. Elastomeric isolators are one of the most employed types of isolation methods in the United States of America [54].

2.6.2 Laminated-rubber seismic isolators

Laminated rubber isolators are composed by rubber layers (natural or synthetic) intercalated by galvanized steel sheets (Figure 2.9). The former is responsible for providing lateral flexibility to the isolation unit, whereas the latter confines laterally the rubber layers while providing vertical stiffness. Therefore, laminated rubber isolators are capable of sustaining large vertical (gravity) loads while still being laterally flexible. Finally, an external rubber cover prevents the steel sheets and the confined rubber layers from being deteriorated by corrosion or ozone [173, 189]. Although natural rubber bearings (NRB) present a viscoelastic behavior, its damping characteristics can be improved by either modifying the rubber composition to create high-damping rubber bearings (HDRB), or a lead core can be introduced in the isolation unit in lead-rubber bearings (LRB) (Figure 2.9b). Lead cores increaseds the characteristic strength of the isolator (or the force intersect at zero displacement), while the rubber dictates the post-elastic stiffness of the device, showing increased capacity to dissipate energy [126].

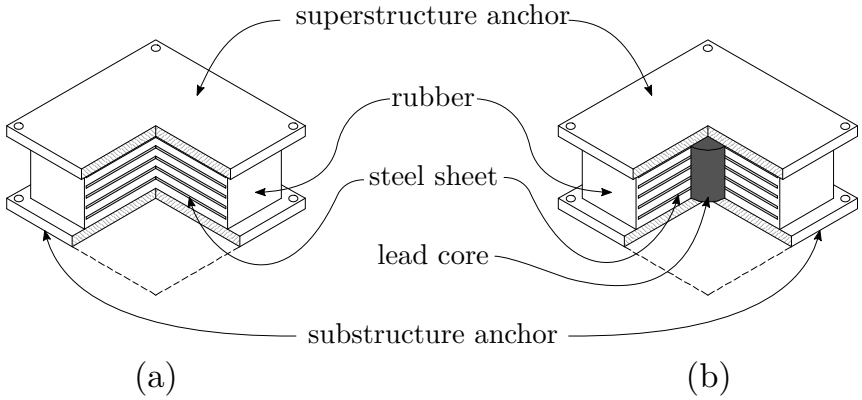

Figure 2.9 Typical rubber isolators: (a) NRB/HDRB and (b) LRB (adapted from Mayes and Naeim [173])

The hysteretic lateral behavior of elastomeric isolators is essentially viscoelastic. To simulate this behavior, several approximative models are found in the literature, varying from simple models superposing a linear behavior to sophisticated models that can take into account effects such as crystallization, strain frequency, and strain history (Figure 2.10). The choice on which model to be used depends on the level of structural complexity, the required accuracy, and the type of mechanical behavior of interest. In practice, the linear viscoelastic and the bilinear models are often chosen for their simplicity. Yet, several approaches are found to model the nonlinear hysteretic behavior of rubber-based isolators [226].

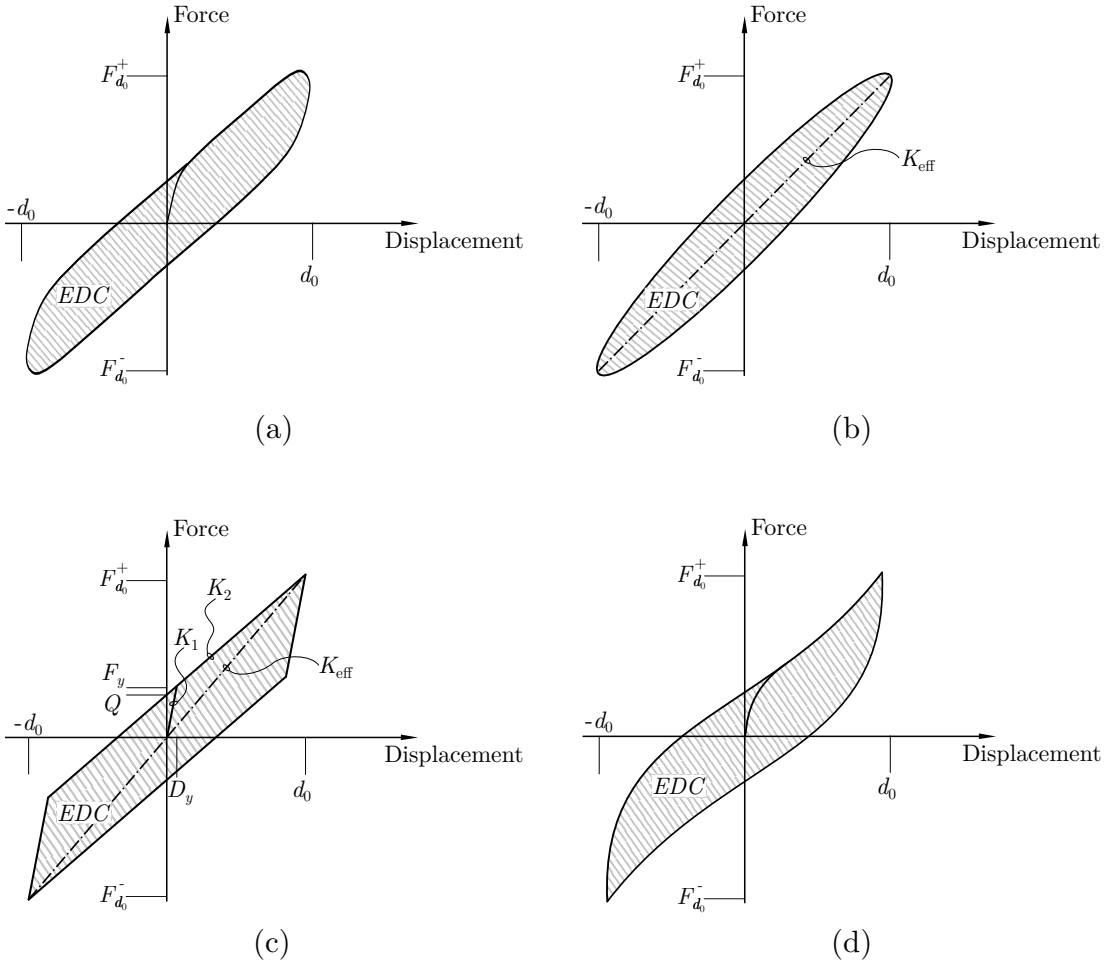

Figure 2.10 Hysteretic behavior of elastomeric isolators: (a) real, (b) linear viscoelastic model, (c) bilinear model, and (d) nonlinear model

The linear viscoelastic model (Figure 2.10b) is the simplest to represent the dynamic behavior of elastomeric isolators. It combines the linear elastic response to a perfectly viscous behavior, and it is fully represented by two parameters: the effective lateral stiffness K_{eff} and the effective damping ratio ξ_{eff}. The effective lateral stiffness can be estimated using the amplitudes of displacements d_0 and respective forces as

$$K_{\text{eff}} = \frac{F^+_{d_0} - F^-_{d_0}}{2d_0} \tag{2.36}$$

while the effective damping ratio is proportional to the energy dissipated per cycle (EDC), measured by the area inclosed by the hysteretic curve

$$\xi_{\text{eff}} = \frac{\text{EDC}}{2\pi K_{\text{eff}} d_0^2} \tag{2.37}$$

The linear viscoelastic model is the basis for modal analysis methods. It predicts with good accuracy the response of elastomeric isolators for small to moderate shear strains (i.e., up to 100%). When lateral deformations are large, the hysteretic curve of the linear viscoelastic model deviates significantly from the real behavior, and a bilinear modeling may be recommended [226].

The bilinear modeling (Figure 2.10c) is the approach most often found in practice. The model is able to represent the response of conventional rubber isolators (NRB and HDRB) and lead-rubber bearings. This idealization can be fully represented by the initial (elastic) stiffness K_1, the post-activation stiffness K_2, and the characteristic strength Q. These parameters are typically obtained from available hysteresis loop of rubber bearing tests. Usually, K_1 varies in the range of 2 to 15 times K_2 for natural rubber bearings (NRB) and high-damping rubber bearings (HDRB) [204]. The post-activation stiffness K_2 can also be based on the effective stiffness, characteristic strength and design displacement [189]. Additionally, according to characterization tests of elastomeric bearings [122], the activation displacement D_y can be approximated as 10% of the total rubber height. The damping capacity of the isolator is intrinsically related to the energy dissipated per cycle (EDC), and the effective damping ratio as in Equation 2.37.

A range of nonlinear hysteretic models (Figure 2.10d) are found in the literature, from simple uncoupled models [137]—which can better capture large strain hardening effects than the preceding linear and bilinear models—to more advanced modeling. For instance, Kumar et al [143] proposed a finite-element formulation comprising: coupled bidirectional motion in horizontal direction, coupled horizontal and vertical motion, cavitation and post-cavitation behavior in tension, strength degradation in cyclic tensile loading due to cavitation, variation in critical buckling load capacity due to lateral displacement, and strength degradation in cyclic shear loading due to heating of lead core (when applicable). This model was proposed for the seismic isolation of nuclear power plants, for which the design ground motion return period is in the order of $10,000$ years, in opposition to $2,475$-year return period for lifeline bridges [143, 57].

Elastomers are produced by the combination of polymers and ingredients that passes through a vulcanization process, which enhances its mechanical properties. Elastomeric compounds typically encountered in structural engineering applications are formed from polychloroprene (neoprene) or polyisoprene (natural rubber) with hardness values ranging between approximately 50 and 70 on the Shore A scale [217, 107]. Although elastomers are often classified by their hardness, the behavior of elastomeric seismic isolators is greatly influenced by the mechanical properties of the rubber layers, mainly by its shear modulus

G, which poorly correlates with hardness [272]. Natural rubber presents a complex nonlinear behavior that depends on several factors such as temperature, strain amplitude, strain history, strain rate, and age [68]. The satisfactory design of an elastomeric isolator should account for all these factors and the respective variation in the seismic response. If the lateral stiffness of an isolating system is underestimated, substructure elements might be damaged by seismic forces that are larger than expected from design. Conversely, in the case that lateral stiffness is overestimated, instability issues may take place due to larger than expected displacements. A safe design of an isolation system requires a thorough comprehension of these factors and their consequences to the response of the isolation units. The present study, however, focuses on the thermal stiffening of rubber at low temperatures and its potential effects on the bridge seismic performance.

2.6.3 Rubber thermal stiffening and its impacts on performance

Elastomers are complex viscoelastic materials, and thermal stiffening may increase significantly their reference (room) temperature stiffness, with two main distinguished processes: the instantaneous and the time-dependent stiffening (Figure 2.11) [267, 68]. The ratio G_θ/G_0 of the shear modulus at low temperature and reference temperature (usually 20 °C) has been reported as high as 4 for natural rubber and 8 for neoprene when conditioned at low temperature for several days [272]. Additionally, rubber may become brittle at extremely low temperatures (approximately -45 °C for neoprene and -65 °C for natural rubber [153]), phenomenon known as glass-transition. All these phenomena are completely reversed as temperature rises back to reference levels [187, 83, 246]. It is noted that the effects of crystallization and thermal stiffening are more pronounced on neoprene than on natural rubber, suggesting that the latter is better for low-temperature applications, as in the case of highway bridges in cold climates like in Northern Canada or Alaska [272]. In effect, the most commonly used elastomer in the U.S. and Canada is natural rubber due to its higher seismic performance when compared to synthetic rubbers like neoprene when high levels shear strains are required [54, 245]. Nevertheless, natural rubber may undergo important stiffening at low temperatures, and its consequences must be considered in the design of natural rubber isolators.

For seismic applications, the effect of low levels of crystallization is highly deleterious to performance even after the yielding produced by a large deformation cycle [267, 268, 101]. Indeed, stiffer isolators may cause the transmission of larger inertial forces to the substructure than expected when designed for reference temperature. Research has been developed on the behavior of elastomeric bearing and isolation devices post-elastic (or post-activation) stiffness and characteristic strength at subfreezing temperatures. Some

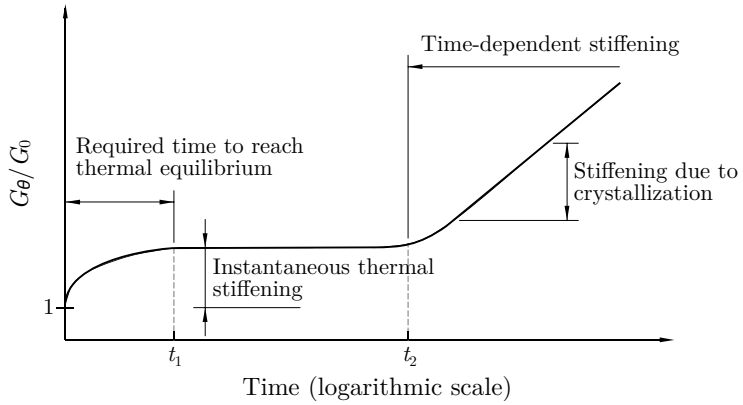

Figure 2.11 Rubber thermal stiffening under subfreezing temperatures (adapted from Constantinou et al. [68])

of these works established modification factors to be multiplied by nominal (at room temperature) properties to obtain the modified mechanical properties under the effect of low temperatures [69, 267, 268, 70]. Design standards often suggest the use of these modification factors when performing bounding analyses to account for the effect of variation of mechanical properties of isolators on the structural response. In simulating cold weather conditions, maximum expected system properties are employed to assess the upper-bound response, which is characterized by highest force levels transmitted to the substructure. For instance, the CSA S6-14 suggests the use of the modification factors proposed by [70] in case no experimental values on the chosen isolation unit are available, while the AASHTO-14 [5] presents their own values for similar cases.

More recently, Cardone et al. [59] and Cardone and Gesualdi [58] reported the results of a comprehensive experimental program on the effects of thermal stiffening on the mechanical properties of rubber compounds typically employed in isolation units. The tests comprised both instantaneous and time-dependent stiffening processes. Empirical equations were defined to translate the low temperature effect on four nominal properties of the rubber compounds, namely secant shear modulus, maximum shear stress, shear stress at zero strain, and effective damping ratio. It was argued, however, that the time-dependent stiffening of rubber was a rather complex phenomenon to be modeled in seismic isolators due to in-service behavior aspects. The rubber shear modulus increased from 1.5 to 2.5 times after 24 h exposed at $-20\,^{\circ}$C at low shear strain amplitudes (compatible to those by seismic isolators under low-intensity earthquake), whilst a lower variation was observed when large strains were applied to the specimens (compatible to those attained by isolators subjected to strong ground shaking). The laboratory results also suggested that the equivalent damping was practically insensitive to prolonged exposure to low

temperatures. Finally, the differences of increasing and constant strain amplitude cyclic tests, and their consequences to rubber thermal stiffening are discussed. While cyclic tests with increasing strain amplitude are deemed to be representative of the structural response to far-fault earthquakes, constant amplitude cyclic tests are more suitable to simulate the seismic response under near-fault conditions. Near-fault earthquakes are characterized by a single large impulse of motion, which forces the structure to absorb a large amount of energy nearly instantaneously, with a few large plastic cycles [65, 172]. The main observed effect of rubber thermal crystallization was an increase of the force levels transmitted by the isolation system to the structure during the first loading cycle. Consequently, the relative importance of cyclic response for structures grows at greater distance from the epicenter, while time-dependent stiffening effects dissipate due to internal heating of the isolator. Conversely, the structural response is governed by the peak response in near-fault conditions, which may be substantially affected by the thermal crystallization.

The CSA S6-14 requires specific cyclic displacement test protocols for designed isolator units to guarantee the adequacy of the tested properties with respect to the design values [57, 56]. At reference temperature, isolators must be tested with a displacement amplitude equal to $0.8d_t$, where d_t is the total design displacement, which comprises the seismic design displacement d_s and any offset displacements caused by other sources, including bridge deformations from shrinkage of concrete or temperature changes. The design displacement is determined according to the design ground motion with a probability of exceedance of 2% in 50 years. At low temperatures, isolation units must be first conditioned for 14 days under minimum service temperature (obtained from an isotherm map of historical minimum mean daily temperatures recorded over at least 30 years up to 1970). Then, the isolator is submitted to nine displacement cycles up to 60% of the seismic design displacement d_s, simulating the demand from a smaller earthquake when the temperature reaches its minimum level. After these nine cycles, the temperature of the specimen is expected to have increased due to energy dissipation. Therefore, the isolator must be cooled again until the core reaches a temperature that equals the concomitant minimum temperature, defined as the average between 15 °C and the minimum service temperature. Finally, the specimen is tested under displacement cycles up to $0.8d_t$, justified as a condition that would be more likely to exist when the displacement demand equals the seismic design displacement.

It is noted that the CSA S6-14 design criteria for isolators propose a compromise between the expected seismic hazard and cold weather conditions with the objective of simplifying the design process for practicing engineers. To assess the efficacy of the code's require-

ments, Guay and Bouaanani [118] evaluated the frequency of reaching low temperatures at several locations in Canada. Climate data collect by almost 6 500 weather stations across the country were analyzed to assess the likelihood of exposing bridge isolators to instantaneous thermal stiffening and to crystallization (time-dependent stiffening). It was suggested that the annual probability of the minimal average daily temperature being lower than the concomitant temperature specified by the Canadian code had a large variability across Canada, attributing it to the fact that the concomitant temperature considered in the code is not based on a probabilistic analysis. A probabilistic framework was thus recommended to establish the concomitant temperature to the design earthquake, even if the concurrent event of prolonged low temperature and earthquake shaking was deemed extremely improbable.

In effect, a few probabilistic assessments of the seismic response of isolated bridges in cold regions have been performed recently. However, none of the previous studies stated whether the bridge was originally isolated or retrofitted. Nassar et al. [190] proposed a reliability-based methodology to estimate the probability of collapse (and the respective reliability index) of isolated bridges using Monte Carlo simulations considering uncertainties with respect to the seismic hazard, temperature, and material properties. Linear elastic spectral analyses on a simplified single-degree-of-freedom system equivalent to a two-span bridge isolated with LRBs was adopted as case study to demonstrate the methodology. Hourly temperature data at Montreal, Canada were used to represent the variation of temperature during the different seasons, and column and isolator limit states were considered for the collapse. It was concluded that not considering the effect of low temperature within the design process led to a larger probability of failure for the case-study bridge, whilst using the minimum average daily temperature of the site concomitantly with the design earthquake would result in an excessively conservative design.

Billah and Todorov [40] used IDA-based fragility curves to investigate the effect of winter temperatures on a seven-span continuous highway bridge isolated with LRBs, also located in Montreal. The mechanical properties of the LRBs were provided by a manufacturer for winter and summer conditions. Fragility curves of the bridge components and the system (using upper and lower bounds according to Equation 2.17) demonstrated the negative impact of winter temperatures on the seismic performance. More precisely, piers, LRBs, and the whole bridge were more likely to undergo moderate, extensive, and complete damage during winter conditions (at $-30\,^{\circ}\mathrm{C}$) compared to summer conditions (at $+25\,^{\circ}\mathrm{C}$). It is important to highlight that intermediate damage states were adopted for the LRBs based on values for typically used for elastomeric bearing pads. Experimental tests suggest,

however, that intermediate damage states on rubber isolators are hardly detected by visual inspection, and signs of damage are usually observed only when the isolator fails by either shear failure or buckling [103, 225].

Finally, also using IDA, Fosoul and Tait [98] investigated the seismic fragility of a nine-span continuous concrete bridge in Ottawa, Canada in room (at $+20\,^{\circ}\mathrm{C}$) and cold (at $-37\,^{\circ}\mathrm{C}$) temperatures. The bridge is seismically isolated by means of unbonded fiber-reinforced elastomeric isolators (U-FREI), which use fiber fabrics as reinforcement layers instead of steel shims, and show a lateral behavior that comprises successive softening and stiffening due to rollover. Modeling properties of the U-FREIs were based on laboratory tests in both temperature conditions to account for thermal stiffening [228]. Cold temperature had a positive impact in reducing the overall fragility of abutment soil in both passive and active actions, whereas columns had their fragility increased in low temperature for slight and moderate damage states. A slight decrease on the fragility of the columns at extensive and complete damage states was observed.

2.7 Summary

A review of the current state-of-the-art has provided insight into the current practice and research gaps relating to assessment of the seismic performance of highway bridges. The main focus of this review is related to the use of analytical seismic fragility analysis in the context of performance-based earthquake engineering. The review exposed the features of a systematic framework to treat uncertainties in seismic risk assessments. First, uncertainties related to the seismic input are based on the site hazard characterization and consistent ground motion record selection. After, from the numerical response history analysis, uncertainties on the observed seismic demand due to record-to-record variability are handled by probabilistic seismic demand models. Two strong assumptions are identified in traditional multivariate probabilistic seismic demand modeling: lognormality and linear dependence. These assumptions have been criticized in past studies and their impact on fragility estimates in not fully understood. The coupling of an optimal strategy for demand data collection (i.e., MSA) with an eminently flexible joint density modeling method (i.e., Gaussian mixture) is presented in Chapter 3 to challenge traditional hypotheses and to assess the potential bias in system fragility analysis.

Finally, research gaps are identified in the seismic performance assessment of retrofitted bridges with rubber isolators in cold regions. First, previous work did not stated if the investigated bridges were either originally isolated or retrofitted with rubber isolators. An important difference between these two types of configuration is related to provided

clearances. While bridges designed with isolators must provide sufficient clearances so the isolators perform without impediment, retrofitted bridges have original clearances that may not respect service displacement requirements. Additionally, temperature has been considered in two discrete scenarios in recent fragility studies (i.e., summer and winter). The continuous impact of low temperatures on the seismic performance cannot be appreciated in this case. The single study that adopted continuous temperature in reliability analysis (e.g., [190]) used a simplified one-degree-of-freedom model of a single-column bent. This model cannot represent the complexity of multicomponent bridges and the interaction between components that may be essential to study the system fragility. To address these gaps, Chapter 4 presents the fragility surfaces generated on the component and system levels for a retrofitted bridge in Eastern Canada considering the concurrent events of seismic and low temperature. This study reveals beneficial interactions between bridge components in ensuring the protection of bent columns and provides meaningful insights for the challenge of retrofitting bridges in extreme environments.

CHAPTER 3

SEISMIC FRAGILITY OF BRIDGES: AN APPROACH COUPLING MULTIPLE-STRIPE ANALYSIS AND GAUSSIAN MIXTURE FOR MULTICOMPONENT STRUCTURES

Avant-propos

Auteurs et affiliation :
P.A.C. Bandini : étudiant au doctorat, Université de Sherbrooke, Faculté de génie, Departement de génie civil et de génie du bâtiment
J.E. Padgett : professeur, Rice University, Department of civil and environmental engineering
P.Paultre : professeur, , Université de Sherbrooke, Faculté de génie, Departement de génie civil et de génie du bâtiment
G.H. Siqueira : professeur, University of Campinas, School of civil engineering, architecture, and urbanism, Department of structures

Date de soumission : 15 avril 2020
État de l'acceptation : accepté pour publication le 7 juillet 2021
Revue : Earthquake Spectra
Titre français : La fragilité sismique des ponts : une approche couplant l'analyse à bandes multiples et mélange gaussien pour des structures à plusieurs componsants
Contribution au document :
Une nouvelle approche est proposée pour modéliser la densité conjointe de la demande sismique des structures multicomposantes, qui bénéficie de la structure en bandes des données de demande générées selon l'analyse à bandes multiples, et de la modélisation raffinée de la densité par des mélanges Gaussiens. La méthodologie proposée est donc éminemment flexible en termes d'hypothèses adoptées et elle est utilisée pour évaluer le biais potentiel introduit dans les calculs de fragilité causé par les hypothèses restrictives trouvées dans les méthodologies plus traditionnelles.
Résumé français :

Une approche est développée pour construire des modèles probabilistes multivariés de demande sismique (PDSM) de structures à composants multiples, basés sur le couplage de l'analyse à bandes multiples et de modèles de mélange gaussien. La méthodologie proposée est éminemment flexible en matière d'hypothèses adoptées. Un pont routier classique dans l'est du Canada est utilisé pour présenter une application de la nouvelle approche et pour étudier son impact sur l'analyse de la fragilité sismique. Les méthodes traditionnelles de PSDM utilisent une distribution lognormale et une corrélation linéaire entre des paires de composants pour ajuster les données de réponse sismique, ce qui peut conduire à une modélisation statistique erronée. En utilisant des accélérogrammes rigoureusement sélectionnés pour le site étudié, les données sont générées par l'analyse de l'historique de la réponse et des tests statistiques appropriés sont ensuite effectués pour montrer que ces hypothèses ne sont pas toujours valables sur les données de réponse du pont étudié. La structure groupée de la méthodologie proposée permet la construction d'une PSDM multivariée qui correspond mieux aux données de réponse corrélées que les méthodes traditionnelles, en introduisant un faible biais dans les fonctions de fragilité et la fréquence annuelle moyenne de violation des états de dommage, qui sont des caractéristiques cruciales pour la prise de décision dans le contexte de l'ingénierie sismique basée sur les performances.
Note :À la suite des corrections demandées par les membres du jury, le contenu de cet article diffère de celui qui a été soumis.

Abstract:
An approach is developed to build multivariate probabilistic seismic demand models (PDSMs) of multicomponent structures based on the coupling of multiple-stripe analysis and Gaussian mixture models. The proposed methodology is eminently flexible in terms of adopted assumptions, and a classic highway bridge in Eastern Canada is used to present an application of the new approach and to investigate its impact on seismic fragility analysis. Traditional PSDM methods employ lognormal distribution and linear correlation between pairs of components to fit the seismic response data, which may lead to poor statistical modeling. Using ground motion records rigorously selected for the investigated site, data are generated via response history analysis, and appropriate statistical tests are then performed to show that these hypotheses are not always valid on the response data of the case-study bridge. The clustering feature of the proposed methodology allows the construction of a multivariate PSDM with refined fitting to the correlated response data, introducing low bias into the fragility functions and mean annual frequency of violating damage states, which are crucial features for decision making in the context of performance-based seismic engineering.

Keywords: Bridges, Seismic fragility, Probabilistic seismic demand model, Component-level, Gaussian mixture, Multiple-stripe analysis

3.1 Introduction

Performance-based earthquake engineering (PBEE) promotes the concept that designed structures are expected to perform according to predefined standards during probable earthquakes, including uncertainties inherent in the evaluation of the potential hazard and in the quantification of the structural response. Intermediate steps of a PBEE probabilistic framework may include the definition of a model that establishes the probabilistic relationship between an engineering demand parameter (EDP) and the seismic intensity measure (IM). This model is known as a probabilistic seismic demand model (PSDM) and is widely employed in constructing analytical fragility functions, common tools for the assessment of seismic performance of structures [158]. In PBEE, performance criteria relate damage limit states to required structural functionality, and for multicomponent structures, such as highway bridges, damage limit states are formulated at two levels: component and system. Often, component level damages are used to estimate repair actions and costs, while system-level performance from this combination of component damages often relates to outcomes such as lane closures, load or speed restrictions [160, 199, 206, 243, 127]. Past studies proposed methodologies to develop PSDMs that consider the contribution of multiple critical components based on system reliability and acknowledging the existence of correlation between pairs of structural component responses [102, 157]; the framework proposed by [199] has been broadly employed in analytical assessments of the seismic fragility of highway bridges since then [206, 250, 273, 243, 216].

Fragility functions are inherently uncertain quantities subject to numerous sources of both aleatory and epistemic uncertainty; one source is intrinsically related to the hypotheses adopted in the development of probabilistic seismic demand models, and significant bias may be introduced if imperfect modeling assumptions are adopted [82, 20]. A crucial step in the construction of a PSDM is the generation of structural response data with typical strategies including (i) cloud analysis (e.g., [158, 199, 206]), (ii) incremental dynamic analysis (IDA) [256], and (iii) multiple-stripe analysis (MSA) [124]. Each collection strategy presents advantages in terms of choice of record selection and scaling, practicality, and adopted hypotheses [161, 87, 104, 22]. Once demand data are gathered, a PSDM is traditionally built using simple techniques such as linear regression (when cloud analysis is used) or fitting parametric distributions—usually lognormal—if IDA or MSA is employed.

It is often assumed, for simplicity and tractability, that (i) demand follows a normal distribution in the logarithmic space (lognormality), (ii) the variability of the demand is constant and independent of the IM level (homoscedasticity), and (iii) component responses are linearly correlated (linear dependence). The impacts of homoscedasticity on fragility are acknowledged, and alternatives to avoid it are the use of a data collection strategy that allows one to calculate the variation of dispersion (for instance, MSA or IDA) [241, 20] or the adoption of piecewise linear regression when cloud analysis is chosen [158, 99]. Lognormality of seismic structural demand has been validated in some studies—usually using either single-degree-of-freedom or two-dimensional frame models (e.g., [237, 77, 10, 123])—and rejected as a general assumption by others—who considered more complex systems such as highway bridges (e.g., [130, 168]). The bias propagated into fragility functions of bridge components due to the lack of fit of seismic response data to a lognormal distribution, however, was deemed generally negligible by [130], whereas [168] suggested that it had lead to low impact on the fragility median and larger effect on the fragility dispersion. With respect to the dependence between pairs of component responses, typical cloud analysis (e.g., [199, 111]) considers the entire dataset of observed demands to estimate linear correlation coefficients, assuming that the correlation of component responses is linear and independent of the seismic intensity level. Still in the scope of cloud analysis, [278] proposed the use of vine copulas to model nonlinear dependence between bridge components and suggested that the assumption of linear dependence may have biased the built seismic fragility functions for a two-span case-study bridge. In contrast, [157] had already investigated the importance of correlation between component responses in long multispan bridges and observed its strong dependence on the level of seismic intensity and on the number of response history analyses (RHA).

Contemporary computational resources and data availability have also allowed the use of alternative machine learning techniques, applying supervised techniques for regression, for instance, polynomial response surfaces [111, 128, 264], artificial neural networks [166], partial least square regression [85], and random forest [168], or unsupervised learning for density modeling, such as kernel density estimator [130]. These learning techniques may employ parametric or nonparametric approaches to better model the observed seismic demand data. Although these approaches are more flexible, some of the resulting models still rely on unverified hypotheses (e.g., linear dependence).

One can thus conclude that there is still no consensus on the validity of traditional hypotheses for the construction of multivariate PSDMs or on their influence on seismic fragility of multicomponent structures. This study proposes a new strategy of probabilistic seis-

mic demand modeling based on MSA and Gaussian mixture (GM) models that relaxes the traditional hypotheses adopted by current strategies by exploiting the ability to better capture the record-to-record variability of multiple-stripe analysis and the flexibility in density modeling provided by parametric unsupervised learning techniques such as finite mixture models. The goal is thus twofold: (i) first to test if bias is propagated into fragility analysis due to limitations of current hypotheses on the distribution and correlation of component seismic demands, and (ii) second to provide an analytical tool for probabilistic seismic demand modeling in a structure-specific context for performance-based design or retrofit (where certain structures may violate traditional assumptions in demand modeling). The proposed model is leveraged for the construction of fragility curves and calculation of the mean annual frequency of violating a damage state using a case-study continuous concrete-girder bridge in Eastern Canada. The case study is also used to further assess the validity of the assumptions on lognormality and linear dependence through appropriate goodness-of-fit tests and visual inspection of data. The impacts of these hypotheses on fragility and mean annual frequency of damage state violation are studied, and the advantages of the proposed method are highlighted.

3.2 Proposed methodology

The method proposed in this paper for probabilistic seismic demand modeling is called MSA-GM, as it couples multiple-stripe analysis and Gaussian mixture models to define joint distributions over seismic component demand at intensity measure levels of interest. Contrary to cloud analysis (in which data are generated for different IM levels providing a cloud of points), MSA organizes demand data at a set of discrete IM levels (stripes), and this strategy allows better capturing locally, the record-to-record variability. Although it can be interpreted as a discrete version of incremental dynamic analysis, MSA is preferred over IDA due to (i) the possibility to use different record sets for each seismic intensity level of interest, (ii) limited scale factor, and (iii) higher efficiency to account for seismic variability (i.e., fewer RHAs are required) [154, 87, 22].

Gaussian mixture models are often employed as unsupervised machine learning tools on the task of clustering (i.e., to determine the number and the location of clusters in unlabeled datasets) or as a mathematical-based approach for density modeling of a wide variety of random phenomena [176, 177, 41]. In the present work, the latter is adopted to model the probability densities of seismic component demands by fitting finite mixtures of multivariate normal distributions to data in the logarithmic space at each stripe that are able to capture the interaction between components in a parametric form. A mathe-

matical description of Gaussian mixture models is provided next along with the steps to build GM-based seismic demand models.

3.2.1 Gaussian mixture seismic demand model

A Gaussian mixture model is a probabilistic model that assumes all the data points are generated from a mixture of a finite number of Gaussian distributions with unknown parameters. The model is defined as the sum of n_k multivariate normal probability density functions (PDFs), each weighted by a probability $\pi_k, \forall k = 1, \ldots, n_k$. Taking $\mathbf{X}$ as a multivariate random variable of an observed dataset $\mathbf{x}$ (e.g., the logarithm of the response of bridge components at a given seismic intensity level EDP|IM), the joint posterior PDF for a Gaussian mixture is thus defined by:

$$f(\mathbf{x}|\boldsymbol{\Psi}) = \sum_{k=1}^{n_k} \pi_k f(\mathbf{x}; \boldsymbol{\mu}_k, \boldsymbol{\Sigma}_k) \tag{3.1}$$

where $\boldsymbol{\Psi} = \left[\boldsymbol{\pi}^{\mathrm{T}}, \boldsymbol{\xi}_1^{\mathrm{T}}, \ldots, \boldsymbol{\xi}_{n_k}^{\mathrm{T}}\right]^{\mathrm{T}}$ is the vector that aggregates all the hyperparameters, being $\boldsymbol{\pi} = [\pi_1, \ldots, \pi_{n_k-1}]^{\mathrm{T}}$ the vector of mixture proportions; each vector $\boldsymbol{\xi}_k$ contains the hyperparameters related to the mean vector $\boldsymbol{\mu}_k$ and the covariance matrix $\boldsymbol{\Sigma}_k$ of the k^{th} mixture cluster [1]; and $f(\mathbf{x}; \boldsymbol{\mu}_k, \boldsymbol{\Sigma}_k)$ is the PDF of a multivariate Gaussian with mean $\boldsymbol{\mu}_k$ and covariance $\boldsymbol{\Sigma}_k$. Figure 3.1 exemplifies the simplicity of the concept by mixing two Gaussian distributions to bivariate data samples of $\mathbf{X} = [\mathrm{EDP}_1, \mathrm{EDP}_2]$. This example illustrates, along with the histograms of the two random variables, the probability distribution functions of: (i) the first cluster (in blue), (ii) the second cluster (in red), and (iii) the resulting Gaussian mixture model (in black). The modeling of the correlation between the random variables EDP_1 and EDP_2 can also be appreciated by the contour plots of the PDF of the fitted Gaussian mixture presented along with the scattered data.

The mean vector indicates the location of the center of each mixture cluster, while the covariance matrix incorporates information about the variance and correlation structures of the data. The complexity of a GM model depends on the number of clusters and the type of covariance structure adopted. Covariance matrices can be diagonal or full and shared or unshared. In the isotropic case, models employ diagonal-shared covariance, assuming a single diagonal covariance matrix for all clusters. Conversely, in the unrestricted case, the most complex GM model (in terms of number of hyperparameters per cluster) adopts a full-unshared covariance structure that fits a full covariance matrix for each cluster [177].

1. The common terminology in finite mixture models is "component", but "mixture cluster" is used instead to avoid confusion with the structural component.

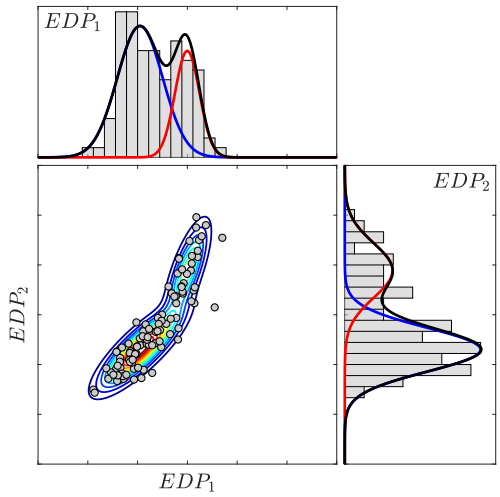

Figure 3.1 Gaussian mixture model of bivariate data with two clusters

The first step to build a GM model is to learn the hyperparameters of the latent clusters that best fit the data; thus, the expectation-maximization (EM) algorithm is employed. This algorithm consists of an iterative approach that alternates between the expectation step, in which missing values are inferred given the estimated hyperparameters, and the maximization step, in which the hyperparameters are optimized given the inferred data [186]. Next, the most suitable number of mixture clusters must be chosen, and this model selection can be performed using information-theoretic criteria for a compromise between the fit and the complexity of the model (represented by the number of clusters and, hence, hyperparameters). In the context of density modeling, the Bayesian information criterion (BIC) is recommended over other information-criterion metrics in the selection of the number of clusters of a GM model, although excessively simple models can be obtained due to the use of finite observed samples and its heavy penalty on complexity [177, 41, 121]. The BIC estimates the lack of fit through the negative log-likelihood and penalizes the model complexity to avoid overfitting:

$$\mathrm{BIC} = -2\ln\left(\mathcal{L}(\hat{\boldsymbol{\Psi}})\right) + p\ln(n) \tag{3.2}$$

where $\mathcal{L}(\hat{\boldsymbol{\Psi}})$ is the likelihood of the data given the learned hyperparameters $\hat{\boldsymbol{\Psi}}$, p is the number of hyperparameters, and n is the number of observations. The intent therefore is to pick a model that minimizes the criterion [177].

The construction of the MSA-GM seismic demand model starts by collecting the seismic demand data using the multiple-stripe analysis. Hence, a suite of ground motions that well represents the seismicity of the site must be initially chosen, and [22] suggests using a conditional IM-based record selection approach, for instance, conditional spectrum (CS)

[21, 125] or generalized conditional intensity measure (GCIM) [43, 45]. Response history analyses are then performed with the selected records, and the seismic demand dataset EDP|IM is generated. After the MSA step, the following steps are performed:

Step 1 Select a covariance structure (e.g., full-unshared);

Step 2 Learn the hyperparameters $\mathbf{\Psi}$ of a Gaussian mixture model with n_k mixture clusters to model the demand data EDP at a given IM level by applying the expectation-maximization algorithm;

Step 3 Compute the Bayesian information criterion for the fitted GM model;

Step 4 Repeat steps 2 and 3 for different numbers of clusters $n_k = 1, 2, \ldots, n_{k,max}$;

Step 5 Select the model with the lowest BIC;

Step 6 Repeat steps 2 to 5 for all the n_{IM} levels of the intensity measure;

Step 7 Repeat steps 1 to 6 for different covariance structures and select the structure that minimizes the BIC (if applicable).

This formulation still assumes lognormality of seismic demand (the model is based on the mixture of Gaussians in the logarithmic space) and linear correlation between components within each mixture cluster. The formulation can be, however, multimodal, providing flexibility to the model in treating probability densities and linear correlation that can locally fit the dependence of observed data within each mixture cluster. Therefore, the models are able to draw samples of correlated seismic demand with good agreement to the data used in the learning process, as will be exemplified subsequently. The obtained seismic demand models are limited to generating samples of correlated component responses only for the IM levels at which they were trained.

3.2.2 Leveraging the MSA-GM approach for fragility analyses

The seismic fragility of a structure is the probability of violating a damage state DS (i.e., limit state exceedance) conditional on the occurrence of a seismic event with intensity IM $= im$, i.e., $\Pr(\mathrm{DS}|\mathrm{IM} = im)$. Structures are composed of several components that can fail separately or at the same time during an extreme event. For instance, bridges are conventionally constituted by a deck, bearings, and supports (abutments and columns), and a holistic assessment of seismic vulnerability for the bridge must be made by combining the effects of the various critical structural elements (or components).

To account for the uncertainty in both demand and capacity in the fragility analysis, samples can be generated from the demand and capacity models (using Monte Carlo or Latin hypercube sampling). Using the MSA-GM seismic demand model, correlated component demand samples are drawn at each IM level (the same used in the construction

of the PSDM). Demand and capacity samples are paired, and the violation of the damage state is verified when the demand is greater than the capacity. An efficient strategy for fragility curve fitting using results from MSA is described by [22], and the assumption that observing a damage state exceedance from each seismic ground motion is independent of the observations from other ground motions is here extrapolated for the generated samples. Thus, the probability of observing z_j cases violating a damage state out of the total number of samples N_j (on the stripe IM $= im_j$) is given by a binomial distribution in which p_j is approximated by the fragility function, i.e., $p_j \approx \Pr(\text{DS}|\text{IM} = im_j)$. Then, adopting the cumulative density function (CDF) of a parametric probability distribution to approximate the fragility $\Pr(\text{DS}|\text{IM} = im) = F(im; \boldsymbol{\Theta})$ with parameters $\boldsymbol{\Theta}$, these parameters can be estimated by maximizing the log-likelihood using the maximum likelihood estimation (MLE) as in:

$$\hat{\boldsymbol{\Theta}} = \arg\max_{\boldsymbol{\Theta}} \sum_{j=1}^{n_{\text{IM}}} \left\{ \ln \binom{N_j}{z_j} + z_j \ln\left[F(im_j; \boldsymbol{\Theta})\right] + (N_j - z_j) \ln\left[1 - F(im_j; \boldsymbol{\Theta})\right] \right\} \tag{3.3}$$

Additionally, throughout its lifetime, a structure is potentially exposed to a range of ground motion intensities at a given site, as characterized by the site-specific seismic hazard curve. For a thorough analysis, the assessment of the annual risk can also be performed, which is measured here by the mean annual frequency (MAF) of violating a specified damage state $\lambda(\text{DS})$. Given that the fragility function is defined for a certain damage state exceedance, this probability can be calculated by convolving the fragility with the hazard curve of the conditioning intensity measure:

$$\lambda(\text{DS}) = \int_{\text{IM}} \Pr(\text{DS}|\text{IM}) \left| \frac{\text{d}\lambda(\text{IM})}{\text{dIM}} \right| \text{dIM} \tag{3.4}$$

where $\frac{\text{d}\lambda(\text{IM})}{\text{dIM}}$ is the derivative of the hazard curve with respect to the IM of interest [87, 20].

Annual risk calculations can be performed using the raw data provided by the seismic hazard curve although for certain sites the hazard data are sparse and significant interpolation between data points may be required. For instance, [52] proposed a hyperbolic model in the log-transformed space to fit the hazard curve to an analytical expression:

$$\lambda(\text{IM}) \approx \hat{\lambda}(\text{IM}) = \lambda_{asy} \left\{ \alpha \left[\ln\left(\frac{\text{IM}}{\text{IM}_{asy}} \right) \right]^{-1} \right\} \tag{3.5}$$

where λ_{asy}, α, and IM_{asy} are the parameters to be estimated from minimizing the error between the data and the proposed curve (using, for example, least-squares minimization).

3.3 Case study: Chemin des Dalles bridge

As a classic multicomponent structural system, the Chemin des Dalles overpass, located in Quebec, Canada, is adopted to illustrate the proposed method. It is a 106.5 m long symmetric continuous concrete girder bridge with three equally spaced spans and a 13.2 m wide deck. The superstructure is composed of a 0.165 m depth deck and six prestressed concrete AASHTO type-V girders directly connected at the bents and supported by elastomeric bearings at the abutments. Pier bents are composed of three circular columns and square section cap beams, with a vertical clearance of 6.2 m. Bent columns are rigidly connected to the shallow foundations in the west bent and free for rotation in the east bent. The substructure also comprises seat-type abutments with wing walls supported by shallow foundations, with a 25.4 mm gap separating the deck from the abutment wing walls. This bridge was designed in 1975 and does not comply with current seismic design standards and detailing. It has been extensively studied and comprehensive data is available on the structural properties, capacity, site conditions, and numerical model [221, 251, 244, 280]. Details on the numerical model, component capacities, and ground motion record selection are presented next.

3.3.1 Numerical model

The three-dimensional finite element model originally built by [251] is revisited in this work. The model was created on the Open System for Earthquake Engineering Simulation (OpenSees) [175], and it uses beam-column elements and zero-length elements to represent the behavior of this structural system and to capture the nonlinear behavior of critical structural components. Superstructure elements, including the deck and girders, are defined as linear-elastic elements, while the substructure is constituted by the nonlinear elements. Bent columns and cap beams are modeled using force-based beam-column elements with their cross-sections discretized with fibers [195]. With the increase of the number of integration points within force-based elements, general improvement of both global and local responses is observed without excessive mesh refinement. Columns are discretized in five elements along their height with five Gauss-Lobatto integration points within each element. Concrete fibers are modeled with *Concrete02* (Kent-Park) material while reinforcement layers are modeled using *Steel02* (Giuffré-Menegotto-Pinto) uniaxial material. Confined concrete properties are calculated according to the formulation proposed by [148]. To verify if lost of objectivity due to localization issues takes place [67, 229], the column analytical model is validated and calibrated against experimental

data. Good agreement is observed from laboratory reversed cyclic-test results of an exact replica of the actual bridge column [280]. Strain-penetration effects at the intersection of columns and footings or cap beams are neglected, and the connection of columns to the cap beams and shallow foundation is modeled by rigid-link objects (Figure 3.2b). Soil-structure interaction is incorporated by adding elastic half-space spring-dashpot systems (using zero-length elements) and mass to the footing nodes [196, 66, 219, 57]. Abutments are modeled as a series of elastic and elastic-gap zero-length elements to account for the back walls, wing walls, embankment and gap between the deck and abutments [74, 261, 262, 158]. Elastomeric bearings are also modeled with zero-length elements to behave as an elastic-perfectly plastic material [4, 63]. Lumped masses are defined for superstructure and substructure elements. Rayleigh damping corresponding to an average damping ratio of 1.5% at the first and second vibration modes is adopted to perform RHA. A similar modeling approach has been adopted on the assessment of the seismic performance of bridges in Eastern Canada [250, 245, 243]. Finally, the numerical model is calibrated against in situ ambient vibration test results (vibration frequencies, mode shapes, and modal dampings) provided by [221]. An overview of the bridge model as well as some details on bents, columns, and abutments are illustrated in Figure 3.2. Further details on the numerical model and its calibration are found elsewhere [251, 244].

3.3.2 Damage states and capacity models

The damage states related to the seismic performance criteria defined in Section 4 of the Canadian highway bridge design code (CHBDC) CSA S6-14 [57] are adopted in this study for the assessment of the bridge's fragility, namely, minimal, repairable, extensive, and probable replacement. These performance criteria indicate gradually progressive damage states that are similar to those established by HazUS [93].

The case-study bridge includes three critical components: abutment wing walls, elastomeric bearings, and bent columns. Other structural components have shown negligible seismic fragility on multi-span continuous concrete girder bridges in Eastern Canada [250, 243]. The associated engineering demand parameters are the deformation on the wing walls and bearings (Δ_{aww} and Δ_{brg}, respectively), and drift of fixed-base bent columns (δ_{col}); all in the transverse direction [244]. Component capacities are assumed to follow lognormal distributions [199, 168], and their median (m_C) and dispersion (ζ_C) values for each damage state are presented in Table 3.1. The median capacities of columns follow the findings of [280] who established column damage states in accordance to the performance criteria of the CHBDC CSA S6-14 based on experimental tests, which included an exact replica of the actual bridge column. The median capacities of the other components

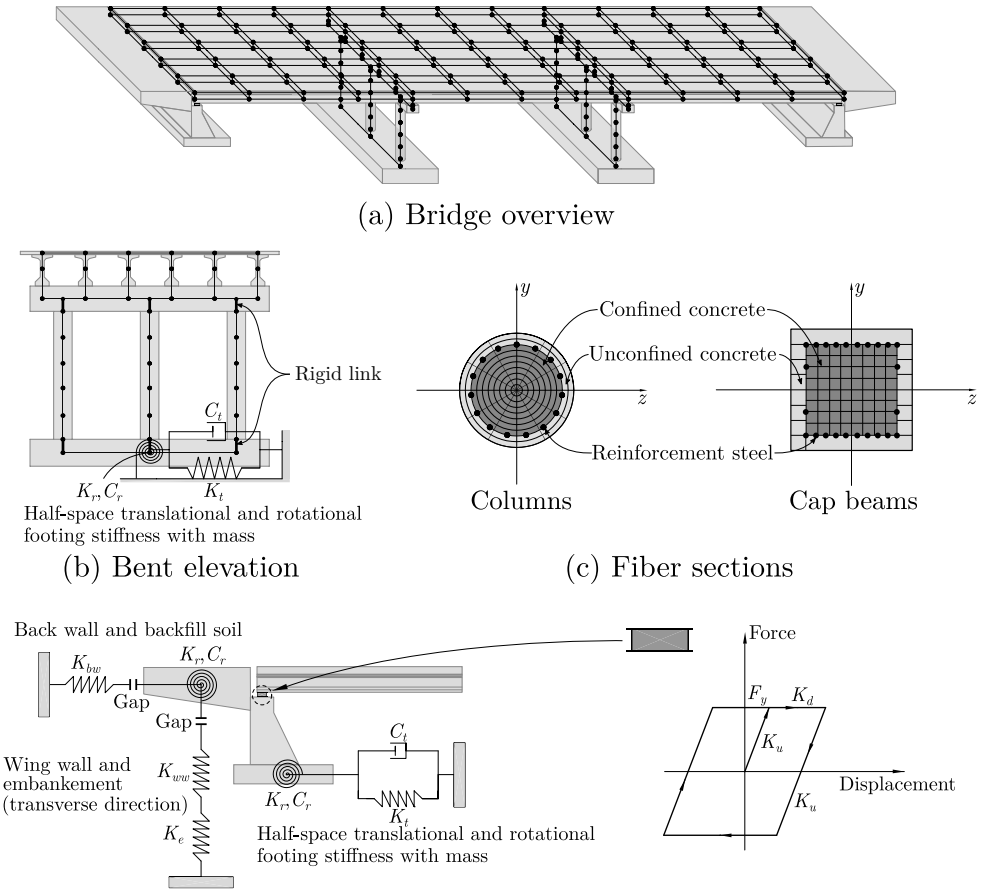

(a) Bridge overview

(b) Bent elevation

(c) Fiber sections

(d) Seat-type abutment with wing walls

(e) Elastomeric bearings

Figure 3.2 Numerical model of the case-study bridge: (a) overview, (b) bent elevation, (c) fiber sections, (d) abutment, and (e) material model for elastomeric bearings

were adapted by [251] for structures in Quebec based on the prescriptive damage states proposed by [64]. Dispersion values follow the recommendations given by [197].

3.3.3 Seismic hazard and record selection

Seismic ground motion record selection is performed using the GCIM approach [43, 45] by adapting an algorithm with greed optimization [125, 27] to include other IMs in addition to spectral acceleration. In the GCIM approach, a multivariate lognormal distribution of intensity measures is built conditioned on the occurrence of an earthquake event with a given intensity level (the conditioning intensity measure). To build this conditional distribution, a conditioning IM must be chosen (referred as IM_j) along with the concomitant conditioned IMs (referred as IM_i). The conditional multivariate lognormal distribution $\mathrm{LN}\left(\mathrm{IM}|\mathrm{IM}_j\right)$ is then used as target for the record selection, in which IM is the vector of conditioned intensity measures IM_i. The choice of the seismic intensity measures depends

Table 3.1 Bridge component damage states

Component EDP	Minimal		Repairable		Extensive		Probable replacement	
	m_C	ζ_C	m_C	ζ_C	m_C	ζ_C	m_C	ζ_C
Δ_{aww} (mm)	7.0	0.25	15.0	0.25	30.0	0.46	60.0	0.46
Δ_{brg} (mm)	30.0	0.25	60.0	0.25	150.0	0.46	300.0	0.46
δ_{col} (%)	0.5	0.25	1.4	0.25	2.0	0.46	2.2	0.46

on the availability of ground motion models (GMM) and correlation models between pairs of IMs at the investigated site.

First, a probabilistic seismic hazard analysis (PSHA) is performed at the bridge site using the software OpenQuake [238] to identify expected earthquake scenarios. The most recent GMMs for Eastern Canada [15] are employed along with the source clusters and logic tree weights considered by the Geological Survey of Canada [120]. These GMMs and logic tree models are the same used in the construction of the Canadian seismic hazard maps adopted by the 2015 edition of the National Building Code of Canada [55]. The resulting hazard curve is presented in Figure 3.3a, and the hyperbolic curve fitted to the hazard data (with parameters $\lambda_{asy} = 6.7 \times 10^{10}$, $\alpha = 607.2$, and $\text{IM}_{asy} = 3.0 \times 10^{7}$) [52] is also shown.

For the record selection, the spectral acceleration (S_a) at the bridge elastic fundamental period in the transverse direction $T_1 = 0.38\,\text{s}$ is chosen as the conditioning intensity measure at six levels: from 0.2 to 1.2 g with steps of 0.2 g, corresponding to seismic events with return periods ranging from 1 400 to 44 000 years [2]. The target distributions of intensity measures are defined by $\text{LN}\left(\text{IM}|S_a(T_1)\right)$ in which the conditioned intensity measures are $\text{IM} = [S_a(T_i), \text{PGV}, \text{PGA}]$ with 20 values of T_i ranging from 0.1 to 2.0 s to account for the effects of higher modes (up to 90% of the effective modal mass in the transverse direction) and period elongation due to nonlinearities [3]. All intensity measures are in the horizontal direction. The same ground motion models used in the PSHA are employed to calculate the mean and standard deviation of the IMs, while the correlation coefficients between IMs are calculated employing the following models: [26] for spectral acceleration at various periods; [44] for S_a and PGA; and [46] for S_a and PGV. With the conditional distributions of intensity measures defined, 100 ground motion records are selected from

2. The upper spectral acceleration level is adopted to agree with past studies that used $S_a(T_1)$ up to 1.56 g [251], although it would represent extremely rare earthquake scenarios.

3. The recommended lower bound period is $0.2T_1$ for the inclusion of higher modes, which would result in periods starting at 0.076 s. Nonetheless, the analysis of the effective modal masses indicated that the third mode shape ($T_3 = 0.13\,\text{s}$) includes more than 90% of the cumulative effective modal mass, and hence, the chosen range of periods is deemed suitable.

the NGA-West2 database [7] per level of $S_a(T_1)$. An example of the selected records conditioned on $S_a(T_1) = 0.2\,\mathrm{g}$ is presented in Figure 3.3b.

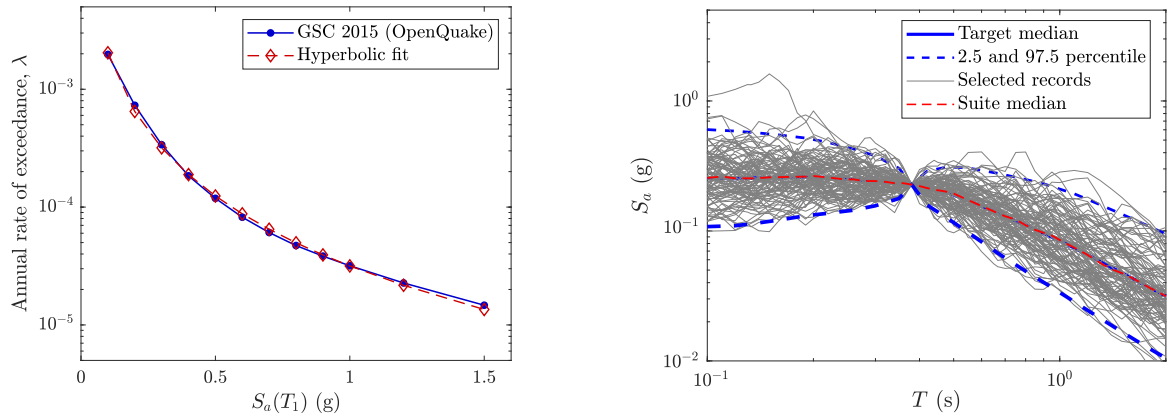

Figure 3.3 Record selection: (a) hazard curve for $S_a(T_1)$ from PSHA and hyperbolic fit; and (b) an example of selected spectra conditioned on $S_a(T_1) = 0.2\,\mathrm{g}$

3.4 Validity of traditional assumptions on seismic demands

For simplicity, a deterministic structural sample (e.g., neglecting material and geometric uncertainty) is considered to illustrate the MSA-GM method. Given that the 600 selected records were grouped into six sets of spectral acceleration at the fundamental period ranging from 0.2 to 1.2 g, the results from the 100 response history analyses at each stripe are deemed significant to assess their statistics (i.e., mean, variance, and correlation). Moreover, the responses of the critical components of the case-study bridge and their interactions are studied in the log-transformed space.

3.4.1 Assumptions on lognormality

Lognormality of seismic demand is often employed in the construction of PSDMs due to its simplicity, while it also assures that only positive values of structural response are sampled from the resulting model. To verify the validity of this hypothesis, a goodness-of-fit test may be performed, and the Kolmogorov-Smirnov (K-S) test is often chosen for this task (e.g., [130, 99, 168]). Nonetheless, when certain parameters of the tested distribution must be estimated from the sample, the K-S test is no longer suitable because its results will be conservative in the sense that the probability of a type I error will be smaller than that given by tabulated values of the K-S statistics [150]. The Lilliefors test is then recommended instead. The test statistic is $L^* = \max_x \left|\hat{F}(x) - G(x)\right|$, where $\hat{F}(x)$ is the

empirical cumulative distribution function (ECDF) of the sample data and $G(x)$ is the CDF of the hypothesized null distribution with estimated parameters equal to the sample parameters. If the value of L^* exceeds the critical tabulated value $L_{n,\alpha}$, one rejects the hypothesis that the n observations come from a normal population in the significance level α.

The marginal distributions of all component seismic demands are tested for the lognormal distribution (null hypothesis) at each stripe against the alternative hypothesis (that the data do not come from the tested distribution). For 100 samples and a significance level $\alpha = 0.05$, the tabulated critical value is $L_{100,0.05} = 0.089$. Figure 3.4 shows the test statistics for each component at all the studied stripes along with the critical value. One can verify that the assumption of lognormality is not always valid, although a reasonably good fit may be observed for elastomeric bearings and columns depending on the seismic intensity level. For the deformation of abutment wing walls, none of the demands generated could be satisfactorily modeled by a lognormal distribution. For spectral accelerations between 0.6 and 1.2 g, unimodal lognormality does not hold, and the distance between the data and the tested distribution is greater than 0.2 in most cases [4]. This value was defined as a threshold by [130] to neglect the impact of imperfect modeling of a PSDM on the fragility analysis. For columns and elastomeric bearings, the test statistics lie in the vicinity of the critical value $L_{100,0.05}$ and do not exceed 0.2.

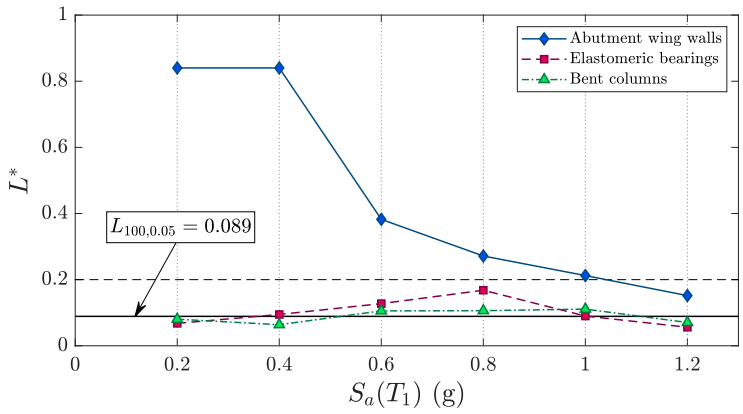

Figure 3.4 Lilliefors test statistics for each bridge component

The lack-of-fit of the seismic demands to the lognormal distribution may be explained by discontinuities in the behavior of the bridge components and their interaction. For instance, the behavior of the elastomeric bearings installed on the abutments of this bridge

4. The first two points of abutment wing walls (i.e., for $S_a(T_1)$ equal to 0.2 and 0.4 g) might be neglected since they represent the distance between a single-valued dataset (undeformed abutment wing walls) and a distribution with virtually null standard deviation.

is intrinsically related to the presence of the gap that separates the deck from the abutment wing walls. The response of the elastomeric bearings may be described by two distinct regimes: (i) the bearing presents deformations that are less than the 25.4 mm and the deck moves freely between the abutment wing walls (while the bearings deform freely within this same range); and (ii) the bearing yields with deformations that are greater than the gap, while the deck closes the gap and mobilizes the spring force that models the wing walls, thus constraining the deformation of the bearings. Bent columns are similarly affected by the presence of the gap. While the gap on the abutments is not closed, the deck moves freely in a "quasi" rigid-body movement with bending of the columns. Once the wing walls are mobilized, the deck will present transverse bending, limiting the lateral displacement of the bent columns.

These different regimes, however, do not occur exclusively at specific levels of seismic intensity and Figure 3.5 is used to illustrate this phenomenon for spectral acceleration at T_1 of 0.8 g. For instance, if one focuses on the response of the elastomeric bearings, the bearing deforms freely with the deck on the verge of overcoming the gap in some cases, whereas, in other cases, the bearing has its deformation limited by the fact that the gap is closed and the wing walls resist the displacement of the ensemble deck/bearing pads. This is observed in Figure 3.5a by a first peak for $\Delta_{\text{brg}} < 25.4$ mm and a second greater peak for $\Delta_{\text{brg}} > 25.4$ mm. One can still notice these peaks after transforming the responses into the logarithmic space with the discontinuity separating the lower tail around $\ln(25.4) \approx 3.2$ (Figure 3.5b). Consequently, this lower tail with deformations that are less than 3.2 causes the statistical test to fail (Figure 3.5c). In the case of deformation on abutment wing walls, one might infer that the fitted dispersion considering a lognormal distribution might be larger than the actual dispersion of the data due to the observation of null deformations (Figures 3.5b,c).

It is therefore verified that, for the number of samples and the adopted significance level, the lognormal distribution may not satisfactorily represent the seismic responses of the components of a bridge at a set of IM levels of interest. A nonparametric approach, for instance, the kernel density estimator or logistic regression, could enhance the performance of the fitted marginal distribution of demand at each stripe [130, 168]. Nevertheless, a parametric approach such as the mixture of Gaussian distributions might also improve the modeling, as proposed in this study and verified later.

3.4.2 Assumptions on linear dependence

To assess the interaction between component responses, the Pearson correlation coefficient ρ_{AB} is usually employed (e.g., [199, 206, 111]), which is a measurement of the linear

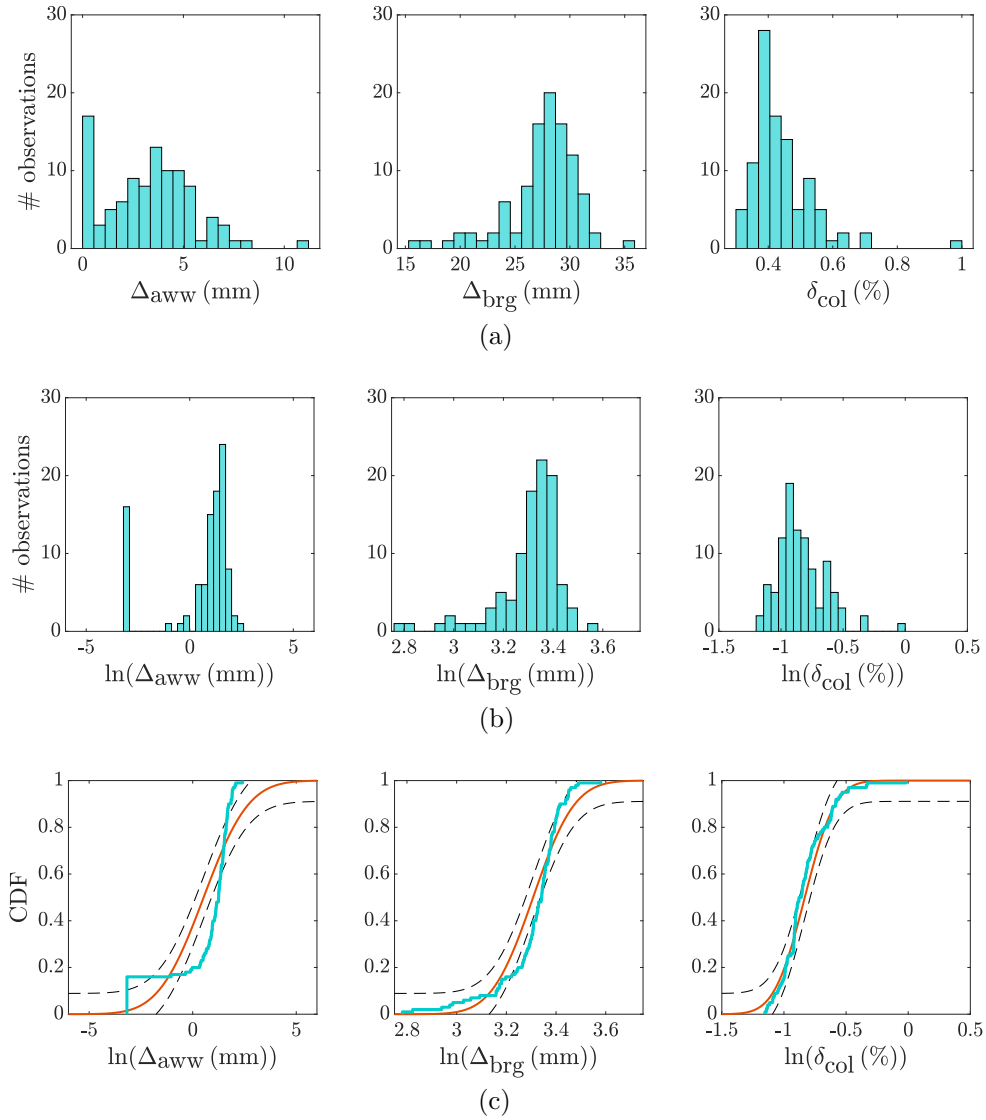

Figure 3.5 Distribution of component demands for $S_a(T_1) = 0.8\,\mathrm{g}$: (a) histogram in original scale, (b) histogram in logarithmic scale, and (c) comparison of ECDF to test bounds (solid orange line represents the fitted lognormal CDF while dashed black lines indicate the bounds of the Lilliefors test)

dependence between two random variables A and B and is bounded between -1 and $+1$. This metric provides a very useful measure of dependence between variables: large values of $|\rho_{AB}|$ imply strong stochastic dependence and a near-linear functional relationship, whereas small values may result from its lack of strong linearity if a functional relationship exists or from the predominance of other sources of variation (and hence low stochastic dependence) [35]. To the best of the authors' knowledge, no study has been conducted on the validity of the assumption on linear dependence of seismic response between bridge components. However, the consequences on the definition of fragility of long bridges under

nonuniform motion (i.e., with the effect of spatial variation of earthquake ground motions) were assessed by [157], who also concluded that the correlation coefficients between piers were strongly dependent on the seismic intensity level and on the number of analyses, observing coefficients lower than unity even for adjacent piers under uniform motion.

Despite these observations, some approaches still disregard the dependence of the correlation with respect to the IM level and compute the correlation coefficient using the whole demand dataset. This interpretation is believed by the authors to distort the real correlation between component demands, in the sense that demands tend to increase with the augmentation of the seismic intensity, and thus, the correlation coefficients would assume values close to unity. These values, however, are affected by the seismic intensity and do not represent the existing correlation between components. Accordingly, considering the entire demand dataset, the correlation coefficients independent of the intensity measure level (ρ_{XY}) are estimated as follows: 0.797 between abutment wing walls and elastomeric bearings; 0.800 between abutment wing walls and bent columns; and 0.954 between elastomeric bearings and bent columns. By leveraging the stripe structure of seismic demand using MSA, the correlation coefficients between component responses conditional on the seismic intensity are also estimated at each level of $S_a(T_1)$ ($\rho_{XY|S_a(T_1)}$). These conditional values are presented in Figure 3.6 along with the independent values ρ_{XY}, in which the variation of the correlation coefficients with respect to intensity level is verified. One can also observe that the correlation coefficients involving the response on bent columns using the entire dataset are always higher than the conditional values.

The correlation between the drift of the two bents is also introduced into Figure 3.6 to assess the dependence between similar structural and spatially close components, although the drift of pinned columns ($\delta_{\text{col-p}}$) are not taken as critical structural elements in the fragility analysis. The correlation coefficient between the columns of the two bents evolves from moderate (≈ 0.5) to rather high correlation values (close to unity) with the increase of spectral acceleration, suggesting the dependence of the degree of correlation between pairs of bent columns to the level of seismic intensity measure even for similar and adjacent structural components, as previously observed by [157].

For low levels of seismic intensity (e.g., $S_a(T_1) = 0.2\,\text{g}$), the observed correlation coefficients are small ($|\rho_{XY|S_a(T_1)}| \leq 0.1$, except between column piers). As shown in Figure 3.6, the values of the correlation coefficient increase with the augmentation of the seismic intensity and values greater than 0.6 are obtained for $S_a(T_1) \geq 0.6\,\text{g}$. This outcome might be seen as a tendency to linear dependence between the component demands from low to high IM levels, although for the in-between intensity levels, however, the relationship is not clear.

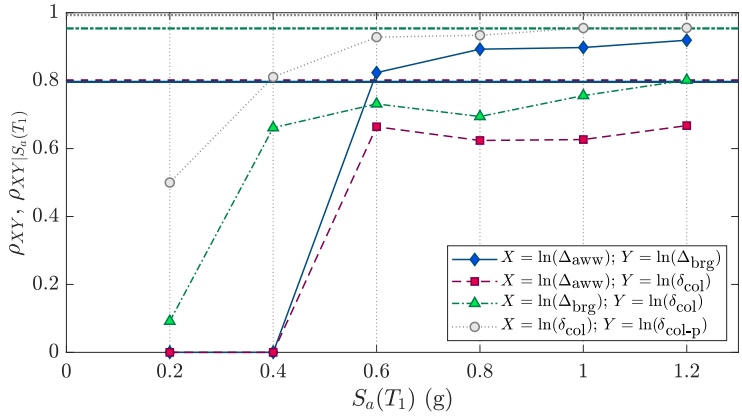

Figure 3.6 Evolution of correlation coefficients between component responses with respect to the seismic intensity

Hence, it is of great importance to base this analysis on the visual inspection of the data as well as (and not only on) the computed correlation coefficients [9]; Figure 3.7 illustrates the correlation plots at all the studied levels of spectral acceleration at the fundamental period.

As observed, lower $S_a(T_1)$ levels (Figures 3.7a and 3.7b) show absent or low linear correlation with horizontally aligned (due to the gap between the abutment wing walls and the deck) or circular shaped graphed data. For responses at intermediate levels of spectral acceleration, for instance, $S_a(T_1) = 0.6$ and $0.8\,\text{g}$ (Figures 3.7c and 3.7d), graphed data indicate functional relationships that are clearly not linear, although correlation coefficients as high as 0.89 may be observed. The closing of the gap may explain this behavior. As discussed in Figure 3.5, two deformation regimes are identified depending on the closure of the gap. Two colors are used on the markers in Figure 3.7 to distinguish the component demands with open (blue) or closed (red) gap, and the impact of this discontinuity on pairwise component correlation becomes evident. In these cases, a linear correlation coefficient may poorly model the dependence of the demand data. Finally, as previously stated, at higher levels of $S_a(T_1)$, responses showed values of $\rho_{XY|S_a(T_1)}$ close to unity, and the expected pattern of data for these values of the correlation coefficient are depicted in Figures 3.7e and 3.7f.

Furthermore, to test the absence of linear correlation between samples of two random variables X and Y (being the null hypothesis $\rho_{XY} = 0$ against the alternative hypothesis $\rho_{XY} \neq 0$), considering that both come from a bivariate normal population, one can use the test statistic T with Student's t-distribution for $n - 2$ degrees of freedom to calculate the p-value of the estimated correlation coefficient [84]. It can also be used to establish the minimum sample size for a significant estimate of ρ_{XY}. For instance, more than 250

samples are required to discard the absence of linear dependence between two random variables with correlation coefficients as low as 0.1 at the 0.05 significance level, whereas as few as 12 samples are required for $\rho_{XY} = 0.5$ at the same significance level. The p-values corresponding to the estimated correlation coefficients are also presented in parentheses in Figure 3.7.

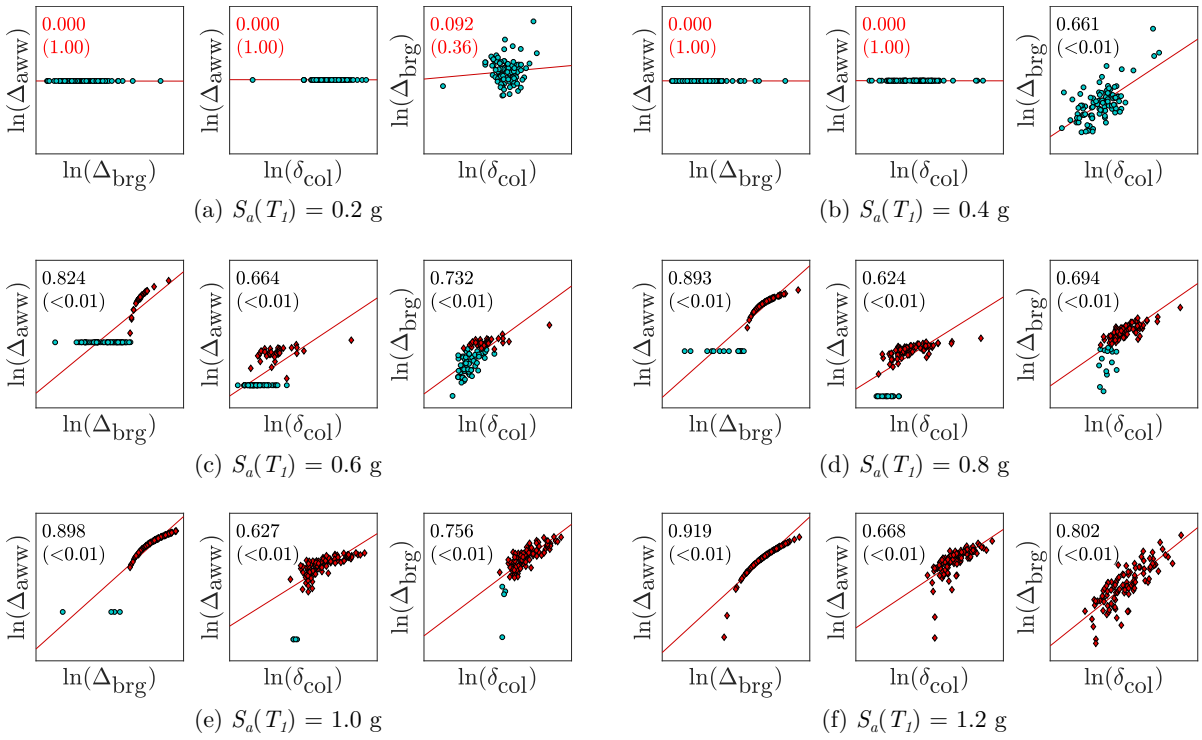

(a) $S_a(T_1) = 0.2$ g (b) $S_a(T_1) = 0.4$ g

(c) $S_a(T_1) = 0.6$ g (d) $S_a(T_1) = 0.8$ g

(e) $S_a(T_1) = 1.0$ g (f) $S_a(T_1) = 1.2$ g

Figure 3.7 Correlation plots of pairwise component demands in the logarithmic space at each level of spectral acceleration (values on the upper corner indicate the correlation coefficients and the respective p-values in between parentheses). Blue and red markers indicate open and closed gap, respectively.

Accordingly, for the lowest considered levels of $S_a(T_1)$ (e.g., Figure 3.7a), the observed p-values of the correlation coefficients were greater than 0.05, which means that there is no strong evidence to show that these responses are linearly correlated. In the other cases (i.e., $S_a(T_1) > 0.4\,\text{g}$), the p-values for the estimated correlation coefficients are always less than 0.05, indicating the rejection of the hypothesis that no correlation exists between the component responses. This rejection, however, does not ensure that the correlation is linear, as verified in Figure 3.7d, for example.

Hence, the linear correlation coefficient may not adequately capture the existing local dependencies between component seismic responses at some levels of seismic intensity, as observed at lower and intermediate levels of spectral acceleration in this case study. The

proposed MSA-GM method considers correlation locally (e.g., within a mixture cluster) and might be more suitable for this task, as tested in the next section.

3.5 Fragility analysis based on MSA-GM

The proposed methodology based on coupling multiple-stripe analysis and Gaussian mixture is first used to construct a GM seismic demand model for the observed data. Several models are fitted, and the capacity of the selected models to represent the observed data are assessed and compared to the unimodal case. The chosen model is then used to build component and system fragility curves for the case-study bridge. Finally, MSA-GM and other conventional strategies are used to assess the impact of some of the traditional hypotheses on fragility analysis.

3.5.1 Construction of the Gaussian mixture seismic demand model

With the seismic demand data already presented and structured in stripes of spectral acceleration at T_1, Gaussian mixture models are fitted for a number of mixture clusters ranging from 1 to 10 at each stripe. The maximum number of clusters is chosen to verify if the chosen information criterion would be useful in selecting models that avoid overfitting. The covariance structure was defined as full-unshared, in which each cluster has its own covariance matrix with variance and correlation coefficients determined within the cluster. Though this option increases the number of hyperparameters per cluster, it tends to use fewer clusters to satisfactorily model the data than simpler covariance structures. The performance of each model is assessed using the Bayesian information criterion, and the values are shown in Figure 3.8. The selected number of mixture clusters are highlighted by red rectangles around the minimum values of BIC, and the color scale indicates the variation between the maximum (dark brown) and the minimum (white) BIC values at each stripe.

The final model is further detailed in Table 3.2, in which the proportion of each mixture cluster is also shown. In some cases, a small mixture proportion (< 0.1) is observed, indicating that small portions of the data are clustered, which might be seen as a sign of overfitting. Nevertheless, all selected models have four or fewer clusters, demonstrating that a reasonable trade-off between complexity and lack of fit is chosen. More stringent criteria could be adopted to choose simpler GM models and avoid selecting clusters with small proportions. For instance, it is observed in Figure 3.8 that GM models with only two mixture clusters perform almost as well as the selected clusters and could be chosen instead. Nevertheless, the chosen approach is to let the demand data speak for themselves.

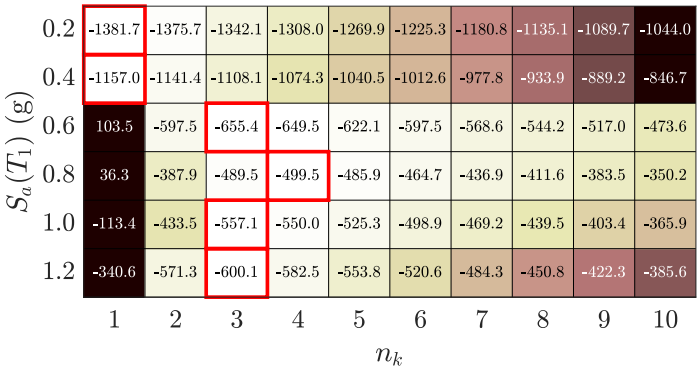

Figure 3.8 BIC values for the Gaussian mixture models at each stripe (red rectangles indicate minima)

Table 3.2 Chosen Gaussian mixture models at each stripe

$S_a(T_1)$ (g)	n_k	BIC	Mixture proportions
0.2	1	-1381.7	[1.00]
0.4	1	-1157.0	[1.00]
0.6	3	-655.4	[0.33, 0.60, 0.07]
0.8	4	-499.5	[0.47, 0.08, 0.29, 0.16]
1.0	3	-557.1	[0.70, 0.04, 0.26]
1.2	3	-600.1	[0.74, 0.22, 0.04]

At low intensity levels ($S_a(T_1)$ of 0.2 or 0.4 g) Gaussian mixture models with a single cluster may seem contradictory with respect to the statistical tests performed on the data (Figure 3.4). However, increasing the number of clusters to model the data at these levels of spectral acceleration does not show significant improvement to the density model as per the values of Bayesian information criterion (Figure 3.8). In the case of the abutment wing walls that are not mobilized at these levels of seismic intensity, as single valued sample sets, they can be represented by a lognormal distribution with median equal to that value and a small dispersion (in the order of 10^{-2}), with the marginal CDF approaching a step function without too much loss of information. Additionally, it is important to notice the difference between the BIC of the chosen models and the one-cluster models for $S_a(T_1)$ in the range 0.6 to 1.2 g; these differences indicate the loss of information and the lack of fit when a unimodal multivariate lognormal distribution is fitted to the demand data at these stripes. This observation agrees with the values of the Lilliefors test statistic presented in Figure 3.4 that exceeds the critical value, especially for the deformation of abutment wing walls. An example to compare the sampling capabilities of the unimodal and the chosen model is graphically depicted in Figure 3.9 for $S_a(T_1) = 0.8$ g. One can recognize

from the correlated samples that the unimodal approach generates a significant quantity of unrealistic demand samples (i.e., that do not agree with the observed data from RHAs), especially for the interactions with abutment wing walls. Although omitted for brevity, similar behavior is observed for spectral accelerations between 0.6 and 1.2 g. Regarding the fragility analysis, these unrealistic drawn samples may introduce bias depending on the relevance of the components to the system fragility for a given damage state. To understand the relevance of each component to the system fragility, component and system fragility curves are determined from the final GM demand model and are presented next.

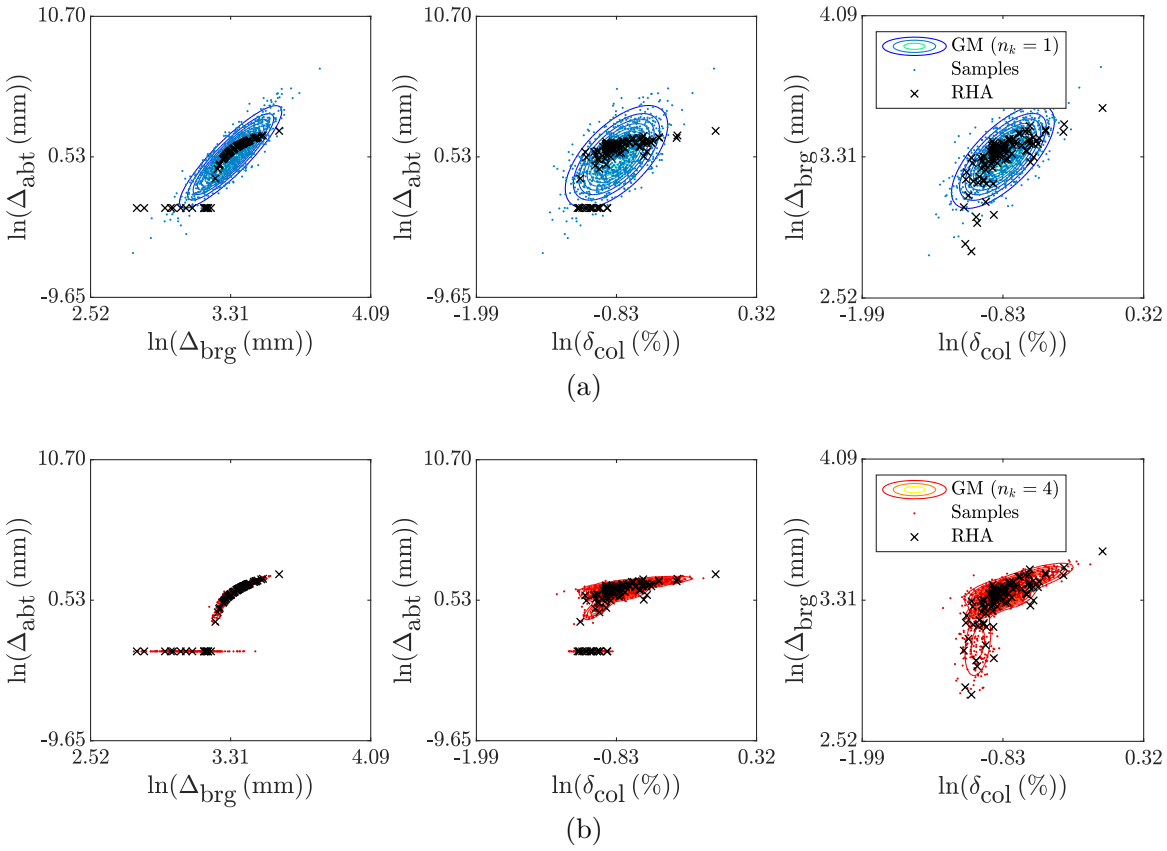

Figure 3.9 Comparison of observed and sampled correlated demand data at $S_a(T_1) = 0.8\,\mathrm{g}$ with: (a) 1 cluster and (b) 4 clusters

3.5.2 Component and system fragilities

Fragility curves are assumed to follow a lognormal distribution with parameters $\boldsymbol{\Theta} = \{\theta, \beta\}$ (i.e., median and dispersion). Hence, the CDF $F(im; \boldsymbol{\Theta})$ used in Equation 3.3 is:

$$F(im; \boldsymbol{\Theta}) = \Pr(\mathrm{DS}|\mathrm{IM} = im) = \Phi\left(\frac{\ln(im/\theta)}{\beta}\right) \tag{3.6}$$

where $\Phi(\cdot)$ is the CDF of the standard normal distribution.

While many alternatives exist in the literature, a series system assumption is often adopted for the system damage state definitions of structures such as bridges (e.g., [199]). Therefore, the violation of the same damage state of the system $\mathcal{F}_{sys}$ is the union of the component violations, i.e., $\mathcal{F}_{sys} = \bigcup_{i=1}^{m} \mathcal{F}_{comp,i}$, and thus, the probability of $\mathcal{F}_{sys}$ is:

$$\Pr(\mathcal{F}_{sys}) = \Pr\left(\bigcup_{i=1}^{m} \mathcal{F}_{comp,i}\right) \tag{3.7}$$

Additionally, to conform the damage states of the components to the consequences to the bridge's performance in terms of closure and repair implications, the components are classified as primary or secondary in accordance with their importance for bridge stability under traffic or a subsequent seismic event [273]. Extensively damaged columns shall be classified as primary components, which are assumed to be the only components contributing to the probable replacement damage state of the bridge. Secondary components (e.g., abutments and bearings) are assumed to contribute to earlier damage states of the whole system (minimal, repairable, and extensive) because their complete failure will not have a similar consequence as that of primary components.

The fragility curves for the bridge components and for the whole system are fitted using the maximum likelihood estimation, as in Equation 3.3. When MSA is performed, [22] recommends choosing IM levels near the lower tail of the fragility function and up to levels slightly above the median (i.e., with a fraction of observed damage state violation greater than 0.5) to ensure a good fit. Figure 3.10 presents the fitted fragility curves for the four damage states for the system and critical components for spectral accelerations up to 1.5 g. Fragility curves for minimal damage follow the aforementioned strategy; conversely, the other fragility curves would show greater uncertainty, but the use of higher values of spectral acceleration would not be reasonable for the current case study.

The three critical components have a significant contribution to the system fragility for the minimal (Figure 3.10a) and repairable (Figure 3.10b) damage states (the latter being less likely with probabilities of less than 5%). Columns are the governing component for the extensive damage state, followed by the abutment wing walls that contribute to a lesser extent to the bridge fragility (Figure 3.10c). Only columns control the probable replacement of the bridge (as previously stated) (Figure 3.10d). Due to the performance criteria and column capacity adopted in the present work, abutment wing walls contribute more to the system's repairable and extensive damage states than in a past study [251]. The system's fragility is directly influenced by the fragility of each of the critical compo-

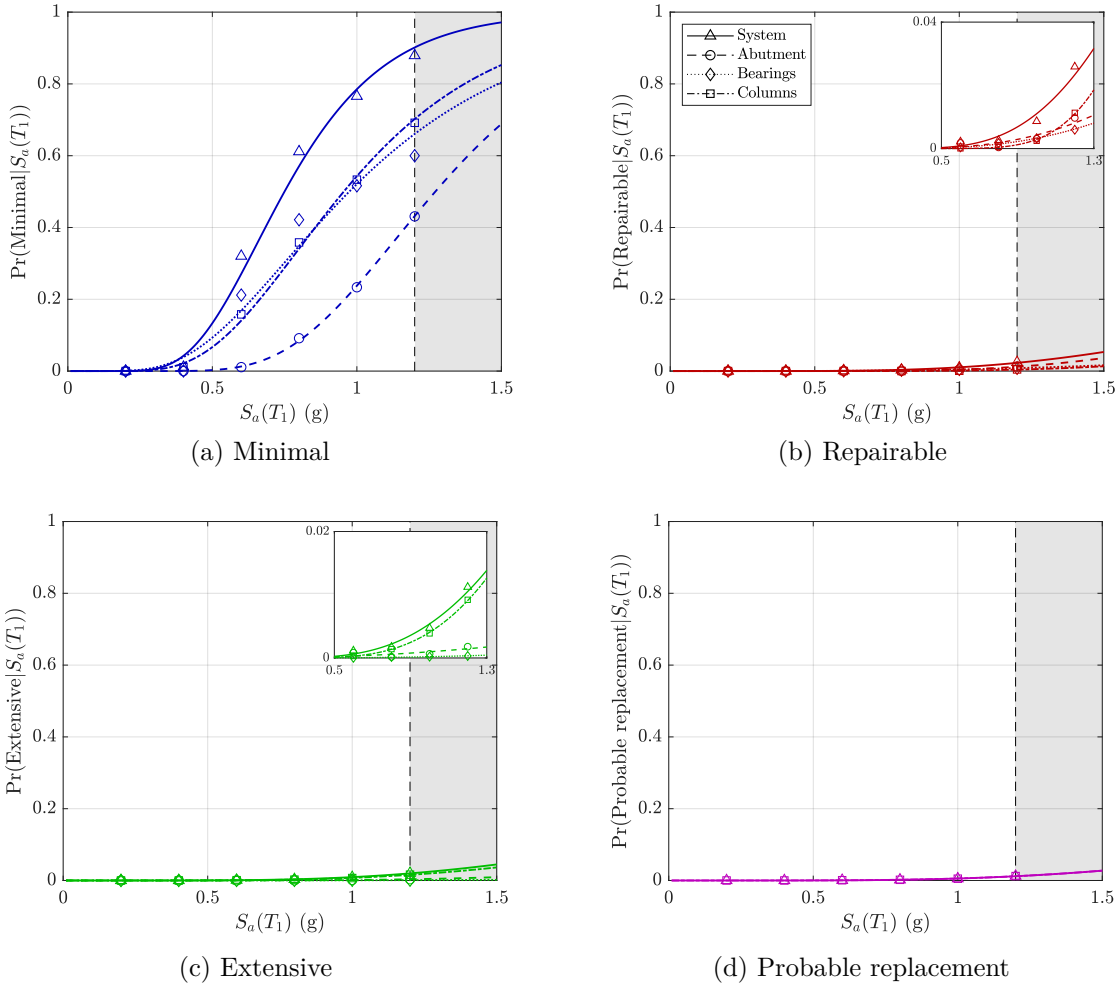

(a) Minimal (b) Repairable

(c) Extensive (d) Probable replacement

Figure 3.10 Fragility curves for components and system based on the MSA-GM model. Markers represent the fraction of observed violation of damage state and gray shaded areas indicate the region where the fragility curves extrapolate the investigated seismic intensity levels

nents for a given damage state, which in turn are intrinsically related to the capability of the PSDM strategy to model the observed demand data. This feature may be crucial when comparing the performance of PSDM strategies with different density modeling capabilities, as presented next.

3.5.3 Comparison of different hypotheses

For this analysis, five different PSDM strategies are defined to isolate the effects of each of the investigated hypotheses, namely, MSA-L1, MSA-L2, MSA-K1, MSA-K2, and MSA-GM; Table 3.3 presents their characteristic assumptions. All strategies employ multiple-stripe analysis for data collection, assuring heteroscedasticity of the demand with respect to the seismic intensity. In the adopted nomenclature, the letters indicate the statistical

fitting of the demand data at each stripe: L stands for a multivariate lognormal distribution, whereas K stands for kernel density estimator (a nonparametric distribution as recommended by [130]). Finally, numbers 1 and 2 indicate, respectively, the assumption of correlation coefficient calculated at each stripe or using the complete dataset. Assuming that MSA-GM is the less constrained strategy, this demand model is taken as reference for comparing the impact of the adopted hypotheses to the results of the respective fragility analyses.

Table 3.3 Hypothesis adopted for each PSDM strategy

Hyphotesis	PSDM strategy				
	MSA-L1	MSA-L2	MSA-K1	MSA-K2	MSA-GM
Lognormality of EDP|IM	✓	✓	–	–	∗
Linear correlation (entire dataset)	–	✓	–	✓	–
Linear correlation (stripe)	✓	–	✓	–	∗

Note: presence (✓), absence (–), and presence within each mixture cluster (∗).

Figure 3.11 presents the system's fragility curves obtained with each of the five PSDM strategies for all the damage states of interest. Strategies MSA-L1 and MSA-L2 performed similar to MSA-GM for minimal and probable replacement damage states, whereas the ratios of DS violation for repairable and extensive damage states are overestimated for intermediate stripes when compared to more flexible modeling strategies. As a consequence, the fitted fragility curves are drastically different from those obtained with the Gaussian mixture model and the kernel method. The overestimation is explained by the significant contribution of the abutment wing walls and columns to these system damage states and by the fact that these intermediate stripes represent S_a at T_1 in the range from 0.6 to 1.2 g, which are the same intensity levels at which the Gaussian mixture models were fitted with more than one mixture cluster (see Table 3.2). Additionally, the ratios of DS violation produced by the lognormal strategies are not conventional, as they appear to oscillate for spectral accelerations between 0.6 and 1.2 g with significant amplitude. This oscillation is attributed to the poor approximation of the lognormal distribution on the abutment wing wall deformation at these levels of spectral acceleration. A larger fitted dispersion than the actual dispersion (Figure 3.5) causes the model to draw unrealistic demand samples (Figure 3.9). As a consequence, the number of generated samples that exceed the component capacity tends to be higher than the actual fragility ratios (Table 3.4), indicating that the assumption of lognormality of the deformation of abutment wing-walls introduced significant bias into the component and system fragility estimates, not being adequate for the investigated structure. Still from Table 3.4, it is worth noting that, despite violating

the Lilliefors test at some intensity levels, the fragility estimates for elastomeric bearings and bent columns obtained with MSA-L1 are in good agreement with those generated with the MSA-GM approach. These results suggest that the unimodal lognormal distribution is a satisfactory approximation for the density modeling of bearing and column responses for the case-study bridge. These findings agree with the recommendations given by [130] that low bias may be introduced into fragility estimates if the maximum deviation between the ECDF and the hypothetical CDF of demand is less than 0.2.

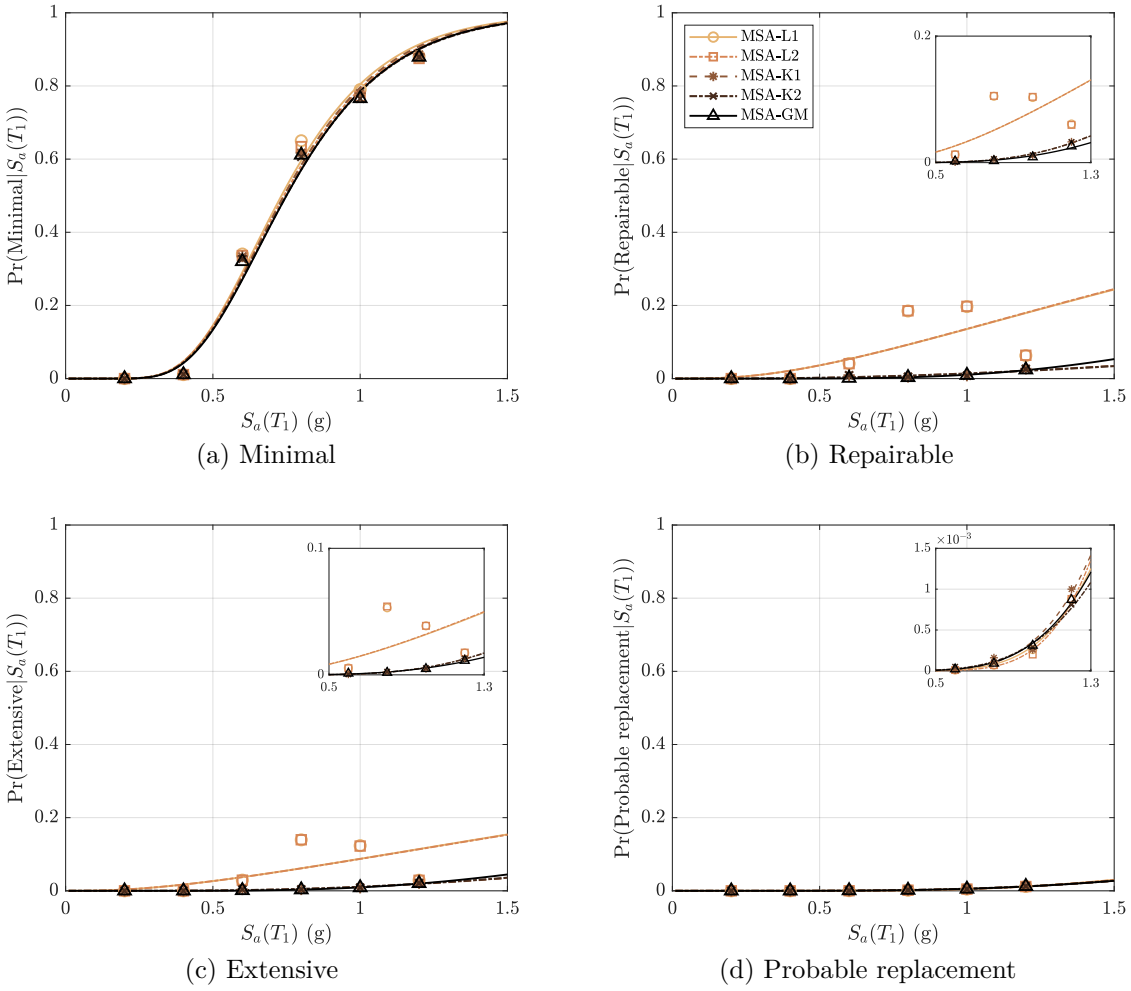

Figure 3.11 System fragility curves for different PSDM strategies with markers representing the fraction of observed violation of damage state

Fragility curves based on strategies MSA-L1 and MSA-L2 are practically superposed. This is also observed in fragility curves for MSA-K1 and MSA-K2. Therefore, one can conclude that the impact of the correlation using the entire dataset compared to the stripewise approach was negligible on the resulting fragilities for the case-study bridge, and Figure 3.6 may explain this finding. Correlation coefficients independent of the level of $S_a(T_1)$ were particularly different from the dependent values for spectral accelerations below 0.4 g, and

Table 3.4 Damage state ratios for strategies MSA-L1 and MSA-GM (multiplied by 10^2)

Damage[1]	Level[2]	MSA-L1[3,4]						MSA-GM					
		$S_a(T_1)$ (g)						$S_a(T_1)$ (g)					
		0.2	0.4	0.6	0.8	1.0	1.2	0.2	0.4	0.6	0.8	1.0	1.2
Minimal	A	0.0	0.0	**4.3**	**22.8**	**30.1**	37.0	0.0	0.0	1.0	7.9	21.3	40.3
	B	0.0	0.1	18.0	37.2	46.7	55.3	0.0	0.0	18.5	38.0	47.1	55.5
	C	0.0	0.7	13.7	32.9	50.7	67.0	0.0	0.7	13.3	32.1	50.0	66.2
	S	0.0	0.8	29.3	60.1	74.7	85.6	0.0	0.8	27.9	56.3	72.9	85.4
Repairable	A	0.0	0.0	**2.3**	**14.0**	**13.6**	**4.9**	0.0	0.0	0.0	0.0	0.3	1.0
	B	0.0	0.0	0.1	0.3	0.4	0.6	0.0	0.0	0.0	0.2	0.4	0.6
	C	0.0	0.0	0.0	0.0	0.2	1.2	0.0	0.0	0.0	0.1	0.2	1.2
	S	0.0	0.0	**2.3**	**14.1**	**13.9**	**6.3**	0.0	0.0	0.1	0.3	0.9	2.7
Extensive	A	0.0	0.0	**1.3**	**8.5**	**6.1**	**0.9**	0.0	0.0	0.0	0.0	0.1	0.2
	B	0.0	0.0	0.0	0.0	0.0	0.0	0.0	0.0	0.0	0.0	0.0	0.0
	C	0.0	0.0	0.0	0.1	0.3	0.9	0.0	0.0	0.0	0.1	0.3	0.9
	S	0.0	0.0	**1.3**	**8.6**	**6.3**	**1.7**	0.0	0.0	0.1	0.2	0.4	1.1

[1] Probable replacement damage state is omitted due to negligible ratios of damage state violation.
[2] A: abutment wing walls, B: elastomeric bearings, C: bent columns, S: system (whole bridge).
[3] Given the similarities to the results generated with MSA-L2, only results from MSA-L1 are shown.
[4] Values in bold indicate deviation greater than 10 % with respect to the MSA-GM approach.

no damage state violation was observed at these stripes. Additionally, the good agreement between the fragility curves fitted with samples from the nonparametric strategies (MSA-K1 and MSA-K2) and the parametric model MSA-GM allows one to conclude that (i) the latter was able to fit a parametric density model that was equivalent to the nonparametric distribution fitted by kernel smoothing and that (ii) the consideration of linear correlation between components did not significantly affect the fragility in the present case study. This second statement contradicts the observations made by [157] for long bridges under nonuniform ground motions. The differences in the investigated structures may explain the divergent conclusions with respect to the impact of the correlation between components.

Finally, the mean annual frequency of violating a damage state is intrinsically related to the fragility. Table 3.5 presents the MAF of damage state λ(DS) calculated with each PSDM strategy investigated for all the considered damage states. As expected, intermediate damage states (repairable and extensive) show the greatest differences due to previously observed nonconform fragility curves. Accordingly, differences of more than 100% are observed when lognormality was incorporated, indicating the bias introduced by

poor statistical modeling. This difference could be crucial in accepting the performance of a structure if a threshold for the probability of failure is to be respected. For instance, the MAFs of repairable damage state calculated using MSA-L1 and MSA-GM represent a difference in terms of probability of exceedance in 50 years of 0.4%. In the case of extensive damage state, however, the difference may be found to be negligible given that it represents extremely rare events with return periods greater than 100 000 years. Despite its outdated seismic detailing, the bridge presents overall satisfactory performance, which may be attributed to its location on a region of low to moderate seismicity.

Table 3.5 Mean annual frequency of damage state violation for different PSDM strategies

Damage state†	$\lambda(\text{DS}) \times 10^{-5}$				
	MSA-L1	MSA-L2	MSA-K1	MSA-K2	MSA-GM
Minimal	7.313	7.209	7.241	7.161	7.180
Repairable	1.265	1.254	0.408	0.404	0.421
Extensive	0.701	0.689	0.283	0.284	0.273

† Probable replacement damage state is omitted due to negligible values.

3.6 Conclusions

A methodology coupling multiple-stripe analysis and Gaussian mixture models is proposed for the construction of multivariate seismic demand models with the objective of improving fragility analysis of specific multicomponent structural systems, such as highway bridges. This methodology exploits the stripe structure provided by MSA to locally assess the statistics of the relationship EDP|IM; and the flexibility of mixture models to find density functions that better fit the data given the cluster structure. This approach is thus less constrained than traditional seismic demand modeling strategies in the sense that it does not rely on the typical hypotheses, namely, unimodal lognormality, homoscedasticity, and linear dependence between components.

A classic multispan continuous concrete girder bridge in Eastern Canada is used as a case study to demonstrate the application of the proposed method and to investigate its performance. Initially, a rigorous ground motion selection is performed to define a statistically significant suite of records to then produce the seismic demand data following the scheme of MSA. The proposed approach showed enhanced capacity in fitting the data when compared to traditional approaches that employ lognormal distribution (which is similar to the single-cluster models). A density function that satisfactorily fits the observed data avoids the introduction of bias into the fragility analysis. This effect is also verified

when the features of the proposed MSA-GM model are leveraged for the construction of system fragility functions and calculation of the mean annual frequency of damage state violation.

In addition to the fragility analysis, the produced demand data are investigated with respect to the validity of lognormality and linear dependence. First, the Lilliefors test—a more suitable test for goodness of fit of normal distributions—is employed in the verification of lognormality, and confirming a general perception, this hypothesis is not valid at several IM levels for all the components (especially in the case of abutment wing walls with a gap). The impacts of this assumption on the system fragility analysis are significant for intermediate damage states, indicating that the governing structural components must be appropriately modeled when assessing the system fragility. The hypothesis on the linear dependence between components is also investigated using graphic inspection and testing the absence of correlation, concluding that this assumption is not always valid either. It is shown that the correlation coefficient varies gradually with the augmentation of the spectral acceleration. This observation does not agree with the commonly adopted approach of a constant correlation coefficient over all IM levels. These assumptions, however, have negligible impact on the fragility analysis of the case-study bridge. The analysis of a conventional bridge under uniform motion may explain this finding.

Due to irregularities, asymmetries, and discontinuities, structural systems with highly complex component interactions or multiple regimes of behavior may indeed violate traditional assumptions. Accordingly, the gap between the deck and the abutment wing walls in the case-study bridge causes a discontinuity in the response not only on the deformation of wing walls but on the other critical components by impacting their statistical distribution and dependence. This discontinuity is identified as a driver that leads to the demand data failing the statistical test on lognormality and to the lack of linearity between components. Two regimes of deformation of the bridge components are distinguished relative to gap closure, which depend on the earthquake intensity although not exclusive to a certain intensity level. The proposed density modeling strategy can identify these two regimes and build a more refined multivariate PSDM. The hypotheses of lognormality and linear correlation may, however, still be valid or represent suitable approximations of the observed data depending on the specific structure and on the level of acceptable error on the risk assessment. The choice on the strategy to perform probabilistic seismic demand modeling that better suites the investigated data remains the analyst's responsibility.

The application of the model is demonstrated using a typical highway bridge with satisfactory seismic performance even though the structure was conceived without stringent

seismic design rules at the time. Structures with insufficient seismic detailing in higher seismicity regions and long bridges may be prime candidates to confirm the advantages of the proposed approach. Poor seismic detailing may be the driver of complex component interactions and multiple regimes of nonlinear behavior, while the effect of multiple support motions in long bridges may require refined component dependence modeling. Structural modeling parameters that are neglected in the present study should be incorporated in future work. For instance, strain penetration at the intersection of columns and footings and bridge joints affects the response of bents, which may impact the complexity of the structural demand. Likewise, as design codes are improved periodically, new performance criteria and corresponding component damage indicators should be updated in future bridge fragility assessments. The application of the proposed approach to the construction of bridge-specific fragility functions should also be expanded and tested for the assessment of bridge classes and regional portfolios. Finally, the model could be employed for a thorough analysis of other multicomponent structures, such as multistory buildings in which the responses of different elements or distinct engineering demand parameters might be correlated.

3.7 Acknowledgements

The authors gratefully acknowledge the financial support from the Natural Science and Engineering Research Council of Canada (Grant No. 37717), the *Fonds de Recherche du Québec – Nature et Technologies* (Grant No. 171443), and the Brazilian National Council for Scientific and Technological Development (CNPq) (Grant No. 233738/2014-2), and all the assistance provided by the *Centre d'Études Interuniversitaire des Structures sous Charges Extrêmes* (CEISCE). Computational resources were provided by *Calcul Québec* and Compute Canada.

CHAPTER 4

SEISMIC PERFORMANCE ASSESSMENT OF A RETROFITTED BRIDGE WITH NATURAL RUBBER ISOLATORS IN COLD WEATHER ENVIRONMENTS USING FRAGILITY SURFACES

Avant-propos

Auteurs et affiliation :
P.A.C. Bandini : étudiant au doctorat, Université de Sherbrooke, Faculté de génie, Departement de génie civil et de génie du bâtiment
G.H. Siqueira : professeur, University of Campinas, School of civil engineering, architecture, and urbanism, Department of structures
J.E. Padgett : professeur, Rice University, Department of civil and environmental engineering
P. Paultre : professeur, , Université de Sherbrooke, Faculté de génie, Departement de génie civil et de génie du bâtiment

Date de soumission : 24 avril 2021
Revue : ASCE Journal of Bridge Engineering
Titre français : Évaluation de la performance sismique d'un pont routier isolé avec des appareils en caoutchouc naturel en basses températures
Contribution au document :
L'approche proposée dans le chapitre précédent est utilisée dans un cadre probabiliste pour évaluer l'impact du raidissement thermique des isolateurs en caoutchouc naturel sur la performance d'un pont réhabilité dans des conditions hivernales sévères. Une compréhension holistique de la performance sismique du pont sous les effets des températures froides est fournie en tenant compte de la corrélation de la demande sismique des composants critiques du pont étudiés, et la contribution individuelle de ces composants à la fragilité de l'ensemble du système. À cette fin, des fonctions de fragilité paramétrées

conditionnées par l'intensité sismique et la température développées pour la première fois dans l'évaluation de la performance d'un pont isolé en région froide. L'aspect global de cette étude fournit un exemple perspicace sur la façon dont la combinaison d'isolateurs et de structures de retenue latérale peut être bénéfique pour la performance d'un pont réhabilité à des températures inférieures au point de congélation.

Résumé français :
Il a été démontré que l'isolation sismique à base de caoutchouc est l'une des mesures les plus efficaces pour protéger les éléments structurels des dommages causés par les tremblements de terre. Le principal constituant de ce système d'isolation est le caoutchouc, un matériau qui est susceptible au raidissement lorsqu'il est exposé à de basses températures de l'air. Dans le cas des ponts routiers isolés, le raidissement thermique peut réduire l'efficacité des isolateurs, transférant des forces plus importantes à la sous-structure. L'évaluation de la réponse sismique des structures isolées dans les régions froides est donc nécessaire. En conséquence, cette étude quantifie l'impact des basses températures sur la performance sismique d'un pont routier isolé avec des isolateurs en caoutchouc naturel en utilisant un cadre probabiliste basé sur des surfaces de fragilité. À partir de ces surfaces au niveau des composants et du système, on révèle que les effets des températures froides sur les ponts routiers équipés d'isolateurs en élastomère peuvent être négligeable selon la configuration des structures de retenue latérale. Cependant, lorsque les isolateurs sont capables de remplir leur fonction sans entrave, leur raidissement thermique peut être significativement préjudiciable à la sous-structure du pont, affectant principalement les piliers.
Note :À la suite des corrections demandées par les membres du jury, le contenu de cet article diffère de celui qui a été soumis.

Abstract:
Rubber-based seismic isolation has been demonstrated to be one of the most effective measures to protect structural elements from damage during earthquakes. The main constituent of these isolation units is rubber, a material that is subject to stiffening when exposed to low air temperatures. In the case of isolated highway bridges, thermal stiffening may reduce the efficiency of isolators, transferring higher forces to the substructure. The assessment of the seismic response of isolated structures in cold regions is thus necessary. Accordingly, this study quantifies the impact of low temperatures on the seismic performance of a highway bridge seismically isolated with natural rubber isolators using a probabilistic framework based on fragility surfaces. From these component- and system-level surfaces, it is revealed that the effects of cold temperatures on highway bridges retrofitted with elastomeric isolators may be negligible depending on the configuration

of lateral restraining structures. However, when isolators are able to perform their function without impediment, their thermal stiffening may be significantly detrimental to the bridge's substructure, mainly affecting bent columns.

Keywords: Bridges, Seismic fragility, Retrofitting, Rubber isolators, Cold regions, Fragility surfaces

4.1 Introduction

In recent decades, seismic isolation has gained attention as one of the most effective measures to mitigate or eliminate damage in the structural elements of bridges and bridge systems during severe earthquake shaking [54, 207, 243]. The rather simple concept behind seismic isolation consists of the introduction of flexibility (and damping) into the structural system of a bridge, which is typically achieved by placing isolators between the superstructure (i.e., deck/girders) and substructure (i.e., piers/bents and abutments). Seismic isolators, hence, decouple the bridge superstructure from the extreme lateral excitations induced at its base. This results in a significant reduction in the transmission of forces between the bridge superstructure and substructure [189]. This reduction in forces allows the bridge substructure to remain in the elastic range and eliminates the occurrence of plastic hinges at the top and bottom of the piers. The seismic performance of a bridge can thus be significantly improved by introducing isolators with low lateral stiffness that are capable of shifting the dominant period of the structure to the displacement sensitive region [68].

Laminated rubber isolators (rubber pads with reinforcing steel plates, with or without lead cores) are widely used for seismic isolation of structures [54]. While the role of steel plates is to increase the vertical stiffness by controlling the bulging of the elastomeric pads under gravity loads, the properties of the elastomeric pads highly influence the lateral response of the isolator. The mechanical properties of rubber are affected by several factors, including the temperature, aging process, strain level, loading history, and strain rate [107]. While higher temperatures have a negligible effect on reducing the stiffness of rubber, elastomers may undergo significant thermal stiffening processes when subjected to low temperatures. The following two processes are identified: (i) instantaneous stiffening, which depends only on the air temperature, and (ii) crystallization, which depends on the air temperature and on the exposure time to low temperature [187, 246, 58]. For seismic applications, the effect of low levels of crystallization is highly detrimental to structural performance even after yielding occurs due to a large deformation cycle [267, 268, 101]. Stiffer isolators may cause the transmission of larger inertial forces to the substructure than expected when designed

for a reference temperature (usually 20 °C). The most commonly used elastomer in the United States and Canada is natural rubber (NR) due to its higher seismic performance when compared to that of synthetic rubbers such as neoprene when high levels of shear strains are required [54, 245]. Moreover, the effects of crystallization and thermal stiffening are stronger on neoprene than on natural rubber, suggesting that the latter is better for low-temperature applications, as in the case of highway bridges in cold climates such as in Northern Canada or Alaska [272]. However, natural rubber may undergo severe stiffening at subfreezing temperatures, and these effects must be considered in the design of NR isolators.

Accordingly, to account for this phenomenon in a simplified manner, design codes such as the AASHTO-14 [5] and the Canadian Highway Bridge Design Code (CHBDC) CSA S6-14 [57] recommend the use of bounding analysis. Additionally, design standards require concomitant minimum service temperatures to be adopted for this bounding analysis, in a compromise between the expected seismic hazard and cold weather conditions. Nevertheless, [118] suggested that the annual probability of the minimal average daily temperature being lower than the concomitant temperature specified by the Canadian code had a large variability across Canada, which was attributed to the fact that the concomitant temperature considered in the code is not based on a probabilistic analysis. A probability-based framework for establishing the concomitant temperature and design earthquake action is still recommended, even if the concurrent event of prolonged low temperature and earthquake shaking is suggested as extremely improbable.

Nevertheless, substantial earthquakes have occurred during winter in North America in locations such as Charlevoix-Kamouraska in February 1663, southern Alaska in January 1912, southern Yukon-Alaska Border in February 1979, Miramichi (New Brunswick) in January 1982, and the Ungava Region (northern Quebec) in December, 1989 [192, 254]. Figure 4.1 links past seismic events [191] and future projected coldest temperatures [213] in Canada, implying that active seismic regions could be subjected to extremely low temperatures, as in the case of eastern Canada.

The stiffening of elastomeric isolators caused by low temperatures reduces the efficiency of isolation devices while increasing the demand on the substructure. Consequently, the question may arise of whether this effect can be harmful to the seismic vulnerability of the bridge or if substructure components (mainly piers) are still protected when rubber isolators undergo severe stiffening. Some deterministic studies have verified the change in the elastomeric response of isolators and on bridge substructure elements caused by the modification of mechanical properties due to low temperatures (e.g., [260, 202, 80]).

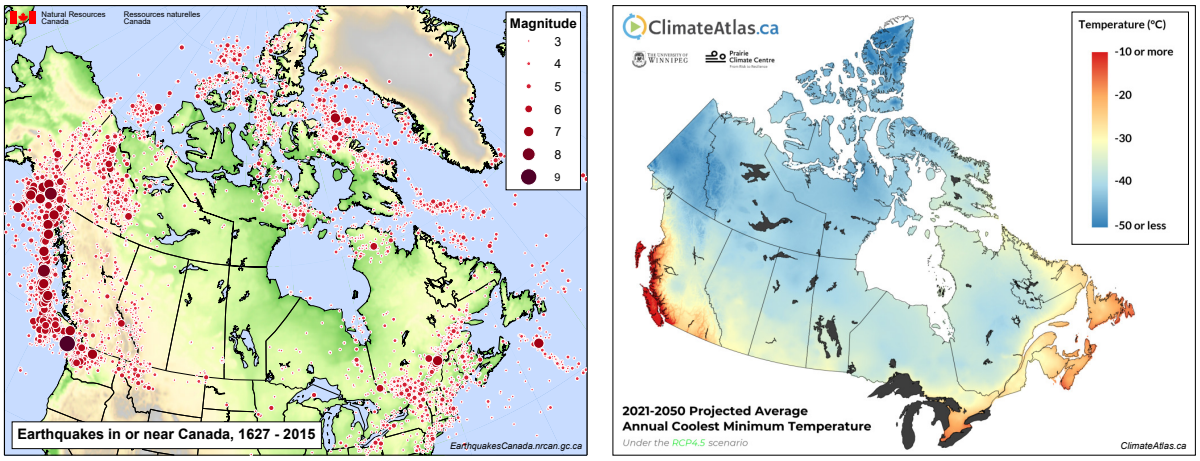

(a) (b)

Figure 4.1 Canada's (a) historical earthquakes (Natural Resources Canada 2018a) and (b) projected annual coldest temperatures (Prairie Climate Centre 2019)

Although relevant, a probabilistic framework that captures the inherent uncertainties is required for a better comprehension of the seismic performance of an isolated bridge. In this case, studies are more scarce and the works developed by [190], [40], and [98] evaluated the concurrent events of earthquake loading and thermal stiffening using either reliability or fragility analysis. Drawbacks of the probabilistic studies are related either to the use of simplified single-degree-of-freedom models—which neglect the interaction between bridge components—or the adoption of damage states of isolators that do not agree with experimental observations—either by neglecting the failure of isolators or by considering intermediate damage states, contrary to studies that suggest that elastomeric isolators hardly exhibit macroscopic signs of damage before failure [225, 103]. To address these gaps in the performance assessment of isolated bridges under earthquakes and extreme cold weather, a case-study bridge is investigated in Quebec, Canada. A three-dimensional numerical model of the retrofitted bridge that comprises its critical components (e.g., columns, abutments, and isolators) is adopted. This model is parameterized to consider the increment of lateral stiffness of natural rubber isolators under low temperatures. The study leverages a multivariate seismic demand modeling approach that handles the interaction between the three critical structural components. Two scenarios are idealized to consider the case of retrofitted bridges with respect to lateral clearances. Finally, fragility surfaces are constructed to assess the bridge's seismic performance at different temperatures, based on consistent damage state models of its components.

4.2 Analytical framework for constructing parameterized fragility functions

Seismic fragility analysis is a valuable tool in performance-based earthquake engineering for strategic planning of aftermath actions and for retrofitting evaluation. Seismic fragility models traditionally estimate the conditional probability of damage state exceedance DS given the occurrence of an earthquake event with a specific intensity measure level IM = im, as indicated by

$$\text{Fragility} = \Pr(\text{DS}|\text{IM} = im) \tag{4.1}$$

Seismic fragility functions are often depicted as curves (e.g., [199, 206, 250, 243]), in which the probability of exceeding a damage state is only dependent on the seismic intensity. More recently, parameterized fragility functions in the form $\Pr(\text{DS}|\text{IM}, \mathbf{P})$ have been developed [110, 218, 129], in which $\mathbf{P} = \{p_1, p_2, \ldots, p_n\}$ represents a set of n structural and/or environmental parameters (also called covariates or predictors). The depiction of a parameterized seismic fragility function with respect to the conditioning intensity measure and a single covariate has the form of a surface [112], and its visualization is useful for assessing the influence of this structural or environmental parameter on the structure's seismic performance.

Several techniques have been studied to develop seismic fragility surfaces (e.g., [110, 231]). Building a parameterized fragility function can be categorized as a problem of distinguishing between two discrete regions of either structural failure (damage state violation) or survival. Supervised learning techniques for discrete data (i.e., classification) are well suited for this task [136], and logistic regression is one option that has often been adopted owing to its simplicity and interpretability [2, 141]. In this case, the parameterized fragility function takes the form of the log odds (logit)

$$\Pr(\text{DS}|\text{IM}, \mathbf{P}) = \frac{\exp\left(\beta_0 + \beta_1 im + \sum_{i=2}^{n+1} \beta_i p_{i-1}\right)}{1 + \exp\left(\beta_0 + \beta_1 im + \sum_{i=2}^{n+1} \beta_i p_{i-1}\right)} \tag{4.2}$$

where β_i with $i = 0, 1, 2, \ldots, n$ is a set of model parameters that are learned from the observed data on damage state exceedance.

To generate the dataset on damage state exceedance within an analytical framework, sampling techniques, such as Monte Carlo sampling, can be employed to determine the values of structural and seismic parameters used in response history analyses (RHA). These techniques may, however, be computationally expensive and time-consuming when employed

to properly cover the domain of the structural and seismic parameters of interest (e.g., [190]). Alternatively, probabilistic seismic demand modeling techniques can be adopted to reduce the computational cost (e.g., [199, 20]). These techniques establish a probabilistic relationship—known as a probabilistic seismic demand model (PSDM)—between the structural responses (or engineering demand parameters, EDP) and the seismic intensity measure IM, based on the results of limited dynamic analyses.

Recently, a PSDM approach was proposed by [32] that locally considers the uncertainty of the seismic response and the correlation between pairs of structural components using Gaussian mixture models. This formulation constructs Gaussian mixture seismic demand models (GMSDM) based on mixtures of multivariate normal distributions on the peak component seismic demands, which are generated using multiple-stripe analysis (MSA) [124]. This density modeling approach relaxes some of the traditional assumptions made by other PSDMs and has been shown to build a more refined model that captures highly complex component interactions or multiple regimes of deformation due to discontinuities, irregularities, and asymmetries found in structural systems [130, 32]. The stripe structure of the MSA allows one to capture the statistics of the peak component responses that depend on the observed seismic intensity measure. In addition, this approach is suited for the selection of ground motion record techniques that are consistent with the site's seismic hazard, such as the conditional spectrum approach [21] or the generalized conditional intensity measure (GCIM) approach [43]. Equation 4.3 expresses the joint posterior probability density function (PDF) of a vector of component EDPs (represented by the random variable $\mathbf{X}$) following a Gaussian mixture (i.e., $\mathbf{X} \sim \text{GM}(\mathbf{x}; \boldsymbol{\Psi})$)

$$f(\mathbf{x}|\boldsymbol{\Psi}) = \sum_{k=1}^{m} \pi_k f(\mathbf{x}; \boldsymbol{\mu}_k, \boldsymbol{\Sigma}_k) \tag{4.3}$$

where $\boldsymbol{\Psi} = \left[\boldsymbol{\pi}^{\mathrm{T}}, \boldsymbol{\xi}_1^{\mathrm{T}}, \ldots, \boldsymbol{\xi}_m^{\mathrm{T}}\right]^{\mathrm{T}}$ is the vector that aggregates all the GM model parameters, in which: $\boldsymbol{\pi}^{\mathrm{T}} = [\pi_1, \ldots, \pi_k, \ldots, \pi_{m-1}]$ is the vector of mixture proportions, with $\sum_{k=1}^{m} \pi_k = 1$; each vector $\boldsymbol{\xi}_k$ contains the model parameters related to the mean vector $\boldsymbol{\mu}_k$ and the covariance matrix $\boldsymbol{\Sigma}_k$ of the k^{th} mixture cluster; and $f(\mathbf{x}; \boldsymbol{\mu}_k, \boldsymbol{\Sigma}_k)$ is the PDF of a multivariate Gaussian distribution on $\mathbf{X}$ with mean $\boldsymbol{\mu}_k$ and covariance $\boldsymbol{\Sigma}_k$. Fitting the GM model to the observed data is accomplished using the expectation-maximization algorithm. Furthermore, it is challenging to find the covariance structure and the required number of clusters m to satisfactorily model this phenomenon. The Bayesian information criterion (BIC) can be used to quantify the goodness-of-fit of the model by calculating

the log-likelihood of the fitted model given the observed data while penalizing the model complexity to prevent overfitting (i.e., preventing overcomplex models) [177].

Within this framework, to evaluate the impact of thermal stiffening of natural rubber isolators on the seismic performance of the isolated bridge, the fragility surfaces must be conditioned on a seismic intensity measure and air temperature. Therefore, the GMSDMs must also be conditioned on pairs of temperature and seismic intensity. The chosen GMSDMs are then used to draw N demand samples at a given IM level and temperature θ (i.e., $D_{i,im,\theta} = D_i|\text{IM} = im, \Theta = \theta$) that are paired with N capacity samples C_i to generate the damage state binary data: $\text{DS}_{i,im,\theta} = 1$ when $D_{i,im,\theta} > C_i$ (i.e., exceedance of the damage state) or $\text{DS}_{i,im,\theta} = 0$ when $D_{i,im,\theta} < C_i$ (i.e., nonexceedance). Temperature is represented here by the Greek leter theta (θ) instead of T to avoid confusion with structural vibration period. This dataset is finally used to train the fragility model given by Equation 4.2. The effect of low temperatures on the global response of the isolated bridge can be incorporated in the numerical model of the isolated bridge through an analytical model that relates temperature and isolator stiffness. The formulation adopted here to represent this phenomenon is described next.

4.3 Modeling of thermal stiffening in rubber isolators

As briefly discussed, the sought mechanical properties for elastomeric seismic isolators are incompressibility (to sustain structural weight), low shear modulus (to lengthen fundamental period), and damping (to avoid excessive displacements). The lateral stiffness K_h is the most important property of a seismic isolator. Typical shape factors (i.e., the ratio of the bounded and vertically loaded rubber area to the free area of one rubber layer of the bearing) of seismic isolators vary between 8 and 20 [103], allowing the calculation of the lateral stiffness based on the rubber shear modulus G (instead of the effective shear modulus of the rubber layer G_{eff}) with negligible error

$$K_h = \frac{GA_r}{T_r} \tag{4.4}$$

where (A_r is the cross-sectional area of rubber, and T_r is the total height of N rubber layers of individual thickness t_r (i.e., $T_r = Nt_r$). For a given lateral displacement Δ_h, the shear strain in the isolator is then calculated as $\gamma = \Delta_h/T_r$.

Although elastomeric isolators essentially behave as viscous-elastic materials with an elliptical hysteric curve, their lateral behavior is commonly idealized by a bilinear model for simplification [189]. Figure 4.2 illustrates this idealization comparing the real behav-

ior to that of the bilinear model, which can be fully represented by the initial (elastic) stiffness K_1, the postactivation stiffness K_2, and the characteristic strength Q. The initial stiffness, the postactivation stiffness, and the characteristic strength are typically obtained from available hysteresis loops of rubber bearing tests. For natural rubber bearings (NRB) and high-damping rubber bearings (HDRB), K_1 is usually assumed to be in the range of 2 to 15 times K_2 [204]. The postactivation stiffness K_2 can also be based on the effective stiffness, characteristic strength and design displacement [189]. Additionally, according to characterization tests of elastomeric bearings [122], the activation displacement Δ_y can be approximated as 10% of the total rubber height. The damping capacity of the isolator is intrinsically related to the energy dissipated per cycle (EDC), and the effective hysteretic damping ratio ξ_{eff} can be estimated as [211]

$$\xi_{\text{eff}} = \frac{\text{EDC}}{2\pi K_{\text{eff}} \Delta_d^2} \tag{4.5}$$

where K_{eff} is the effective lateral stiffness of the ensemble isolators and substructure, and Δ_d is the design displacement. When substructures present a lateral stiffness much larger than the isolation units, the effective lateral stiffness of the combination of a substructure and isolators can only be approximated by the isolator lateral stiffness without introducing significant errors (i.e., $K_{\text{eff}} \approx K_h$).

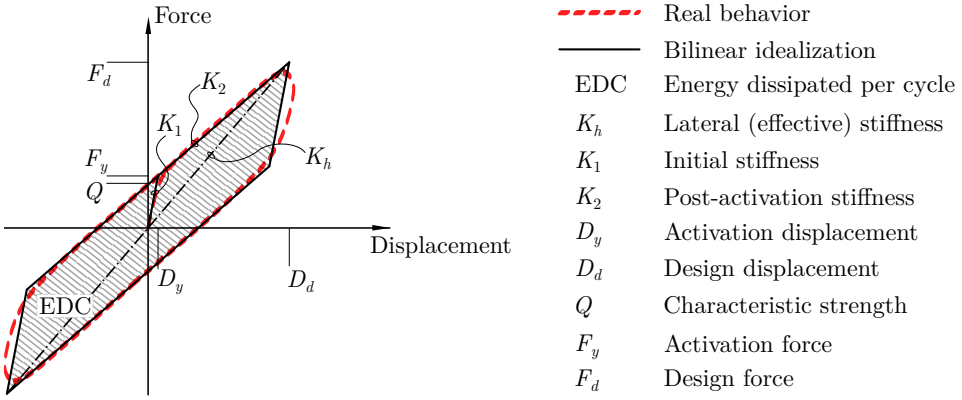

Figure 4.2 Bilinear idealization of the lateral hysteretic behavior of elastomeric isolators

This approximation is useful for the preliminary design of seismic isolators using simplified methods, such as uniform-load and single-mode spectral analysis in CSA S6-14 [57]. In this case, considering the segment of the superstructure with weight W, the effective period of

the isolated structure can be estimated as

$$T_{\text{eff}} = 2\pi\sqrt{\frac{W}{K_{\text{eff}}\,\text{g}}} \tag{4.6}$$

where g is the acceleration of gravity. Based on a chosen target effective period, the effective stiffness can be estimated from Equation 4.6. Furthermore, the design displacement Δ_d depends on the target effective period and damping. Hence, an iterative process may be adopted to estimate these isolator properties until convergence of the bridge displacement is achieved. Further details on the design of elastomeric isolators are discussed along with the case-study bridge.

The mechanical properties of elastomeric isolators depend intrinsically on the shear modulus of rubber, which is prone to undergo significant stiffening under low air temperatures. Thermal stiffening may significantly increase the reference temperature stiffness of rubber compounds, with two main processes distinguished: instantaneous and time-dependent stiffening. In extreme cases, the elastomer may become brittle and fail, which is a phenomenon known as glass transition. All these phenomena are fully reversed once the temperature increases back to the reference conditions. The actual increase in stiffness depends on many factors, including the rubber compound, temperature, and exposure time [187, 83, 246]. Modification factors to be multiplied by nominal (at reference temperature) properties have been recommended to obtain the modified mechanical properties under the effect of low temperatures [69, 267, 268, 70]. More recently, [58] performed an extensive experimental program to assess the thermal effects on the mechanical properties of elastomeric compounds typically employed in isolation units. The following continuous empirical relationship for instantaneous stiffening was established between the rubber shear stiffness and air temperature

$$G(\theta) = G_0\left(0.0005\theta^2 - 0.03\theta + 1.4\right) \tag{4.7}$$

where G_0 is the secant shear modulus at the reference temperature $\theta_0 = +20\,^{\circ}\text{C}$.

The thermal crystallization process (or time-dependent stiffening) of rubber in seismic isolators is, however, a rather complex phenomenon to be empirically modeled due to in-service behavior aspects. In summary, the results reported by [58] suggested that the influence of the exposition time at low temperature on the response of rubber were conditioned on the strain amplitudes and the type of displacement protocol. In fact, thermal crystallization showed lower influence on the specimen stiffness when large shear strains

(compatible with those attained by isolators subjected to strong ground shaking) were applied compared to that of low strains. Regarding, the displacement protocol, cyclic tests with increasing strain amplitude are deemed to be representative of the structural response to far-source earthquakes, whereas cyclic tests with constant amplitude are more suitable to simulate the seismic response under near-source conditions. Near-source earthquakes are characterized by a single large impulse of motion, which forces the structure to absorb a large amount of energy nearly instantaneously, with a few large plastic cycles [65, 172]. The main observed effect of rubber thermal crystallization was an increase in the force levels transmitted by the isolation system to the structure during the first loading cycle. Consequently, the relative importance of cyclic responses for structures grows at a greater distance from the epicenter, while time-dependent stiffening effects dissipate due to internal heating of the isolator. Conversely, the structural response is governed by the peak response in near-source conditions, which may be substantially affected by the thermal crystallization.

Finally, Equations 4.4 and 4.7 are coupled to the effective stiffness of NR isolators when subjected to instantaneous thermal stiffening. The presented formulation is integrated into a parameterized numerical model of the case-study bridge to modify the mechanical properties of natural rubber isolators. Details on the case-study bridge and the seismic isolation system are described in the following section. Moreover, as is described in later sections, the ground motions used in this study are only representative of far-source earthquakes. Hence, the time-dependent stiffening of natural rubber is neglected hereafter.

4.4 Case-study bridge

The seismic performance of the Chemin des Dalles overpass (Figure 4.3a), located in Quebec, Canada, is assessed here in an idealized isolated configuration. This bridge was designed in 1975 and does not comply with current seismic design standards and detailing. The bridge has been extensively studied, and data have been gathered on its structural properties, capacity, site conditions, and numerical model [221, 251, 244, 280]. It is a three-span continuous concrete girder bridge, with a 106.5 m long and 13.2 m wide deck, and a vertical underclearance of 6.2 m. The superstructure is supported by two concrete piers and two seat-type wing-wall abutments. The piers are moment-resisting frames in the transverse direction consisting of a transverse beam supported by three circular reinforced concrete (RC) columns with diameters of 0.9 m resting on shallow foundations (Figure 4.3b). Details on the numerical model, design of isolation units, damage states of the critical bridge components, site consistent seismic ground motion record selection, and historical temperature data are presented hereafter.

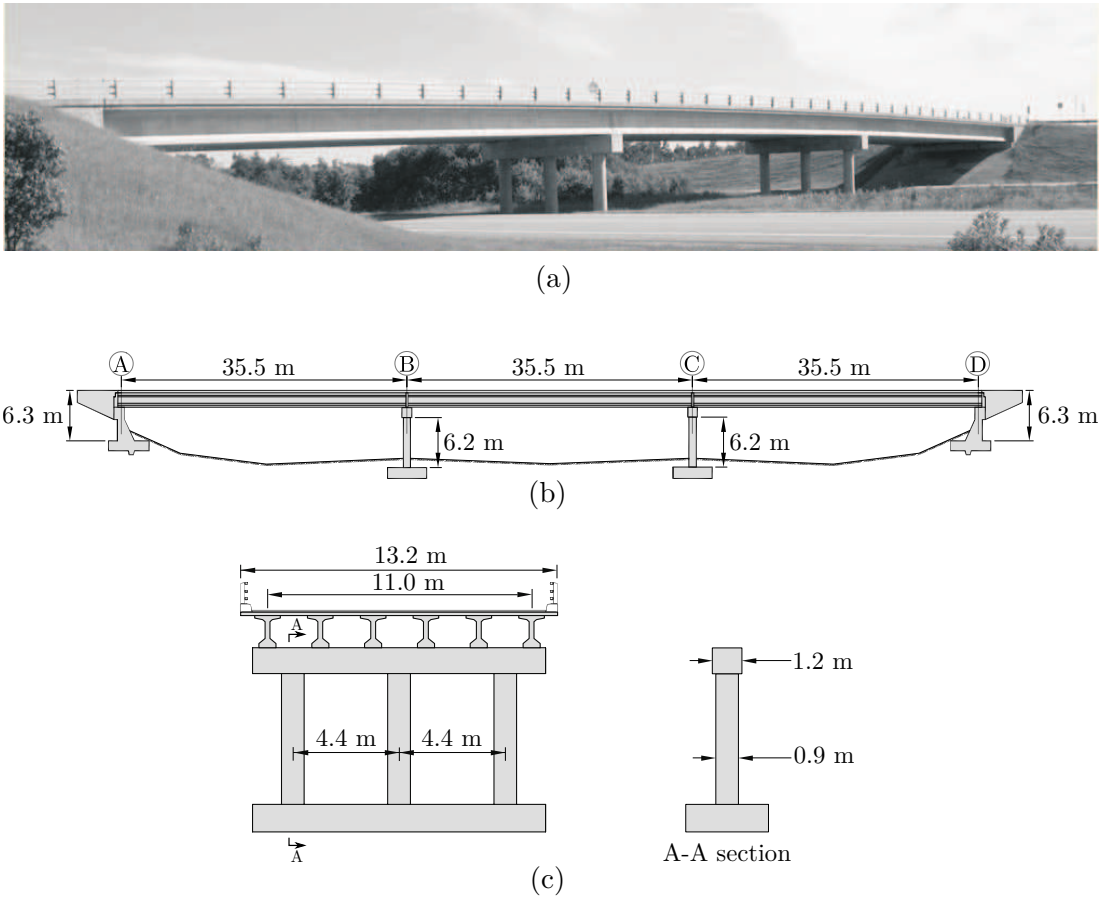

Figure 4.3 Case-study bridge over highways in Quebec: (a) overview (photography credits to Roy et al. 2010), (b) elevation, and (c) bent details

4.4.1 Numerical modeling

The numerical model, which was originally created by [251] based on construction drawings and calibrated with previous in situ ambient vibration tests by [221], and was later modified by [244] for the introduction of natural rubber isolators, is leveraged and updated for the present work. The model is built in the Open System for earthquake engineering simulation (OpenSees) [175] and is parameterized to enable the modifications of the mechanical properties of the NRB isolators. Figure 4.4a shows an overview of the three-dimensional (3D) model constructed with OpenSees, which uses beam-column elements and nonlinear zero-length spring elements to represent the behavior of this structural system. The nonlinear behavior of the bent columns and cap beams is captured with force-based beam-column elements with fiber cross sections [195] while concrete confinement effects are modeled according to [148] using *Concrete02* and *Steel02* prebuilt material models in OpenSees (Figures 4.4d, f, and g). The natural rubber isolation units replace the original elastomeric bearings on the abutments and the pinned connections on

bents, and are inserted as zero-length elements with bilinear material behavior between the six AASHTO-type V precast concrete girders and the top of the bent cap beams and the seat-type abutments (Figures 4.4b, c, and e). Associations of zero-length elements and zero-length elements with gaps are employed to simulate the behavior of abutments and footings (Figures 4.4b and c). Further details on the numerical model can be found elsewhere [251, 244, 32].

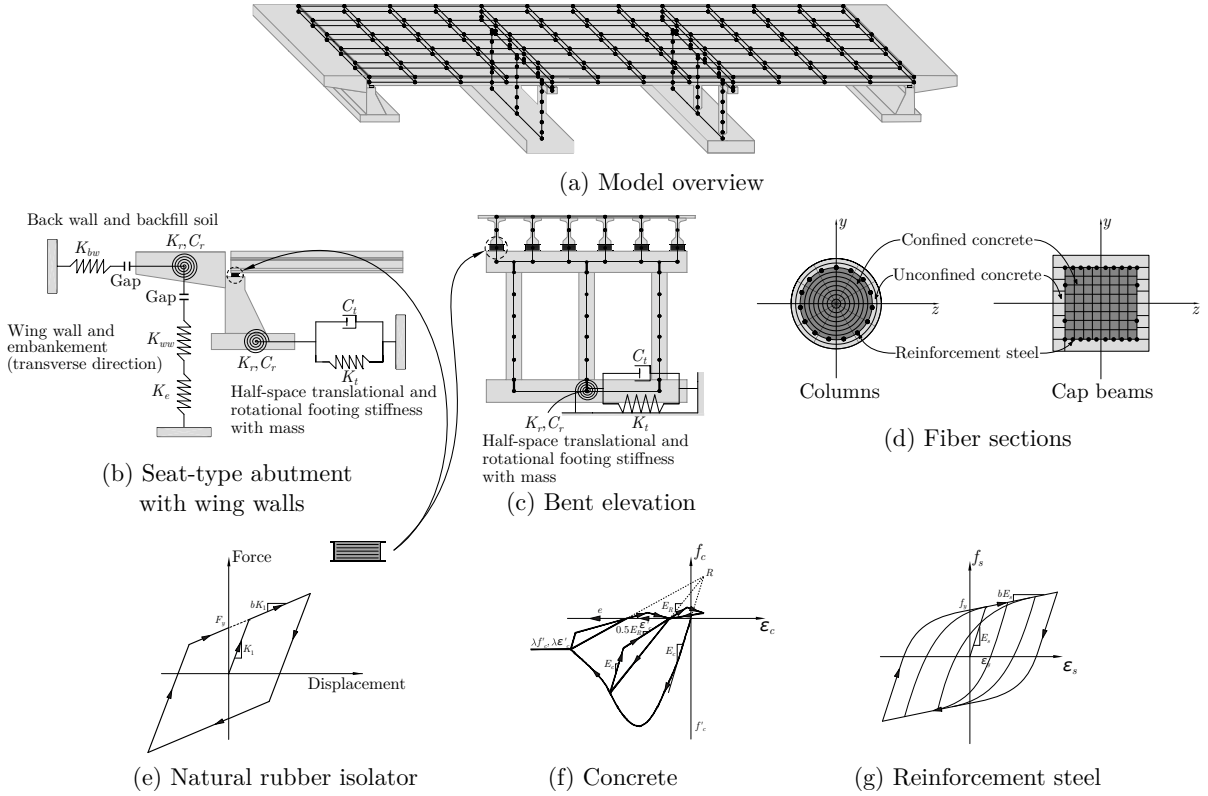

Figure 4.4 Numerical model of the case-study bridge

The isolation units are redesigned according to CSA S6-14 to account for important modifications related to performance-based design requirements, recent developments of seismic hazard in Canada, and lower damping effects observed under motions rich in high frequencies [142]. The shear strain of natural rubber at the reference temperature and effective damping are set to $G_0 = 0.75\,\text{MPa}$ and $\xi_{\text{eff}} = 7.5\%$, respectively. These values are representative of natural rubber in service conditions found in structural engineering applications in Quebec [243]. Isolation units are designed to assure a fundamental period of 2.0 s in both the transverse and longitudinal directions. Given the target period and the effective damping ratio, the design displacement of the isolators is calculated as $\Delta_d = 70\,\text{mm}$ using the site specific spectral data for a probability of exceedance of 2% in 50 years, according to the hazard calculator of Natural Resources Canada [193]. Given the different weights

supported by bents and abutments, the effective stiffness of the isolators installed on the bents is $K_{\text{eff}} = 0.86\,\text{kN/mm}$, whereas that of isolators installed on the seat-type abutments is $K_{\text{eff}} = 0.52\,\text{kN/mm}$.

Because the isolators are preliminarily designed using the simplified approach of CSA S6-14, modal analysis of the whole bridge is performed using the effective stiffness of the NRB isolators to ensure that the first two vibration modes behave as expected. Figure 4.5 illustrates these two fundamental modes of the isolated bridge along with the first two vibration modes of the as-built bridge. Accordingly, modal information demonstrates the effective design of the isolator units in (i) lengthening the fundamental period in the two orthogonal directions with good agreement with the target effective period $T_{\text{eff}} = 2.0\,\text{s}$, and (ii) decoupling the bridge deck from the substructure with fundamental modes mobilizing more than 90% of the modal masses in each horizontal direction.

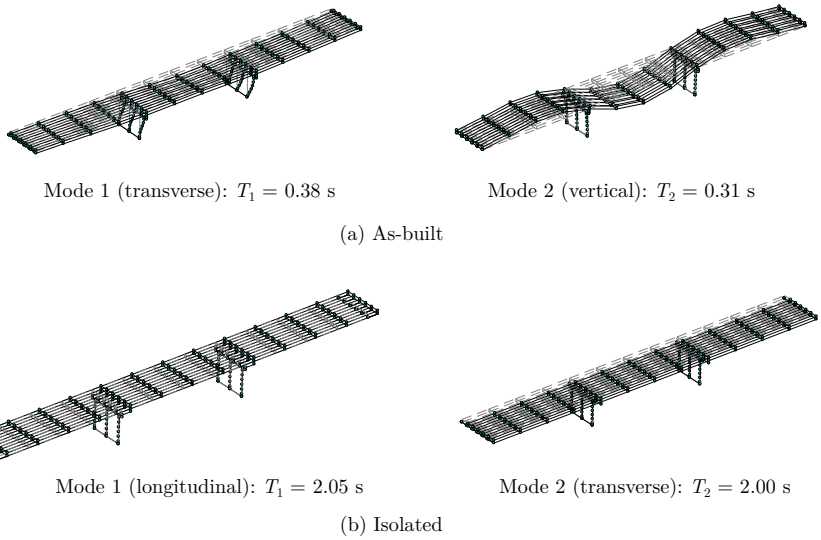

Figure 4.5 First two vibration modes of the (a) as-built and (b) isolated bridge

Finally, two scenarios are idealized with respect to lateral restraining structures, represented in this case study by the abutment wing walls. The CHBDC requires that sufficient clearances be provided such that the isolation units can perform their function without impediment. Because this is an existing structure with deficient seismic detailing, two values for the gap between the deck and the abutment wing walls are considered. In scenario I, the original 25.4 mm gap remains unchanged, as if these lateral structures are expected to be sacrificed during severe ground shaking action. In scenario II, the gap is augmented to 100 mm, simulating a situation where the wing walls would be modified to comply with the code requirement. Nonlinear response history analyses according to the

MSA technique are conducted using the suite of seismic ground motion records described below.

4.4.2 Component capacities and performance levels

An essential step in performing seismic fragility analysis is the definition of structural component capacity models. For highway bridges, these capacities are defined in terms of damage states relating expected damage to components and the bridge's postevent service level. In this study, mechanics-based capacity values corresponding to the damage state descriptions presented in the CSA S6-14 are adopted. The four damage states are defined in progressive order of severity as minimal, repairable, extensive, and probable replacement and are renamed DS1 to DS4 hereafter for brevity. The case-study bridge includes three critical components: abutment wing walls, NRB isolators, and bent columns, while other structural components have shown negligible seismic fragility for multispan continuous concrete girder bridges in eastern Canada [250, 243]. The parameters associated with the engineering demand of each component are taken only in the transverse direction [244] and are described in Table 4.1 under normal operating conditions (i.e., at the reference temperature of 20 °C). For completeness, the effect of the uncertainty on the capacity should be included in the analysis [20]. Therefore, the capacities of the components are assumed to follow lognormal distributions [199, 168] with median m_C and dispersion ζ_C values fully characterizing each damage state model.

Table 4.1 Damage state capacities of bridge components at the reference temperature ($\theta_0 = 20\,^{\circ}\mathrm{C}$)

Component EDP	DS1		DS2		DS3		DS4	
	m_C	ζ_C	m_C	ζ_C	m_C	ζ_C	m_C	ζ_C
Abutment wing wall deformation, Δ_{aww} (mm)	7.0	0.25	15.0	0.25	30.0	0.46	60.0	0.46
NRB isolator shear strain, γ_{iso} (%)	n/a	n/a	n/a	n/a	n/a	n/a	267	0.46
Column drift ratio, δ_{col} (%)	0.5	0.25	1.4	0.25	2.0	0.46	2.2	0.46

Note: n/a – not available

The median capacities of the columns follow the findings of [280], who experimentally established column damage states in accordance with the performance criteria of the CSA S6-14 (including an exact replica of the actual bridge column). The median capacities of the abutment wing walls were adapted by [251] for structures in Quebec based on the prescriptive capacity models proposed by [64]. The CHBDC also indicates the expected levels of performance and the respective damage states for seismically isolated bridges, which suggests that intermediate damage will occur for isolation devices. Conversely, experimental observations on elastomeric isolators (e.g., [225, 103, 223]) suggest

that isolators are either macroscopically undamaged or fail due to shear or buckling (i.e., intermediate damage states are hard to define by visual inspection). Moreover, elastomeric isolators may be classified as slender or short depending on their slenderness ratio, a parameter that controls the type of failure (either buckling for the former or shear failure for the latter) [243, 103]. The isolators designed for the case-study bridge are considered slender and, therefore, are expected to present instability issues before showing any sign of shear failure. Finally, dispersion values follow the recommendations given by [197].

Freezing temperatures can alter a material's response to loading and, consequently, affect the element's capacity. For instance, experimental data on flexural-dominated columns tested at low temperatures ($-40\,^{\circ}$C) exhibit an increase in the flexural strength (explained by the enhancement in the mechanical properties of plain concrete and steel reinforcement in extreme cold conditions) and a decrement in the displacement capacity. This decrement was attributed to a substantial reduction in the spread of plasticity of the specimens tested at low temperatures, causing an increment in the curvature demand at the base of the column [183]. A numerical parametric study was then performed with finite element models of bridge bents calibrated against experimental data to represent the reduction in the ductility capacity of RC columns at low temperatures [184]. Equation 4.8 expresses the relationship between the displacement ductility at the reference temperature and low (-40 °C) temperatures

$$\frac{\mu_{\Delta(-40)}}{\mu_{\Delta(+20)}} = 0.88\left(\mu_{\Delta(+20)}\right)^{-0.17} \tag{4.8}$$

where $\mu_{\Delta(\theta)}$ is the displacement ductility at temperature θ in °C. Although defined at $-40\,^{\circ}$C, this relationship is recommended for temperatures below $0\,^{\circ}$C, thereby producing a conservative result [184].

Although the parametric study considered transverse reinforcement, it is worth noting that ratios as low as 0.4% (close to the 0.34% were found for the columns of the case study bridge), and the flexural-dominated experimental specimens presented a transverse reinforcement ratio of 1.2%. In addition, the numerical model did not consider bond slip between the reinforcing bar and concrete, which was observed during laboratory tests on a replica of the actual bridge column at ambient temperature [280]. Therefore, the real decrement on the displacement capacity of the columns of the case-study bridge may deviate from that of the analytical model expressed by Equation 4.8. This analytical model is, nonetheless, deemed adequate in the present study due to the scarcity of more refined models. The adopted engineering demand parameter for the bent columns is the drift ratio, and a simple conversion of the ductility levels to drift ratios is required. Thus, the reference column drift median capacities (Table 4.1) are multiplied by 0.88, 0.74, 0.70, and

0.68, from minimal to probable replacement damage states to account for the decrement in the displacement capacity at subfreezing temperatures.

Finally, to the best of the authors' knowledge, no study on NRB isolators has quantitatively determined the impact of low temperatures on the shear strain capacity, except for those that undergo glass transition, which occurs at approximately $-65\,^{\circ}\mathrm{C}$ for natural rubber [153] and is beyond the scope of the present study. However, one advantage of the analytical framework employed in this study is that a decrement in the shear strain capacity of the NRB isolators can be idealized and have an effortless impact on the assessed performance of the structure. Therefore, two hypothetical decrements of 20 and 40% on the shear strain capacity of the NRBs due to freezing temperatures are investigated.

4.4.3 Ground motion record selection

Another crucial step of seismic fragility analysis involves the selection of ground motion records that are consistent with the site's seismic hazards, and the generalized conditional intensity measure approach [43, 45] is adopted for this purpose. For this approach, target multivariate lognormal distributions of intensity measures conditioned on the observation of earthquake events with specific values of a conditioning IM are constructed; and the ground motion records that best match these target conditional distributions are selected. Spectral acceleration at the target isolation period is discarded as a conditioning IM because the thermal stiffening on the NRB isolators causes a shift in the fundamental period of the structure. Hence, a structure-independent intensity measure is selected instead, and peak ground velocity (PGV) is chosen, which has been recently identified as a sufficient and efficient seismic IM for the assessment of the seismic performance of highway bridge portfolios [275] and isolated bridges [19], even when ordinary (non pulse-like) ground motions are observed.

First, a probabilistic seismic hazard analysis (PSHA) is performed to determine the mean annual frequency of exceedance of the PGV (i.e., the hazard curve). The ground motion models employed by Natural Resources Canada (NRC) [120] in the construction of the hazard maps for the 2015 edition of the National Building Code of Canada [55] are adopted here for consistency with the design of the isolation units. Then, for the selected levels of the conditioning IM, seismic deaggreation [34] is performed to define the expected earthquake scenario (i.e., the expected values of magnitude, distance, and ε are estimated). The ε value is the deviation of the mean seismic intensity calculated from the ground motion model to the target value of the intensity measure, divided by the standard deviation of the GMM. Both PSHA and deaggregation are performed on the OpenQuake (OQ) engine [238].

Target conditional distributions are then constructed based on these GMMs using a modified version of the algorithm proposed by [27] to include IMs other than spectral acceleration. Forty (40) records are selected for each expected earthquake scenario of interest. An example illustrating the process for record selection is shown in Figure 4.6 for a 9 975-year return period of the earthquake scenario (i.e., 0.5 % probability of exceedance in 50 years). Finally, Kolmogorov-Smirnov tests are performed to ensure the fit of the selected suites to the target conditional IM distributions for each conditioned intensity measure. Six PGV levels are chosen corresponding to probabilities of exceedance of 5, 2, 1, 0.5, 0.2, and 0.1 % in 50 years. Thus, 240 ground motion records compose the selected suite for the response history analyses to be performed in OpenSees. The process illustrated in Figure 4.6 is repeated for each chosen level of PGV.

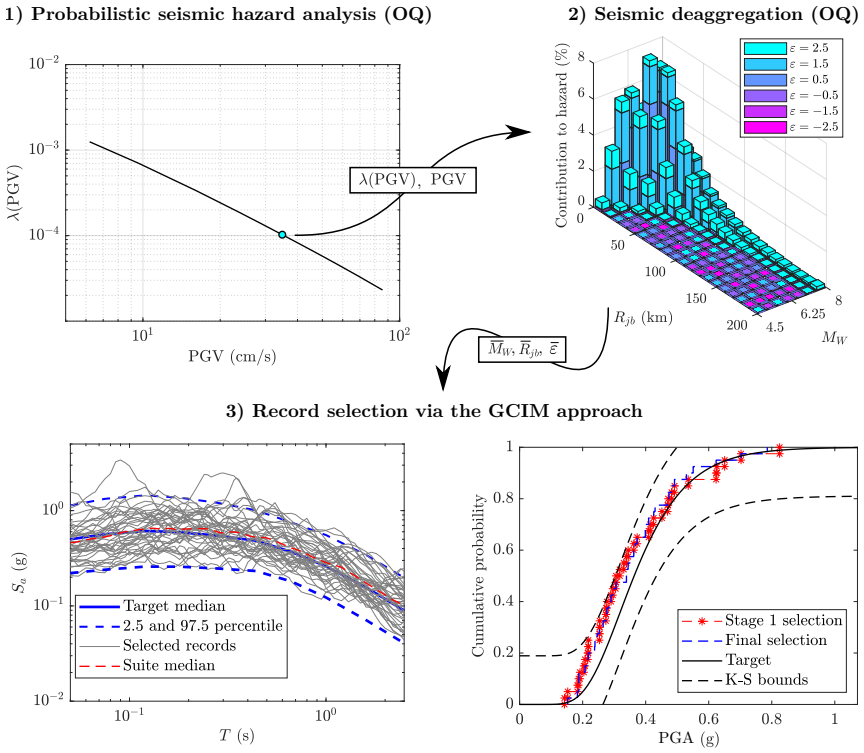

Figure 4.6 Steps for ground motion record selection using the GCIM approach

Records are selected from the PEER NGA-West2 database [7] due to the scarcity of recorded strong ground motions in Eastern Canada. Two limitations are usually highlighted within this approach: (i) when compared to western regions in North America, eastern events tend to generate high amplitudes at low periods; and (ii) ground acceleration attenuates more slowly in eastern North America than in western regions [38, 230]. Two measures are adopted to address these limitations. First, a prescreening of the database is performed with respect to the magnitude, source-to-site distance, and soil type to limit

the selection of records to those that closely match the seismic characteristics at the bridge site. Only ground motions with the following properties are available for selection after screening: $5.5 \leq M_W \leq 7.5$, $20 \leq R_{jb} \leq 200\,\text{km}$, and $200 \leq V_{S30} \leq 760\,\text{m/s}$, where M_W is the moment magnitude, R_{jb} is the Joyner-Boore source-to-site distance, and V_{S30} is the shear wave velocity. This screening criterion also ensures that only far-source ground motion records are selected. Finally, the acceleration spectra of the selected suite are ensured to satisfactorily match the target GCIM distributions at low periods [23, 154].

4.4.4 Climate historical data at the bridge's site

To assess the thermal effects on the seismic performance of the isolated bridge in this case study, daily mean temperature data collected at two stations in Shawinigan, Quebec, Canada [178] are gathered. These stations are located approximately 13.5 km away from the bridge site and report temperature measurements from 1902 to 2020. The histograms of the daily mean temperature ($\bar{\theta}_{daily}$) at each station are shown in Figure 4.7. Climate identifiers (CID) of the stations are 7018000 and 7018001. The former reports temperature data from 1902 to 2004 (Figure 4.7a), while the latter has been collecting data since 1998 (Figure 4.7b).

Despite the different time spans covered by each station, the daily mean temperatures appear to follow the same trend, with a minimum mean temperature of approximately $-30\,^{\circ}\text{C}$ and a maximum not exceeding $+30\,^{\circ}\text{C}$. The Canadian code requires that the concomitant minimum service temperature be taken as the average of $+15\,^{\circ}\text{C}$ and the minimum service temperature. For the case-study bridge, the concomitant minimum service temperature is therefore $-7.5\,^{\circ}\text{C}$. However, for a holistic seismic fragility analysis, a range from -30 to $+20\,^{\circ}\text{C}$ is adopted in this study. This range is deemed adequate because the thermal effects of warmer temperatures on the seismic isolators are assumed to be negligible [70, 58].

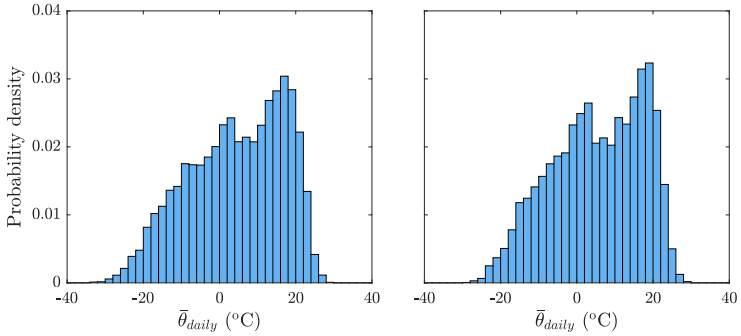

(a) CID 7018000 (b) CID 7018001

Figure 4.7 Mean daily temperature from two stations in Shawinigan, Quebec, Canada based on Environment and Climate Change Canada data

4.5 Assessment of the isolated bridge seismic performance in cold regions

The 240 selected records were used to perform RHAs on the numerical model at six values of air temperature ranging from +20 to −30 °C, for a total of 1440 RHAs in OpenSees for each idealized scenario regarding the width of the abutment wing wall gap. A deterministic numerical model of the isolated bridge is employed, neglecting any material uncertainty or thermal effects of the concrete and steel strengths, based on past studies that showed the low influence of these mechanical properties on the peak responses of multispan continuous concrete bridges in Quebec for both as-built and isolated configurations (e.g., [250, 243, 33]).

4.5.1 Probabilistic seismic demand model

The peak responses from the nonlinear RHAs performed in OpenSees are extracted and used to build the probabilistic seismic demand models based on Gaussian mixtures (Equation 4.3). The peak demand values (conditioned on the six PGV levels and six temperature levels) are first transformed into the (natural) logarithmic space. Then, 36 GMSDMs are built considering a maximum of ten clusters and full-unshared covariance matrices (i.e., each cluster has a full covariance matrix) to fit the observed correlated demand data. The GM seismic demand models are chosen according to minima BIC values and have a number of clusters varying from 1 to 4, indicating that overcomplex models are avoided. For three-variable GM models, a single cluster corresponds to nine model parameters plus its mixture proportion. Therefore, for brevity, the GM model parameters are not discussed.

These GMSDMs are used to generate 10^3 correlated demand samples at each combination of temperatures and PGVs for a total of 36 000 samples for each gap scenario, which are shown along with the observed peak responses in Figure 4.8. The good agreement of the sampled demands and the RHA peak responses demonstrates the refined fit of the GMSDMs, which are capable of capturing the discontinuities (caused by the abutment wing-wall gap) and the nonlinear dependence between the component responses. This feature may avoid the propagation of density modeling bias into the fragility analysis [32].

4.5.2 Construction of component and system fragility surfaces

In seismic fragility analysis, performance criteria relate damage limit states to required structural functionality, and for highway bridges, damage limit states are formulated at two levels, i.e., the component and system levels. Component-level damage is typically used to estimate repair actions and costs, while system-level performance combined with the component damages relates to outcomes such as lane closures, load restrictions or

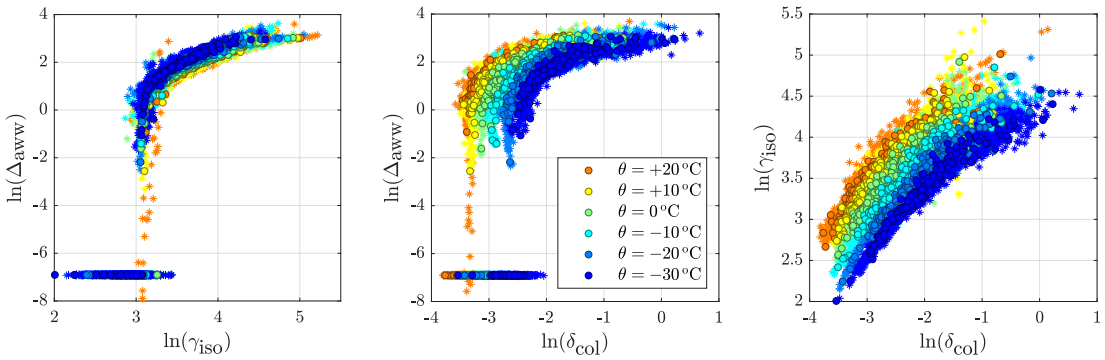

(a) Scenario I (25.4 mm gap)

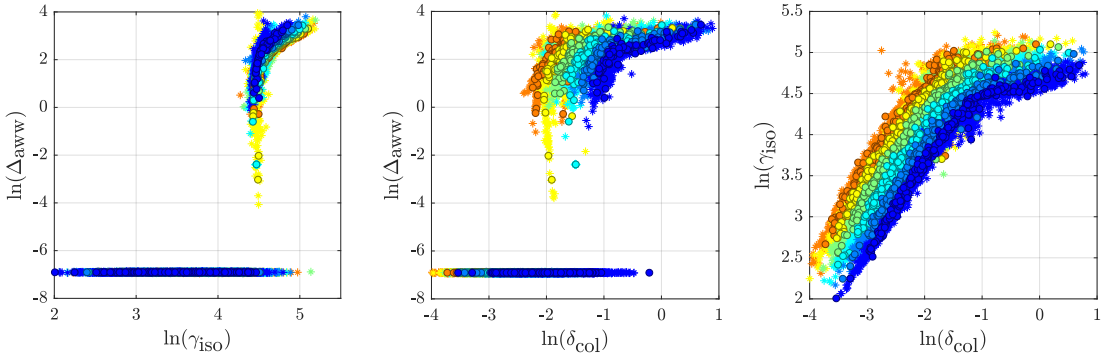

(b) Scenario II (100 mm gap)

Figure 4.8 Peak responses (circle markers) and samples generated from GM seismic demand models (∗) in each scenario

speed restrictions [160, 206, 127]. While many alternatives exist in the literature, bridges are commonly assumed to be a series system (e.g., [199, 248, 243]). Thus, violating the same damage state of the system $\mathcal{F}_{sys}$ is the union of the component violations, i.e., $\mathcal{F}_{sys} = \bigcup_{i=1}^{m} \mathcal{F}_{comp,i}$. Hence, the probability of exceeding the bridge's damage state is expressed as

$$\Pr(\mathcal{F}_{sys}) = \Pr\left(\bigcup_{i=1}^{m} \mathcal{F}_{comp,i}\right) \tag{4.9}$$

Adapting the methodology detailed by [110] to the use of the Gaussian mixture seismic demand models, the generated demand samples are then paired to the same number of samples from the capacity models at each damage state (Table 4.1). Then, binary vectors indicating component DS exceedance are built for the construction of the seismic fragility functions. To better conform the damage states of the components to the consequences to the bridge's level of service, the components can be classified as primary or secondary in accordance with their importance for bridge stability under traffic or subsequent seismic events [273]. Extensively damaged columns and isolation units shall be classified as

primary components, which are assumed to be the only components contributing to the probable replacement damage state of the bridge. Abutment wing walls are considered secondary components, contributing to the initial damage states of the whole system (i.e., minimal, repairable, and extensive) because their complete failure will not have a similar consequence as that of the primary components. To translate these assumptions into the fragility functions, the binary matrix in Table 4.2 connects the component damage states to the damage state of the whole bridge.

Table 4.2 Adopted binary matrix relating the component damage state to the overall performance of the bridge

Bridge component	Damage state			
	DS1	DS2	DS3	DS4
Abutment wing walls	1	1	1	0
NRB isolators	0	0	0	1
Bent columns	1	1	1	1

To compare the effects of the covariates having different units on the fitted logistic regression model, covariates are first standardized with respect to their mean and standard deviation values [2]. In the present case, only the peak ground velocity (PGV) and air temperature (θ) are considered predictors, and the fragility function (Equation 4.2) takes the following form

$$\Pr(\mathrm{DS}|\mathrm{PGV},\theta) = \frac{\exp\left(\beta_0 + \beta_1 z_{\mathrm{PGV}} + \beta_2 z_\theta\right)}{1 + \exp\left(\beta_0 + \beta_1 z_{\mathrm{PGV}} + \beta_2 z_\theta\right)} \tag{4.10}$$

where z_{PGV} and z_θ are the standardized values of the PGV and temperature. Table 4.3 presents the fitted model parameters ($\hat{\beta}_i$) for all the components and system, at each studied scenario. The average accuracy from the 5-fold cross-validation is also shown, suggesting good agreement between the observed damage data and that of the fitted models. Although omitted here for brevity, the p-values of all the logistic regression coefficients are less than 0.001, demonstrating the relevance of the investigated covariates for the fragility. The resulting fragility surfaces are depicted in Figures 4.9 to 4.12 for damages states DS1 to DS4, respectively.

As mentioned above, one of the advantages of the logistic regression model is the interpretability of the model parameters. Accordingly, the positive model parameter of a given covariate indicates that the increment on this covariate increases the odds of observing damage. As expected, all the fitted model parameters related to the seismic intensity

Table 4.3 Summary of the fitted logistic regression models for the fragility data

DS	Level†	Scenario I (25.4 mm gap)				Scenario II (100 mm gap)			
		$\hat{\beta}_0$	$\hat{\beta}_1$	$\hat{\beta}_2$	Accuracy (%)‡	$\hat{\beta}_0$	$\hat{\beta}_1$	$\hat{\beta}_2$	Accuracy (%)‡
DS1	AWW	-0.693	2.168	0.127	83.79	-1.902	2.799	0.580	88.88
	ISO	n/a	n/a	n/a	n/a	n/a	n/a	n/a	n/a
	COL	-6.234	2.076	-1.484	97.90	-4.087	2.149	-1.456	92.29
	SYS	-0.667	2.169	0.139	83.58	-1.770	2.753	0.368	88.29
DS2	AWW	-3.488	1.617	0.153	92.56	-3.388	2.097	0.188	88.59
	ISO	n/a	n/a	n/a	n/a	n/a	n/a	n/a	n/a
	COL	-10.887	2.817	-2.210	99.84	-7.057	2.331	-1.698	98.34
	SYS	-3.505	1.653	0.108	92.44	-3.358	2.095	0.145	88.33
DS3	AWW	-5.298	1.412	0.122	98.80	-5.182	1.882	0.121	97.66
	ISO	n/a	n/a	n/a	n/a	n/a	n/a	n/a	n/a
	COL	-10.335	2.672	-1.183	99.92	-7.613	2.329	-1.724	98.95
	SYS	-5.286	1.499	0.006	98.67	-5.161	2.057	-0.215	97.01
DS4	AWW	n/a	n/a	n/a	n/a	n/a	n/a	n/a	n/a
	ISO	-9.381	1.294	1.179	99.97	-4.629	1.236	0.357	98.04
	COL	-12.476	3.288	-1.975	99.95	-8.481	2.397	-1.913	99.38
	SYS	-8.420	1.886	-0.328	99.89	-4.799	1.598	-0.093	97.63

† AWW: abutment wing walls, ISO: NRB isolators, COL: bent columns, SYS: system (whole bridge)

‡ Average accuracy from 5-fold cross-validation

n/a: not available

measure ($\hat{\beta}_1$) are positive. In contrast, the temperature model parameter $\hat{\beta}_2$ varies depending on the studied level (component or system), abutment wing wall gap length, and damage state, with negative values indicating that seismic fragility increases as the air temperature decreases.

For the minimal damage state DS1, the abutment wing walls seem to govern the system fragility in both investigated scenarios. Indeed, the fitted model parameters at the levels of the abutment wing walls and system are close, suggesting that the first signs of yielding of the longitudinal reinforcement in the bent columns occurs concomitantly with the minimal damage of the abutment wing walls. This finding can also be observed through the similarity of the fragility surfaces of the abutment wing walls (Figure 4.9a) and the whole bridge (Figure 4.9c). Additionally, regression coefficients and the depiction of the fragility surfaces suggest that the enlargement of the gap between the deck and the wing walls has a slight impact on reducing the seismic fragility. Indeed, the slightly larger value of $\hat{\beta}_2 = 0.580$ in scenario II, compared to $\hat{\beta}_2 = 0.127$ in scenario I, demonstrates the minor positive effect of colder temperatures on the system's fragility, which can be explained

by the lower lateral displacement of the stiffer NRB isolators causing less damage on the abutment wing walls. Conversely, low temperatures are detrimental to the fragility of columns in DS1 for both investigated scenarios, a result of the increased forces transmitted to the substructure when thermal stiffening takes place on the elastomeric isolators. At the reference temperature, it is unlikely that columsn will undergo minimal damage even under strong shaking. The column's seismic fragility, however, increases rapidly as temperature decreases, and the close values of the logistic regression coefficients for temperature (-1.484 and -1.456) may suggest that the effects of temperature are similar in both gap scenarios. Nevertheless, as observed in Figure 4.9b, the larger clearance (which allows the isolators to deform more freely) has a negative impact on the column's seismic fragility. Therefore, sacrificing the abutment wing wall in the minimal damage state seems to be beneficial to the seismic fragility of the bent columns in the case-study bridge.

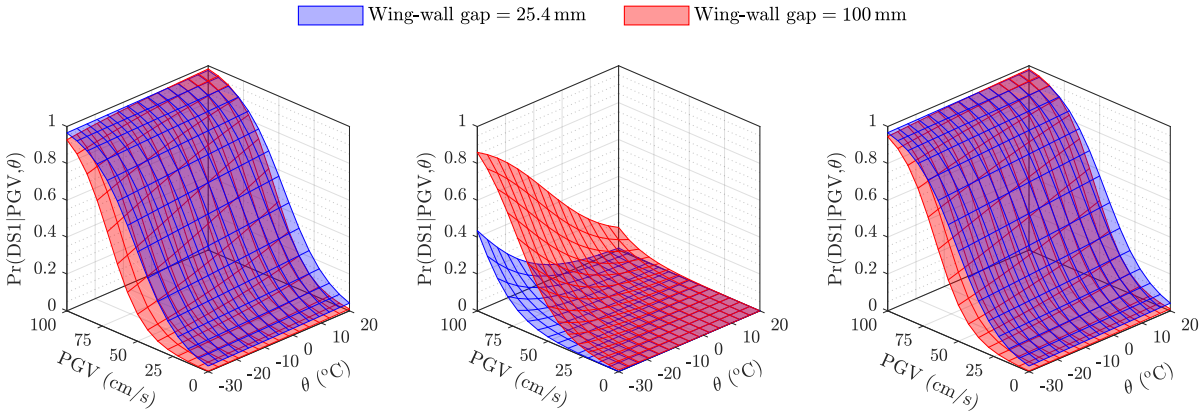

(a) Abutment wing wall (b) Bent column (c) System

Figure 4.9 Fragility surfaces for the minimal damage state (DS1)

In the case of the repairable damage state, the bridge must present a limited service level, and the abutment wing walls still govern the system's fragility (Figures 4.10a and c). In scenario II, the slight reduction in the fragility of abutment wing walls at $-30\,^{\circ}\mathrm{C}$ (compared to that of the reference temperature) and high PGV levels is compensated by a rapid augmentation of fragility of the columns (Figure 4.10b). Contrarily to the behavior observed in DS1, the enlargement of the wing-wall gap appears to be detrimental to the abutment's fragility, and the same phenomenon is observed at the system level. The larger PGV regression coefficient in scenario II compared to scenario I (2.097 against 1.617) indicates that the fragility increases more rapidly when the clearance respects the design code requirements. This could be explained by the fact that wider gap allows the deck to pound against the wing walls with greater velocity and potentially more damaging energy. For the bent columns, similar observations to that of the minimal damage states can be drawn: lower temperatures show an adverse effect on the seismic fragility. However,

the restraining effect of the wing walls at their original position results in improbable occurrence of repairable damage on the columns. When the gap increases to 100 mm, the odds of observing inelastic behavior and moderate damage of the columns becomes larger for PGV $>$ 50 cm/s and subfreezing temperatures.

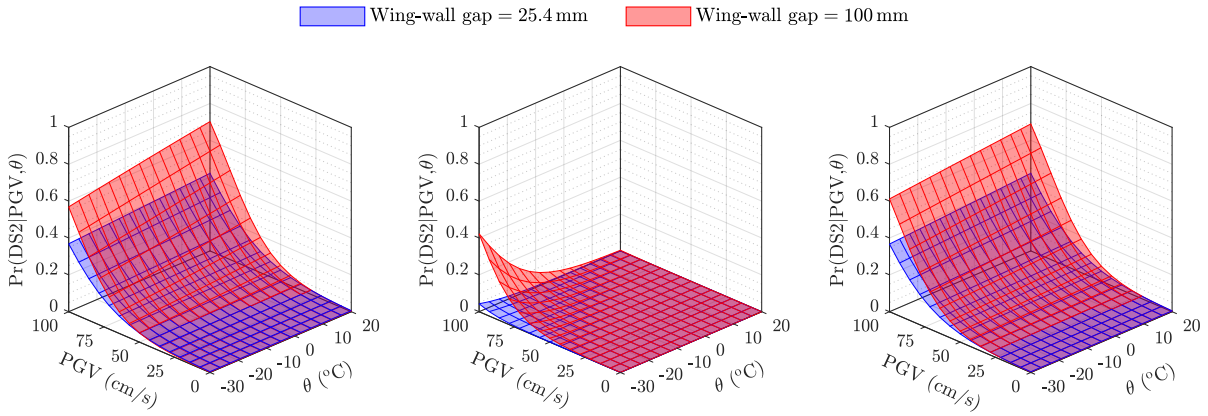

(a) Abutment wing wall (b) Bent column (c) System

Figure 4.10 Fragility surfaces for the repairable damage state (DS2)

Extensive damage characterizes the bridge's service disruption. The bridge fragility in DS3 is practically controlled by the abutments when the original 25.4 mm gap is maintained, with a negligible contribution of the bent columns and irrelevant impact of temperature ($\left|\hat{\beta}_2\right| < 0.01$). Conversely, when the gap is enlarged to 100 mm, the control of the system fragility progressively migrates from the abutment wing walls to the bent columns as the air temperature gets lower. As observed in the repairable damage state, the bridge and its components are less prone to be extensively damaged with a narrower clearance between the deck and the abutment wing walls, with the latter being damaged while the bent columns are protected.

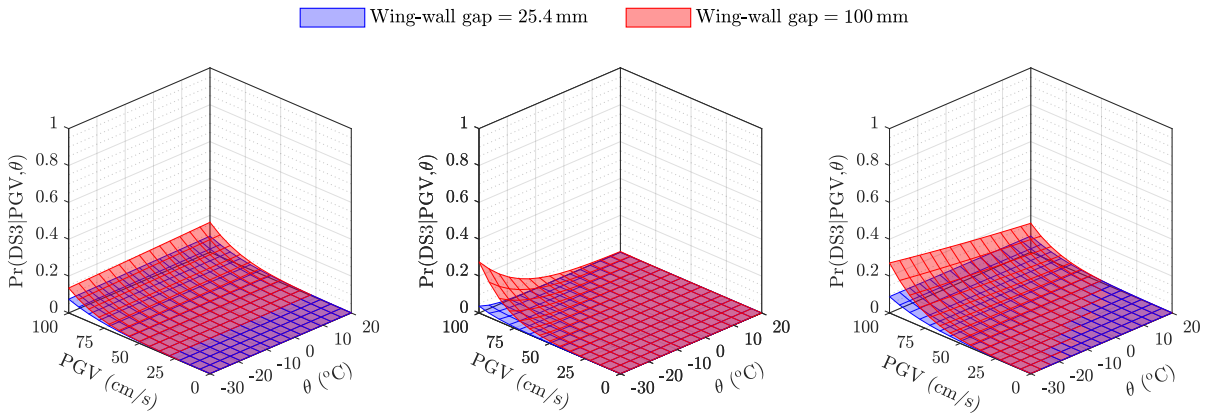

(a) Abutment wing wall (b) Bent column (c) System

Figure 4.11 Fragility surfaces for the extensive damage state (DS3)

Finally, for the life safety level of service, characterized by probable replacement damage state (DS4), the abutment wing walls present negligible seismic fragility (the fitting of the logistic regression model to the observed fragility data does not converge) in any investigated scenario (see Table 4.3). As indicated in Tables 4.1 and 4.2, the NRB isolators are considered in this damage state and may contribute to the system's fragility. Accordingly, the isolators control the bridge fragility in the probable replacement condition. The isolators could practically only fail by buckling when not impeded by the abutment wing walls (i.e., in scenario II) and when subjected to severe shaking (PGV $> 75\,\mathrm{cm/s}$), which would be followed by deck unseating. As thermal stiffening takes place, the seismic fragility of the isolators is slightly reduced (as indicated by the negative temperature logistic regression coefficient in Table 4.3 and illustrated in Figure 4.12a). This phenomenon is expected as the lateral displacement of the NRB isolators diminishes for subfreezing temperatures. The instability of longitudinal reinforcement in columns is very unlikely to occur and has a slight contribution on the system's fragility only under extremely low temperatures and severe ground shaking (Figure 4.12b).

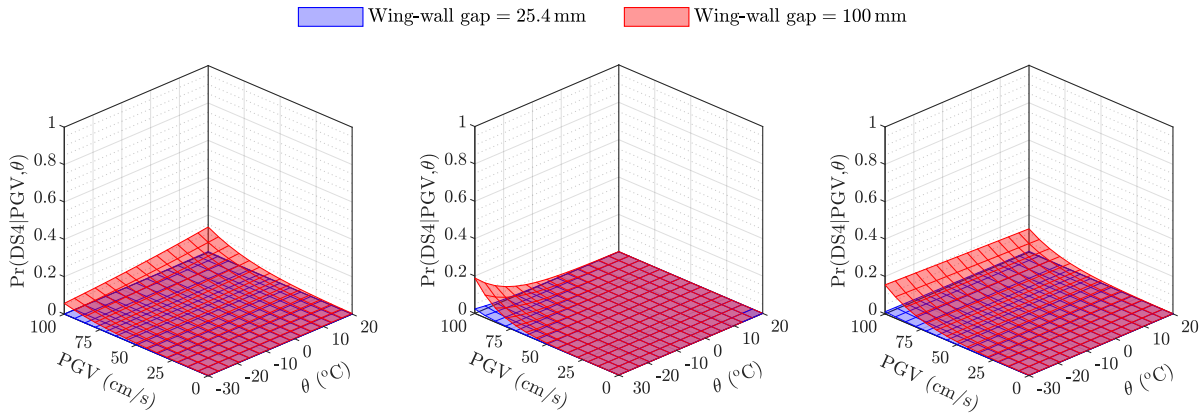

(a) NRB isolator (b) Bent column (c) System

Figure 4.12 Fragility surfaces for the probable replacement damage state (DS4)

Finally, the analytical framework adopted in this study is leveraged to investigate the potential impact that a decrease in the shear strain capacity of the NRB isolators (due to low temperatures) could have on their fragility. Accordingly, two hypothetical decrements are idealized: 20 and 40% (i.e., the median capacity in Table 4.1 of the NRB is multiplied by 0.8 and 0.6, respectively). The coefficients of the logistic regression models for these capacity levels are summarized in Table 4.4 along with the nominal capacity (i.e., no reduction). In both gap scenarios, the progressive decrement in the NRB capacity gradually cancels the beneficial effect of low temperatures on the fragility of the isolators, as the values of $\hat{\beta}_2$ change from positive to negative.

Table 4.4 Logistic regression models for the probable replacement damage state of the NRB isolators considering capacity reduction

Variation on shear strain capacity	Scenario I (25.4 mm gap)				Scenario II (100 mm gap)			
	$\hat{\beta}_0$	$\hat{\beta}_1$	$\hat{\beta}_2$	Accuracy (%)‡	$\hat{\beta}_0$	$\hat{\beta}_1$	$\hat{\beta}_2$	Accuracy (%)‡
No reduction	-9.381	1.294	1.179	99.97	-4.629	1.236	0.357	98.04
20% reduction	-7.639	1.191	0.229	99.91	-3.967	1.213	-0.020	96.59
40% reduction	-6.320	1.442	-0.177	99.54	-3.061	1.176	-0.354	92.44

‡ Average accuracy from 5-fold cross-validation

The fragility surfaces indicate that the restraining action of the abutment wing walls is still beneficial to the fragility of the isolators when the original gap is maintained (Figure 4.13). Conversely, the effects of the reduction in the shear capacity of the isolator are more important when the NRBs function without impediment (100 mm gap). Although temperature effects on the shear capacities of NRB isolators are not reported in the current literature, the results show that even a 20% reduction in capacity would still lead to a minimal probability of limit state exceedance (Figure 4.13b). A greater decrement on the NRB shear capacity would then lead to a detrimental impact of low temperatures on the isolator fragility and, consequently, to the system fragility for this case study (Figure 4.13c).

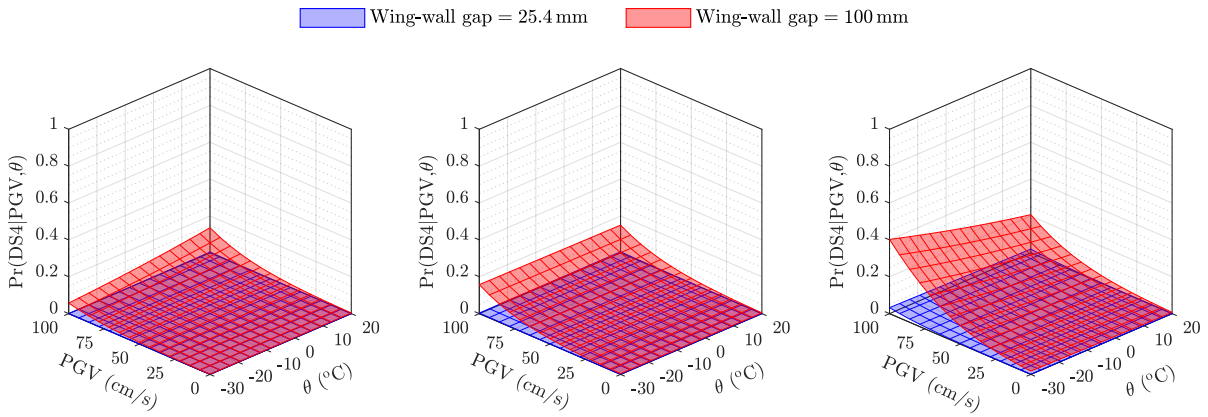

(a) No reduction (b) 20% reduction (c) 40% reduction

Figure 4.13 Fragility surfaces for the probable replacement damage state (DS4) of the NRB isolators considering capacity reduction

4.5.3 Compliance to the CHBDC performance criteria

Due to their importance to bridge stability and as the main component of the substructure that is protected by the isolation system in the case-study bridge, the performance of the bent columns is studied in more detail. Table 4.5 presents the values of the seismic fragility at the minimal damage state of the columns (Equation 4.10 and Table 4.3)

for cases combining reference, concomitant minimum service (−7.5 °C), and daily minimum temperatures with specific seismic ground motion return periods. According to the CHBDC's performance-based seismic design criteria, columns with minimal damage indicate the onset of spalling of the unconfined concrete cover and first yielding of longitudinal reinforcement. This damage state is related to the immediate service level, in which the bridge may be fully serviceable for normal traffic, with repair work not causing any service disruption.

Table 4.5 Probability of bent columns undergoing minimal damage according to the CSA S6-14 performance criteria at reference, concomitant, minimum service temperatures (values in percentage)

Gap scenario	θ (°C)	Seismic ground motion return periods (years)					
		975	2 475	4 975	9 975	24 975	49 975
I (25.4 mm)	+20	**<0.1**	**<0.1**	**<0.1**	**<0.1**	0.1	0.8
	-7.5	**<0.1**	**<0.1**	**<0.1**	0.2	1.0	6.8
	-30	0.2	0.3	0.5	1.1	5.1	30.2
II (100 mm)	+20	**<0.1**	**<0.1**	**<0.1**	0.2	1.1	7.6
	-7.5	0.3	0.4	0.7	1.6	8.5	41.2
	-30	1.4	2.2	3.8	8.5	34.9	80.1

At reference temperature, the columns show satisfactory performance in both studied scenarios even at the occurrence of extremely rare seismic events, with conditional probabilities of showing any sign of minor damage that are lower than 1%. The concomitant minimum service temperature is set for the assessment of 2 475-year return period seismic events. Again, the observed results suggest that the columns are likely to remain essentially elastic in the two gap scenarios. Finally, assuming that the case-study bridge is a lifeline structure according to the CHBDC's importance categories, this bridge would be expected to reach its immediate service level in the event of seismic ground motion with a 975-year return period. Therefore, it would be rather unlikely that the bent columns of the case-study bridge undergo minimal damage even at the combination of the wider gap scenario and minimum temperature, which results in the largest displacements at the top of the columns and, consequently, the largest strains at its base. These observations on the performance of the columns based on the fact that the widening of the gap does not substantially reduce the fragility of the abutment wing walls are gathered (Figure 4.9a), and these results suggest that seismically isolating the case study bridge using natural rubber devices without relocation of its wing walls could be a viable retrofitting option even in extremely cold weather conditions.

4.6 Conclusion

A probabilistic framework based on seismic fragility analysis is leveraged to assess the impact of thermal stiffening of natural rubber isolators on the performance of a bridge in Eastern Canada with an isolation system designed according to CSA S6-14. A holistic understanding of the seismic performance of the bridge under the effects of cold weather temperatures is provided considering the correlation of the seismic demand of the critical components of the bridge and the individual contribution of these components on the fragility of the entire system. Two scenarios are idealized regarding the clearance between the bridge deck and the abutment wing walls: in the first scenario, the original 25.4 mm gap is maintained (which does not comply with code requirements and would demand strengthening), while in the second scenario, the gap is enlarged to 100 mm to respect the service displacement of the isolators.

Typical winter temperatures in cold regions may be detrimental to the seismic performance of the isolators, which may not function as designed at reference temperature. The poorer performance of the rubber isolators is followed by an increased displacement demand on the bent columns, which are, in turn, more prone to damage during an earthquake. This reiterates the importance of considering thermal stiffening effects in the design of rubber-based isolation systems. The reported results suggest, however, that these effects may be less important when restraining structures act in combination with the isolator. From the performance assessment, the following key findings are highlighted:

1. The vulnerability of the abutment wing walls is not significantly affected by the thermal stiffening of the isolators when the original gap is maintained, whereas a slight positive effect due to low temperatures is generally observed in the fragility of this component when the gap is enlarged. Moreover, the probability of observing repairable and extensive damage increases in the latter scenario compared to the former, as a result of the deck developing greater velocities within the wider gap. Consequently, more damaging energy of the deck pounding on the wing walls is observed when the gap is modified to comply with the requirements of CSA S6-14.

2. Bent columns are the main components of the substructure that are protected in the case-study bridge by the installation of natural rubber isolators. At reference temperature, the columns are efficiently protected and are likely to remain in the elastic regime even during severe ground shaking. When the wing walls are kept at their original position, the thermal stiffening of the isolator is detrimental to the fragility of bent columns only for the minimal damage state. Conversely, when the gap is enlarged, a poorer performance of the isolation system is observed, with larger

seismic forces transmitted to the bent columns, thus increasing the displacement demand on these substructure elements. The columns are consequently more prone to damage when earthquakes take place during extreme cold weather conditions. These observations suggest that the combination of isolation and restraining effects of the wing walls considerably reduced the fragility of the columns when the elastomeric isolators undergo thermal stiffening.

3. The system's fragility is mainly controlled by the abutment wing walls for the minimal, repairable, and extensive damage states in both gap scenarios. NRB isolators govern the probable replacement fragility of the system only when performing without impediment of the wing walls. In this case, thermal stiffening shows a slight positive impact on the NRBs fragility due to reduced lateral displacement. Bent columns only contribute to the fragility of the whole bridge in the enlarged gap scenario, which is more considerable when the structure is subjected to combined subfreezing temperatures and strong seismic events. Otherwise, if the original gap remains unchanged, the restraining effect of the wing walls, although adverse to the vulnerability of the abutments, improves the seismic performance of the columns and, therefore, of the entire bridge.

The results of this case study reveal the beneficial combination of lateral restraining structures (e.g., abutment wing walls) and elastomeric seismic isolators when the latter undergo important thermal stiffening in extreme cold weather conditions. For the case-study bridge, sacrificing the abutment wing walls reduces the probability of observing even minor damage to the bent columns, which are usually the most expensive bridge components to be repaired or retrofitted. However, in practice, the abutment wing walls would require strengthening, and these costs should also be considered. Additionally, different deck displacement restraining mechanisms, such as keeper plates and restraining cables, have already been show to enhance the seismic performance of bridges, and could be studied in companions of elastomeric isolators subject to subfreezing temperatures. Alternatively, a retrofitting plan could comprise the installation of NRB isolators only on top of the bents while keeping the original elastomeric bearing pads on the abutments. This option still remains unexplored and should be investigated further. In this case, the deck would not be expected to move as a rigid body though, and its ability to remain elastic under transverse bending should be incorporated in the analysis. The case study involves a bridge supported by shallow foundation on stiff soil. Isolated bridges on soils that require the use of piles should be investigated regarding the combined effect of rubber thermal stiffening and freezing soil. Other aspects of seismic risk analysis could be incorporated into this performance assessment to evaluate the impact of this combination in terms of repair

costs and return-to-service times for repair and restoration. Finally, a more thorough analysis could combine seismic hazard and air temperature data in an effort to calculate the mean annual frequency of observing each of the assessed damage states and their general acceptance by asset managers.

4.7 Data availability

The following data that support the findings of this study are available from the corresponding author upon reasonable request: selected ground motion records, peak demand data from response history analyses, and fitted Gaussian mixture seismic demand models.

4.8 Acknowledgements

The authors gratefully acknowledge the financial support from the Natural Science and Engineering Research Council of Canada (Grant No. 37717), the *Fonds de Recherche du Québec – Nature et Technologies* (Grant No. 171443), and the Brazilian National Council for Scientific and Technological Development (CNPq) (Grant No. 233738/2014-2), and all the assistance provided by the *Centre d'Études Interuniversitaire des Structures sous Charges Extrêmes* (CEISCE). Computational resources were provided by *Calcul Québec* and Compute Canada for probabilistic seismic hazard analysis and deaggregation.

CHAPTER 5

CONCLUSION

5.1 Summary and conclusions

In Quebec, where the bridge inventory is ageing, and where the scarcity of empirical data on damage caused by earthquakes resulted in structures with poor seismic detailing, the assessment of the seismic vulnerability of the highway infrastructure is a priority. In effect, seismic fragility studies performed at the beginning of the last decade confirmed the susceptibility of the provincial bridge portfolio to likely earthquakes to happen in the future. This led to the investigation on the use of natural rubber isolators to retrofit these bridges, which demonstrated to effectively improve their seismic performance. Elastomers, the main component of laminated rubber isolators, are prone to severe thermal stiffening at low temperatures. Typical winter temperatures in cold regions can therefore cause substantial stiffening of the elastomeric compounds used in seismic isolators, which may not function as designed at reference temperature. Given the poorer performance of the isolators at low temperatures, increased displacement demands are expected to substructure elements, which are, in turn, more prone to be damaged during an earthquake. By the time that NRBs were identified as a potential retrofitting scheme for the bridge inventory in Quebec, the effects related to thermal stiffening on the natural rubber isolators were considered in a simplified manner. This motivated the present work to further investigate the impact of thermal stiffening of rubber isolators on the seismic performance of retrofitted bridges. To achieve this goal, this study was based on a probabilistic analytical framework comprised by the seismic demand density modeling and the generation of seismic fragility functions.

First, a multicomponent bridge located in Quebec, the Chemin des Dalles overpass, was chosen as case-study structure owing to the comprehensive information gathered on this bridge by past studies, which included a three-dimensional finite element model and experimental capacity estimates of the bridge elements. More precisely, the numerical model on OpenSees accounted for the nonlinear behavior of the main bridge components: reinforced concrete bent columns and cap beams, elastomeric bearings (as-built), seat-type abutments, shallow foundations, and natural rubber isolators (retrofitted); while the capacity estimates were obtained through previous laboratory test programs on the RC bent columns and natural rubber bearings. To perform nonlinear response history analyses on

the numerical model, a suite of hazard consistent ground motion records was selected from the NGA-West2 database. To this end, a refined characterization of the seismic hazard at the bridge site was performed based on probabilistic seismic hazard analysis on the OpenQuake-engine. This analysis employed the 5^{th} generation seismic hazard model of eastern Canada to account for the uncertainties relative to ground motion models and seismic sources in the region. The results of the PSHA were then used as input for a rigorous ground motion record selection using the GCIM approach, which guaranteed a hazard consistent propagation of the record-to-record variability into the seismic demand analysis.

Acknowledging the importance of the interaction between multiple component seismic responses and their potential contribution to the whole bridge fragility, the first part of this study was focused on the construction of multivariate PSDMs. Traditional PSDM approaches rely on assumptions that can significantly facilitate the density modeling of the uncertainty on structural responses to earthquake excitation. These same assumptions, however, are responsible for carrying errors throughout risk-based analyses when a poor density modeling is obtained. Besides, some of these assumptions were largely tested on other structural types, engineering demand parameters, and seismic intensity measure (e.g., maximum inter-story drift ratio on multistory moment-resisting frames conditioned on spectral acceleration at the fundamental period). Bridges are composed of several different components with distinguished behaviors and complex interactions under seismic excitation. The validity of the assumptions on lognormality and linear dependence of bridge component demands has been criticized and their impact on fragility estimates was identified as an open question to be potentially responded.

The difficulty in translating the richness in the response of multicomponent structures to earthquake loadings, coupled with the emergence of conditional-IM-based record selection approaches and multiple-stripe analysis, motivated the development of a novel approach for probabilistic seismic demand modeling. Inspired by the potential of machine-learning techniques in treating uncertainty, this work explored an algorithm commonly used for clustering, Gaussian mixtures, as density modeling rather than using regression-based algorithms. The proposed method relies on the flexibility of GM models to estimate the density of multivariate demand systems conditioned on a certain level of seismic intensity. The model concomitantly captures the uncertainty and the correlation of multiple component responses using a simple linear combination of weighted normal distributions. This new PSDM strategy was then leveraged to assess the potential propagation of bias due

to poor seismic demand density modeling into the fragility analysis of a multicomponent structure.

Accordingly, the gap between the deck and the abutment wing walls in the case-study bridge caused a discontinuity in the response in transverse direction not only on the deformation of wing walls but on the other critical components by impacting their statistical distribution and dependence. This discontinuity was recognized as a driver that led to the demand data failing the Lilliefors test on lognormality and to the nonlinear dependence between components. Two regimes of deformation of the bridge components were identified relative to gap closure, which depended on the earthquake intensity although not exclusive to a certain intensity level. By locally assessing the statistics of the relationship EDP|IM using MSA and clusters, the proposed density modeling strategy was able to identify these two regimes, constructing a more refined multivariate PSDM. By comparing system fragility curves build upon different PSDM strategies, the impact of poor density modeling was investigated on the bridge's fragility and mean annual frequency of exceeding damage states. The lack of lognormality of the demand data showed to propagate more bias than poor modeling by linear dependence, depending on the damage state and governing components.

Later, the preliminary perception that the GM-based seismic demand models propagated low bias into fragility- and risk-based analyses was validated when compared against the outcomes of a nonparametric bootstrap approach. This validation also confirmed the general impression that the lack of lognormality of the seismic demand data can propagate great bias into fragility estimates, while the impact of the assumption of linear dependence was deemed negligible for the case study. The objective of this part of the research was, thus, not to be conclusive, but rather complementary to the ongoing discussion on the validity of typical assumptions and on their impact on seismic risk assessment. The hypotheses of lognormality and linear correlation may, however, still be valid or represent suitable approximations of the observed data depending on the specific structure and on the level of acceptable error on the risk assessment. The choice on the strategy to perform probabilistic seismic demand modeling remains the analyst's responsibility.

In the second part of the present study, the performance of the case study was assessed in its retrofitted configuration with isolators considering the concurrent event of earthquake loading and subfreezing temperatures. Combining the novel PSDM with logistic regression, the vulnerability of the case-study bridge was investigated in both component and system levels. Accordingly, fragility surfaces were conditioned on peak ground velocity and environmental temperature. While seismic hazard was characterized using PSHA,

mean daily temperature collected for more than 100 years was used. Due to the fact that the bridge is not originally isolated, as-built clearances may not comply with code requirements that demand that isolators should perform without impediment. Consequently, two scenarios were idealized with respect to the gap between the bridge deck and the abutment wing walls. In the first, the original 25.4 mm gap is kept as in the as-built bridge. This gap is smaller than isolators' design displacement of 70 mm. Thus, it does not comply with code requirements and abutment wing walls should be strengthened. In the second scenario, the gap is enlarged to 100 mm to accommodate the service displacement of the isolators.

Bent columns were the main bridge substructure elements sought to be protected by the proposed retrofitting scheme. In effect, at reference temperature 20 °C, the columns were efficiently protected by the isolators in both gap scenarios. Even minor signs of damage are not likely to be observed as minimal damage state fragilities are less than 10% for extremely rare seismic events (0.02% per annum probability of exceedance). Column fragility surfaces, however, depicted the increase of the bridge column's fragility with the decrease of the environmental temperature as expected given, the important stiffening suffered by isolators. This reiterates the relevance of considering thermal stiffening effects during the design of rubber-based seismic isolation systems. The reported results suggest, however, that these effects were less important when restraining structures acted in combination to the isolators. Correspondingly, in the modified gap scenario, the columns are more prone to undergo any damage state than when the original gap was kept. The beneficial action of the abutment wing walls was evidenced in avoiding the transmission of larger seismic forces to the bent columns, while the seismic isolator effectively decoupled the bridge superstructure from the substructure.

Intuitively, it would be expected that the abutment wing walls would undergo less damage when modified to accommodate the service displacement of the isolators. The vulnerability of wing walls was, however, not substantially affected by the different gap values. More precisely, the fragility of these lateral structures was practically the same for the minimal damage states. Conversely, a slight increase of the fragility at more severe damage states was noted. This increase could be explained by a greater and, consequently, more damaging pounding energy of the deck on the wing walls when the gap is modified to comply with the requirements of the CSA S6-14. The fragility of the wing walls seemed generally insensitive to the thermal stiffening of the isolators. Based on the results of this case study, one can thus conclude that the abutment wing walls would require strengthening independently of the clearance provided between the bridge deck and the lateral

walls. Furthermore, keeping the abutment wing walls at their original position was also beneficial to the NRBs, which did not fail by buckling. In the modified scenario, however, isolators were more susceptible to instability issues, especially in the case of a potential decrement on the isolator's capacity caused by low temperatures.

At last, the system's fragility was mainly governed by the abutment wing walls for the minimal, repairable, and extensive damage states in both gap scenarios. NRB isolators controlled the probable replacement fragility of the system only when performing without impediment of the wing walls. In this case, thermal stiffening demonstrated a slight positive impact on NRB's fragility due to reduced lateral displacement. Bent columns mainly contributed to the fragility of the whole bridge in the enlarged gap scenario, more considerably when the structure is submitted to subfreezing temperatures combined to rare seismic events. Otherwise, if the original gap was kept unchanged, the restraining effect of the wing walls, although averse to the vulnerability of the abutments, improved considerably the seismic performance of the columns. In this case, if the capacity of abutment wing walls was to be enhanced, the entire bridge could have a satisfactory seismic performance when isolated with NRBs in spite of their thermal stiffening.

In summary, the general objective stated for this research was accomplished by means of a probabilistic analytical framework. Analytical seismic fragility analyses were rigorously performed based on (1) seismic hazard and climate data, (2) refined ground motion record selection, (3) nonlinear RHAs on a calibrated finite element model of a real case-study bridge, and (4) recent bridge component capacity experimental data generated at the UdeS's laboratory of structures. This study contributed to ongoing discussions on the validity of traditional hypotheses on multivariate seismic demand density modeling by proposing a novel PSDM strategy that leverages the strengths of multiple-stripe analysis and finite mixture models. The relevance of integrating powerful statistical tools in seismic risk assessment is thus acknowledged. Besides, the detrimental impact of low temperatures on the seismic performance of the case-study bridge was quantified in terms of fragility, reinforcing the need to account for thermal effects on the design of rubber-based isolation systems in cold weather environments. Once again, the distinguished consideration of component- and system-level fragilities demonstrated its importance in providing local and global perspectives of vulnerability. Although thermal effects were detrimental to minimal damage of columns, the system's fragility was mainly governed by abutment wing walls, which in turn were insensitive to low temperature effects. Therefore, an insightful example was provided on the potential challenges in retrofitting bridges in cold regions with natural rubber isolators, such as Quebec.

5.2 Recommendations and future work

The work performed in this research could be complemented by future studies on the following subjects:

- The number of data points used to fit Gaussian mixture models on the observed demand (i.e., the number of seismic ground motion records at each stripe) might affect the fitted model. Further investigation should be performed on the satisfactory size of the dataset to avoid the introduction of bias, and its relationship with the number of structural components and model parameters.
- The novel multivariate PSDM approach was, at first, tested in a structure-specific framework, using a case-study bridge that has been extensively studied. The application of the proposed approach, however, should be expanded and tested for the assessment of bridge classes and regional portfolios. Based on the results of this study, the potential impacts that the methodology would have at a regional portfolio scale cannot be inferred yet. Future work to extend its application to structural classes and inventories is thus needed. Moreover, structures with even more insufficient seismic detailing (where complex interactions and multiple regimes of nonlinear behavior or pounding may be common) or long bridges (where refined modeling of correlation between component responses may have a more crucial role) may be prime candidates for future applications of the proposed method.
- The adopted methodology was supported by a rigorous record selection, which in turn relied on the results of probabilistic seismic hazard analysis. The ground motion models and seismic sources in Canada have been recently fully integrated into the Global Earthquake Model (GEM) Foundation's OpenQuake engine to deliver the sixth generation seismic hazard model of Canada, which should be incorporated in future regional seismic risk assessments.
- The present work used accelerograms from the NGA-West2 database, which comprises ground motions recorded Western North America, New Zealand, China, Japan, Middle East, and Southern Europe. Characteristics of these ground motions can be significantly different from those recorded in Eastern North America. With the release of the NGA-East database, more consistent strong ground motion record selection could be accomplished for seismic assessments in Eastern Canada.
- Contrarily to multistory buildings, bridges may demonstrate a more complex dynamic response, which is not governed by the first vibration modes. Owing to this, the average spectral acceleration $S_{a,Avg}$ over a range of vibration periods (discussed in Chapter 2) has shown to be an optimal intensity measure for seismic risk assessment

of bridges and should be incorporated in future studies on either structure-specific or portfolio cases.

- The present study was conducted when the 2014 edition of the Canadian highway bridge design code CSA S6-14 was in force. The 2019 edition of the code was published in November 2019 and available in early 2020, when the major part of the analyses of the present work had already been performed and could not possibly include the revisions. The revised performance criteria of the CHBDC's 2nd generation performance-based seismic design provisions have brought changes specially to damage indicators of concrete substructure elements. However, capacity models of reinforced concrete columns have not been updated yet to account for the new damage indicators. These changes are likely to affect the results of the seismic fragility assessment and can be easily considered in future studies. The new criteria will be naturally incorporated in future work, conditioned upon the development of consistent capacity models.
- The case-study bridge was supported by shallow foundation on stiff soil. Isolated bridges on soils that require the use deep foundation should be investigated regarding the combined effect of rubber thermal stiffening and frozen soil. Widespread damage on deep foundations has been reported on bridges located on frozen soil during past earthquakes. The potential amplification of damage caused by larger-than-expected forces transmitted to the substructure by stiffer isolators should be studied.
- In the eventual emergence of experimental data demonstrating the occurrence of intermediate damage states on laminated-rubber seismic isolators, the capacity estimates of these components should be updated and incorporated into fragility analyses of isolated bridges. For instance, the effects of imperfections and yielding of the reinforcement steel plates in the behavior and capacity of these isolators should be investigated. Moreover, if low temperatures affect the capacity of these devices, this phenomenon should be considered in a more accurate estimation of the bridge's seismic vulnerability in cold regions.
- The results of this case study reported the beneficial combination of lateral restraining structures (e.g., abutment wing walls) and laminated-rubber seismic isolators when the latter undergo important thermal stiffening in extreme cold weather conditions. For the case-study bridge, sacrificing the abutment wing walls reduced the probability of observing even minor damage on bent columns, which are usually the most expensive bridge components to be repaired or retrofitted. Additionally, different deck displacement restraining mechanisms have already shown to enhance

the seismic performance of bridges, such as keeper plates and restraining cables, and should be studied in companion of elastomeric isolators in cold regions.

– Finally, the decreased serviceability of bridges after the occurrence of an extreme event can significantly impact transportation systems and affect a community's recovery process. Estimation of the fragility of a bridge under seismic hazard can facilitate the evaluation of its functionality and ultimately its resilience after the occurrence of an earthquake. In this case, other aspects of seismic risk analysis should still be incorporated into the performance assessment to evaluate the impact of potential combinations of retrofitting measures in potential scenarios. Variables such as retrofitting and repairing costs and return-to-service times for repair and restoration should be integrated. Yet, in this more thorough analysis of concurrent extreme events (e.g., seismic and thermal), seismic hazard and air temperature data should be convolved to the fragility in an effort to calculate the mean annual frequency of observing each of the assessed damage states and their general acceptance by asset managers.

In summary, tools for performance-based earthquake engineering have progressed considerably in the past twenty years, achieving the adoption of performance-based seismic design by standards in the past half-decade. Despite the large progress made in the field, the implementation of risk-consistent analysis by practicing engineers is still rare and additional work is required before probabilistic methods evolve as the standard approach for decision making processes in structural engineering. The propagation of uncertainty from seismic hazard analysis, passing through seismic fragility assessment, and ending in computing the probability of exceeding a target decision variable have been widely employed by the academia, whereas a still modest interest by practicing engineers is observed. It is, however, consensus that the probabilistic performance-based earthquake engineering methods are gaining popularity and they may be adopted as standard procedures soon. Future research should thus continue on providing engineers and decision makers with the necessary sensibility to judge structural performance in terms of probabilities of exceedance of decision variables.

5.3 Sommaire et conclusions

Au Québec, où l'inventaire des ponts est vieillissant et où la rareté des données empiriques sur les dommages causés par les tremblements de terre a donné lieu à des structures dont les détails sismiques sont déficients, l'évaluation de la vulnérabilité sismique de l'infrastructure routière est une priorité. En effet, les études de fragilité sismique réalisées au début de la dernière décennie ont confirmé la sensibilité du portefeuille de ponts provinciaux aux

séismes susceptibles de se produire dans le futur. Cela a conduit à l'étude de l'utilisation d'isolateurs en caoutchouc naturel pour réhabiliter ces ponts, ce qui a permis d'améliorer efficacement leur performance sismique. Les élastomères, principal composant des isolateurs en caoutchouc laminé, sont sujets à un raidissement thermique important à basse température. Les températures hivernales typiques des régions froides peuvent donc provoquer un changement significatif des propriétés d'élastomères utilisées dans les isolateurs sismiques, qui peuvent ne pas fonctionner comme prévu à la température de référence. Étant donné la performance moindre des isolateurs à basse température, on s'attend à des demandes de déplacement accrues des éléments de la structure, qui sont, à leur tour, plus susceptibles d'être endommagés pendant un tremblement de terre. Au moment où les NRB ont été identifiées comme un schéma de réhabilitation potentiel pour l'inventaire des ponts du Québec, les effets liés au raidissement thermique sur les isolateurs en caoutchouc naturel ont été considérés de manière simplifiée. Ceci a motivé le présent travail à étudier plus en profondeur l'impact de la rigidité thermique des isolateurs en caoutchouc sur la performance sismique des ponts réhabilités. Pour atteindre cet objectif, cette étude s'est basée sur un cadre analytique probabiliste comprenant la modélisation de la densité de la demande sismique et la génération de fonctions de fragilité sismique.

Tout d'abord, un pont à plusieurs composantes situé au Québec, le pont du Chemin des Dalles, a été choisi comme structure d'étude de cas en raison de l'information exhaustive recueillie sur ce pont par de recherches antérieures. Y sont compris un modèle tridimensionnel par éléments finis et des estimations expérimentales de la capacité des éléments du pont. Plus précisément, le modèle numérique sur OpenSees a pris en compte le comportement non linéaire des principaux composants du pont : piller et poutres de couronnement en béton armé, appuis élastomères (structure telle que construite), culées de type siège avec des murs en aile, fondations peu profondes et isolateurs en caoutchouc naturel (structure réhabilitée). Tandis que les estimations de capacité ont été obtenues grâce à des programmes d'essais en laboratoire sur les piliers en béton armé et les appuis en caoutchouc naturel. Pour effectuer des analyses dynamiques non linéaires sur le modèle numérique, une série d'accélérogrammes cohérents avec les d'aléa sismique de la région a été sélectionnée à partir de la base de données NGA-West2. À cette fin, une caractérisation raffinée de l'aléa sismique sur le site du pont a été effectuée sur la base d'une analyse probabiliste de l'aléa sismique sur OpenQuake-engine. Cette analyse a utilisé le modèle d'aléa sismique de la $5^{\text{ème}}$ génération pour l'est du Canada pour tenir compte des incertitudes relatives aux modèles de mouvement du sol et aux sources sismiques de la région. Les résultats de l'analyse PSHA ont ensuite été utilisés pour une sélection rigoureuse d'accélérogrammes

à l'aide de l'approche GCIM, ce qui a garanti une propagation cohérente des incertitudes à la réponse de la structure.

En reconnaissant l'importance de l'interaction entre les réponses sismiques des structures à composants multiples et leur contribution potentielle à la fragilité de l'ensemble du pont, la première partie de cette étude s'est concentrée sur la construction de PSDM à variables multiples. Les approches PSDM traditionnelles reposent sur des hypothèses qui peuvent faciliter de manière significative la modélisation de la densité de l'incertitude sur les réponses structurelles aux excitations sismiques. Ces mêmes hypothèses, cependant, sont responsables d'erreurs tout au long des analyses basées sur le risque lorsqu'une mauvaise modélisation de la densité est obtenue. De plus, certaines de ces hypothèses ont été largement testées sur d'autres types de structures, de paramètres de demande d'ingénierie et de mesures d'intensité sismique (par exemple, le rapport de dérive interétage maximum sur les cadres résistants aux moments à plusieurs étages conditionnés par l'accélération spectrale à la période fondamentale). Les ponts sont composés de plusieurs éléments différents ayant des comportements distincts et des interactions complexes sous excitation sismique. La validité des hypothèses sur la log-normalité et la dépendance linéaire des demandes des composants du pont a été critiquée et leur impact sur les estimations de fragilité a été identifié comme une question ouverte à laquelle il faut potentiellement répondre.

La difficulté de traduire la richesse de la réponse des structures multicomposantes aux charges sismiques, couplée à l'émergence d'approches de sélection d'enregistrements basées sur des approches conditionnelles aux mesures d'intensité et l'analyse de bandes multiples, a motivé le développement d'une nouvelle approche pour la modélisation probabiliste de la demande sismique. Inspiré par le potentiel des techniques d'apprentissage automatique dans le traitement de l'incertitude, ce travail a exploré un algorithme de regroupement couramment utilisé pour les problèmes de *clustering*, les mélanges gaussiens, comme approche de modélisation de la densité, plutôt que d'utiliser des algorithmes basés sur la régression. La méthode proposée s'appuie sur la flexibilité des modèles GM pour estimer la densité de systèmes de demande multivariés conditionnés par un certain niveau d'intensité sismique. Le modèle capture de manière concomitante l'incertitude et la corrélation des réponses à composantes multiples à l'aide d'une simple combinaison linéaire de distributions normales pondérées. Cette nouvelle stratégie PSDM a ensuite été utilisée pour évaluer la propagation potentielle du biais dû à une mauvaise modélisation de la densité de la demande sismique dans le modèle de fragilité d'une structure multicomposante.

En conséquence, l'écart entre le tablier et les murs d'aile de la culée dans le pont de l'étude de cas a provoqué une discontinuité dans la réponse dans la direction transversale,

non seulement sur la déformation des murs d'aile, mais aussi sur les autres composants critiques en ayant un impact sur leur distribution statistique et leur dépendance. Cette discontinuité a été reconnue comme un facteur qui a conduit les données de demande à échouer au test de Lilliefors sur la log-normalité et à la dépendance non linéaire entre les composants. Deux régimes de déformation des composants du pont ont été identifiés par rapport à la fermeture de l'écart entre le tablier et la culée, qui dépendaient de l'intensité du tremblement de terre, sans toutefois être exclusifs à un certain niveau d'intensité. En évaluant localement les statistiques de la relation EDP|IM à l'aide de MSA et de clusters, la stratégie de modélisation de la densité proposée a permis d'identifier ces deux régimes, construisant ainsi un PSDM multivarié plus raffiné. En comparant les courbes de fragilité du système calculées à partir de différentes stratégies PSDM, l'impact d'une mauvaise modélisation de la densité a été étudié sur la fragilité du pont et la fréquence annuelle moyenne de dépassement des états de dommages. La déviation de la densité des données de demande de la loi lognormale a montré qu'il propageait plus de biais que la mauvaise hypothèse de dépendance linéaire, en fonction de l'état d'endommagement et des composants de gouvernance.

Par la suite, la perception préliminaire que les modèles de demande sismique basés sur le GM propageaient un faible biais dans les analyses basées sur la fragilité et le risque a été validée lorsqu'elle a été comparée aux résultats d'une approche bootstrap non paramétrique. Cette validation a également confirmé l'impression générale que la mauvaise modélisation probabiliste de la loi lognormale sur les données de demande sismique peut propager un biais important dans les estimations de fragilité, tandis que l'impact de l'hypothèse de dépendance linéaire a été jugé négligeable pour l'étude de cas. L'objectif de cette partie de la recherche n'était donc pas d'être conclusif, mais plutôt d'être complémentaire la discussion en cours sur la validité des hypothèses typiques et sur leur impact sur l'évaluation du risque sismique. Les hypothèses de lognormalité et de corrélation linéaire peuvent cependant être valides ou représenter des approximations appropriées des données observées, en fonction de la structure spécifique et du niveau d'erreur acceptable lors d'une évaluation du risque. Le choix de la stratégie pour effectuer une modélisation probabiliste de la demande sismique reste de la responsabilité de l'analyste.

Dans la deuxième partie de la présente étude, la performance du même pont a été évaluée dans sa configuration réhabilitée avec des isolateurs en considérant l'événement simultané d'un chargement sismique et des basses températures. En combinant le nouveau PSDM avec la régression logistique, la vulnérabilité du pont de l'étude de cas a été étudiée à la fois au niveau des composants et du système. En conséquence, les surfaces de fragilité ont

été conditionnées par la vitesse maximale du sol et la température ambiante. Alors que l'aléa sismique a été caractérisé à l'aide de PSHA, la température quotidienne moyenne recueillie pendant plus de 100 ans a été obtenue. Étant donné que le pont n'est pas isolé à l'origine, les écarts tels que construits peuvent ne pas être conformes aux exigences des codes qui demandent que les isolateurs fonctionnent sans entrave. Par conséquent, deux scénarios ont été idéalisés en ce qui concerne l'espace entre le tablier du pont et les murs en ailes des culées. Dans le premier, l'écart original de $25,4\,\text{mm}$ est conservé comme dans le pont tel que construit. Cet espace est plus petit que le déplacement de conception des isolateurs de $70\,\text{mm}$. Par conséquent, il n'est pas conforme aux exigences du code et les murs des ailes des culées doivent être renforcés. Dans le second scénario, l'espace est agrandi à $100\,\text{mm}$ pour tenir compte du déplacement de service des isolateurs.

Les piliers en béton armé étaient les principaux éléments de la sous-structure du pont que l'on cherchait à protéger par le schéma de réhabilitation proposé. En effet, à la température de référence ($20\,^{\circ}\text{C}$), les piliers ont été efficacement protégés par les isolateurs dans les deux scénarios d'écart. Même des signes mineurs de dommages ne sont pas susceptibles d'être observés, car les fragilités de l'état de dommage minimal sont inférieures à 10% pour des événements sismiques extrêmement rares ($0,02\%$ par an de probabilité de dépassement). Les surfaces de fragilité des piliers, cependant, ont montré l'augmentation de la fragilité des piliers du pont avec la diminution de la température ambiante, comme prévue étant donné l'important raidissement subi par les isolateurs. Ceci réitère la pertinence de la prise en compte des effets de raidissement thermique lors de la conception de systèmes d'isolation sismique à base de caoutchouc. Les résultats rapportés suggèrent, cependant, que ces effets étaient moins importants lorsque les structures de retenue agissaient en combinaison avec les isolateurs. En conséquence, dans le scénario de l'écart modifié, les piliers sont plus susceptibles de subir un état de dommage que lorsque l'écart original a été conservé. L'action bénéfique des murs en aile des culées a été mise en évidence en évitant la transmission de forces sismiques plus importantes aux piliers, tandis que l'isolateur sismique a effectivement découplé la superstructure du pont de la sous-structure.

Intuitivement, on pourrait s'attendre à ce que les murs en aile des culées subissent moins de dommages lorsqu'ils sont modifiés pour tenir compte du déplacement de service des isolateurs. La vulnérabilité des murs en aile n'a cependant pas été affectée de manière substantielle par les différentes valeurs d'écart. Plus précisément, la fragilité de ces structures latérales était pratiquement la même pour les états de dommages minimaux. Inversement, une légère augmentation de la fragilité à des états de dommages plus sévères a été notée. On pourrait expliquer cette augmentation par une énergie de martèlement du tablier plus

élevée et, par conséquent, plus dommageable, sur les murs en aile lorsque l'espacement est modifié pour se conformer aux exigences du CSA S6-14. La fragilité des murs en aile semblait généralement insensible au raidissement thermique des isolateurs. Sur la base des résultats de cette étude de cas, on peut donc conclure que les murs en aile des culées auraient besoin d'être renforcés indépendamment de l'espace disponible entre le tablier du pont et les murs latéraux. En outre, le maintien des murs en aile de culée dans leur place d'origine était également bénéfique pour les NRB, qui ne se sont pas effondrés par flambage. Dans le scénario modifié, cependant, les isolateurs étaient plus sensibles aux problèmes d'instabilité, en particulier dans le cas d'une éventuelle diminution potentielle de la capacité de l'isolateur causée par les basses températures.

Enfin, la fragilité du système était principalement régie par les parois en ailes des culées pour les états de dommages minimaux, réparables et étendus dans les deux scénarios d'écart. Les isolateurs NRB ne contrôlaient la fragilité de remplacement probable du système que lorsqu'ils fonctionnaient sans l'entrave des murs en aile. Dans ce cas, le raidissement thermique a démontré un léger impact positif sur la fragilité du NRB en raison de la réduction du déplacement latéral. Les piliers ont principalement contribué à la fragilité de l'ensemble du pont dans le scénario de l'espace élargi, et plus encore lorsque la structure est soumise à des températures inférieures au point de congélation et des événements sismiques rares. Dans le cas contraire, si l'espace d'origine est conservé, l'effet de retenue des murs en aile, bien que défavorable à la vulnérabilité des culées, a considérablement amélioré la performance sismique des piliers. Dans ce cas, si la capacité des murs en aile des culées devait être améliorée, l'ensemble du pont pourrait avoir une performance sismique satisfaisante lorsqu'il est isolé avec des NRBs, malgré leur raidissement thermique.

En résumé, l'objectif général de cette recherche a été atteint au moyen d'un cadre probabiliste analytique. Des analyses de fragilité sismique analytique ont été rigoureusement basées sur (1) des données sur les risques sismiques et le climat, (2) une sélection raffinée d'accélérogrammes, (3) des RHA non linéaires sur un modèle d'éléments finis calibré d'un pont réel, et (4) des données récentes de la capacité des composants du pont génerées au laboratoire de structures de l'UdeS. Cette étude a contribué aux discussions en cours sur la validité des hypothèses traditionnelles sur la modélisation multivariée de la densité de la demande sismique en en proposant une nouvelle stratégie de PSDM qui exploite les forces de l'analyse de bandes multiples et des modèles de mélanges finis. La pertinence de l'intégration d'outils statistiques puissants dans l'évaluation du risque sismique est ainsi reconnue. En outre, l'impact négatif des basses températures sur la performance sismique

du pont de l'étude de cas a été quantifié en matière de fragilité, en renforçant la nécessité de tenir compte des effets thermiques dans la conception des systèmes d'isolation à base de caoutchouc dans les dans des environnements froids. Encore une fois, la prise en compte distinguée des fragilités au niveau des composants et du système a démontré son importance pour fournir des informations locales et globales de la vulnérabilité sismique d'une structure. Bien que les effets thermiques aient été préjudiciables à l'endommagement minimal des piliers, la fragilité du système était principalement régie par les murs en aile de culée, qui étaient à leur tour insensibles aux effets des basses températures. Par conséquent, un exemple perspicace a été fourni sur les défis potentiels de la modernisation des ponts dans les régions froides avec des isolateurs en caoutchouc naturel, comme au Québec.

5.4 Recommendations et travaux futurs

Le travail effectué dans cette recherche pourrait être complété par de futures études sur les sujets suivants :

- Le nombre de points de données utilisés pour ajuster les modèles de mélange gaussien (c'est-à-dire le nombre d'enregistrements de mouvements sismiques du sol à chaque bande) pourrait affecter le modèle choisi. On doit mener des études supplémentaires sur la taille satisfaisante de l'ensemble de données pour éviter l'introduction de biais. En plus, on doit évaluer la relation entre la taille de l'ensemble de données avec le nombre de composants structurels et les paramètres du modèle.
- La nouvelle approche PSDM multivariée a d'abord été testée dans un cadre spécifique à la structure, en utilisant un pont d'étude de cas qui a été largement étudié. L'application de l'approche proposée doit cependant être étendue et testée pour l'évaluation de classes de ponts et de portfolios régionaux. En se basant sur les résultats de cette étude, les impacts potentiels que la méthodologie aurait à l'échelle d'un portefeuille régional ne peuvent pas encore être déduits. Des travaux futurs visant à étendre son application à des classes et des inventaires structurels sont donc nécessaires. De plus, les structures dont les détails sismiques sont encore plus insuffisants (où des interactions complexes et des régimes multiples non-linéaires peuvent se produire) ou de longs ponts (où une modélisation raffinée de la corrélation entre les réponses des composants peut avoir un rôle plus crucial) peuvent être des candidats de choix pour l'application de la méthode proposée.
- La méthodologie adoptée s'est appuyée sur une sélection rigoureuse d'accélérogrammes, qui s'est elle-même appuyée sur les résultats régionaux de l'analyse probabiliste de l'aléa sismique. Les modèles de mouvement du sol et les sources sismiques du Canada

ont récemment été entièrement intégrés dans le logiciel OpenQuake-engine de la Global Earthquake Model (GEM) Foundation afin de produire la sixième génération du modèle de risque sismique du Canada, qui devrait être incorporé dans les futures évaluations régionales du risque sismique.

– Le présent travail a utilisé les accélérogrammes de la base de données NGA-West2, qui comprend les mouvements du sol enregistrés dans l'ouest de l'Amérique du Nord, en Nouvelle-Zélande, en Chine, au Japon, au Moyen-Orient et au sud de l'Europe. Les caractéristiques de ces séismes peuvent être sensiblement différentes de celles enregistrées dans l'est de l'Amérique du Nord. Avec la publication de la base de données NGA-East, une sélection plus cohérente des enregistrements de mouvements du sol forts pourrait être réalisée pour les évaluations sismiques dans l'est du Canada.
– Contrairement aux bâtiments multiétagés, les ponts peuvent présenter une réponse dynamique plus complexe, qui n'est pas régie par ses premiers modes de vibration. Pour cette raison, l'accélération spectrale moyenne $S_{a,Avg}$ sur une gamme de périodes de vibration (discutée dans le chapitre 2) s'est avérée être une mesure d'intensité optimale pour l'évaluation du risque sismique des ponts et devrait être incorporée dans les études futures sur des cas spécifiques de structure ou de portfolios.
– La présente étude a été réalisée lorsque l'édition 2014 du code canadien de conception des ponts routiers CSA S6-14 était en vigueur. L'édition 2019 du code a été publiée en novembre 2019 et disponible au début de 2020, alors que la majeure partie des analyses du présent travail avait déjà été effectuée et ne pouvait éventuellement pas inclure les révisions. Les critères de performance révisés des dispositions de conception sismique basée sur la performance de deuxième génération du CHBDC ont apporté des changements spécialement aux indicateurs de dommages des éléments de sous-structure en béton. Cependant, les modèles de capacité des piliers en béton armé n'ont pas encore été mis à jour pour tenir compte des nouveaux indicateurs de dommages. Ces changements sont susceptibles d'affecter les résultats de l'évaluation de la fragilité sismique et peuvent être facilement pris en compte dans les études futures. Les nouveaux critères seront naturellement intégrés dans les travaux futurs, sous réserve du développement de modèles de capacité cohérents.
– Le pont de l'étude de cas était soutenu par des fondations peu profondes sur un sol rigide. Cependant, on devrait étudier les ponts isolés sur des sols qui nécessitent l'utilisation de fondations profondes en ce qui concerne l'effet combiné du raidissement thermique du caoutchouc et du sol gelé. Des dommages étendus sur des fondations profondes ont été signalés sur des ponts situés sur des sols gelés lors de tremblements de terre antérieurs. L'amplification potentielle des dommages causés

par des forces plus importantes que prévues transmises à sous-structure par des isolateurs plus rigides devrait être étudiée.

- Dans l'éventuelle émergence de données expérimentales démontrant l'apparition d'états de dommages intermédiaires sur les isolateurs sismiques en caoutchouc laminé, les estimations de capacité de ces composants devraient être mises à jour et incorporées dans les analyses de fragilité des ponts isolés. Par exemple, les effets des imperfections et de la plastification des plaques de renforcement en acier sur le comportement et la capacité de ces isolateurs doivent être étudiés. De plus, si les basses températures affectent la capacité de ces dispositifs, ce phénomène devrait être pris en compte dans une estimation plus précise de la vulnérabilité sismique du pont dans les régions froides.
- Les résultats de cette étude de cas ont montré qu'il est avantageux de combiner des structures de retenue latérale (par exemple, des murs en aile de culée) et des isolateurs sismiques en caoutchouc laminé lorsque ces derniers subissent un raidissement thermique important dans des conditions de froid extrême. Pour le pont de l'étude de cas, le sacrifice des murs en aile de culée a réduit la probabilité d'observer des dommages, même mineurs, sur les piliers, qui sont généralement les éléments du pont les plus coûteux à réparer ou à réhabiliter. En outre, il a déjà été démontré que différents mécanismes de retenue des déplacements du tablier, tels que les plaques de retenue et les câbles de retenue, améliorent les performances sismiques des ponts. Ces mécanismes devraient être étudiés en complément des isolateurs en élastomère dans les régions froides.
- Enfin, la diminution de la fonctionnalité des ponts après l'occurrence d'un événement extrême peut avoir un impact significatif sur les systèmes de transport et affecter le processus de récupération d'une communauté. L'estimation de la fragilité d'un pont sous l'effet d'un risque sismique peut faciliter l'évaluation de sa fonctionnalité et finalement de sa résilience après l'occurrence d'un tremblement de terre. Dans ce cas, d'autres aspects de l'analyse du risque sismique doivent tout de même être intégrés à l'évaluation des performances afin d'évaluer l'impact des combinaisons potentielles de mesures de modernisation dans des scénarios potentiels. Des variables telles que les coûts de modernisation et de réparation et les délais de remise en service pour la réparation et la restauration devraient être intégrées. En outre, dans cette analyse plus approfondie des événements extrêmes simultanés (par exemple, sismiques et thermiques), les données relatives aux risques sismiques et à la température de l'air devraient être convoluées à la fragilité dans le but de calculer la fréquence annuelle

moyenne d'observation de chacun des états de dommages évalués et leur acceptation générale par les gestionnaires d'actifs.

En résumé, les outils du génie parasismique basée sur la performance ont considérablement progressé au cours des vingt dernières années, pour aboutir à l'adoption de normes de conception sismique basées sur la performance au cours de dernière demi-décennie. Malgré les grands progrès réalisés dans le domaine, la mise en œuvre de l'analyse cohérente avec le risque par les ingénieurs praticiens est encore rare et des travaux supplémentaires sont nécessaires avant que les méthodes probabilistes ne deviennent l'approche standard pour les processus de prise de décision en génie des structures. La propagation de l'incertitude à partir de l'analyse de l'aléa sismique, en passant par l'évaluation de la fragilité sismique, et aboutissant au calcul de la probabilité de dépasser une variable de décision cible, a été largement utilisée dans le monde universitaire, alors qu'un intérêt encore modeste de la part des ingénieurs praticiens est observé. Il y a, cependant, un consensus sur le fait que les méthodes probabilistes du génie parasismique basé sur la performance gagnent en popularité et pourraient être adoptées comme des procédures standard dans l'avenir. Les recherches futures devraient donc continuer à fournir aux ingénieurs et aux décideurs la sensibilité nécessaire pour juger de la performance structurelle en matière de probabilités de dépassement des variables de décision.

APPENDIX A
THE AVERAGE BRIDGE IN QUEBEC

The 2 672 multi-span bridges in Quebec were categorized by Tavares [250] with respect to an exhaustive criteria list, which included the construction year, type of superstructure, number of spans, span length, material, type of abutment, type of bent, number of columns per bent, and shape of column cross-section, to name a few. From this dataset, the seven major bridge classes could be statistically represented and have their seismic fragility assessed. In addition, an average bridge for Quebec was defined based on the collected data. This average bridge shares numerous similar characteristics with the Chemin des Dalles bridge (Table A.1). More precisely, they match on 15 out of 28 criteria, with small deviation in some mismatching aspects (e.g., the number of girders). These similarities suggest that, although a specific bridge is the object of the present study, the expected performance of other similar structures in the region may be inferred based on the results presented.

Table A.1 Characteristics of the average bridge in Quebec and the Chemin des Dalles bridge

Parameter	Average bridge [248]	Chemin des Dalles bridge
	General information	
Type of superstructure	Concrete girder bridge	Concrete girder bridge
Number of spans	3	3
Support condition	Continuous	Continuous
Highway type	Local	Local
Construction year	1967	1979
Maximum length	69 m	106.5 m
Maximum span length	28 m	35.5 m
Deck width	13 m	13.2 m
Average column height	6 m	6.2 m
Maximum column height	7 m	6.2 m
Skew angle	0°	0°
Number of girders	5	6
	Span information	
Span length	28 m	35.5 m
Slab type	Reinforced concrete	Reinforced concrete
Deck surface type	Asphalt	Asphalt
	Substructure information	
Type of substructure unit	Seat-type abutment with integral wall and either wall bent or multicolumn bent	Seat-type abutment with integral wall and multicolumn bent
Material	Concrete	Concrete
Height	3 m abutment and 8 m bent	6.3 m abutment and 6.2 m bent
Foundation type	Superficial	Superficial
Soil type	Rock	Stiff soil
Bearing type	Elastomer with steel plates or non-existant	Elastomer with steel plates
Joint type	Non-existant	Non-existant
	Column information	
Number of bents	2	2
Number of columns per bent	4	3
Cross-section shape	Rectangular	Circular
Cross-section diameter	1140 mm	904 mm
Cross-section depth	2074 mm	n.a.
Cross-section width	1367 mm	n.a.

APPENDIX B

HAZARD CHARACTERIZATION AT THE BRIDGE SITE

The seismic hazard at the site of the case-study bridge is characterized by means of probabilistic seismic hazard analysis with respect to spectral acceleration and peak ground velocity. The

B.1 Seismic hazard

Although earthquakes occur in all regions in Canada, certain regions present a higher probability of experiencing damaging ground motion caused by seismic events than others. Because eastern Canada is located in a stable continental region within the North American Plate, a relatively low rate of earthquake activity is found. Nevertheless, large and damaging earthquakes have occurred in the past and will certainly occur in the future [194]. Seismic activity in these locations is apparently related to the regional stress fields, with the earthquakes concentrated in regions of crustal weakness. According to Natural Resources Canada [194], every year eastern Canada experiences approximately 450 earthquakes. Four of these seismic events will exceed magnitude 4, thirty will exceed magnitude 3, and about 25 will be reported felt. Other than that, within a decade, three earthquakes will occur with magnitude greater than 5, which is generally considered the threshold of damage to civil engineering facilities. Although earthquakes can and do occur throughout most of eastern Canada, years of instrumental recordings have recognized certain clusters of earthquake activity, where earthquakes occur at depths varying from the surface to 30 km [96]. One can observe that highest relative seismic hazard is concentrated along the Saint Lawrence River (Figure B.1) and that the case-study bridge is located on a region of moderate relative hazard. In Canada, the evaluation of the seismic hazard is the responsibility of the Geological Survey of Canada (GSC), a sector of Natural Resources Canada (NRC). With the sophistication and better understanding of probabilistic seismic hazard modeling, Canada's national hazard mapping efforts have evolved from qualitative assessment in 1953, to fully probabilistic in 2015 [1].

The 2015 edition of the hazard maps in Canada yields many important advances on its predecessors, including reconfigured seismic sources, and special consideration of large rare eastern earthquakes [3], besides the adoption of ground motion models proposed by Atkinson and Adams [15] with additional details by Atkinson's white paper [18] for Eastern North America (ENA) [120]. These GMMs are themselves based on five other GMMs [16, 13, 17, 212, 240] for ENA to account for epistemic uncertainties. This time, however, the GMM are not provided as equations. Instead, lookup tables define the models for a reference B/C site condition (with average seismic shear-wave velocity from the surface to a depth of 30 m $V_{s30} = 760\,\mathrm{m/s}$), whereas those present in GSC's Open File 7576 [120] are provided for the site C category ($V_{s30} = 450\,\mathrm{m/s}$). Soil conditions are

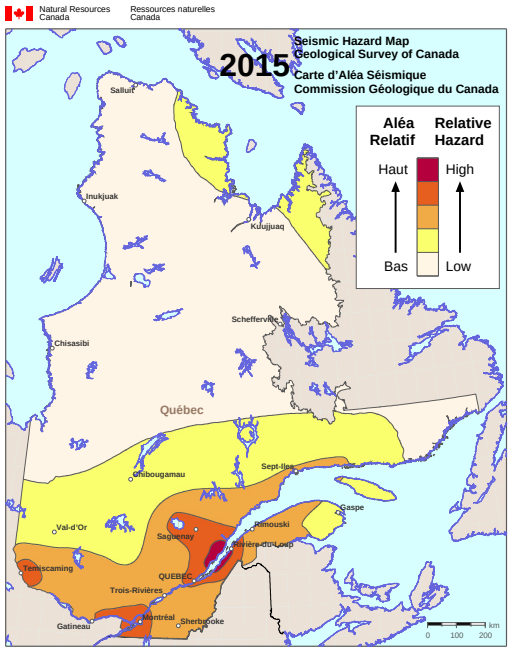

Figure B.1 Simplified seismic hazard map for Quebec [194].

defined by the 2015 edition of the National Building Code of Canada [55] (NBCC-2015). The latter were adopted by the GSC for the construction of the national seismic hazard maps of Canada, which are still in force according to the 2015 edition of the National Building Code of Canada [55]. Also, these GMMs are implemented on the OpenQuake-engine [113], an open-source platform for seismic hazard and risk calculation developed by the Global Earthquake Model (GEM) Foundation. Consequently, this software is adopted in the present study to perform the required probabilistic seismic hazard analyses.

These GMMs are determined for a moment magnitude (M_W) range between 4.5 and 8 and hypocentral distance (R_{hypo}) ranging from 10 to approximately 800 km. Finally, the models are defined for (pseudo) spectral acceleration (S_a) at periods ranging from 0.05 to 10 s, peak ground acceleration (PGA), and peak ground velocity (PGV). The source-to-site distance simplified conversions presented in Atkinson's white paper [18] were adopted to transform hypocentral distances (R_{hypo}) to Joyner-Boore distances (R_{jb}). Figure B.2a illustrates acceleration spectra generated by the three GMMs for $V_{s30} = 450\,\text{m/s}$, $M_W = 6$, and $R_{jb} = 80\,\text{km}$. To include the effect of site class soil condition into the prediction equations, the coefficients established in tables 4.1.8.4.-B to 4.1.8.4.-I in the NBCC-2015 [55] are adopted in accordance with the procedure defined by article 4.1.8. of the code. The site categories are considered according to the values of the average shear-wave velocity to a depth of 30 m. The effects of the soil conditions on the acceleration spectrum (based on the central GMM) can be appreciated in Figure B.2b. The spectral accelerations are amplified as the average shear-wave velocity is lower, and reduced otherwise.

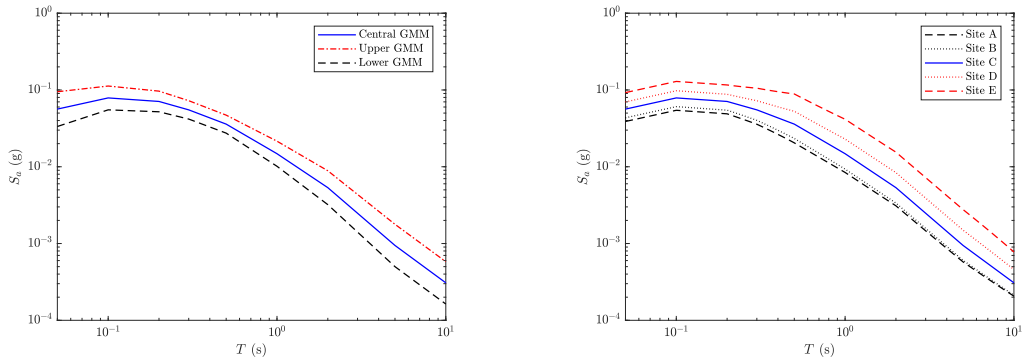

(a) **(b)**

Figure B.2 Acceleration spectra: (a) from upper, central, and lower GMMs for $V_{s30} = 450$ m/s; and (b) from central GMM for two site categories

For this study, the OpenQuake (OQ) engine [238] is employed to perform the PSHA at the bridge location To define the hazard curve for the pseudo-spectral acceleration S_a at the fundamental period of the Chemin des Dalles bridge $T_1 = 0.38\,\text{s}$; and peak ground velocity. The PSHA procedure provides a systematic framework for the consideration of both epistemic and aleatory uncertainties about the seismic model. Aleatory uncertainty is treated by modelling the GMM with a lognormal distribution that is characterized by a mean value and by the standard deviation of the logarithmic of the ground motion parameter of interest at a given magnitude and distance. Historically, the standard deviation has been assumed constant for all magnitudes and distances. Epistemic uncertainty arises from the modelling assumptions, unknown properties and parameters, and extrapolation of data beyond their observed range. The use of logic trees provides a convenient framework for the explicit treatment of epistemic uncertainty in seismic hazard analysis [239]. The longitude and latitude of the bridge are obtained in the inventory of structures provided by the Quebec Ministry of transportation, sustainable mobility, and transport electrification [179]. Besides the ground motion models, seismic source models are required for the PSHA. In Eastern Canada, three source clusters are established: Historical (H2), Hybrid (HY), and Regional (R2) [120]. The logic tree for the PSHA at the bridge site is presented in Figure B.3, in which the weights for each source cluster and ground motion model are also indicated.

Once each ground motion model (central, upper, and lower) is combined with each source cluster (H2, HY, and R2), nine individual hazard curves are produced, and the total hazard is obtained by the combining the weighted individual hazard curves (Figure B.4). The results of the hazard curves are then deaggregated for each couple of GMM and source cluster to identify the expected earthquake scenarios at the bridge site. Then, seismic deaggregation is performed to identify the expected earthquake scenario at the site of interest according to a given exceedance recurrence rate. Figure B.5 illustrates the deaggregation results for ground motions with 1% probability of exceedance in 50 years. The expected seismic scenarios evolve from lower magnitudes, larger distances, and

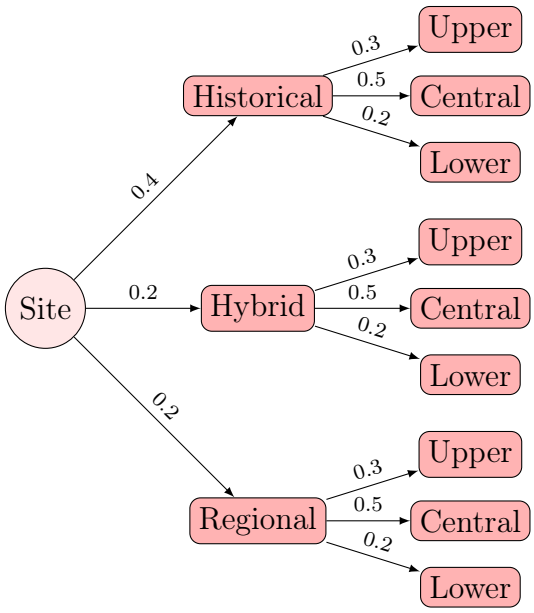

Figure B.3 Logic tree for probabilistic seismic hazard analysis on the OQ-engine based on sources and GMMs for eastern Canada

lower epsilons for more likely seismic events (low intensity levels) to higher magnitudes, shorter distances, and higher epsilons for more rare earthquake scenarios. Nevertheless, low intensity seismic events have more spread contributions to hazard, with significant contribution even from larger magnitudes (7.5–8) and longer distances (200 km). This could impact the definition of the conditional spectrum based on a single expected scenario and the consideration of all possible scenarios could be used instead for improvement [151]. The outcomes of the seismic deaggregations are used as input for the record selection via the GCIM approach. The construction of the target conditional distribution on IMs and the derived algorithm for record selection are described in Appendix C.

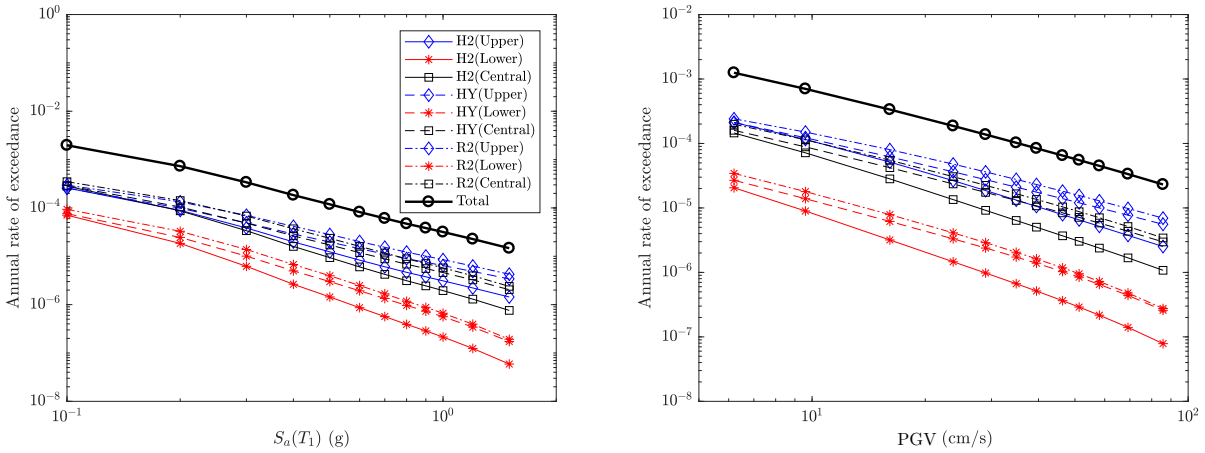

(a) **(b)**

Figure B.4 Total and ground motion model hazard curves from the PSHA on OpenQuake for (a) $S_a(T_1)$ and (b) PGV

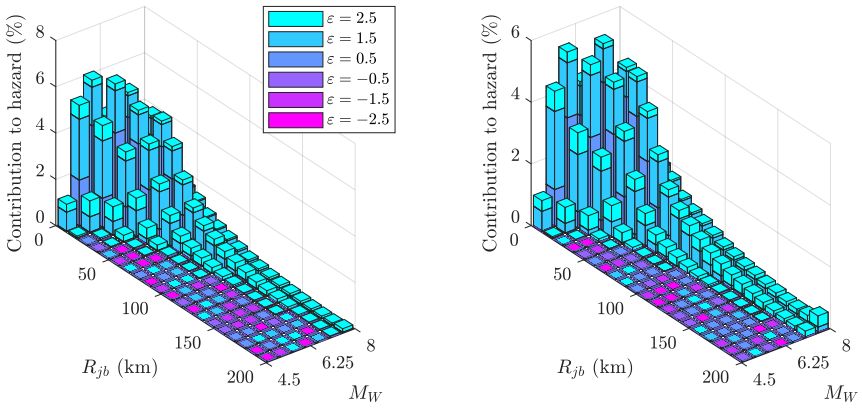

Figure B.5 Seismic deaggregation for (a) $S_a(T_1)$ and (b) PGV for a probability of exceedance of 1% in 50 years

B.2 Climate

The design and structural safety evaluation of many civil engineering facilities require the evaluation of thermal effects. In the case of bridges, temperature variations generate thermal strains and corresponding displacements of the bridge superstructure that should be adequately accommodated by bearings and expansion joints. In the case of isolated bridges, thermal stiffening of elastomeric isolators can be detrimental to the bridge performance during a seismic event by significantly affecting the load transfer between the bridge substructure and its superstructure. Rubber thermal stiffening depends on temperature and exposure time. For instance, the CHBDC-14 demands displacement tests on rubber isolators that are conditioned at negative temperatures for 14 days to simulate thermal stiffening effects. Two levels of temperature are defined for the tests: minimum service temperature and concomitant minimum temperature (see Section 2.6.3 for details). To assess the adequacy of this code criteria, a large database of meteorological records including recorded temperatures provided by Environment Canada was processed by Guay and Bouaanani [118] to build temperature contour maps. An example is illustrated in Figure B.6.

The number of consecutive days of observing temperatures below a given level are easily read in these maps. For instance, at the site of the case-study bridge, for a frequency of 5% per annum, the bridge is subjected to 1, 2, and 4 days with temperatures below -25, -20, and $-15\,^{\circ}\mathrm{C}$. At a lower annual frequency of 1%, the bridge is subjected to 2, 1, and 0 days with temperatures below -25, -20, and $-15\,^{\circ}\mathrm{C}$, respectively. This information is crucial to consider thermal crystallization effects during the design of rubber isolators.

Regarding the instantaneous thermal stiffening of rubber isolators, historical climate data comprehending daily temperature (minimum, mean, and maximum) are gathered from two stations in Shawinigan, Quebec, Canada [178]. These stations are located approximately 13.5 km away from the bridge site and report temperature measurements from 1902 to 2020. The histograms of the daily mean temperature ($\bar{\theta}_{daily}$) at each station are shown in Figure B.7. Climate identifiers (CID) of the stations are 7018000 and 7018001. The

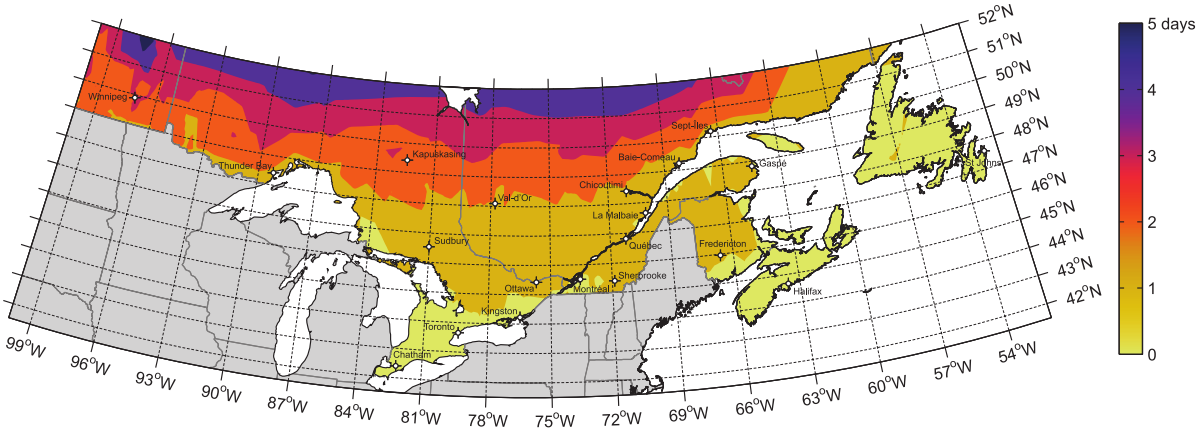

Figure B.6 Number of consecutive days below −20 °C in eastern Canada for a frequency of 5% (adapted from Guay and Bouaanani [118])

former reports temperature data from 1902 to 2004 (Figure B.7a), while the latter has been collecting data since 1998 (Figure B.7b). Gaussian mixtures are fit to the mean daily temperature data to facilitate the calculation of annual probabilities of observing temperatures below a given value. Four weighted normal distributions demonstrate the best fit to the observed data.

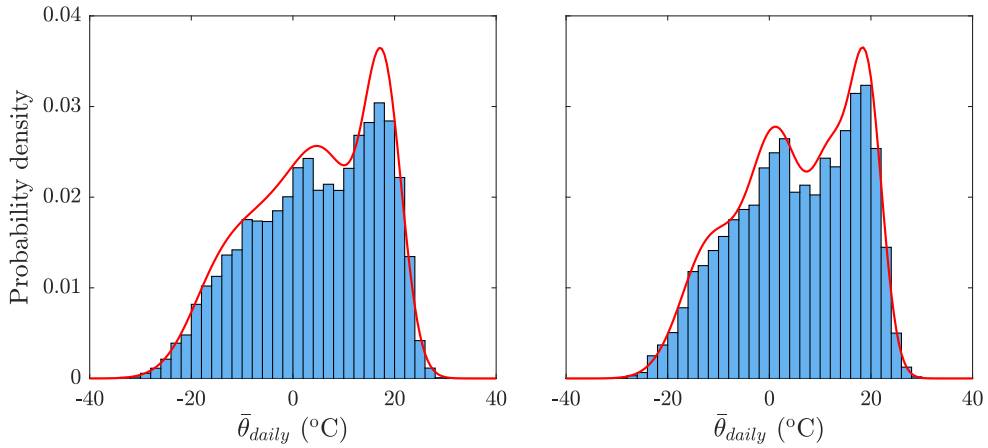

(a) CID 7018000 (b) CID 7018001

Figure B.7 Mean daily temperature from two stations in Shawinigan, Quebec, Canada based on Environment and Climate Change Canada data [178]

The CHBDC-14 requires that the concomitant minimum service temperature to be taken as the average of +15 °C and the minimum service temperature, which is −30 °C in this case. Hence, at the location of the Chemin des Dalles bridge, the concomitant minimum service temperature is −7.5 °C. According to the Gaussian mixture fitted model, temperatures below −30 °C have a probability of 0.01% per annum, while temperatures below the concomitant temperature have an annual probability of 19.07% (Figure B.8).

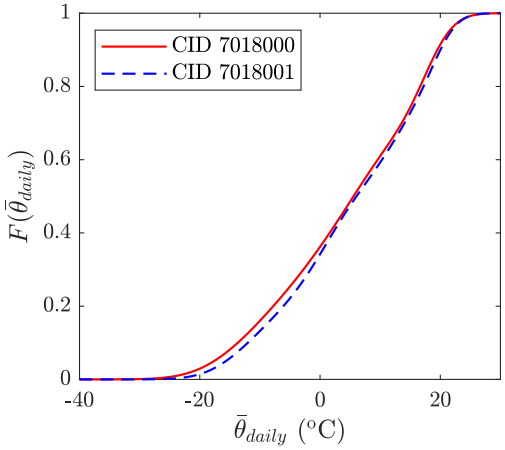

Figure B.8 Cumulative distribution function of mean daily temperature at the bridge site

APPENDIX C

THE GENERALIZED CONDITIONAL INTENSITY MEASURE APPROACH FOR RECORD SELECTION

Bradley [43] proposed the generalized conditional intensity measure (GCIM) approach aiming to overcome the restrictions of the conditional spectrum approach. In this generalized approach, a framework is established in which the distribution of any ground motion intensity measure can be obtained given the occurrence of another specific ground motion IM (which are commonly gathered from probabilistic seismic hazard analysis). The GCIM approach allows any number of intensity measures, identified as important in a particular seismic response problem, to be considered. Details on the construction of target conditional distribution and the adopted algorithm for record selection are further explained in this appendix.

C.1 Target conditional distribution of the GCIM

The basis of the GCIM approach is similar to the conditional spectrum method, whereas, instead of assuming that only spectral accelerations have a multivariate lognormal distributions, all intensity measures of interest $\mathbf{IM} = \{\mathrm{IM}_1, \mathrm{IM}_2, \ldots, \mathrm{IM}_n\}$ are assumed to follow a multivariate lognormal distribution conditioned on the occurrence of a specific ground motion intensity measure $\mathrm{IM}_j = im_j$. From the assumption that $\mathbf{IM}|Rup$ has a multivariate lognormal distribution (given the occurrence of an earthquake scenario characterized by rupture parameters Rup), it follows that $\mathrm{IM}|Rup, \mathrm{IM}_j$ is also lognormally distributed, and in particular, that for each IM_i in IM, the marginal conditional $\mathrm{IM}_i|Rup, \mathrm{IM}_j$ has a univariate lognormal distribution. It can be expressed as

$$f_{\mathrm{IM}_i|Rup,\mathrm{IM}_j} \sim \mathrm{LN}(im_i; \mu_{\ln \mathrm{IM}_i|Rup,\mathrm{IM}_j}, \sigma^2_{\ln \mathrm{IM}_i|Rup,\mathrm{IM}_j}) \tag{C.1}$$

where $f_X \sim \mathrm{LN}(x; \mu_{\ln X}, \sigma^2_{\ln X})$ is the short-hand notation for a random variable X following a lognormal distribution with mean $\mu_{\ln X}$ and variance $\sigma^2_{\ln X}$.

The conditional mean and standard deviation of each marginal distribution are calculated as

$$\mu_{\ln \mathrm{IM}_i|Rup,\mathrm{IM}_j} = \mu_{\ln \mathrm{IM}_i|Rup} + \sigma_{\ln \mathrm{IM}_i|Rup}\rho_{\ln \mathrm{IM}_i,\ln \mathrm{IM}_j}\varepsilon_{\ln \mathrm{IM}_j} \tag{C.2}$$

$$\sigma_{\ln \mathrm{IM}_i|Rup,\mathrm{IM}_j} = \sigma_{\ln \mathrm{IM}_i|Rup}\sqrt{1 - \rho^2_{\ln \mathrm{IM}_i,\ln \mathrm{IM}_j}} \tag{C.3}$$

where $\mu_{\ln \mathrm{IM}_i|Rup}$ and $\sigma_{\ln \mathrm{IM}_i|Rup}$ are the mean and standard deviation of $\ln \mathrm{IM}_i$ provided by a ground motion model (GMM); $\rho_{\ln \mathrm{IM}_i,\ln \mathrm{IM}_j}$ is the correlation coefficient for $\ln \mathrm{IM}_i$ and $\ln \mathrm{IM}_j$; and $\varepsilon_{\ln \mathrm{IM}_j}$ is the difference between the logarithm of the target IM_j and the mean

predicted by the GMM $\mu_{\ln \mathrm{IM}_j|Rup}$, in terms of the standard deviation $\sigma_{\ln \mathrm{IM}_j|Rup}$

$$\varepsilon_{\ln \mathrm{IM}_j} = \frac{\ln \mathrm{IM}_j - \mu_{\ln \mathrm{IM}_j|Rup}}{\sigma_{\ln \mathrm{IM}_j|Rup}} \tag{C.4}$$

Recently, Baker and Bradley [24] defined correlation coefficients for several intensity measures based on the NGA-West2 [8] database. These coefficients were compared to those calculated previously based on alternative databases and showed good agreement. Additionally, they provided further evidence that the IM correlation coefficients are independent of the reference ground motion model, ground motion database and rupture and site parameters (e.g., magnitude, distance, and soil category).

C.2 Algorithm for record selection

Bradley [45] provided an algorithm for record selection based on the GCIM approach. The construction of the multivariate distribution is performed in the open-source software OpenSHA while the record selection is carried out in a Matlab program. For the present study, however, it was opted to expand the Matlab program provided by Baker and Lee [27] (originally built for the conditional spectrum approach) to consider other intensity measures, given the similarities between the two approaches. Furthermore, the program supplied by Baker and Lee [27] allows the easy inclusion of different GMMs and the use of results from PSHA performed elsewhere (e.g., on OpenQuake as in the current study). The script was modified to consider other intensity measures in addition to the already contemplated spectral acceleration at multiple periods. Here, only peak ground acceleration PGA and peak ground velocity PGV were included, which can be predicted by the most recent GMMs for Eastern Canada [120].

First, the target multivariate conditional lognormal distribution is built based on the ground motion models and correlation models. Once the GCIM distribution is defined, samples of the IM_i are drawn from it and ground motions from a database are selected to match such samples individually in a first row of selection, i.e, the selected records are those that present the lowest residual compared to the samples. The residual $r_{m,sim}$ of a prospective ground motion m with respect to a simulation sim from the GCIM distribution is

$$r_{m,sim} = \sum_{i=1}^{N_{\mathrm{IM}_i}} w_i \left[\frac{\ln \mathrm{IM}_i^{sim} - \ln \mathrm{IM}_i^{m}}{\sigma_{\ln \mathrm{IM}_i|Rup,\mathrm{IM}_j}} \right]^2 \tag{C.5}$$

where w_i is the weight of ith intensity measure and $\sigma_{\ln \mathrm{IM}_i|Rup,\mathrm{IM}_j}$ is the conditional standard deviation of $\ln \mathrm{IM}_i$ given the rupture scenario and the occurrence of $\mathrm{IM}_j = im_j$.

The IM weights w_i are normalized (i.e., $\sum_i w_i = 1$) and indicate the importance of each IM_i for the ground motion selection. Thus, by setting the weight w_{IM_k} of an intensity measure IM_k to zero, this intensity measure is neglected for the record selection. However, the values of IM_k are still collected for the chosen records and, therefore, the effect of its disregard may be assessed in comparison to the marginal conditional distribution that it should follow.

Since the records are selected by individually matching the simulated samples, the set is deemed to be representative of the target GCIM distribution. Nevertheless, given the finite number of selected records N_{gm}, a comparison of the suitability of the whole suite to the target distribution must be assessed via statistical goodness-of-fit measures. Differently to the approach proposed by Bradley [45], a greedy optimization algorithm is used instead of the comparison of different selected sets. The greedy optimization technique adopted by Jayaram et al. [125] is utilized here to further improve the record selection. For such, each ground motion selected initially is replaced one at a time with a ground motion from the database that causes the best improvement to the whole suite in comparison to the target distribution. In this way, two options to evaluate the suite's goodness-of-fit are available: (i) a weighted sum (over all intensity measures) of squared errors in the mean values and standard deviations; and (ii) a global residual based on Kolgomorov-Smirnov (K-S) test statistics.

For the former, the sum of squared errors SSE for the set s is calculated as

$$SSE_s = \sum_{i=1}^{N_{\mathrm{IM}_i}} w_i \left[w_\mu (m_{\ln \mathrm{IM}_i,s} - \mu_{\ln \mathrm{IM}_i|Rup,\mathrm{IM}_j})^2 + w_\sigma (s_{\ln \mathrm{IM}_i,s} - \sigma_{\ln \mathrm{IM}_i|Rup,\mathrm{IM}_j})^2 \right] \tag{C.6}$$

where w_μ and w_σ are the weights for the means and standard deviations, respectively, $m_{\ln \mathrm{IM}_i,s}$ and $s_{\ln \mathrm{IM}_i,s}$ are the mean and standard deviation of $\ln IM_i$ of the suite s of selected records, and

The second criterion calculates a global residual for the set R_s over all IM_i and all records as

$$R_s = \sum_{i=1}^{N_{\mathrm{IM}_i}} w_i (D_{\mathrm{IM}_i,s})^2 \tag{C.7}$$

in which $D_{\mathrm{IM}_i,s}$ is the K-S test-statistic for the set s that is calculated as

$$D_{\mathrm{IM}_i,s} = \max_m \left\{ F_{\mathrm{IM}_i|IM_j} - S_{\mathrm{IM}_i,s} \right\} \tag{C.8}$$

where m indicates the ground motions in the set, $F_{\mathrm{IM}_i|\mathrm{IM}_j}$ is the cumulative distribution function (CDF) of the GCIM distribution, and $S_{\mathrm{IM}_i,s}$ is the empirical distribution function (EDF) of the suite of ground motions selected.

The following observations are made when the selection parameters and testing criteria are modified:

1. when using only one IM that is independent of the structure (i.e., $w_i = 0$ for either PGV or PGA), the optimization brings the other structure-independent IM to conformity to the target distribution. Intuitively, if $w_i = 0$ for both PGA and PGV, the selected records do not match the target conditional distributions for these structure-independent intensity measures regardless the number of further optimization loops;
2. when the optimization criterion is based on the sum of squared errors, the final discrepancies on means and standard deviations are usually further reduced and often fall within 10% tolerance. The empirical distribution functions are not guaranteed

to show the best fit to the GCIM target distributions, although the K-S bounds are usually respected (i.e., the null hypothesis of the K-S tests are not verified);

3. conversely, when the optimization criterion is based on the K-S test statistics, the final EDPs match well the theoretical conditional CDFs in detriment of the deviation of the final selection with respect to target means and standard deviations, which often do not show improvement compared to the initial selection. It is also noticed that the EDPs frequently show really good fit for cumulative probability with values less than 0.8 whereas the right tail seem to be lengthened to match the target CDFs. Additionally, the optimization using K-S test statistics is slower than the other option, as also verified by Baker and Lee [27].

The ground motion records selected for use in this study and the adopted criteria are presented in Appendix D. The benefits of the greedy optimization algorithm proposed by Jayaram et al. [125] are evidenced in the graphs presented in the next appendix.

APPENDIX D
SELECTED GROUND MOTION RECORDS

Due to the lack of real ground motion records in Eastern Canada, synthetic accelerograms were generated by Atkinson [14] for moment magnitudes of 6.0 and 7.0 and near and far distances. Nevertheless, the availability of strong ground motion records in Eastern Canada is very limited. Another option is to select records from other databases, such as the Pacific Earthquake Engineering Research (PEER) Next Generation Attenuation Relationships for Western US Phase 2 (NGA-West2), which is composed of more than 20,000 three-component records [8, 7]. It is recognized that use of such ground motions in Eastern North America might underestimate the response of the case study structure and western records might be too weak for periods near the fundamental period of the structure. Nevertheless, ground motions from the NGA-West2 database can still be adequate if they match well the conditional spectrum at low periods. Actually, past studies have shown that if the spectral shape of the selected records is similar to the target spectra, they will adequately estimate the structural response [38]. The spectral shape of the records is one of the most important properties to match when selecting records with the CS or GCIM method, whereas other characteristics of the records can be seen as of less importance [23, 154].

D.1 Records conditioned on spectral acceleration

The selected ground motion records conditioned on the spectral acceleration at the bridge's elastic fundamental period in the transverse direction $S_a(T_1)$ are illustrated here in terms of selected spectra, standard deviation of the selected spectra, and the Kolmogorov-Sminorv (K-S) test on the conditioned distributions of peak ground acceleration (PGA) and peak ground velocity (PGV) (Figures D.1 to D.6). All intensity measures are considered in the horizontal direction. The levels of conditioning spectral acceleration at $T_1 = 0.38\,\text{s}$ are 0.2, 0.4, 0.6, 0.8, 1.0, and 1.2 g. One hundred (100) records are selected at each of these levels.

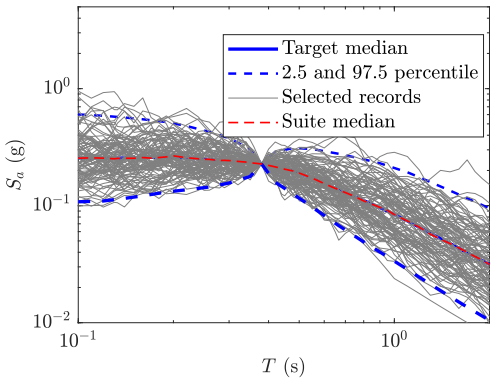

(a) Selected spectra

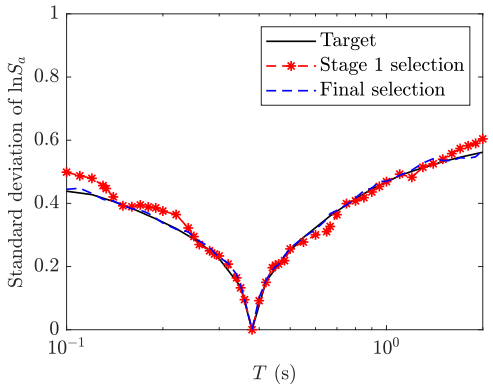

(b) Conditional standard deviation of selected spectra

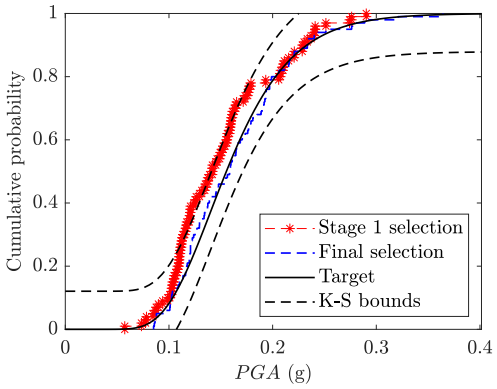

(c) K-S test on PGA

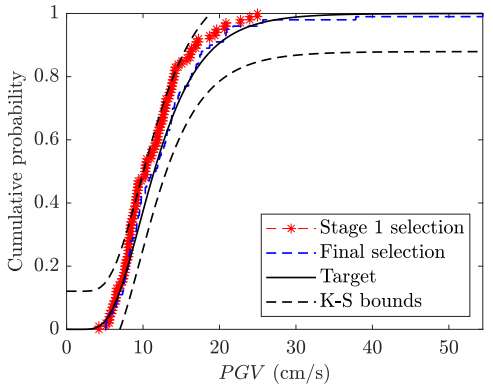

(d) K-S test on PGV

Figure D.1 Selected records conditioned on $S_a(T_1) = 0.2\,\mathrm{g}$

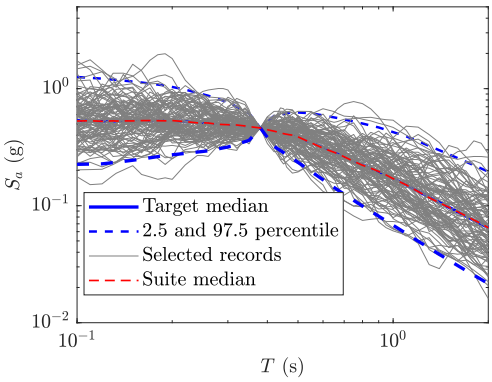

(a) Selected spectra

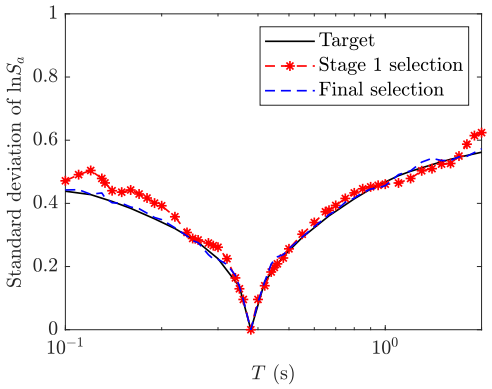

(b) Conditional standard deviation of selected spectra

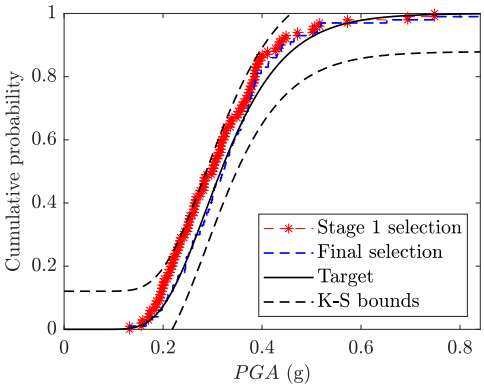

(c) K-S test on PGA

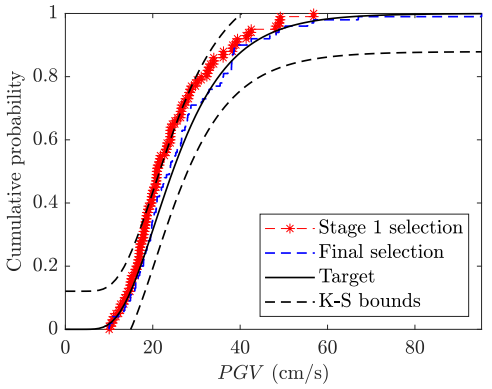

(d) K-S test on PGV

Figure D.2 Selected records conditioned on $S_a(T_1) = 0.4\,\mathrm{g}$

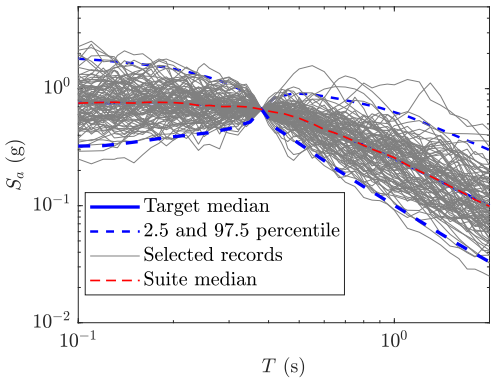

(a) Selected spectra

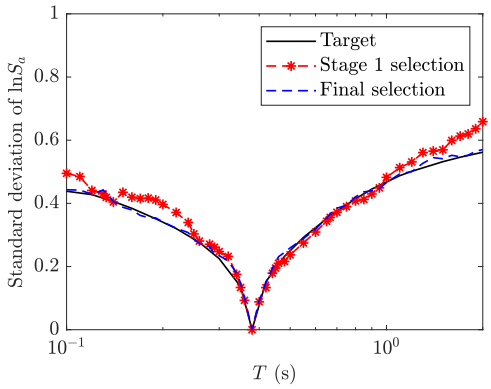

(b) Conditional standard deviation of selected spectra

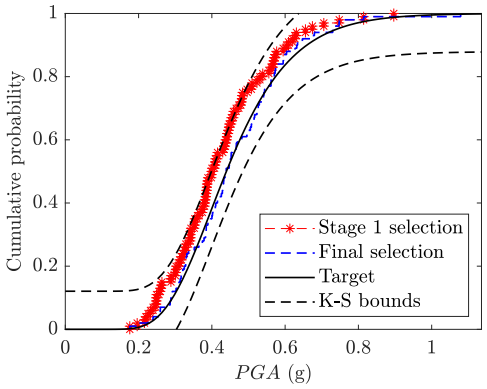

(c) K-S test on PGA

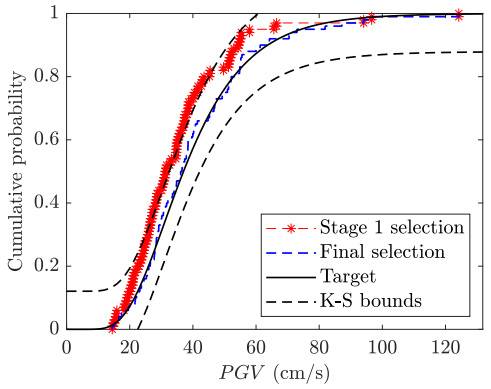

(d) K-S test on PGV

Figure D.3 Selected records conditioned on $S_a(T_1) = 0.6\,\mathrm{g}$

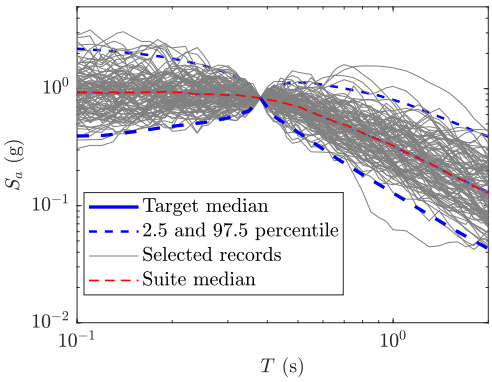

(a) Selected spectra

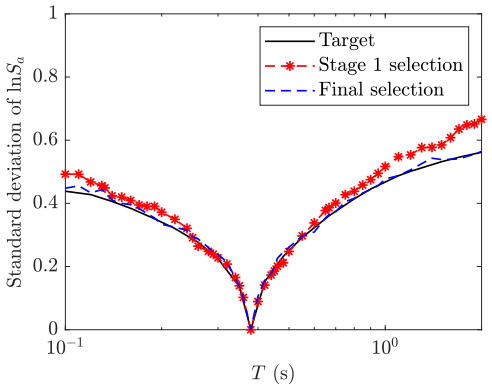

(b) Conditional standard deviation of selected spectra

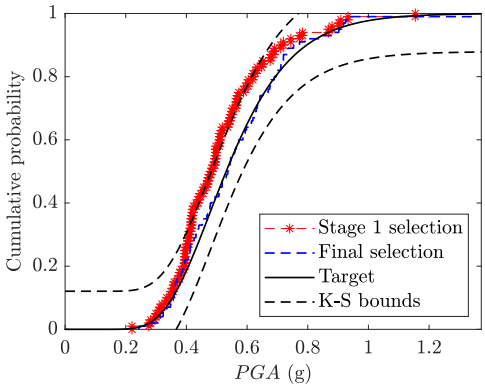

(c) K-S test on PGA

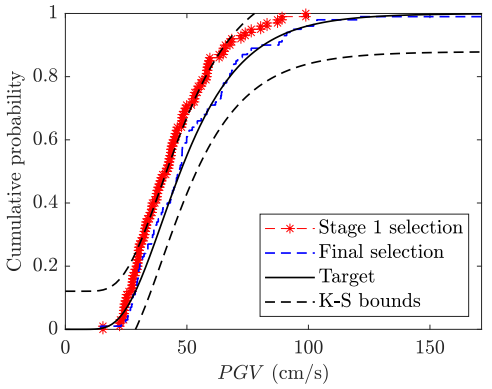

(d) K-S test on PGV

Figure D.4 Selected records conditioned on $S_a(T_1) = 0.8\,\mathrm{g}$

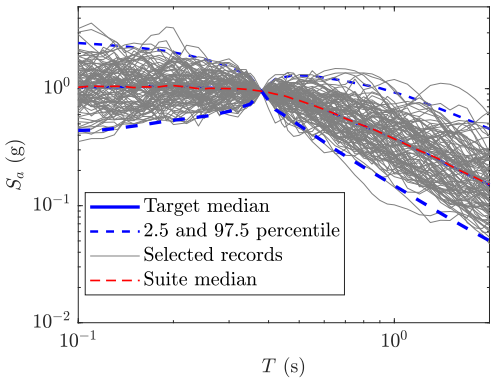

(a) Selected spectra

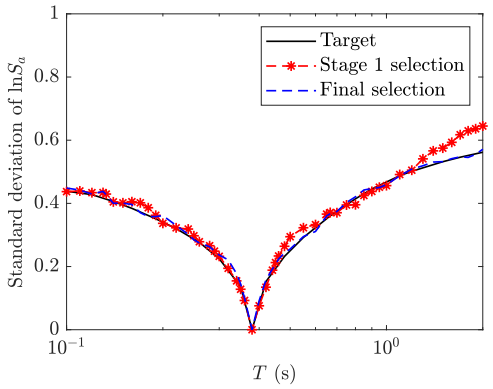

(b) Conditional standard deviation of selected spectra

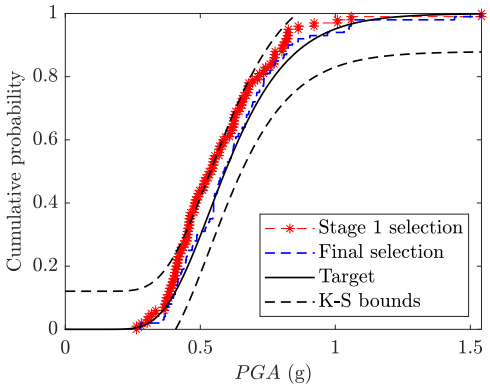

(c) K-S test on PGA

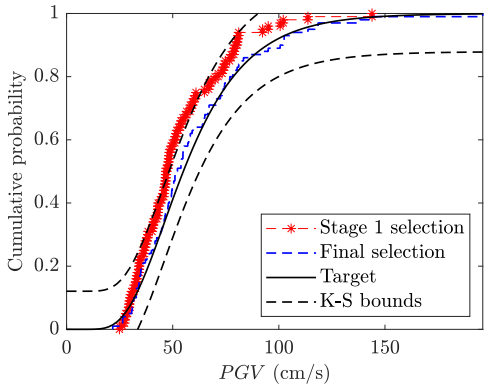

(d) K-S test on PGV

Figure D.5 Selected records conditioned on $S_a(T_1) = 1.0\,\mathrm{g}$

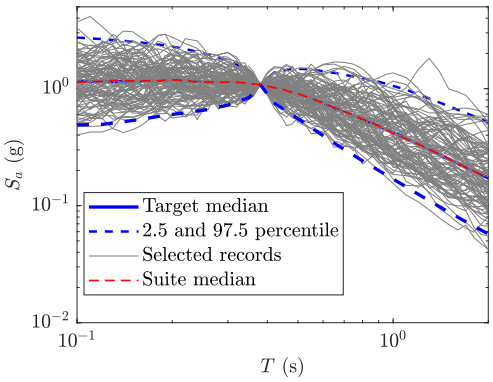

(a) Selected spectra

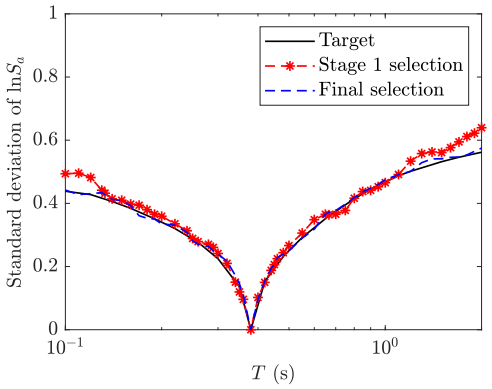

(b) Conditional standard deviation of selected spectra

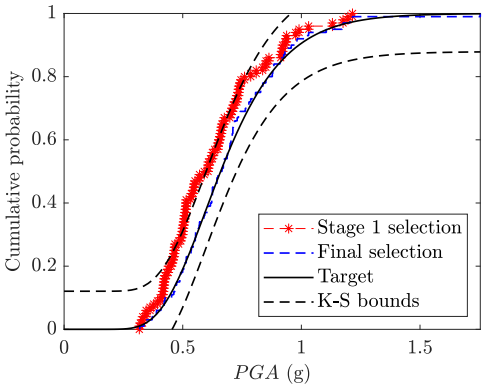

(c) K-S test on PGA

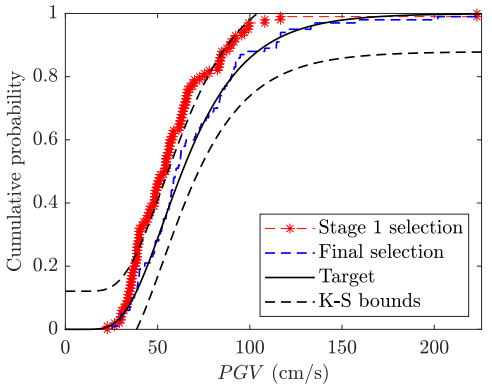

(d) K-S test on PGV

Figure D.6 Selected records conditioned on $S_a(T_1) = 1.2\,\mathrm{g}$

D.2 Records conditioned on peak ground velocity

The selected ground motion records conditioned on peak ground velocity (PGV) are illustrated here in terms of select spectra, standard deviation of the selected spectra, and the Kolmogorov-Sminorv (K-S) test on the conditioned distributions of peak ground acceleration (PGA) (Figures D.7 to D.12). All intensity measures are considered in the horizontal direction. The levels of conditioning peak ground velocity are 7.2, 14.1, 22.7, 35.5, 62.1, and 92.8 cm/s. Forty (40) records are selected at each of these levels.

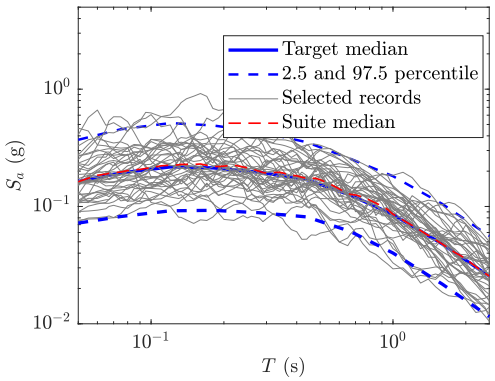

(a) Selected spectra

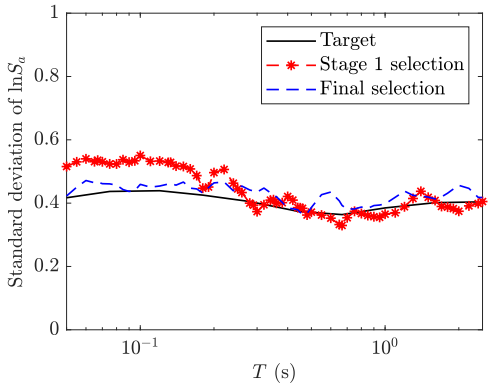

(b) Conditional standard deviation of selected spectra

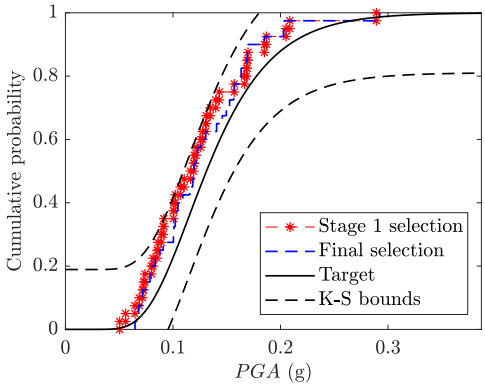

(c) K-S test on PGA

Figure D.7 Selected records conditioned on PGV = 7.2 cm/s

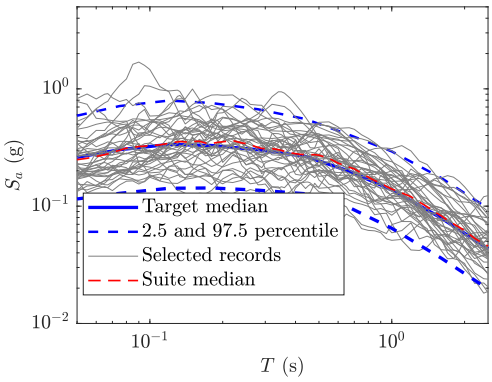

(a) Selected spectra

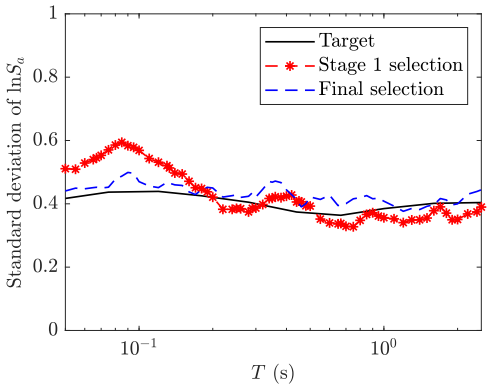

(b) Conditional standard deviation of selected spectra

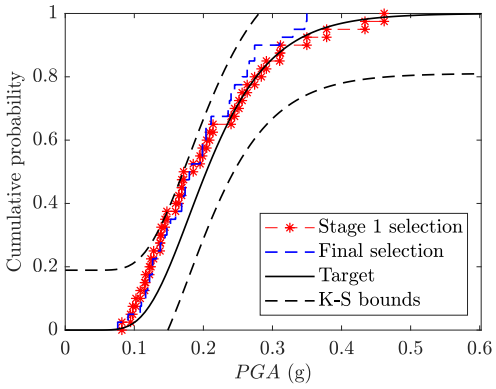

(c) K-S test on PGA

Figure D.8 Selected records conditioned on PGV = 14.1 cm/s

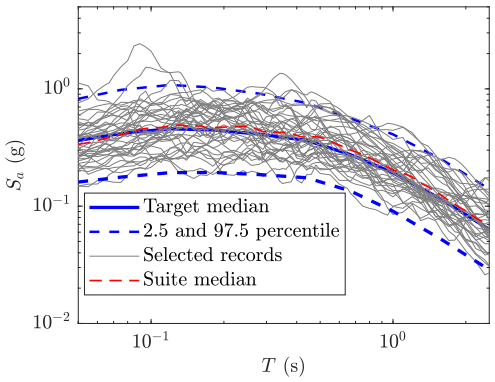

(a) Selected spectra

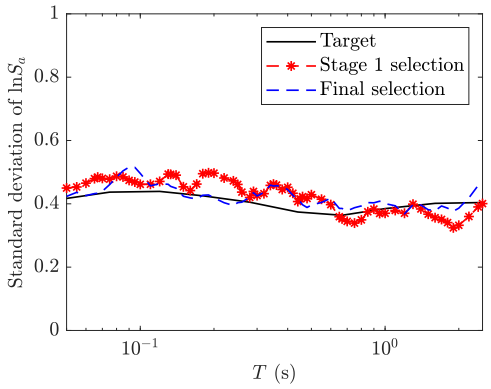

(b) Conditional standard deviation of selected spectra

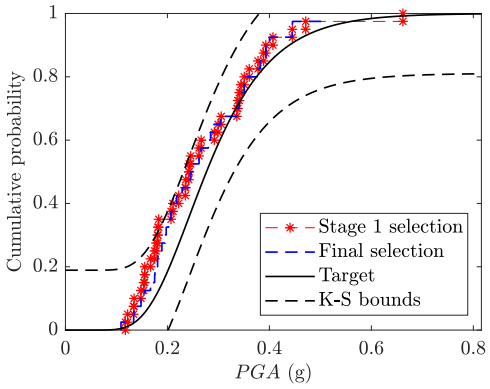

(c) K-S test on PGA

Figure D.9 Selected records conditioned on PGV = 22.7 cm/s

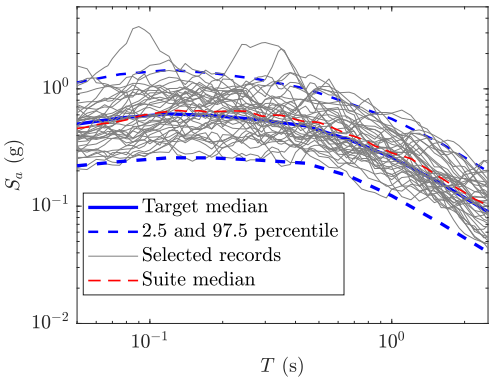

(a) Selected spectra

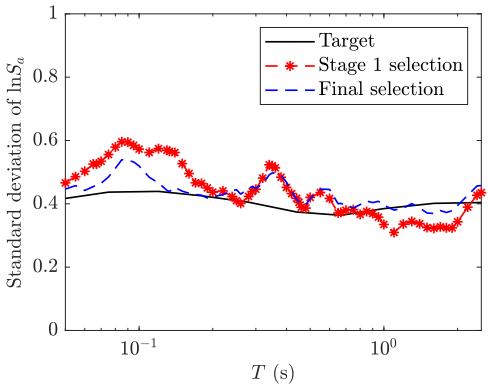

(b) Conditional standard deviation of selected spectra

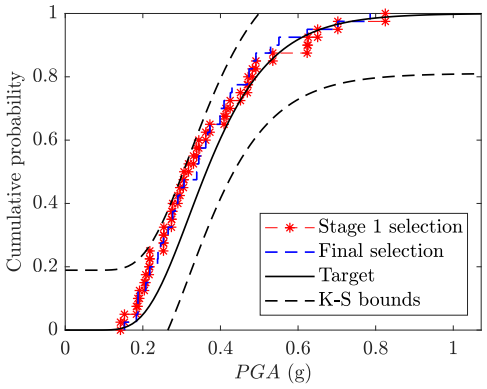

(c) K-S test on PGA

Figure D.10 Selected records conditioned on PGV = 35.5 cm/s

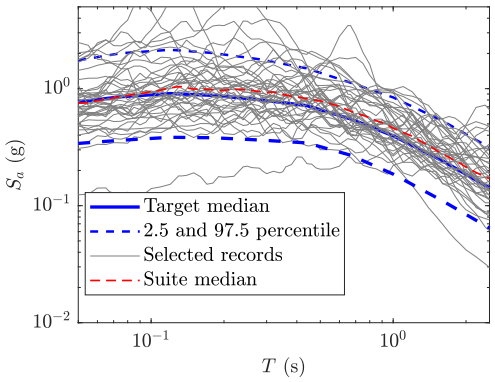

(a) Selected spectra

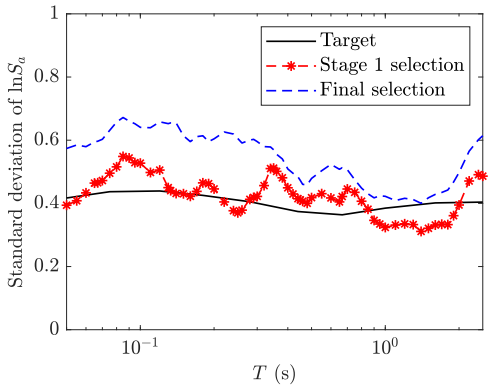

(b) Conditional standard deviation of selected spectra

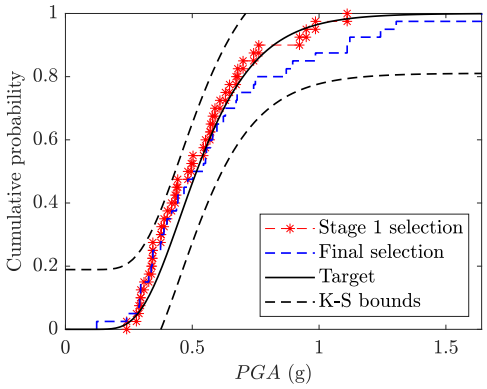

(c) K-S test on PGA

Figure D.11 Selected records conditioned on PGV = 62.1 cm/s

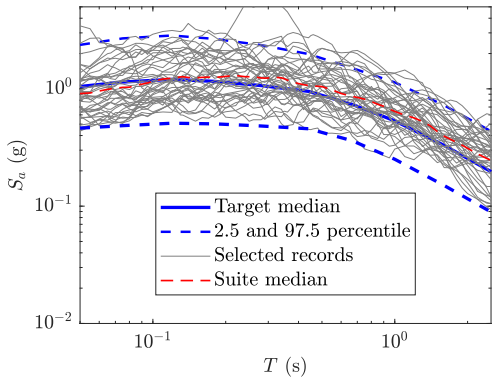

(a) Selected spectra

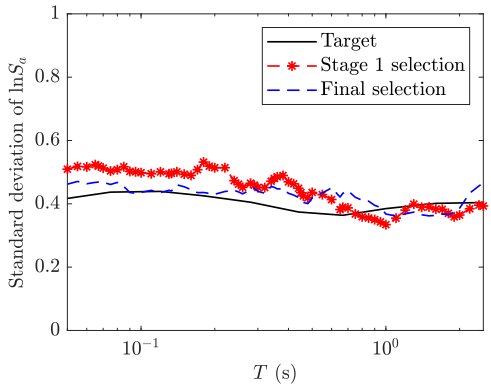

(b) Conditional standard deviation of selected spectra

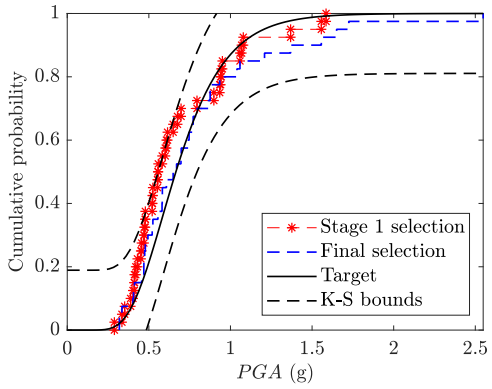

(c) K-S test on PGA

Figure D.12 Selected records conditioned on PGV = 92.8 cm/s

APPENDIX E

INFERENCE ON FRAGILITY AND RISK ESTIMATES

The fragility analyses performed in Chapter 3 based on the Gaussian mixture seismic demand models were deemed less biased than the other PSDM approaches due to the inherent flexibility of the density model used to fit the observed seismic demand data. At that point, however, no further verification was provided to check the accuracy of the proposed approach. The analyses presented in this appendix are thus aimed to address this limitation. To this end, bootstrap-based fragility curves are generated, allowing the assessment of confidence intervals of the fragility functions for the case-study bridge. From the bootstrap fragility curve replications, the corresponding mean annual frequency of damage state exceedance are estimated to give an indication of bias of the investigated PSDM strategies. Bootstraping has already been adopted in other fragility and risk studies to quantify the uncertainty (e.g.,[87, 104, 62]).

E.1 Bootstrap seismic fragility curves

The development of analytical system fragility curves is a rather complex process. Indeed, a thorough approach treating uncertainty on both demand and capacity involves: (1) the generation of a seismic demand dataset and its joint probabilistic modeling, (2) the adoption of probabilistic capacity models of critical components, and (3) the assessment of the conditional probability of exceeding a damage state. The common assumptions on the demand modeling and their limitations were previously discussed on Chapter 3. With respect to the capacity models, it is common to suppose that they are lognormally distributed [197, 168]. Finally, fragility curves are often fitted to parametric CDFs such as lognormal, normal, Weibull, or logistic [200, 207, 39, 230].

If a poor model results from one the adopted hypothesis, significant bias may be propagated into seismic risk analysis [82, 20]. To avoid the adoption of parametric assumptions on seismic demand and given the complexity of the construction of fragility curves, a nonparametric bootstrap-based approach seems to be a suitable strategy to build fragility functions and to perform statistical inference on the results—e.g., estimate a mean and a confidence interval of the resulting fragility curves. Bootstrapping estimates the distribution of a statistic by repeatedly resampling from the observed data with replacement [88]. In this case, a bootstrap estimate of the fraction of ground motions that cause structural collapse at an intensity level is made by sampling n peak demands with replacement from the original n RHAs performed at that intensity level. To incorporate the uncertainty on component capacities, one hundred capacity estimates are first sampled from the lognormal capacity models of each critical component (Table 3.1). Then, by sampling n capacity estimates with replacement and pairing them with the bootstrap sampled demands, a bootstrap replication of the ratio of damage state exceedance $z_{j,b}/n$ is obtained,

based on the series system assumption. Finally, a replication system fragility curve is fitted to the resampled fractions of ground motions causing DS violation at all N_{IM} intensity levels, and the corresponding mean annual frequency of DS exceedance is then estimated.

Therefore, the nonparametric aspect of the adopted procedure to develop bootstrap fragility curves relies only on the resampled demand data, because these are the limited dataset generated from the response history analyses. The capacity models are assumed to follow lognormal distributions, and the shape of the fragility curves is assumed as the lognormal CDF given the good fit to the observed data in this study. Thus, applying maximum likelihood estimation to the replication number of DS exceedance, Equation 3.3 takes the following form:

$$\left\{\hat{\theta},\hat{\beta}\right\}_b = \arg\max_{\boldsymbol{\theta},\boldsymbol{\beta}} \sum_{j=1}^{N_{\mathrm{IM}}} \left\{ \ln \binom{n}{z_{j,b}} + z_{j,b} \ln \Phi\left(\frac{\ln(im_j/\theta)}{\beta}\right) + (n - z_{j,b}) \ln\left[1 - \Phi\left(\frac{\ln(im_j/\theta)}{\beta}\right)\right] \right\} \quad \text{(E.1)}$$

where the subscript b relates to the bootstrap replication, $\Phi(\cdot)$ is the standard normal CDF, n is the number of bootstrap samples at each seismic intensity level (equal to the number of selected ground motion records conditioned at each level of IM). The corresponding mean annual frequency of damage state exceedance λ(DS) is then calculated according to Equation 3.4.

E.2 Inference on fragility and risk estimates

Ten thousand bootstrap replications of the system fragility curves are performed for each of the four damage states of the CHBDC-14 (see Table 2.2), based on $n = 100$ bootstrap samples of demand at each of the six levels of $S_a(T_1)$ used in Chapter 3. A subset of the bootstrap fragility curves is depicted in Figure E.1 along with the fragility curves built according to the investigated PSDM strategies (see Table 3.3). For the minimal damage state, all the PSDM-based fragility curves agree with the bootstrap replications, which in turn show a rather small variation. The 95% confidence interval (c.i.) of the median and the dispersion of the bootstrap fragility curves are inferred using percentile confidence intervals [88], and are presented in Tables E.1 and E.2, respectively. Effectively, the observed small variation is confirmed by the narrow confidence intervals for the minimal damage state, while the parameters of the PSDM-based fragility curves fall within the c.i. thresholds.

These observations are not valid for the repairable and extensive damage states. Accordingly, while the fragility curves built upon the Gaussian mixture and kernel smoothing PSDMs (MSA-GM, MSA-K1 and MSA-K2) follow the general trend of the bootstrap replications, those curves built upon lognormal-based PSDMs (MSA-L1 and MSA-L2) deviate significantly from this trend. This graphical impression is validated by the bootstrap confidence intervals. The parameters of the MSA-L1 and MSA-L2 are the only that are found out of the bootstrap confidence intervals. This is explained by the lack of fit of

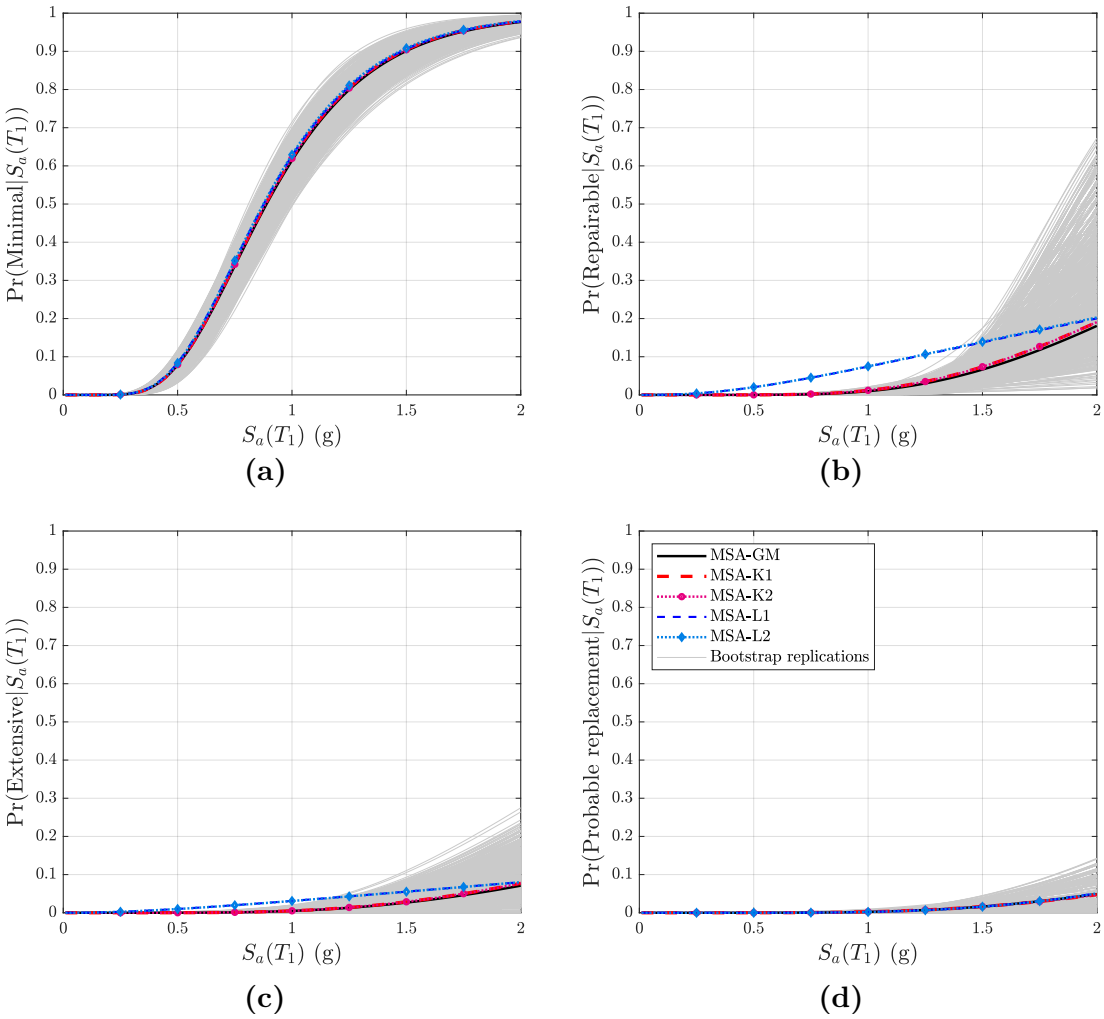

Figure E.1 Comparison of fragility curves generated with bootstrap and different seismic demand modeling strategies

the lognormal distribution to the deformation of the abutment wing walls for intermediate levels of $S_a(T_1)$ (see Chapter 3 for more details). Additionally, a great variation of the bootstrap fragility curves is noted for these damage states, as confirmed by the large estimated confidence intervals of the curve parameters. These large variations are due to the low ratios of damage state exceedance observed for the levels of spectral acceleration adopted in this study. Consequently, the fragility curves are restrained only by the lower tail, and a large variation is allowed for the rest of the curve. To reduce this variation, higher levels of spectral acceleration at the bridge's fundamental period could be used, according to the recommendations by Baker [22]. For this specific case, however, this would mean using ground motions of excessively large return periods ($> 50\,000$ years). Moreover, selecting records for this order of return period that satisfactorily match the GCIM target distribution can be rather challenging [50, 135].

For the probable replacement damage state, all the PSDM-based fragility curves show good agreement to the bootstrap fragility curves. In this case, as discussed in Chapter 3,

Table E.1 Comparison of the median of the fitted fragility curves to the bootstrap confidence interval (values in g)

Damage state	Bootstrap 95% c.i.	MSA-GM	MSA-K1	MSA-K2	MSA-L1	MSA-L2
Minimal	(0.84, 0.97)	0.89	0.88	0.89	0.87	0.88
Repairable	(1.95, 4.66)	3.12	3.09	3.07	5.13	5.16
Extensive	(3.02, 15.28)	4.88	4.62	4.60	16.46	16.30
Probable replacement	(3.63, >20)	5.22	5.62	5.48	4.98	5.05

Table E.2 Comparison of the dispersion of the fitted fragility curves to the bootstrap confidence interval

Damage state	Bootstrap 95% c.i.	MSA-GM	MSA-K1	MSA-K2	MSA-L1	MSA-L2
Minimal	(0.39, 0.41)	0.40	0.40	0.40	0.41	0.41
Repairable	(0.24, 0.63)	0.48	0.50	0.50	1.14	1.14
Extensive	(0.47, 0.97)	0.61	0.59	0.59	1.50	1.49
Probable replacement	(0.46, 0.80)	0.58	0.62	0.61	0.56	0.57

only the columns participate on the system's fragility. Owing to the reasonably good fit of the lognormal distribution to the peak column drift ratios, the fragility curves built upon the MSA-L1 and MSA-L2 strategies show once again a good agreement with the other curves, as observed for the minimal damage state. This time, however, the variation of the bootstrap fragility curves is large. Although not evidenced in Figure E.1, the large variation for this damage state is indicated by the wide confidence interval of the median (Table E.1). Again, this large variation is justified by fitting the fragility curves with low fractions of damage state exceedance.

From the 10 000 bootstrap fragility curve replications, the corresponding mean annual frequencies of damage state exceedance are calculated. A standardization of the MAFs is adopted as follows to facilitate the comparison:

$$z_{\lambda(\mathrm{DS})} = \frac{\lambda(\mathrm{DS}) - \bar{\lambda}(\mathrm{DS})_{boot}}{s\left(\lambda(\mathrm{DS})_{boot}\right)} \tag{E.2}$$

where $\bar{\lambda}(\mathrm{DS})_{boot}$ and $s\left(\lambda(\mathrm{DS})_{boot}\right)$ are, respectively, the sample mean and standard deviation of the mean annual frequency of exceeding the damage state DS from the bootstrap replications. It is, therefore, expected that the bootstrap standardized MAF replications are normally distributed with null mean and standard deviation equal to unity. Consequently, considering bias as the deviation of the estimated value from the expected (true) value, the bias of each PSDM strategy is here inferred as the distance of the standardized MAF from zero. Figure E.2 presents the histograms of the bootstrap replications of $\bar{\lambda}(\mathrm{DS})$ along with the standardized MAFs estimated upon each PSDM strategy.

For the minimal damage state, the MAF replications are normally distributed. This was expected given the low variation of the fragility curves, owing to the appropriate fragility ratios used to fit the curves. The good agreement of all the PSDM-based fragility curves

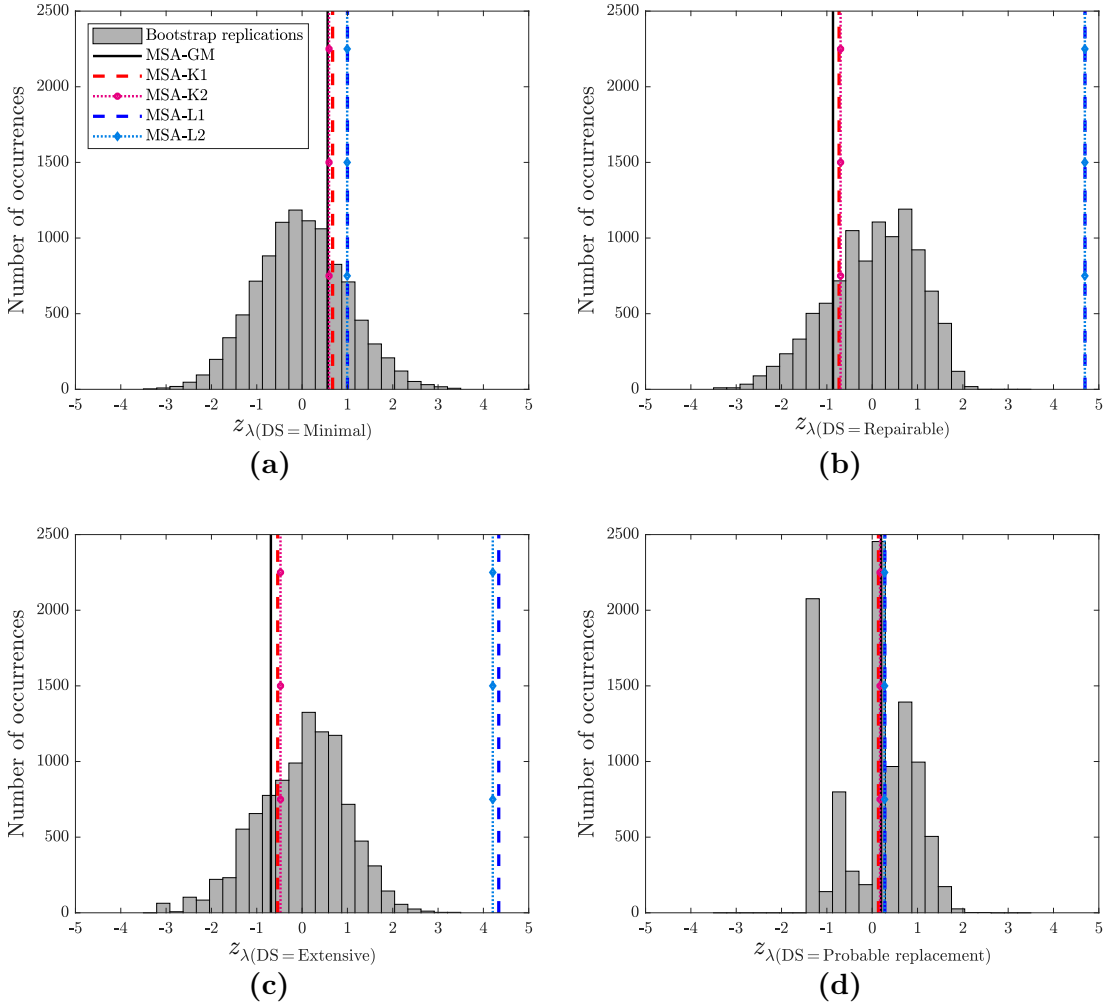

Figure E.2 Mean annual frequency of system damage state exceedance generated with bootstrap and different seismic demand modeling strategies

with the bootstrap replications in this DS are responsible for the low bias of the corresponding MAFs (Figure E.2a). For the repairable and extensive damage states, the error introduced by the poor seismic demand density modeling is propagated into the MAFs based on MSA-L1 and MSA-L2. In effect, while the other PSDM strategies introduced an error that is less than one standard deviation, the bias caused by MSA-L1 and MSA-L2 are greater than 4 times the standard deviation of the bootstrap replications. The histograms of the MAF replications for these damage states present negative skew, which could again be explained by fitting the fragility curves with low fractions of DS violation. For instance, in the case of the repairable damage state, fragility curves with low dispersion (the lower bound of the confidence interval is 0.24 in Table E.2) are accompanied by lower medians, generating positive standardized MAF replications, which justify the negative skew (Figure E.2b). The same can be inferred over the extensive damage state, whereas to a lesser extent (Figure E.2c). Contrarily to the damage states with unimodal MAF histograms discussed until now, the probable replacement damage state presents a multimodal histogram (Figure E.2d), which is justified by the too low fragility fractions used to fit the

curves. In this case, the large median values ($> 20\,\mathrm{g}$) of part of the bootstrap fragility curve replications are responsible for the negative standardized MAFs. As seen on the fragility curves, the MAF values estimated upon the different PSDM strategies. Finally, the differences between the estimates based on strategies that rely on the correlation coefficients conditioned on IM levels and those using the whole demand dataset are negligible. This observation indicates the low impact of using the entire dataset to estimate the correlation between component responses. Besides, the close MAFs estimated from MSA-GM, MSA-K1, and MSA-K2, indicate that the nonlinear correlation of the demand (which is only modeled by the MSA-GM) had a low impact on the risk assessment.

E.3 Closure

A nonparametric bootstrap approach is proposed to perform inference on the system fragility curves and the corresponding estimates of MAF of damage state exceedance. In this way, no assumption is made on the distribution or correlation of the seismic demand of the bridge components. This complementary study assesses the uncertainties on the fragility analyses presented in Chapter 3 by quantifying the confidence interval of the fragility curves and the potential bias caused by poor density modeling of the investigated PSDM strategies. Ten thousand bootstrap replications are performed for each damage state, which demonstrate that only the estimated values for minimal damage state show reasonable uncertainty. The greater uncertainty observed for the other damage states are caused by the low fragility fractions used to fit the respective fragility curves. The large variation is carried into the estimated mean annual frequencies, whose standardized replications deviate from a standard normal distribution, especially for the probable replacement damage state. Although these results may be indicative of the need for ground motions of greater return periods, they also suggest that the MSA-GM was able to capture the uncertainty of the seismic demand, propagating low error into the fragility- and risk-based analyses, in spite of the limitations relative to seismic intensity levels. The performance of the parametric Gaussian mixture model is comparable to the nonparametric kernel smoothing approach. This complementary study, hence, supports the initial perception that the MSA-GM introduces lower bias than traditional PSDM approaches, owing to its flexibility to model the joint density of multiple component structural systems.

LIST OF REFERENCES

[1] J. Adams, T. Allen, S. Halchuk, and M. Kolaj. Canada's 6th Generation Seismic Hazard Model, as Prepared for the 2020 National Building Code of Canada. In *12th Canadian Conference on Earthquake Engineering*, Quebec City, Canada, 2019.

[2] A. Agresti. *Categorical data analysis*. Wiley-Interscience, New Jersey, 2nd edition edition, 2002.

[3] T. I. Allen, J. Adams, and S. Halchuk. The seismic hazard model for Canada : Past , present and future. In *Proceedings of the Tenth Pacific Conference on Earthquake Engineering*, page 8, 2015.

[4] American Association of State Highway and Transportation Officials. *LRFD bridge design specifications, SI unit*. AASHTO, Washington, D.C., 4th edition, 2007.

[5] American Association of State Highway and Transportation Officials. *Guide Specifications for Seismic Isolation Design, 4th Edition*. AASHTO, Washington, DC, 2014.

[6] American Society of Civil Engineers. *Minimum design loads and associated criteria for buildings and other structures : ASCE/SEI 7-16*. 2017.

[7] T. D. Ancheta, R. B. Darragh, J. P. Stewart, E. Seyhan, W. J. Silva, B. S.-J. Chiou, K. E. Wooddell, R. W. Graves, A. R. Kottke, D. M. Boore, T. Kishida, and J. L. Donahue. NGA-West2 database. *Earthquake Spectra*, 30(3):989–1005, 2014.

[8] T. D. Ancheta, R. B. Darragh, J. P. Stewart, W. J. Silva, B. S.-J. Chiou, K. E. Wooddell, R. W. Graves, A. R. Kottke, D. M. Boore, T. Kishida, and J. L. Donahue. PEER NGA-West2 Database. Technical report, Pacific Earthquake Engineering Research Center, Berkeley, 2013.

[9] F. J. Anscombe. Graphs in Statistical Analysis. *The American Statistician*, 27(1):17–21, 1973.

[10] H. Aslani and E. Miranda. Probability-based seismic response analysis. *Engineering Structures*, 27(8):1151–1163, 2005.

[11] N. Ataei and J. E. Padgett. Probabilistic Modeling of Bridge Deck Unseating during Hurricane Events. *Journal of Bridge Engineering*, 18(4):275–286, 2012.

[12] N. Ataei and J. E. Padgett. Fragility surrogate models for coastal bridges in hurricane prone zones. *Engineering Structures*, 103:203–213, 2015.

[13] G. M. Atkinson. Ground-motion prediction equations for Eastern North America from a referenced empirical approach: Implications for epistemic uncertainty. *Bulletin of the Seismological Society of America*, 98(3):1304–1318, 2008.

[14] G. M. Atkinson. Earthquake time histories compatible with the 2005 national building code of Canada uniform hazard spectrum. *Canadian Journal of Civil Engineering*, 36(6):991–1000, 2009.

[15] G. M. Atkinson and J. Adams. Ground motion prediction equations for application to the 2015 Canadian national seismic hazard maps. *Canadian Journal of Civil Engineering*, 40(July 2013):988–998, 2013.

[16] G. M. Atkinson and D. M. Boore. Earthquake ground-motion prediction equations for eastern North America. *Bulletin of the Seismological Society of America*, 96(6):2181–2205, 2006.

[17] G. M. Atkinson and D. M. Boore. Modifications to existing ground-motion prediction equations in light of new data. *Bulletin of the Seismological Society of America*, 101(3):1121–1135, 2011.

[18] G. M. Atkinson, G. Rogers, T. Onur, and K. Assatourians. White paper on proposed ground-motion prediction equations (GMPEs) for 2015 National Seismic Hazard Maps, 2012.

[19] Ö. Avşar and G. Özdemir. Response of Seismic-Isolated Bridges in Relation to Intensity Measures of Ordinary and Pulselike Ground Motions. *Journal of Bridge Engineering*, 18(3):250–260, 2013.

[20] K. Bakalis and D. Vamvatsikos. Seismic Fragility Functions via Nonlinear Response History Analysis. *Journal of Structural Engineering*, 144(10):04018181, 2018.

[21] J. W. Baker. Conditional Mean Spectrum: Tool for ground motion selection. *Journal of Structural Engineering*, 137(3):322–331, 2011.

[22] J. W. Baker. Efficient Analytical Fragility Function Fitting Using Dynamic Structural Analysis. *Earthquake Spectra*, 31(1):579–599, 2015.

[23] J. W. Baker and C. Allin Cornell. Spectral shape, epsilon and record selection. *Earthquake Engineering & Structural Dynamics*, 35(9):1077–1095, 2006.

[24] J. W. Baker and B. A. Bradley. Intensity Measure Correlations Observed in the NGA-West2 Database, and Dependence of Correlations on Rupture and Site Parameters. *Earthquake Spectra*, 33(1):145–156, 2017.

[25] J. W. Baker and C. A. Cornell. A vector-valued ground motion intensity measure consisting of spectral acceleration and epsilon. *Earthquake Engineering & Structural Dynamics*, 34(10):1193–1217, 2005.

[26] J. W. Baker and N. Jayaram. Correlation of spectral acceleration values from NGA ground motion models. *Earthquake Spectra*, 24(1):299–317, 2008.

[27] J. W. Baker and C. Lee. An Improved Algorithm for Selecting Ground Motions to Match a Conditional Spectrum. *Journal of Earthquake Engineering*, 22(4):708–723, 2018.

[28] J. W. Baker, T. Lin, and S. K. Shahi. New Ground Motion Selection Procedures and Selected Motions for the PEER Transportation Research Program. Technical report, Pacific Earthquake Engineering Research Center, Berkeley, 2011.

[29] G. P. Balomenos, Y. Hu, J. E. Padgett, and K. Shelton. Impact of Coastal Hazards on Residents' Spatial Accessibility to Health Services. *Journal of Infrastructure Systems*, 25(4):04019028, Dec. 2019. Publisher: American Society of Civil Engineers.

[30] G. P. Balomenos, S. Kameshwar, and J. E. Padgett. Parameterized fragility models for multi-bridge classes subjected to hurricane loads. *Engineering Structures*, 208:110213, 2020.

[31] G. P. Balomenos and M. D. Pandey. Finite element reliability and sensitivity analysis of structures using the multiplicative dimensional reduction method. *Structure and Infrastructure Engineering*, 12(12):1553–1565, 2016. Publisher: Taylor & Francis.

[32] P. Bandini, J. E. Padgett, P. Paultre, and G. H. Siqueira. Seismic fragility of bridges: an approach coupling multiple-stripe analysis and Gaussian mixture for multicomponent structures. *Earthquake Spectra*, (under review), 2020.

[33] P. A. C. Bandini, J. E. Padgett, and P. Paultre. Seismic Fragility of a Highway Bridge in Quebec via metamodelling. In *12th Canadian Conference on Earthquake Engineering*, Quebec City, Canada, 2019.

[34] P. Bazzurro and C. A. Cornell. Disaggregation of seismic hazard. *Bulletin of the Seismological Society of America*, 89(2):501–520, 1999.

[35] J. R. Benjamin and C. A. Cornell. *Probability, Statistics, and Decision for Civil Engineers*. McGraw-Hill, New York, 1970.

[36] C. Bernier. *Courbes de fragilité pour la vulnerabilité sismique de barrages-poids en béton*. Msc thesis, Université de Sherbrooke, 2015.

[37] C. Bernier, I. Gidaris, G. P. Balomenos, and J. E. Padgett. Assessing the accessibility of petrochemical facilities during storm surge events. *Reliability Engineering & System Safety*, 188:155–167, Aug. 2019.

[38] C. Bernier, R. Monteiro, and P. Paultre. Using the Conditonal Spectrum Method for Improved Fragility Assessment of Concrete Gravity Dams in Eastern Canada. *Earthquake Spectra*, 32(3):1449–1468, 2016.

[39] C. Bernier, J. E. Padgett, J. Proulx, and P. Paultre. Seismic Fragility of Concrete Gravity Dams With Modeling Parameter Uncertainty and Spatial Variation. *Journal of Structural Engineering*, 142(5):05015002, 2016.

[40] A. H. M. M. Billah and B. Todorov. Effects of subfreezing temperature on the seismic response of lead rubber bearing isolated bridge. *Soil Dynamics and Earthquake Engineering*, 126(April):105814, 2019.

[41] C. M. Bishop. *Pattern recognition and machine learning*. Springer Science+Business Media, New York, 2006.

[42] P. Bocchini and D. M. Frangopol. A stochastic computational framework for the joint transportation network fragility analysis and traffic flow distribution under extreme events. *Probabilistic Engineering Mechanics*, 26(2):182–193, 2011.

[43] B. A. Bradley. A generalized conditional intensity measure approach and holistic ground-motion selection. *Earthquake Engineering & Structural Dynamics*, 39:1321–1342, 2010.

[44] B. A. Bradley. Empirical correlation of PGA, spectral accelerations and spectrum intensities from active shallow crustal earthquakes. *Earthquake Engineering & Structural Dynamics*, 40:1707–1721, 2011.

[45] B. A. Bradley. A ground motion selection algorithm based on the generalized conditional intensity measure approach. *Soil Dynamics and Earthquake Engineering*, 40:48–61, 2012.

[46] B. A. Bradley. Empirical correlations between peak ground velocity and spectrum-based intensity measures. *Earthquake Spectra*, 28(1):17–35, 2012.

[47] B. A. Bradley. The seismic demand hazard and importance of the conditioning intensity measure. *Earthquake Engineering & Structural Dynamics*, 41:1417–1437, 2012.

[48] B. A. Bradley. A comparison of intensity-based demand distributions and the seismic demand hazard for seismic performance assessment. *Earthquake Engineering & Structural Dynamics*, 42:2235–2253, 2013.

[49] B. A. Bradley. A critical examination of seismic response uncertainty analysis in earthquake engineering. *Earthquake Engineering & Structural Dynamics*, 42:1717–1729, 2013.

[50] B. A. Bradley. Practice-oriented estimation of the seismic demand hazard using ground motions at few intensity levels. *Earthquake Engineering & Structural Dynamics*, 42:2167–2185, 2013.

[51] B. A. Bradley, L. S. Burks, and J. W. Baker. Ground motion selection for simulation-based seismic hazard and structural reliability assessment. *Earthquake Engineering & Structural Dynamics*, 44:2321–2340, 2015.

[52] B. A. Bradley, R. P. Dhakal, M. Cubrinovski, J. B. Mander, and G. A. MacRae. Improved seismic hazard model with application to probabilistic seismic demand analysis. *Earthquake Engineering & Structural Dynamics*, 36(14):2211–2225, 2007.

[53] S. J. Brandenberg, J. Zhang, P. Kashighandi, Y. Huo, and M. Zao. Demand Fragility Surfaces for Bridges in Liquefied and Laterally Spreading Ground. Technical Report March, Pacific Earthquake Engineering Research Center, Berkeley, 2011. Publication Title: Pacific Earthquake Engineering Research Center Volume: 2011/01.

[54] I. G. Buckle, M. C. Constantinou, M. Dicleli, and H. Ghasemi. Seismic isolation of highway bridges. Research report 06-SP07, Multidisciplinary Center for Earthquake Engineering Research, Buffalo, NY, 2006.

[55] Canadian Commission on Building and Fire Codes and National Research Council Canada. *National Building Code of Canada*. National Research Council Canada, Ottawa, Ontario, 14 edition, 2015.

[56] Canadian Standards Association. *Commentary on CSA S6-14, Canadian Bridge Design Code*. CSA Group, Toronto, 2014.

[57] Canadian Standards Association. *CSA S6-14 Canadian Highway Bridge Design Code*. CSA Group, Mississauga, 2014.

[58] D. Cardone and G. Gesualdi. Experimental evaluation of the mechanical behavior of elastomeric materials for seismic applications at different air temperatures. *International Journal of Mechanical Sciences*, 64(1):127–143, 2012.

[59] D. Cardone, G. Gesualdi, and D. Nigro. Effects of air temperature on the cyclic behavior of elastomeric seismic isolators. *Bulletin of Earthquake Engineering*, 9(4):1227–1255, 2011.

[60] R. Chandramohan, J. W. Baker, and G. G. Deierlein. Impact of hazard-consistent ground motion duration in structural collapse risk assessment. *Earthquake Engineering & Structural Dynamics*, 45:1357–1379, 2016.

[61] R. Chandramohan, J. W. Baker, and G. G. Deierlein. Quantifying the influence of ground motion duration on structural collapse capacity using spectrally equivalent records. *Earthquake Spectra*, 32(2):927–950, 2016. ISBN: 0041103111446.

[62] R. Chandramohan, J. W. Baker, and G. G. Deierlein. Quantifying the influence of ground motion duration on structural collapse capacity using spectrally equivalent records. *Earthquake Spectra*, 32(2):927–950, 2016.

[63] E. Choi. *Seismic Analysis and Retrofit of Mid-America Bridges*. PhD thesis, Georgia Institute of Technology, Atlanta, USA, 2002.

[64] E. Choi, R. DesRoches, and B. G. Nielson. Seismic fragility of typical bridges in moderate seismic zones. *Engineering Structures*, 26(2):187–199, 2004.

[65] A. K. Chopra and C. Chintanapakdee. Comparing response of SDF systems to near-fault and far-fault earthquake motions in the context of spectral regions. *Earthquake Engineering & Structural Dynamics*, 30(12):1769–1789, Dec. 2001. Publisher: John Wiley & Sons, Ltd.

[66] R. W. Clough and J. Penzien. *Dynamics of Structures*. McGraw-Hill, New York; Montréal, 1975.

[67] J. Coleman and E. Spacone. Localization issues in force-based frame elements. *Journal of Structural Engineering*, 127(11):1257–1265, 2001.

[68] M. C. Constantinou, I. V. Kalpakidis, A. Filiatrault, and R. A. Ecker Lay. LRFD-based analysis and design procedures for bridge bearings and seismic isolators. Technical report 11-0004, Multidisciplinary Center for Earthquake Engineering Research, Buffalo, NY, 2011.

[69] M. C. Constantinou, P. Tsopelas, A. Kasalanati, and E. D. Wolff. Property modification factors for seismic isolation bearings. Technical Report MCEER-99-0012, 1999.

[70] M. C. Constantinou, A. S. Whittaker, Y. Kalpakidis, D. M. Fenz, and G. P. Warn. Performance of seismic isolation hardware under service and seismic loading. Technical Report MCEER-07-0012, Multidisciplinary Center for Earthquake Engineering Research, 2007.

[71] C. A. Cornell. Engineering seismic risk analysis. *Bulletin of the Seismological Society of America*, 58(5):1583–1606, 1968.

[72] C. A. Cornell, F. Jalayer, R. O. Hamburger, and D. A. Foutch. Probabilistic basis for 2000 SAC Federal Emergency Management Agency Steel Moment Frame Guidelines. *Journal of Structural Engineering*, 128(4):526–533, 2002.

[73] C. A. Cornell and H. Krawinkler. Progress and challenges in seismic performance assessment. *PEER Center News*, 3(2):1–4, 2000.

[74] C. B. Crouse, B. Hushmand, and G. R. Martin. Dynamic soil–structure interaction of a single-span bridge. *Earthquake Engineering & Structural Dynamics*, 15(6):711–729, 1987.

[75] P. Daneshvar, N. Bouaanani, and A. Godia. On computation of conditional mean spectrum in Eastern Canada. *Journal of Seismology*, 19(2):443–467, 2015.

[76] P. Daneshvar, N. Bouaanani, and P. Léger. Application of conditional mean spectra for evaluation of a building's seismic response in Eastern Canada. *Canadian Journal of Civil Engineering*, 41:769–773, 2014.

[77] L. Decanini, L. Liberatore, and F. Mollaioli. Characterization of displacement demand for elastic and inelastic SDOF systems. *Soil Dynamics and Earthquake Engineering*, 23(6):455–471, 2003.

[78] G. G. Deierlein. Overview of a comprehensive framework for earthquake performance assessment. In P. Fajfar and H. Krawinkler, editors, *Performance-based seismic design concepts and implementation – Proceedings of an international workshop*, pages 15–26, Bled, Slovenia, 2004. Pacific Earthquake Engineering Research Center.

[79] L. Deng, W. Wang, and Y. Yu. State-of-the-Art Review on the Causes and Mechanisms of Bridge Collapse. *Journal of Performance of Constructed Facilities*, 30(2):04015005, 2015.

[80] P. Deng, Z. Gan, T. Hayashikawa, and T. Matsumoto. Seismic response of highway viaducts equipped with lead-rubber bearings under low temperature. *Engineering Structures*, 209:110008, 2020. Publisher: Elsevier.

[81] A. Der Kiureghian. *Structural and System Reliability: Lecture Notes for CE229*. University of California, Berkeley, 2013.

[82] A. Der Kiureghian and O. Ditlevsen. Aleatory or epistemic? Does it matter? *Structural Safety*, 31(2):105–112, 2009.

[83] C. J. Derham and A. G. Thomas. The design and use of rubber bearings for vibration isolation and seismic protection of structures. *Engineering Structures*, 2(3):171–175, 1980.

[84] J. L. Devore. *Probability and statistics for engineering and the sciences*. Thomson-Brooks/Cole, Southbank, Victoria, Australia, 2004.

[85] A. Du and J. E. Padgett. Investigation of multivariate seismic surrogate demand modeling for multi-response structural systems. *Engineering Structures*, 207, 2020.

[86] J. D. Dukes. *Application of Bridge Specific Fragility Analysis in the Seismic Design Process of Bridges in California*. Phd thesis, Georgia Institute of Technology, 2013.

[87] L. Eads, E. Miranda, H. Krawinkler, and D. G. Lignos. An efficient method for estimating the collapse risk of structures in seismic regions. *Earthquake Engineering & Structural Dynamics*, 42:25–41, 2013.

[88] B. Efron and R. J. Tibshirani. *An Introduction to the Bootstrap*. Chapman and Hall/CRC, Boca Raton, 1998.

[89] B. Ellingwood. Validation studies of seismic PRAs. *Nuclear Engineering and Design*, 123(2-3):189–196, 1990.

[90] B. R. Ellingwood, O. C. Celik, and K. Kinali. Fragility assessment of building structural system in Mid-America. *Earthquake Engineering & Structural Dynamics*, 36:1935–1952, 2007.

[91] B. R. Ellingwood and P. B. Tekie. Seismic Fragility Analysis of Concrete Gravity Dams. *Journal of Infrastructure System*, 7(2):41–48, 2001.

[92] A. S. Elnashai and L. Di Sarno. *Fundamentals of earthquake engineering: from source to fragility*. John Willey & Sons, Chichester, 2nd edition, 2015.

[93] Federal Emergency Management Agency. *Multi-hazard Loss Estimation Methodology - Earthquake Model - Hazus-MH 2.1: Technical Manual*. Washington, D.C., 2015.

[94] Federal Emergency Management Agency and Applied Technology Council. *Seismic performance assessment of buildings – Volume 1 – Methodology*, volume 1 of *FEMA P-58*. Washington, D.C., 2nd edition, 2018.

[95] Federal Emergency Management Agency (FEMA). *HAZUS-MH MR4 Technical Manual*. National Institute of Building Sciences and Federal Emergency Management Agency (NIBS and FEMA), Washington, D.C., 2003.

[96] A. Filiatrault, R. Tremblay, C. Christopoulos, B. Folz, and D. Pettinga. *Elements of earthquake engineering and structural dynamics*. Presses internationales Polytechnique, Montréal, 3rd edition, 2013.

[97] A. I. J. Forrester, A. Sóbester, and A. J. Keane. *Engineering design via surrogate modelling: A practical guide*. John Willey & Sons, Chichester, 2008.

[98] S. A. S. Fosoul and M. J. Tait. Seismic fragility assessment of isolated bridges in cold regions: a case study for Eastern Canada. In *17th World Conference on Earthquake Engineering*, Sendai, Japan, 2020.

[99] F. Freddi, J. E. Padgett, and A. Dall'Asta. Probabilistic seismic demand modeling of local level response parameters of an RC frame. *Bulletin of Earthquake Engineering*, 15(1):1–23, 2017.

[100] J. H. Friedman. Multivariate Adaptive Regression Splines. *The Annals of Statistics*, 19(1):1–141, 1991.

[101] K. N. G. Fuller, J. Gough, and A. G. Thomas. The Effect of Low-Temperature Crystallization on the Mechanical Behavior of Rubber. *Journal of Polymer Science: Part B: Polymer Physics*, 42:2181–2190, 2004.

[102] P. Gardoni, K. M. Mosalam, and A. Der Kiureghian. Probabilistic seismic demand models and fragility estimates for RC bridges. *Journal of Earthquake Engineering*, 7(S1):79–106, 2003.

[103] O. Gauron, A. Saidou, A. Busson, G. H. Siqueira, and P. Paultre. Experimental determination of the lateral stability and shear failure limit states of bridge rubber bearings. *Engineering Structures*, 174(1):39–48, 2018.

[104] P. Gehl, J. Douglas, and D. Seyedi. Influence of the number of dynamic analyses on the accuracy of structural response estimates. *Earthquake Spectra*, 31(1):97–113, 2015.

[105] P. Gehl, D. Seyedi, J. Douglas, and M. Khiar. Introduction of Fragility Surfaces for a More Accurate Modeling of the Seismic Vulnerability of Reinforced Concrete Structures. In M. Papadrakakis, N. D. Lagaros, and M. Fragiadakis, editors, *EC-COMAS Thematic Conference on Computational Methods in Structural Dynamics and Earthquake Engineering*, page 11, Rhodes, Greece, 2009.

[106] P. Gehl, S. Sy, and D. Seyedi. Developing Fragility Surfaces for More Accurate Seismic Vulnerability Assessment of Masonry. In M. Papadrakakis, M. Fragiadakis, and V. Plevris, editors, *3rd ECCOMAS Thematic Conference on Computational Methods in Structural Dynamics and Earthquake Engineering*, page 16, Corfu, Greece, 2011.

[107] A. N. Gent. *Engineering with rubber : how to design rubber components.* Hanser, Munich, 2001.

[108] J. Ghosh and J. E. Padgett. Aging Considerations in the Development of Time-Dependent Seismic Fragility Curves. *Journal of Structural Engineering*, 136(12):1497–1511, 2010.

[109] J. Ghosh, J. E. Padgett, and L. Dueñas-Osorio. Surrogate modeling and failure surface visualization for efficient seismic vulnerability assessment of highway bridges. *Probabilistic Engineering Mechanics*, 34:189–199, 2013.

[110] J. Ghosh, K. Rokneddin, L. Dueñas-Osorio, and J. E. Padgett. Seismic reliability assessment of aging highway bridge networks with field instrumentation data and correlated failures, I: Methodology. *Earthquake Spectra*, 30(2):819–843, 2014. ISBN: 9781138000865.

[111] J. Ghosh, K. Rokneddin, L. Dueñas-Osorio, and J. E. Padgett. Seismic reliability assessment of aging highway bridge networks with field instrumentation data and correlated failures, I: Methodology. *Earthquake Spectra*, 30(2):819–843, 2014.

[112] I. G. Gidaris, J. E. Padgett, A. R. Barbosa, S. Chen, D. T. Cox, B. Webb, and A. Cerato. Multiple-Hazard Fragility and Restoration Models of Highway Bridges for Regional Risk and Resilience Assessment in the United States : State-of-the-Art Review. *Journal of Structural Engineering*, 04016188:1–17, 2016.

[113] Global Earthquake Model Foundation (GEM). OpenQuake Engine 2.7, 2017.

[114] S. Günay and K. M. Mosalam. PEER Performance-Based Earthquake Engineering Methodology, Revisited. *Journal of Earthquake Engineering*, 17(6):829–858, Aug. 2013. Publisher: Taylor & Francis.

[115] K. Goda. Statistical modeling of joint probability distribution using copula: Application to peak and permanent displacement seismic demands. *Structural Safety*, 32(2):112–123, Mar. 2010.

[116] K. Goda and S. Tesfamariam. Multi-variate seismic demand modelling using copulas: Application to non-ductile reinforced concrete frame in Victoria, Canada. *Structural Safety*, 56:39–51, Sept. 2015.

[117] J.-A. Goulet. *Probabilistic Machine Learning for Civil Engineers.* MIT Press, 2020.

[118] L.-P. Guay and N. Bouaanani. Assessment of low temperature exposure for design and evaluation of elastomeric bridge bearings and seismic isolators in Canada. *Canadian Journal of Civil Engineering*, 43(9):851–863, 2016.

[119] X. Guo, Y. Wu, and Y. Guo. Time-dependent seismic fragility analysis of bridge systems under scour hazard and earthquake loads. *Engineering Structures*, 121:52–60, 2016.

[120] S. Halchuk, T. I. Allen, J. Adams, and G. C. Rogers. Fifth generation seismic hazard model input files as proposed to produce values for the 2015 National Building Code of Canada - 7576. Technical report, Geological Survey of Canada, 2014.

[121] T. Hastie, R. Tibshirani, and J. Friedman. *The elements of statistical learning: data mining, inference, and prediction*. Springer, Stanford, second edition, 2017.

[122] Highway Innovatice Technology Evaluation Center (HITEC). Summary of evaluation findings for the testing of seismic isolation and energy dissipating devices. Technical evaluation report 40404, Civil Engineering Research Foundation (CERF), 1998.

[123] L. F. Ibarra and H. Krawinkler. Global collapse of frame structures under seismic excitations. Technical report TR152, The John A. Blume Earthquake Engineering Center, Stanford, California, 2005.

[124] F. Jalayer and C. A. Cornell. Alternative non-linear demand estimation methods for probability-based seismic assessment. *Earthquake Engineering & Structural Dynamics*, 38:951–972, 2009.

[125] N. Jayaram, T. Lin, and J. W. Baker. A Computationally efficient ground-motion selection algorithm for matching a target response spectrum mean and variance. *Earthquake Spectra*, 27(3):797–815, 2011.

[126] I. V. Kalpakidis and M. C. Constantinou. Effects of heating on the behavior of lead-rubber bearings. I: Theory. *Journal of Structural Engineering*, 135(12):1440–1449, 2009.

[127] S. Kameshwar, S. Misra, and J. E. Padgett. Decision tree based bridge restoration models for extreme event performance assessment of regional road networks. *Structure and Infrastructure Engineering*, 16(3):431–451, 2020.

[128] S. Kameshwar and J. E. Padgett. Multi-hazard risk assessment of highway bridges subjected to earthquake and hurricane hazards. *Engineering Structures*, 78:154–166, 2014.

[129] S. Kameshwar and J. E. Padgett. Effect of vehicle bridge interaction on seismic response and fragility of bridges. *Earthquake Engineering and Structural Dynamics*, 47(3):697–713, 2018.

[130] A. Karamlou and P. Bocchini. Computation of bridge seismic fragility by large-scale simulation for probabilistic resilience analysis. *Earthquake Engineering & Structural Dynamics*, 44:1959–1978, 2015.

[131] A. Karamlou and P. Bocchini. From Component Damage to System-Level Probabilistic Restoration Functions for a Damaged Bridge. *Journal of Infrastructure Systems*, 23(3):04016042, 2017.

[132] A. Karamlou and P. Bocchini. Functionality-fragility surfaces. *Earthquake Engineering & Structural Dynamics*, 46(10):1687–1709, 2017. ISBN: 6507252573.

[133] K. R. Karim and F. Yamazaki. A simplified method of constructing fragility curves for highway bridges. *Earthquake Engineering & Structural Dynamics*, 32(10):1603–1626, 2003.

[134] A. I. Khuri and S. Mukhopadhyay. Response surface methodology. *Wiley Interdisciplinary Reviews: Computational Statistics*, 2(2):128–149, 2010.

[135] J. Kiani, C. Camp, and S. Pezeshk. On the number of required response history analyses. *Bulletin of Earthquake Engineering*, 16(11):5195–5226, 2018.

[136] J. Kiani, C. Camp, and S. Pezeshk. On the application of machine learning techniques to derive seismic fragility curves. *Computers and Structures*, 218:108–122, 2019. Publisher: Elsevier Ltd.

[137] M. Kikuchi and I. D. Aiken. An analytical hysteresis model for elastomeric seismic isolation bearings. *Earthquake Engineering & Structural Dynamics*, 26:215–231, 1997.

[138] M. Kohrangi, P. Bazzurro, D. Vamvatsikos, and A. Spillatura. Conditional spectrum-based ground motion record selection using average spectral acceleration. *Earthquake Engineering & Structural Dynamics*, 46(10):1667–1685, Aug. 2017. Publisher: John Wiley & Sons, Ltd.

[139] M. Kohrangi, S. R. Kotha, and P. Bazzurro. Ground-motion models for average spectral acceleration in a period range: direct and indirect methods. *Bulletin of Earthquake Engineering*, 16(1):45–65, Jan. 2018.

[140] M. Kohrangi, D. Vamvatsikos, and P. Bazzurro. Implications of Intensity Measure Selection for Seismic Loss Assessment of 3-D Buildings. *Earthquake Spectra*, 32(4):2167–2189, Nov. 2016. Publisher: SAGE Publications Ltd STM.

[141] P. S. Koutsourelakis. Assessing structural vulnerability against earthquakes using multi-dimensional fragility surfaces: A Bayesian framework. *Probabilistic Engineering Mechanics*, 25:49–60, 2010.

[142] V. Koval, C. Christopoulos, and R. Tremblay. Improvements to the simplified analysis method for the design of seismically isolated bridges in CSA-S6-14. *Canadian Journal of Civil Engineering*, 43:891–907, 2016.

[143] M. Kumar, A. S. Whittaker, and M. C. Constantinou. An advanced numerical model of elastomeric seismic isolation bearings. (April):1955–1974, 2014.

[144] N. Kurata, T. Kobori, and N. Koshika. Performance-based design with semi-active structural control technique. *Earthquake Engineering & Structural Dynamics*, 31:445–458, 2002.

[145] O.-S. Kwon and A. S. Elnashai. Probabilistic seismic assessment of structure, foundation, and soil interacting systems. Technical report, Mid-America Earthquake Center, Urbana, Illinois, 2007.

[146] N. D. Lagaros. Probabilistic fragility analysis: A tool for assessing design rules of RC buildings. *Earthquake Engineering and Engineering Vibration*, 7(1):45–56, 2008.

[147] M.-A. Laplante. *Courbes de fragilité pour la détermination de la vulnérabilité sismique de bâtiments en maçonnerie armée à partir du spectre conditionnel.* Msc thesis, Université de Sherbrooke, 2016.

[148] F. Légeron and P. Paultre. Uniaxial Confinement Model for Normal- and High-Strength Concrete Columns. *Journal of Structural Engineering*, 129(2):241–252, 2003.

[149] D. E. Lehman and J. P. Moehle. Seismic performance of well-confined concrete bridge columns. Technical report, Pacific Earthquake Engineering Research Center, Berkeley, 2000.

[150] H. W. Lilliefors. On the Kolmogorov-Smirnov Test for Normality with Mean and Variance. *Journal of the American Statistical Association*, 62(318):399–402, 1967.

[151] T. Lin, S. C. Harmsen, J. W. Baker, and N. Luco. Conditional spectrum computation incorporating multiple causal earthquakes and ground-motion prediction models. *Bulletin of the Seismological Society of America*, 103(2 A):1103–1116, 2013.

[152] T. Lin, C. B. Haselton, and J. W. Baker. Conditional spectrum-based ground motion selection. Part I: Hazard consistency for risk-based assessments. *Earthquake Engineering & Structural Dynamics*, 42(12):1847–1865, 2013.

[153] J. E. Long. *Bearings in structural engineering*. Newnes-Butterworths, London, 1974.

[154] N. Luco and P. Bazzurro. Does amplitude scaling of ground motion records result in biased nonlinear structural drift responses? *Earthquake Engineering & Structural Dynamics*, 36(June):1813–1835, 2007.

[155] H. Luo and S. G. Paal. Machine Learning-Based Backbone Curve Model of Reinforced Concrete Columns Subjected to Cyclic Loading Reversals. *Journal of Computing in Civil Engineering*, 32(5):1–14, 2018. ISBN: 87507587.

[156] H. Luo and S. G. Paal. A locally weighted machine learning model for generalized prediction of drift capacity in seismic vulnerability assessments. *Computer-Aided Civil and Infrastructure Engineering*, 34(11):935–950, 2019.

[157] G. Lupoi, P. Franchin, A. Lupoi, and P. E. Pinto. Seismic Fragility Analysis of Structural Systems. *Journal of Engineering Mechanics*, 132(4):385–395, 2006.

[158] K. R. Mackie and B. Stojadinovic. Seismic Demands for Performance-Based Design of Bridges. Technical Report PEER 2003/16, Pacific Earthquake Engineering Research Center, Berkeley, 2003.

[159] K. R. Mackie and B. Stojadinovic. Fragility curves for reinforced concrete highway overpass bridges. In *13th World Conference on Earthquake Engineering*, page 14, Vancouver, BC, 2004.

[160] K. R. Mackie and B. Stojadinovic. Post-earthquake function of highway overpass bridges. In P. Fajfar and H. Krawinkler, editors, *Performance-based seismic design concepts and implementation – Proceedings of an international workshop*, pages 53–64, Bled, Slovenia, 2004. Pacific Earthquake Engineering Research Center.

[161] K. R. Mackie and B. Stojadinovic. Comparison of Incremental Dynamic, Cloud, and Stripe Methods for Computing Probabilistic Seismic Demand Models. In *Structures Congress 2005*, page 11, 2005.

[162] K. R. Mackie and B. Stojadinović. R-Factor Parameterized Bridge Damage Fragility Curves. *Journal of Bridge Engineering*, 12(4):500–510, 2007.

[163] S. N. Mahmoudi and L. Chouinard. Seismic fragility assessment of highway bridges using support vector machines. *Bulletin of Earthquake Engineering*, 14(6):1571–1587, June 2016.

[164] J. B. Mander. Fragility Curve Development for Assessing the Seismic Vulnerability of Highway Bridges. In *Research Progress and Accomplishments 1997-1999*, pages 1–10. Buffalo, 1999.

[165] S. Mangalathu, G. Heo, and J.-S. Jeon. Artificial neural network based multi-dimensional fragility development of skewed concrete bridge classes. *Engineering Structures*, 162(February):166–176, 2018. Publisher: Elsevier.

[166] S. Mangalathu, G. Heo, and J.-S. Jeon. Artificial neural network based multi-dimensional fragility development of skewed concrete bridge classes. *Engineering Structures*, 162(February):166–176, 2018.

[167] S. Mangalathu and J. S. Jeon. Classification of failure mode and prediction of shear strength for reinforced concrete beam-column joints using machine learning techniques. *Engineering Structures*, 160(November 2017):85–94, 2018. Publisher: Elsevier.

[168] S. Mangalathu and J.-S. Jeon. Stripe-based fragility analysis of concrete bridge classes using machine learning techniques. *Earthquake Engineering & Structural Dynamics*, pages 1–18, 2019.

[169] S. Mangalathu, J.-S. Jeon, and R. DesRoches. Critical uncertainty parameters influencing seismic performance of bridges using Lasso regression. *Earthquake Engineering & Structural Dynamics*, 47(3):784–801, 2018. ISBN: 1001-6538.

[170] S. Mangalathu, J. S. Jeon, J. E. Padgett, and R. DesRoches. ANCOVA-based grouping of bridge classes for seismic fragility assessment. *Engineering Structures*, 123(2016):379–394, 2016.

[171] M. Maniglio, G. P. Balomenos, J. E. Padgett, and G. P. Cimellaro. Parameterized coastal fragilities and their application to aging port structures subjected to surge and wave. *Engineering Structures*, 237:112235, June 2021.

[172] G. P. Mavroeidis and A. S. Papageorgiou. Effect of Fault Rupture Characteristics on Near-Fault Strong Ground Motions. *Bulletin of the Seismological Society of America*, 100(1):37–58, Feb. 2010.

[173] R. L. Mayes and F. Naeim. Design of Structures with Seismic Isolation. In F. Naeim, editor, *The Seismic Design Handbook*, pages 723–756. Springer Science+Business Media, New York, 2001. Section: 14.

[174] R. K. McGuire. Probabilistic Seismic Hazard Analysis and Design Earthquakes : Closing the Loop. *Bulletin of the Seismological Society of America*, 85(5):1275–1284, 1995.

[175] F. McKenna, M. H. Scott, and G. L. Fenves. Nonlinear Finite-Element Analysis Software Architecture Using Object Composition. *Journal of Computing in Civil Engineering*, 24(1):95–107, 2010.

[176] G. J. McLachlan and K. E. Basford. *Mixture models: Inference and applications to clustering*. Marcel Dekker, New York, 1988.

[177] G. J. McLachlan and D. Peel. *Finite mixture models*. Wiley, New York; Toronto, 2000.

[178] Meteorological Service of Canada, Environment and Climate Change Canada. Historical climate data, 2020.

[179] Ministère des Transports, de la Mobilité durable et de l'Électrification des transports du Québec. Inventaire et inspection des structures, 2018.

[180] S. Misra and J. E. Padgett. Seismic Fragility of Railway Bridge Classes: Methods, Models, and Comparison with the State of the Art. *Journal of Bridge Engineering*, 24(12):1–12, 2019.

[181] D. Mitchell, S. Huffman, R. Tremblay, M. Saatcioglu, D. Palermo, R. Tinawi, and D. Lau. Damage to bridges due to the 27 February 2010 Chile earthquake. *Canadian Journal of Civil Engineering*, 40(8):675–692, 2013.

[182] J. Moehle and G. G. Deierlein. A framework methodology for performance-based earthquake engineering. In *13th World Conference on Earthquake Engineering*, pages 3812–3814, Vancouver, B.C., 2004.

[183] L. A. Montejo, M. J. Kowalsky, and H. Tasnim. Seismic Behavior of Flexural Dominated Reinforced Concrete Bridge Columns at Low Temperatures. *Journal of Cold Regions Engineering*, 23(1):18–42, Mar. 2009. Publisher: American Society of Civil Engineers.

[184] L. A. Montejo, E. Marx, and M. J. Kowalsky. Seismic design of reinforced concrete bridge columns at subfreezing temperatures. *ACI Structural Journal*, 107(4), 2010.

[185] A. H. M. Muntasir Billah and M. Shahria Alam. Seismic fragility assessment of highway bridges: a state-of-the-art review. *Structure and Infrastructure Engineering*, 11(6):804–832, 2015.

[186] K. P. Murphy. *Machine learning: a probabilistic perspective*. MIT Press, Cambridge, MA, 2012.

[187] R. M. Murray and J. D. Detenber. First and Second Order Transitions in Neoprene. *Rubber Chemistry and Technology*, 34(2):668–685, 1961.

[188] F. Naeim, H. Bhatia, and R. M. Lobo. Performance-Based Seismic Engineering. In F. Naeim, editor, *The Seismic Design Handbook*, chapter 15, pages 757–792. Springer Science+Business Media, New York, 2001.

[189] F. Naeim and J. M. Kelly. *Design of seismic isolated structures*. John Willey & Sons, New York, 1999.

[190] M. Nassar, L. Guizani, M.-j. Nollet, and A. Tahan. A probability-based reliability assessment approach of seismic base-isolated bridges in cold regions. *Engineering Structures*, 197(Pre-Print):109353, 2019.

[191] Natural Resources Canada. Earthquake map of Canada, 2018.

[192] Natural Resources Canada. Important Canadian Earthquakes, Oct. 2018.

[193] Natural Resources Canada. National Building Code of Canada seismic hazard values, 2019.

[194] Natural Resources Canada (NRC). Hazard calculator – Determine 2015 National Building Code of Canada seismic hazard values, 2016.

[195] A. Neuenhofer and F. C. Filippou. Geometrically nonlinear flexibility-based frame finite element. *Journal of Structural Engineering*, 124(6):704–711, 1998.

[196] N. M. Newmark and E. Rosenblueth. *Fundamentals of earthquake engineering*. Prentice-Hall, Englewood Cliffs, 1971.

[197] B. G. Nielson. *Analytical fragility curves for highway bridges in moderate seismic zones*. PhD Thesis, Georgia Institute of Technology, 2005.

[198] B. G. Nielson and R. DesRoches. Analytical seismic fragility curves for typical bridges in the central and southeastern United States. *Earthquake Spectra*, 23(3):615–633, 2007.

[199] B. G. Nielson and R. DesRoches. Seismic fragility methodology for highway bridges using a component level approach. *Earthquake Engineering & Structural Dynamics*, 36:823–839, 2007.

[200] B. G. Nielson and R. DesRoches. Seismic Performance Assessment of Simply Supported and Continuous Multispan Concrete Girder Highway Bridges. *Journal of Bridge Engineering*, 12(5):611–620, 2008.

[201] B. G. Nielson and W. C. Pang. Effect of ground motion suite size on the uncertainty estimation is seismic brigde fragility modeling. In *Structures Congress 2011*, Las Vegas, 2011.

[202] Y. Okui, K. Nakamura, T. Sato, and T. Imai. Seismic response of isolated bridge with high damping rubber bearings: Self-heating effect at subzero temperatures. *Steel Construction*, 12(1):2–9, 2019.

[203] J. E. Padgett. *Seismic Vulnerability Assessment of Retrofitted Bridges Using Probabilistic Methods Seismic Vulnerability Assessment of Retrofitted Bridges Using Probabilistic*. Phd thesis, Georgia Institute of Technology, 2007.

[204] J. E. Padgett. *Seismic Vulnerability Assessment of Retrofitted Bridges Using Probabilistic Methods Seismic Vulnerability Assessment of Retrofitted Bridges Using Probabilistic*. PhD thesis, Georgia Institute of Technology, 2007.

[205] J. E. Padgett, K. Dennemann, and J. Ghosh. Risk-based seismic life-cycle cost–benefit (LCC-B) analysis for bridge retrofit assessment. *Structural Safety*, 32(3):165–173, 2010.

[206] J. E. Padgett and R. DesRoches. Methodology for the development of analytical fragility curves for retrofitted bridges. *Earthquake Engineering & Structural Dynamics*, 37(8):1157–1174, 2008.

[207] J. E. Padgett and R. DesRoches. Retrofitted bridge fragility analysis for typical classes of multispan bridges. *Earthquake Spectra*, 25(1):117–141, 2009.

[208] J. E. Padgett, B. G. Nielson, and R. DesRoches. Selection of optimal intensity measures in probabilistic seismic demand models of highwat bridge portfolios. *Earthquake Engineering & Structural Dynamics*, 37:711–725, 2008.

[209] A. J. Papazoglou and A. S. Elnashai. Analytical and Field Evidence of the Damaging Effect of Vertical Earthquake Ground Motion. *Earthquake Engineering & Structural Dynamics*, 25(March):1109–1137, 1996.

[210] J. Park and P. Towashiraporn. Rapid seismic damage assessment of railway bridges using the response-surface statistical model. *Structural Safety*, 47(2014):1–12, 2014.

[211] P. Paultre. *Dynamics of Structures*. ISTE; John Wiley & Sons, London; Hoboken, NJ, 2010.

[212] S. Pezeshk, A. Zandieh, and B. Tavakoli. Hybrid empirical ground-motion prediction equations for Eastern North America using NGA models and updated seismological parameters. *Bulletin of the Seismological Society of America*, 101(4):1859–1870, 2011.

[213] Prairie Climate Centre. The Climate Atlas of Canada (version 2), 2019.

[214] M. J. N. Priestley, F. Seible, and G. M. Calvi. *Seismic design and retrofit of bridges*. John Willey & Sons, New York, 1996.

[215] K. Ramanathan, R. DesRoches, and J. E. Padgett. A comparison of pre- and post-seismic design considerations in moderate seismic zones through the fragility assessment of multispan bridge classes. *Engineering Structures*, 45:559–573, 2012.

[216] K. Ramanathan, J. E. Padgett, and R. DesRoches. Temporal evolution of seismic fragility curves for concrete box-girder bridges in California. *Engineering Structures*, 97:29–46, 2015.

[217] C. W. Roeder, J. F. Stanton, and T. Feller. Low-Temperature Performance of Elastomeric Bearings. *Journal of Cold Regions Engineering*, 4(3):113–132, 1990.

[218] K. Rokneddin, J. Ghosh, L. Dueñas-Osorio, and J. E. Padgett. Seismic reliability assessment of aging highway bridge networks with field instrumentation data and correlated failures, II: Application. *Earthquake Spectra*, 30(2):819–843, 2014. ISBN: 9781138000865.

[219] R. K. Rowe. *Geotechnical and geoenvironmental engineering handbook*. Kluwer Academic Publishers, Boston, 2001.

[220] N. Roy. *Réhabilitation parasismique performantielle des ponts avec des polymères renforcés de fibre de carbone*. PhD thesis, Université de Sherbrooke, 2006.

[221] N. Roy, P. Paultre, and J. Proulx. Performance-Based Seismic Retrofit of a Bridge Bent: Design and Experimental Validation. *Canadian Journal of Civil Engineering*, 37(3):367–379, 2010.

[222] L. F. Z. Rubio. *États limites de piliers de ponts en béton armés de cerces avec recouvrement à la base*. Msc thesis, Université de Sherbrooke, 2015.

[223] A. Saidou, O. Gauron, A. Busson, and P. Paultre. High-order finite element model of bridge rubber bearings for the prediction of buckling and shear failure. *Engineering Structures*, Preprint, 2021.

[224] H. Salehi and R. Burgueño. Emerging artificial intelligence methods in structural engineering. *Engineering Structures*, 171(May):170–189, 2018. Publisher: Elsevier.

[225] J. Sanchez, A. Masroor, G. Mosqueda, and K. Ryan. Static and dynamic stability of elastomeric bearings for seismic protection of structures. *Journal of Structural Engineering*, 139(7):1149–1159, 2013.

[226] A. S. Sanda. *Étude du comportement en compression-cisaillement d'isolateurs sismiques en caoutchouc*. Msc thesis, Université de Sherbrooke, 2012.

[227] M. T. Schultz, B. P. Gouldby, J. D. Simm, and J. L. Wibowo. Beyond the Factor of Safety : Developing Fragility Curves to Characterize System Reliability-US Army Corps of Engineers. Technical report, US Army Corps of Engineers, Washington, D.C., 2010.

[228] A. Sciascetti and M. Tait. Effect of Temperature on the Response of Unbonded Fiber-Reinforced Elastomeric Isolators. *Journal of Structural Engineering*, 145(11):04019124, Nov. 2019. Publisher: American Society of Civil Engineers.

[229] M. H. Scott and G. L. Fenves. Plastic hinge integration methods for force-based beam-column elements. *Journal of Structural Engineering*, 132(2):244–252, 2006.

[230] R. Segura, C. Bernier, R. Monteiro, and P. Paultre. On the Seismic Fragility Assessment of Concrete Gravity Dams in Eastern Canada. *Earthquake Spectra*, 35(1):211–231, 2019.

[231] R. L. Segura, J. E. Padgett, and P. Paultre. Metamodel-based seismic fragility analysis of concrete gravity dams. *Journal of Structural Engineering*, 146(7):04020121, 2020.

[232] J. Seo and D. G. Linzell. Horizontally curved steel bridge seismic vulnerability assessment. *Engineering Structures*, 34:21–32, 2012.

[233] J. Seo and D. G. Linzell. Use of response surface metamodels to generate system level fragilities for existing curved steel bridges. *Engineering Structures*, 52:642–653, 2013.

[234] M. N. Sheikh and F. Légeron. Performance based seismic assessment of bridges designed according to Canadian Highway Bridge Design Code. *Canadian Journal of Civil Engineering*, 41(9):777–787, 2014.

[235] M. Shinozuka, M. Q. Feng, J. Lee, and T. Naganuma. Statistical analysis of fragility curves. *Journal of Engineering Mechanics*, 126:1224–1231, 2000.

[236] M. Shinozuka, M. Q. Feng, J. Lee, and T. Naganuma. Statistical Analysis of Fragility Curves. Technical report, Multidisciplinary Center for Earthquake Engineering Research, Stanford, 2001.

[237] N. Shome. *Probabilistic Seismic Demand Analysis of Nonlinear Structures*. PhD thesis, Stanford, CA, USA, 1999. AAI9924607.

[238] V. Silva, H. Crowley, M. Pagani, D. Monelli, and R. Pinho. Development of the OpenQuake engine, the Global Earthquake Model's open-source software for seismic risk assessment. *Natural Hazards*, 72(3):1409–1427, 2014.

[239] V. Silva, H. Crowley, M. Pagani, R. Pinho, and D. Monelli. Development and Application of OpenQuake, an Open Source Software for Seismic Risk Assessment. In *15th World Conference on Earthquake Engineering*, page 10, Lisboa, Portugal, 2012.

[240] W. Silva, N. Gregor, and R. Darragh. Development of regional hard rock attenuation relations for Central and Eastern North America. Technical report, Pacific Engineering and Analysis, El Cerrito, California, 2002.

[241] J. Simon and L. G. Vigh. Seismic fragility assessment of integral precast multi-span bridges in areas of moderate seismicity. *Bulletin of Earthquake Engineering*, 14:3125–3150, 2016.

[242] T. W. Simpson, J. D. Poplinski, P. N. Koch, and J. K. Allen. Metamodels for Computer-based Engineering Design: Survey and recommendations. *Engineering With Computers*, 17(2):129–150, 2001.

[243] G. H. Siqueira, A. S. Sanda, P. Paultre, and J. E. Padgett. Fragility curves for isolated bridges in eastern Canada using experimental results. *Engineering Structures*, 74(2014):311–324, 2014.

[244] G. H. Siqueira, D. H. Tavares, and P. Paultre. Seismic fragility of a highway bridge in Quebec retrofitted with natural rubber isolators. *IBRACON Structures and Materials Journal*, 7(4):534–547, 2014.

[245] G. H. Siqueira, D. H. Tavares, P. Paultre, and J. E. Padgett. Performance evaluation of natural rubber seismic isolators as a retrofit measure for typical multi-span concrete bridges in eastern Canada. *Engineering Structures*, 74:300–310, 2014. ISBN: 0141-0296 Publisher: Elsevier Ltd.

[246] A. Stevenson. The effect of shear and compressive strain on the low temperature crystallization of natural rubber. *Polymer*, 27:1211–1218, 1986.

[247] O. Taskari and A. Sextos. Multi-angle, multi-damage fragility curves for seismic assessment of bridges. *Earthquake Engineering & Structural Dynamics*, 44:2281–2301, 2015.

[248] D. H. Tavares. *Évaluation de la vulnerabilité sismique des ponts routiers au Québec à l'aide des courbes de fragilité*. Phd thesis, Université de Sherbrooke, 2012.

[249] D. H. Tavares, L. I. Cardona, and P. Paultre. Bridge reinforced concrete column limit state definition. In *Congresso Brasileiro do Concreto*, number 52, pages 1–16, 2010.

[250] D. H. Tavares, J. E. Padgett, and P. Paultre. Fragility curves of typical as-built highway bridges in eastern Canada. *Engineering Structures*, 40(2012):107–118, 2012.

[251] D. H. Tavares, J. R. Suescun, P. Paultre, and J. E. Padgett. Seismic Fragility of a Highway Bridge in Quebec. *Journal of Bridge Engineering*, 18(11):1131–1139, 2013.

[252] P. Tehrani, K. Goda, D. Mitchell, G. M. Atkinson, and L. E. Chouinard. Effects of Different Record Selection Methods on the Transverse Seismic Response of a Bridge in South Western British Columbia. *Journal of Earthquake Engineering*, 18(4):611–636, 2014.

[253] Transportation Research Board. *NCHRP Synthesis 440: Performance-Based Seismic Bridge Design - A Synthesis of Highway Practice*. Washington, D.C., 2013.

[254] United States Geological Survey. USGS ANSS Comprehensive Catalog, 2021.

[255] D. Vamvatsikos. Performance-based seismic design in real life: the good, the bad, and the ugly. In *17th Congress of the Italian National Association of Earthquake Engineering*, Pistoia, Italy, 2017.

[256] D. Vamvatsikos and C. A. Cornell. Incremental dynamic analysis. *Earthquake Engineering & Structural Dynamics*, 31(3):491–514, 2002.

[257] D. Vamvatsikos and C. A. Cornell. The Incremental Dynamic Analysis and Its Application To Performance-Based Earthquake Engineering. In *12th European Conference on Earthquake Engineering*, page 10, London, 2002.

[258] N. Vishnu and J. E. Padgett. Interaction of life-cycle phases in a probabilistic life-cycle framework for civil infrastructure system sustainability. *Sustainable and Resilient Infrastructure*, 5(5):289–310, Sept. 2020. Publisher: Taylor & Francis.

[259] Y. Wang, L. Ibarra, and C. Pantelides. Seismic Retrofit of a Three-Span RC Bridge with Buckling-Restrained Braces. *Journal of Bridge Engineering*, 3(14):04016073, 2016.

[260] G. P. Warn and A. S. Whittaker. Property modification factors for seismically isolated bridges. *Journal of Bridge Engineering*, 11(3):371–377, 2006.

[261] J. C. Wilson. Stiffness of non-skew monolithic bridge abutments for seismic analysis. *Earthquake Engineering & Structural Dynamics*, 16:867–883, 1988.

[262] J. C. Wilson and B. S. Tan. Bridge abutments: formulation of simple model for earthquake response analysis. *Journal of Engineering Mechanics*, 116(8):1828–1837, 1990.

[263] Wright Timothy, DesRoches Reginald, and Padgett Jamie E. Bridge Seismic Retrofitting Practices in the Central and Southeastern United States. *Journal of Bridge Engineering*, 16(1):82–92, Jan. 2011. Publisher: American Society of Civil Engineers.

[264] Y. Xie and R. DesRoches. Sensitivity of seismic demands and fragility estimates of a typical California highway bridge to uncertainties in its soil-structure interaction modeling. *Engineering Structures*, 189(January):605–617, 2019.

[265] Y. Xie, M. E. Sichani, J. E. Padgett, and R. Desroches. The promise of implementing machine learning in earthquake engineering: A state-of-the-art review. *Earthquake Spectra*, 36(4):1769–1801, 2020.

[266] Y. Xie and J. Zhang. Evaluating the Effectiveness and Optimal Design of Isolation Bearings and Fluid Dampers for a Highway Bridge Using a Fragility Function Method and Genetic Optimization. In *Geotechnical and Structural Engineering Congress 2016*, pages 1317–1330, ???, 2016.

[267] A. Yakut and J. A. Yura. Evaluation of elastomeric bearing performance at low temperatures. *Journal of Structural Engineering*, 128(8):995–1002, 2002.

[268] A. Yakut and J. A. Yura. Parameters influencing performance of elastomeric bearings at low temperatures. *Journal of Structural Engineering*, 128(8):986–994, 2002.

[269] F. Yamazaki, H. Motomura, and T. Hamada. Damage assessment of expressway networks in Japan based on seismic monitoring. In *12th World Conference on Earthquake Engineering*, page 8, Auckland, New Zeland, 2000.

[270] C. S. W. Yang, S. D. Werner, and R. DesRoches. Seismic fragility analysis of skewed bridges in the central southeastern United States. *Engineering Structures*, 83(2015):116–128, 2015.

[271] T. Yilmaz, S. Banerjee, and P. A. Johnson. Performance of Two Real-Life California Bridges under Regional Natural Hazards. *Journal of Bridge Engineering*, 21(3):1–15, 2016.

[272] J. Yura, A. Kumar, A. Yakut, C. Topkaya, E. Becker, and J. Collingwood. Elastomeric bridge bearings: Recommended test methods. Technical report 449, National Research Council, Washington, D.C., 2001.

[273] B. Zakeri, J. E. Padgett, and G. G. Amiri. Fragility Analysis of Skewed Single-Frame Concrete Box-Girder Bridges. *Journal of Performance of Constructed Facilities*, 28(3):571–582, 2014.

[274] B. Zakeri, J. E. Padgett, and G. G. Amiri. Fragility assessment for seismically retrofitted skewed reinforced concrete box girder bridges. *Journal of Performance of Constructed Facilities*, 29(2):04014043 (12 pp.), 2015.

[275] C. Zelaschi, R. Monteiro, and R. Pinho. Critical Assessment of Intensity Measures for Seismic Response of Italian RC Bridge Portfolios. *Journal of Earthquake Engineering*, 23(6):980–1000, 2019. Publisher: Taylor & Francis.

[276] Q. Zhang, M. S. Alam, S. Khan, and J. Jiang. Seismic performance comparison between force-based and performance-based design as per Canadian Highway Bridge Design Code (CHBDC) 2014. *Canadian Journal of Civil Engineering*, 43(8):741–748, 2016.

[277] Y. Zhang and G. Wu. Seismic Vulnerability Analysis of RC Bridges Based on Kriging Model. *Journal of Earthquake Engineering*, 23(2):242–260, Feb. 2019. Publisher: Taylor & Francis.

[278] T. Zhou and A. Q. Li. Seismic fragility assessment of highway bridges using D-vine copulas. *Bulletin of Earthquake Engineering*, 17(2):927–955, 2019.

[279] T. Zhou, A. Q. Li, and Y. F. Wu. Copula-based seismic fragility assessment of base-isolated structures under near-fault forward-directivity ground motions. *Bulletin of Earthquake Engineering*, 16(11):5671–5696, 2018. Publisher: Springer Netherlands.

[280] L. F. Zuluaga Rubio, Y. Le Tartesse, C. Calixte, G. Chancy, P. Paultre, and J. Proulx. Cyclic behaviour of full scale reinforced concrete bridge columns. In *12th Canadian Conference on Earthquake Engineering*, Quebec City, Canada, 2019.